MAGNETIC HELICITY AND FORCE-FREE EQUILIBRIA IN THE SOLAR CORONA AND IN LABORATORY DEVICES

Andrew Michael Dixon

A Thesis Submitted for the Degree of PhD
at the
University of St Andrews

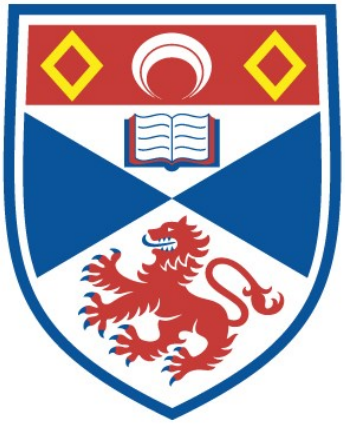

1988

MAGNETIC HELICITY AND FORCE-FREE EQUILIBRIA IN THE SOLAR CORONA AND IN LABORATORY DEVICES.

A. M. DIXON

THESIS SUBMITTED FOR THE DEGREE OF DOCTOR OF PHILOSOPHY
OF THE UNIVERSITY OF ST. ANDREWS

ProQuest LLC.
789 East Eisenhower Parkway
P.O. Box 1346
Ann Arbor, MI 48106 – 1346

ABSTRACT

Force-free equilibria are believed to be important in both an astrophysical and a laboratory context as minimum-energy configurations (see, for example, Woltjer, 1958; Taylor, 1974). Associated is the study of magnetic helicity and its invariance.

In Chapter Two of this thesis we put forward a means of heating the corona by the rotation of the foot-points of a coronal "sunspot" magnetic field anchored in the photosphere. The method adopted is essentially that of Heyvaerts and Priest (1984), employing Taylor's Hypothesis (Taylor, 1974) and a magnetic helicity evolution equation.

A characteristic of the Reversed-Field Pinch device is the appearance, at high enough values of the quantity "volt-seconds over toroidal flux", of a helical distortion to the basic axi-symmetric state. In Chapter Three we look for corresponding behaviour in the "sunspot equilibrium" of the previous chapter, with limited success. However, we go on to formulate a method of calculating general axi-symmetric fields above a sunspot given the normal field component at the photosphere.

Chapters Four, Five and Six are concerned with equilibrium force-free fields in a sphere. The main aim here is the calculation minimum-energy configurations having magnetic flux crossing the boundary, and so we employ "relative helicity" (Berger and Field, 1984). In Chapter Four we consider the "$P_1(\cos\theta)$" boundary radial field, finding that the minimum-energy state is always purely symmetric. In Chapter Five we treat the "$P_2(\cos\theta)$" boundary condition. We find in this case that a "mixed state" is theoretically possible for high enough values of the helicity. In Chapter Six, we consider a general boundary field, which we use to model point sources of magnetic flux at the boundary of a spheromak, finding that in practice an axi-symmetric configuration is always the minimum-energy state.

Finally, in Chapter Seven we present an extension to the theorem of Woltjer (1958), concerning the minimization of the magnetic energy of a magnetic structure, to include the case of a free boundary subjected to external pressure forces. To illustrate the theory, we have provided three applications, the first to a finite cylindrical flux and the remainder to possible spheromak configurations.

CONCERTINO

A. M. Dixon

I. Allegro con Brio * Full Score *

For AEE

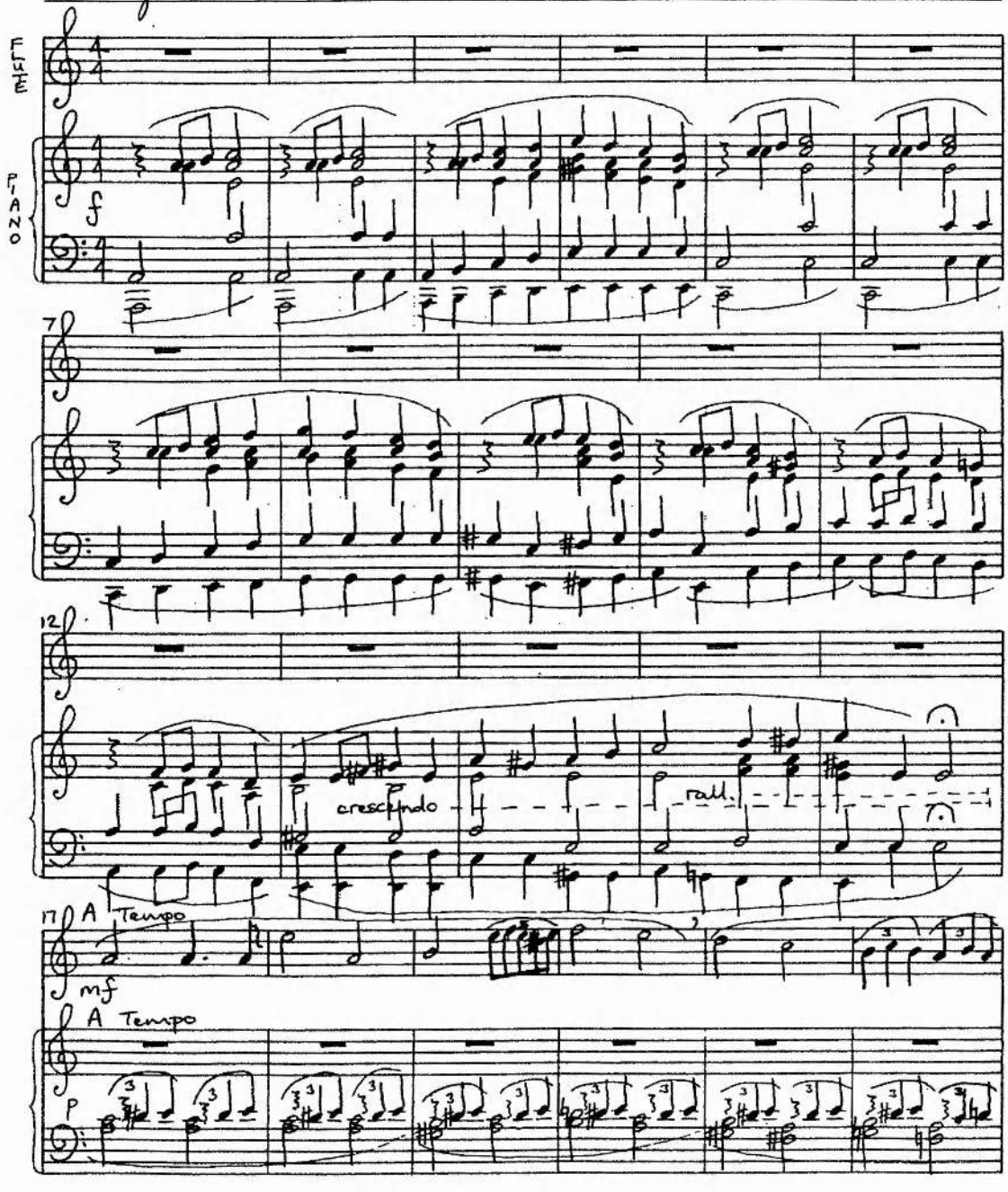

DECLARATION

I, Andrew Michael Dixon, hereby certify that this thesis has been composed by myself, that it is a record of my own work, and that it has not been accepted in partial or complete fulfilment of any other degree or professional qualification.

Signed

Date 24/5/88

POSTGRADUATE CAREER

I was admitted to the faculty of Science of the University of St. Andrews under Ordinance General No.12 in January, 1985 and as a candidate for the degree of Ph.D. in November, 1985.

Signed . Date 24/5/88

CERTIFICATE

I hereby certify that the candidate has fulfilled the conditions of the Resolution and Regulations appropriate to the Degree of Ph.D.

Signature of Supervisor ... Date 24.5.89

ACKNOWLEDGEMENTS

The author would like to thank the following (among others) who have provided advice or support of one kind or another during the production of this thesis : Professor Eric Priest (for help and supervision at St. Andrews); Drs. Mike Bevir and Chris Gimblett (for supervision at Culham); U.K. Science and Engineering Reasearch Council, U.K.A.E.A. Culham Laboratory, Department / Division of Applied Mathematics of the University of St. Andrews, and John Dixon, Esq. (for financial support); Drs. Philippa Browning and Mitchell A. Berger (for collaboration in publications and for providing astonishing insight into the mysteries of magnetic helicity); Dr. Brian Taylor of Culham Laboratory (for helpful discussions); Drs. Alan Hood, Alastair Robertson, Marco Velli and Mr. Terry Martin (for assistance in computational problems); Dr. Bernard Roberts (for showing how a wave interpretation may well be more appropriate); Rev. Lawson and Mrs. Sheila Brown (for a listening ear and moral guidance); the rest of the solar group at St. Andrews (for providing an atmosphere of controlled hysteria) and Anita Forrest (for playing the flute). The author apologises for any inadvertent omissions from this list!

CONTENTS

CHAPTER ONE : INTRODUCTION

1.1 Force-Free Fields

This thesis is concerned largely with the study of those magnetic fields which are termed "force-free". Such fields coexist with (and are strongly coupled to) a plasma , which in the present work is situated either in the solar corona or in a laboratory fusion device such as the spheromak or the reversed-field pinch (RFP). The "force-free equation" is derived from the equation of motion, which in the case of a plasma which possesses bulk electrical neutrality may be written (e.g. Priest,1982)

$$\rho \frac{D\underline{v}}{Dt} = -\nabla p + \underline{j} \times \underline{B} - \rho g(r)\, \hat{\underline{r}} , \qquad (1.1)$$

where ρ is the mass density, $\underline{v}$ is the fluid velocity, p is the plasma pressure, $\underline{j}$ is the electric current density, $\underline{B}$ is the magnetic induction, g is the gravitational acceleration and r is the radial co-ordinate which points out from the centre of the sun or the earth The terms on the right-hand side of (1.1) represent , respectively, the pressure gradient, the Lorentz force and the gravitational force, all of these per unit volume. Other effects, such as viscosity, may also be included if required for a particular application.

We shall be confining our attention here to the situation when the Lorentz force term in (1.1) dominates all the others. From an order-of-magnitude analysis, one can show that this will be the case when the plasma flow speed, the sound speed and the gravitational free-fall speed are all much smaller than the Alfven speed. Under this set of conditions we may justifiably approximate (1.1) by

$$\underline{j} \times \underline{B} = \underline{0} , \qquad (1.2)$$

which we shall refer to as the "force-free equation". This equation is often used to model

magnetohydrostatic equilibria in so-called "low-beta" plasmas, that is , those in which the ratio of gas pressure to magnetic pressure is much smaller than unity. This state of affairs is amply satisfied in the case of the solar corona , particularly in regions of high magnetic field strength such as those above sunspot groups. In the laboratory , plasma betas of 10% or less have been achieved in practice (see, for example, the review by Bodin and Newton,1980).

The physical interpretation of Equation (1.2) is that the electric current density is everywhere parallel to the magnetic field. Using Ampere's Law, the electric current may be eliminated from (1.2) to produce the alternative form of the force-free equation, namely

$$\nabla \times \underline{B} = \alpha \underline{B} , \tag{1.3}$$

where α is a spatially-varying function . By taking the divergence of both sides of (1.3) one obtains the condition

$$(\underline{B} \cdot \nabla) \alpha = 0 , \tag{1.4}$$

which indicates that α is invariant on any particular field-line, but in general varies from one field-line to another. Equation (1.4) is non-linear, except in the special case where α takes the same value over all space , under which condition we have what is known as a *linear* or *constant-* α force-free field. Applying the curl operator to both sides of (1.3) when α is uniform gives the Helmholtz equation

$$(\nabla^2 + \alpha^2) \underline{B} = \underline{0} , \tag{1.5}$$

which is linear in $\underline{B}$. As will be seen subsequently, fields which are solutions to (1.5) play an important role in both solar and terrestrial plasma physics. This is partly because is it is much easier to construct solutions to (1.5) than of the more general equation (1.3), but also because it is widely believed that linear force-free fields do in fact approximate well to many astrophysical and laboratory magnetic field structures.

1.2 Magnetic Helicity

Consider some volume V at each point of which is defined a magnetic field vector $\underline{B}$ which is a function of position. Then the integral

$$H = \int_V \underline{A} \cdot \underline{B} \, dV \tag{1.6}$$

defines the *magnetic helicity* of the field, where $\underline{A}$ is a magnetic vector potential given by

$$\nabla \times \underline{A} = \underline{B} . \tag{1.7}$$

In ideal magnetohydrodynamics (ideal MHD), magnetic helicity has an interpretation in terms of the topology of magnetic field lines. The quantity (1.6) is a measure of the degree of self-twist of elementary flux tubes and of the amount of linkage between distinct flux tubes (Moffatt,1969; Berger and Field,1984).

The definition (1.6) as it stands has certain drawbacks. One of these is that if the boundary S of V is not a magnetic surface, then (1.6) does not uniquely define the helicity. To see this, add the gradient of an arbitrary function of position to the vector potential and substitute this into (1.6). After applying a vector identity it is evident that the new value of helicity differs from the old value by a surface integral term which depends on the *gauge* of the vector potential, thus giving different results for different gauges. Another difficulty arises when V is not simply-connected, as for example is the case when V is the volume bounded by a torus. Here the helicity integral (1.6) is unsatisfactory because the value calculated depends on how much external flux is linking the torus through its centre.

To rectify these, and other, deficiences in the original definition, various authors have proposed more satisfactory alternatives which all possess the desired property of gauge-invariance,and in some cases additional modifications designed to suit specialist applications (Berger and Field,1984; Finn and Antonsen,1985; Hammer,1983). One of

these formulations has been adopted for use in this thesis, and is described in detail in Section 4.9 for application to spheromak fields with inhomogenous boundary conditions.

One can readily show from (1.6) by taking the derivative with respect to time and using the ideal MHD form of the Induction Equation, namely

$$\frac{\partial \underline{B}}{\partial t} = \nabla \times (\underline{v} \times \underline{B}) , \tag{1.8}$$

that the magnetic helicity integral is conserved for simply-connected volumes V which are bounded by magnetic surfaces S.

Woltjer (1958) showed that in an ideal-MHD flux tube if one minimizes the *magnetic energy* , defined as

$$W = \frac{1}{2\mu_0} \int_V B^2 dV , \tag{1.9}$$

subject to the constraint that the magnetic helicity (1.6) remains constant, one finds the minimizing field to be *linear force-free* of the type given by (1.3). Taylor (1974) extended Woltjer's astrophysical theorem to the realm of laboratory plasma physics by putting forward a proposition regarding the nature of relaxed states in a *slightly resistive* plasma. In ideal MHD, there is an infinite number of topological constraints, essentially one for every field-line . On each of these infinitesimal flux-tubes magnetic helicity is conserved and we have associated one particular value of α. Since field-lines in non-resistive MHD cannot break or merge, the topological identity of all field-lines remains fixed for all time. However, if some small resistivity is introduced into the plasma, then field-lines may break and reconnect, exchanging magnetic helicity between flux-tubes in the process and destroying all previous constraints, with one exception : Taylor reasoned that the *total* helicity of the volume would remain approximately constant in the process. Associated with this single global constraint would be just one value of α , which would be the same throughout the volume. Hence *Taylor's Hypothesis* states that in a plasma which possesses slight resistivity, the final state obtained after some intermediate turbulent

process is a constant- α force-free field of the form (1.3) with α uniform.

Such theoretical "Taylor States" have been observed in some cases to correspond closely to fields measured in laboratory discharges, notably in RFP and Spheromak experiments. The phenomenon of toroidal field reversal in the outer regions of RFPs was first satisfactorily explained using Taylor's theory, and also the onset of helical equilibria in cylindrical geometry was predicted (see Chapter 3).

More recently, Heyvaerts and Priest (1984) have adapted Taylor's original hypothesis for use in application to the solar corona, which has magnetic flux crossing the photospheric boundary. They derived an appropriate evolution equation for the magnetic helicity in terms of slow motions of the footpoints of magnetic field-lines anchored in the photosphere. This was then incorporated into a theory of coronal heating based on Taylor relaxation during the shearing of a coronal arcade structure. Dixon, Browning and Priest (1988) performed the same type of calculation , but for the twisting of the magnetic field above a sunspot (see Chapter 2) . Browning, Sakurai and Priest (1985) also used the method to estimate the coronal heating in a set of twisted and closely-packed flux-tubes.

Relaxation theories which employ the restraint of conservation of magnetic helicity rely on the decay time for helicity being much longer than that of magnetic energy. In the solar corona this assumption seems to be justified, since helicity in, for example, a coronal loop has a decay time of the order of 10^{12} seconds (Berger, 1984) , whereas the time-scale for decay of typical magnetic features is of the order of 10^4 seconds (hours or days). Because helicity decays on a diffusion time-scale, namely

$$\tau_D = \frac{L^2}{\eta} , \qquad (1.10)$$

in which L is a typical length-scale and η is the coefficient of diffusivity, the time-scale for significant helicity decay in the case of laboratory plasmas is many orders of magnitude shorter than in the corona. However, energy is still observed to decay preferentially with respect to helicity, typical time-scales being 10^{-3} seconds and about 1 second, respectively. Hence in some laboratory experiments also it remains a good approximation

to assume that decay of magnetic helicity is insignificant compared with the resistive decay of typical magnetic field structures.

1.3 The Solar Corona

The corona is the outermost layer of the sun's atmosphere. It is bounded below by the *transition region* , which separates it from the *chromosphere* , and extends outwards as far as the orbit of the Earth and beyond, where it is much more rarified than in the immediate neighbourhood of the sun.

Two main characteristics of the corona are its high temperature (typically 10^6 K, compared with about 10^3 K in the photosphere) and low number density (of the order of 10^{12} m^{-3} at a height of one solar radius above the photosphere, compared with about 10^{23} m^{-3} in the photosphere). As a result of its high temperature, the material which makes up the corona is ionized to a very high degree, and thus the corona is *highly conducting* . Hence the magnetic Reynolds number of the plasma is very large, and we may use the approximation that the magnetic field-lines are *frozen in* to the plasma. Also, as discussed earlier, since the corona is so tenuous the plasma pressure is small compared with the pressure produced by the magnetic field, so in many cases it is valid to assume that the field is force-free.

Topologically, the corona may be divided into so-called *open* - and *closed-field* regions, depending on the open or closed property of the magnetic field-lines. Open-field regions correspond to the location of *coronal holes* , which are the dark regions observed in X-ray images of the corona. These regions are the origin of the *solar wind* , which is a fast stream of plasma expelled from the sun into the interplanetary medium.

In the visible part of the spectrum, the corona (whose luminosity is about 10^{-6} that of the photosphere) may be seen to advantage using a *coronograph* , which blocks off the

light from the sun's disc. Images produced with the aid of such an instrument show the outlines of both open and closed magnetic structures, such as *streamers* and *coronal transients* . Transients are associated with the eruption of prominences , which are cool (around 10^4 K), dense (about 10^2 times that of the surrounding corona) sheets of plasma . They are often observed to be remarkably stable , as in the case of *quiescent prominences* , which may have a lifetime of several months. MHD models put forward as possible solutions to the problem of the support of prominences in the corona include those by Kippenhahn and Schlüter (1957) and Kuperus and Raadu (1974). In both cases it is magnetic tension forces which are used to balance the pull of gravity on the prominence.

1.4 Laboratory Machines

Two important topological types of plasma confinement device in the laboratory are the *toroidal* and *spherical* systems (Taylor, 1986). Members of the former class include the *tokamak* and *RFP*, whilst the latter group includes the *spheromak* and the *flux-core spheromak* . The ultimate goal in the construction of these machines is the sustainment of controlled thermo-nuclear reactions as a source of useful power. A major problem associated with this is that of *confinement* of plasma within the reaction vessel. Much effort has been spent in the search for stable magnetic field configurations which are efficient in isolating the plasma from the walls of the vessel (to prevent heat losses by conduction) for sufficiently long *energy containment times* . It is important that the plasma temperature is high , since otherwise energy losses due to bremsstrahlung radiation are greater than the energy output of the thermonuclear reactions themselves (Hugill,1981). An important relationship is *Lawson's Criterion* (Lawson, 1957) which is the condition for net production of energy from fusion reactions. It may be expressed in the form (Hugill, 1981)

$$n\tau \geq \frac{3kT}{\left\{\frac{\tilde{\eta}}{1-\tilde{\eta}}\,\frac{\gamma\langle\sigma v\rangle Q}{4} - \tilde{\alpha}\,T^{1/2}\right\}} \qquad (1.11)$$

for the product of the electron number density n with the energy containment time τ as a function of the plasma temperature T. Other quantities in equation (1.11) are Boltzmann's constant k, the efficiency of conversion of plasma energy into electrical energy η , the energy released per reaction Q, and the nuclear reaction rate averaged over a Maxwellian velocity distribution $\langle\sigma v\rangle$. γ is a factor which depends on the isotopes reacting and α is the constant of proportionality in the expression for the bremsstrahlung energy loss.

1.4.1 The Reversed-Field Pinch Configuration.

The RFP is a toroidal confinement system in which the *toroidal* (ϕ) and *poloidal* (θ) components of the magnetic field are of approximately the same magnitude. If a and R represent the *minor* and *major radii* of the torus, the *safety factor* is the quantity

$$q = \frac{a B_\phi}{R B_\theta} , \qquad (1.12)$$

which in the case of the RFP is much less than unity (Bodin and Newton,1980). The *inverse* of the safety factor measures the total number of times the field makes a circuit in the poloidal direction for each tour in the toroidal direction. Hence the RFP configuration has high shear of the field-lines. Another property of the RFP is the spontaneous *reversal* of the toroidal field in the outer region of the plasma near the container wall (Taylor, 1974).

In general, in the RFP the plasma pressure is significant, that is, there is a high plasma beta. However, RFPs lie close to minimum- energy configurations, and so a low-beta approximation is provided by a Taylor state (Bodin and Newton, 1980) . Finite-beta models have been developed which include a pressure varying with radius. Also, since the field twists many times in one toroidal circuit, the effect of the curvature of the container may in most cases be neglected , and a cylindrical coordinate system may be adopted for simplicity (see Chapter 3).

1.4.2 The Spheromak Configuration.

The spheromak differs from, for example, the RFP because it is topologically a sphere rather than a torus. Whereas the latter device has coils placed through its centre to generate a toroidal field, this is obviously not possible in the former. For practical reasons the actual shape of a spheromak device is invariably not a perfect sphere, but nevertheless it is always a sphere topologically speaking, because the volume contained is simply-connected and so topologically deformable into a sphere. However, the spheromak is closely related to the RFP in that it is also a configuration which is nearly force-free and also has 'toroidal' and 'poloidal' fields of comparable magnitude (Hammer,1984). In both these systems, therefore, the role of external coils is small or completely absent, with most of the magnetic field being produced by internal electric currents flowing along field-lines.

One notable feature of this kind of *compact torus* is the absence of a flux conservation condition. In the RFP the toroidal flux is taken as an invariant, but for a simple spheromak consisting of nested flux surfaces, the net flux round any toroidal path is zero. In fact, for the classical spheromak , the only relaxed states are those determined by certain eigenvalues of α(Rosenbluth and Bussac, 1979), assuming that the bounadary is a magnetic surface. What happens when this is not the case is considered in this thesis in Chapters 4, 5 and 6. Turner (1984) has produced analytical force-free solutions for a spheromak idealized as a cylindrical 'can' with point sources of magnetic flux located on the boundary to model isolated electrodes.

Another aspect of spheromak research is the field of *helicity injection* . This is the process whereby plasma is projected by means of a 'gun' into the chamber where the spheromak is to be formed (Jarboe et al., 1984). The basic principle involved is that field-lines initially lying across the entrance to the chamber are carried into it by the injected plasma since the field is 'frozen in'. The field re-connects near the entrance to produce the isolated spheromak in the cavity. The linkage of the field-lines has been increased in the process, and so helicity has thus been injected

1.5 Overview of Thesis

We shall now give a summary of the contents of the main body of the thesis.

In Chapter 2 we start by giving a calculation of the heating in the corona produced by the twisting of magnetic field-lines above a single sunspot, driven by foot-point motions in the photosphere. The method used is based on that of Heyvaerts and Priest (1984), who treated the problem of the heating of the corona due to the shearing of a coronal arcade. The subject matter of this chapter forms the basis of the paper "Coronal Heating by Relaxation in a Sunspot Magnetic Field" by A. M. Dixon, P.K. Browning and E.R.Priest (1988).

Chapter 3 begins with a summary of the analysis of Taylor (1974, 1986) for the onset of helical deformations in initially axi-symmetric force-free fields in a low aspect-ratio torus. This is used as a basis for a search for corresponding classes of solution in the solar corona. The effect of the differing nature of the boundary conditions on the two problems is explored, and a theory developed for coronal fields.

Chapters 4, 5 and 6 are all concerned with solutions in spherical geometry of the force-free equation in which magnetic flux is allowed to cross the boundary. The idea is to model equilibrium spheromak fields with inhomogeneous boundary conditions. The boundary condition is expressed in general as a sum of Legendre polynomials in the cosine of the angle θ. The effect of the first term in this series is analysed in Chapter 4 ('dipole boundary condition') and in Chapter 5 we discuss the solutions with only the second term present ('quadrupole boundary condition'). Deductions regarding the nature of possible solutions are made. As an example of the most general form of the boundary condition, we consider in Chapter 6 the case of boundary point sources, for which we model the radial field on the boundary by delta functions. The work of the three chapters has been submitted to the Journal of Plasma Physics as "Relaxed States in a Spheromak with Inhomogeneous Boundary Fields" by A.M. Dixon, P.K.Browning, M.K. Bevir, C.G. Gimblett and E.R. Priest.

Chapter 7 contains the extension of the theorem of Woltjer (1958) for force-free fields to the case in which the boundary of the region is free to move in response to external pressure forces. This work has been submitted to the Journal of Astronomy and Astrophysics as "A Generalization of the Woltjer Minimum-Energy Principle" by A.M. Dixon, M.A. Berger, P.K. Browning and E.R. Priest.

Finally in Chapter 8 we present some concluding remarks.

1.6 Summary of the Equations of M.H.D.

No thesis seems to be complete without a list of our old friends the MHD equations, so, in keeping with current practice, here they are for reference.

1.6.1 The Fluid Equations.

The following two equations describe properties of the plasma regarded as a continuous fluid. The first of these is the *equation of mass conservation* , also known as the *continuity equation* . For a plasma of density ρ with a velocity field $\underline{v}$, this is

$$\frac{\partial \rho}{\partial t} + \nabla \cdot (\rho \underline{v}) = 0 . \tag{1.13}$$

The second of these equations is the *ideal gas law* , which may be written in the form

$$p = \frac{k_B}{m} \rho T , \tag{1.14}$$

where p is the gas pressure, k_B is Boltzmann's constant, m is the mean particle mass and T is the temperature.

1.6.2 The Momentum Equation.

The *equation of conservation of momentum* (*'equation of motion'*) which includes the effect of a pressure gradient, a gravitational field, the Lorentz force and viscosity respectively can be written

$$\rho \frac{d\underline{v}}{dt} = -\nabla p + \rho \underline{g} + \underline{j} \times \underline{B} + \rho \nu \nabla^2 \underline{v} \,, \qquad (1.15)$$

where g is the gravitational acceleration field and ν is the coefficient of kinematic viscosity. Note that the Lorentz force is the only magnetic term appearing in (1.15).

1.6.2 The Maxwell Equations.

Normally only three of the four *Maxwell Equations* are included in the system of MHD equations.

The *solenoidal* condition, describing the closure of magnetic field lines, is given by

$$\nabla \cdot \underline{B} = 0 \,. \qquad (1.16)$$

Thus the magnetic field is 'divergence-free', which implies that there are no 'sources' or 'sinks' present.

The curl of the magnetic field $\underline{B}$ is related to the electric current density $\underline{j}$ by *Ampere's Law* , which is usually quoted in the form where the displacement current is neglected, namely

$$\nabla \times \underline{B} = \mu_0 \underline{j} \,, \qquad (1.17)$$

where μ_0 is the permeability of free space. This approximation holds good for fluid flow speeds which are much less than the speed of propagation of light.

Faraday's Law of Induction , relating the electric field to the time-variation of the magnetic field, is

$$\frac{\partial \underline{B}}{\partial t} = -\nabla \times \underline{E} \ . \qquad (1.18)$$

1.6.3 Ohm's Law.

Ohm's Law , describing the ease of passage of electric currents in a conductor, is for many purposes amply approximated by the form

$$\underline{j} = \sigma (\underline{E} + \underline{v} \times \underline{B}) \qquad (1.19)$$

for a moving conductor, where σ is the *electrical conductivity.*

1.6.4 The Energy Equation.

The final equation we shall consider describes the interchange of energy among various forms. It may be written in the form

$$\frac{e^{\gamma}}{\gamma - 1} \frac{d}{dt}\left(\frac{p}{e^{\gamma}}\right) = -\nabla \cdot (\kappa \nabla T) - e^2 Q(T) + \frac{j^2}{\sigma} + H \ , \qquad (1.20)$$

where the terms on the right-hand side of the equation represent respectively energy losses by heat conduction, radiation, ohmic (joule) heating and a term due to some (unknown) mechanical heating mechanism. κ is the coefficient of thermal conduction parallel to the magnetic field, and Q(T) is a (known) optically-thin radiative loss function.

The above constitute the usual equations of MHD.

1.6.5 The Induction Equation.

A derived equation, known as the *Induction Equation* , is obtained by eleminating both E and j from (1.16), (1.17), (1.18) and (1.19) to give

$$\frac{\partial \underline{B}}{\partial t} = \nabla \times (\underline{v} \times \underline{B}) + \eta \nabla^2 \underline{B} \ , \tag{1.21}$$

where η is the magnetic diffusivity, given by

$$\eta = \frac{1}{\mu_0 \sigma} \tag{1.22}$$

and assumed to be constant.

1.6.6 Some Characteristic Parameters.

The *magnetic Reynolds number*

$$R_M = \frac{vL}{\eta} \tag{1.23}$$

is determined by the ratio (in order of magnitude) of the first to the second of the terms on the right-hand side of (1.21). If it is small, diffusive effects may be important; if it is large, the field is *frozen in* to the flow.

The *plasma beta* is given by

$$\beta = \frac{P}{B^2/2\mu_0} \tag{1.24}$$

and is a measure of the extent to which the plasma pressure dominates the magnetic pressure.

The plasma *sound speed* is given by the formula

$$c_s = \left(\frac{\gamma p}{\rho}\right)^{1/2}, \tag{1.25}$$

and the *Alfven speed* by

$$V_A = \frac{B}{(\mu_0 \rho)^{1/2}}, \tag{1.26}$$

which is the characteristic speed of propagation of magnetic disturbances.

CHAPTER TWO : EVOLUTION OF A SUNSPOT FIELD

2.1 Introduction

The physical mechanism by which the solar corona is heated to temperatures of the order of 2×10^6 K is now widely considered to be principally magnetic, although there is still considerable speculation as to the precise nature of the processes involved. (For reviews of recent ideas see, for example, Kuperus and Heyvaerts, 1980; Priest, 1982; Chiuderi, 1983; Hollweg, 1983 and Heyvaerts,1984).

One group of theories is based on the idea that the corona may be heated as a result of direct currents generated by slow motions of the photospheric footpoints of the coronal magnetic field. In this context *slow* means that the time-scale of fluid motions (τ_V) is much longer than the Alfven transit time across the structure (τ_A). A mechanism based on such a theory was proposed by Heyvaerts and Priest (1984), who were able to relate the heating-rate by magnetic reconnection to the driving photospheric motions, although necessarily incorporating an unknown *reconnection time* τ_R, which is taken to be much shorter than τ_V. The basic idea is that very slow motions of the photospheric footpoints generate finite stresses in the coronal field which subsequently becomes prone to resistive instabilities. The field then relaxes by reconnection to the minimum-energy state accessible over a reconnection time, conserving the value of the magnetic helicity. Their calculation employs Taylor's hypothesis (see Section 1.2) which was suitably modified to take into account the fact that the photospheric boundary of the corona is not a magnetic surface. The theory does not provide, however, a detailed account of the actual dissipation mechanism, which remains unknown.

The helicity of the corona is changed by motions which twist or shear the footpoints of the magnetic field, which are embedded in the relatively dense photosphere. According

to the (generalized) Taylor theory, the coronal field will relax to a linear force-free field (1.5) whilst preserving the value of the magnetic helicity (1.6). In the limit of *immediate relaxation* ($\tau_R/\tau_V \rightarrow 0$), the field evolves quasi-statically through a sequence of constant-α states which are described by the helicity evolution equation

$$\frac{dH}{dt} = \int_S (\underline{A} \cdot \underline{v})(\underline{B} \cdot d\underline{S}) \tag{2.1}$$

where S represents the photospheric boundary and $\underline{v}$ the velocity field. The vector potential $\underline{A}$ evolves according to the equation

$$\frac{\partial \underline{A}}{\partial t} = \underline{v} \times \underline{B} \tag{2.2}$$

on the boundary S. The force-free parameter α also evolves in time, in a manner which depends on the photospheric velocity field.

There is an apparent difficulty in generalizing Taylor's hypothesis to regions such as the corona which are not bounded by a magnetic surface : since an arbitrary gauge function may always be added to the vector potential $\underline{A}$, the magnetic helicity is not uniquely defined (see Section 1.2). Thus, if $\underline{A}_2 = \underline{A}_1 + \nabla G_2^1$, then

$$H_2 - H_1 = \int_S G_2^1 (\underline{B} \cdot d\underline{S}) \tag{2.3}$$

where H_1 and H_2 are the magnetic helicities which correspond to the two vector potentials $\underline{A}_1$ and $\underline{A}_2$. However, Browning and Priest (1986) have shown that the results of the method are independent of the gauge chosen, as long as changes in the gauge on the boundary are followed closely. The physical interpretation of this is that it is not the actual value of the helicity , but rather the *changes* in value of the helicity which are significant. Much of this difficulty may in fact be bypassed if one uses one of the gauge-invariant forms of magnetic helicity, such as the relative helicity of Berger and Field (1984), throughout the calculation.

The generalized Taylor method enables the coronal heating rate to be calculated (in terms of the reconnection time), since the magnetic energy released as heat is the difference between the energy of the field induced by the boundary motions and the energy of the relaxed linear force-free state. No energy may be dissipated in the immediate relaxation limit, since finite stresses must be built up in order to produce heating (Browning and Priest, 1986). Thus finite relaxation times must be considered if heating is to be achieved.

The theory outlined above is known as the *Resistive Turbulence Model* of coronal heating, and has certain points in common with Parker's theory of *non-equilibrium* (Parker 1972, 1981, 1983a,b). This theory is based on the idea that current sheets are formed in the corona as a result of complex asymmetric footpoint motions, and that as a result the corona is in a state of non-equilibrium and reconnects rapidly to dissipate some of its energy as heat. Whether such a state of non-equilibrium actual exists is unclear (Van Ballegooijen, 1985). Browning, Sakurai and Priest (1986) calculated the heating produced by an array of closely-packed flux-tubes, corresponding to Parker's (1983a) paper. The final state is also determined. Although the two theories do in fact give the same order-of-magnitude heating rate (Parker, 1983b), Parker's theory does not give the final state reached after the onset of non-equilibrium or put a bound on the energy actually available to produce heating.

Previous applications of the Resistive Turbulence Model of coronal heating were to an arcade of loops sheared by photospheric motions (Heyvaerts and Priest, 1984; Browning and Priest, 1986) and to a single coronal loop twisted up by cellular footpoint motions (Browning *et al* ., 1986). These studies have shown that resistive turbulence can adequately heat the corona, and that heating is most efficient when the time-scale of the photospheric motions is of the same order of magnitude as the reconnection time-scale. The present chapter is concerned mainly with the application of the theory developed by Heyvaerts and Priest (1984) to the twisting of the magnetic field above a single sunspot. The equilibrium configuration which we shall adopt is that given by Schatzman (1965). Before this is discussed, we first consider some features which arise from the original work of Heyvaerts and Priest (1984), namely which velocity profiles are most efficient in

injecting helicity into the corona, the relation between the helicity injection rate and the Poynting flux, and finally the reason why the quadratic form for the function g(a) in the original Heyvaerts and Priest (1984) theory was rejected.

2.2 Comments on the Coronal Arcade Problem.

2.2.1 Maximization of the Helicity Injection Rate: the Most Efficient Velocity Profile

For the "arcade" equilibrium considered by Heyvaerts and Priest (1984), having magnetic field components

$$(B_x, B_y, B_z) = \left(\frac{l}{k}\cos kx, -\frac{(k^2-l^2)^{1/2}}{k}\cos kx, \sin kx\right) B_0 e^{-lz} \qquad (2.4)$$

the particular form taken by the helicity evolution equation (2.1) is

$$\frac{dH}{dt} = \frac{B_0}{k^2}\int_{-\pi/2k}^{\pi/2k} k\, v(x,t) \sin kx \cos kx \, dx \;, \qquad (2.5)$$

which describes how the magnetic helicity (H) changes with time as a function of the photospheric velocity field v(x,y) $\hat{\underline{y}}$. The shear (α) is directly proportional to the helicity. It is of interest to discover which velocity profiles, subject to approriate normalization, are most efficient in increasing the coronal helicity. As a first approach we consider the class of functions

$$k\, v(x,t) = \sin pkx \qquad (2.6)$$

where p is a dimensionless parameter representing the ratio of the magnetic length-scale to the velocity length-scale. Thus (2.5) becomes

$$\frac{dH}{dt} = 2\frac{B_0^2}{k^3}\int_0^{\pi/2} \sin\theta \cos\theta \sin p\theta \, d\theta \qquad (2.7)$$

$$= \begin{cases} \frac{1}{2}\frac{B_0^2}{k^3}\left\{\frac{1}{(p+2)} - \frac{1}{(p-2)}\right\}\sin\frac{1}{2}\pi p, & p \neq \pm 2 \quad (2.8) \\ \pm\frac{1}{4}\pi\frac{B_0^2}{k^3}, & p = \pm 2 . \quad (2.9) \end{cases}$$

Part of the graph of dH/dt for p≥0 is shown in Figure 2.1. This shows that the maximum helicity injection rate occurs when the velocity length-scale is a factor 1.7 shorter than the magnetic length-scale 2π/k.

At the dominant peak of dH/dt, at $p=p_0\approx 1.7$, we have in fact

$$\frac{dH(p_0)}{dt} = 0.82\,\frac{B_0^2}{k^3} \qquad (2.10)$$

and from (2.6) the velocity profile that maximizes dH/dt is

$$kv(x,t) = \sin(1.7kx). \qquad (2.11)$$

Much shorter velocity scales (larger values of p) are very inefficient at increasing the helicity (and hence the shear) of the coronal field.

2.2.2 The Relation Between the Helicity Injection Rate and the Poynting Flux.

A physically important quantity is the Poynting flux F through the plane z=0, which is the rate at which magnetic energy is injected into the corona from the photosphere. For the same arcade equilibrium, F as a function of the velocity field v(x,t) at z=0 is

$$F = \frac{B_0^2(k^2-l^2)^{1/2}}{\mu_0 k^3}\int_0^{\pi/2} kv\left(\frac{\theta}{k},t\right)\sin 2\theta\, d\theta \qquad (2.12)$$

and if stresses relax instantaneously it can be shown that in addition we have

$$\frac{1}{4}\pi\frac{(k^2-l^2)^{1/2}}{l} = \int_0^{\pi/2} k\lambda\left(\frac{\theta}{k},t\right)\sin 2\theta\, d\theta \qquad (2.13)$$

where

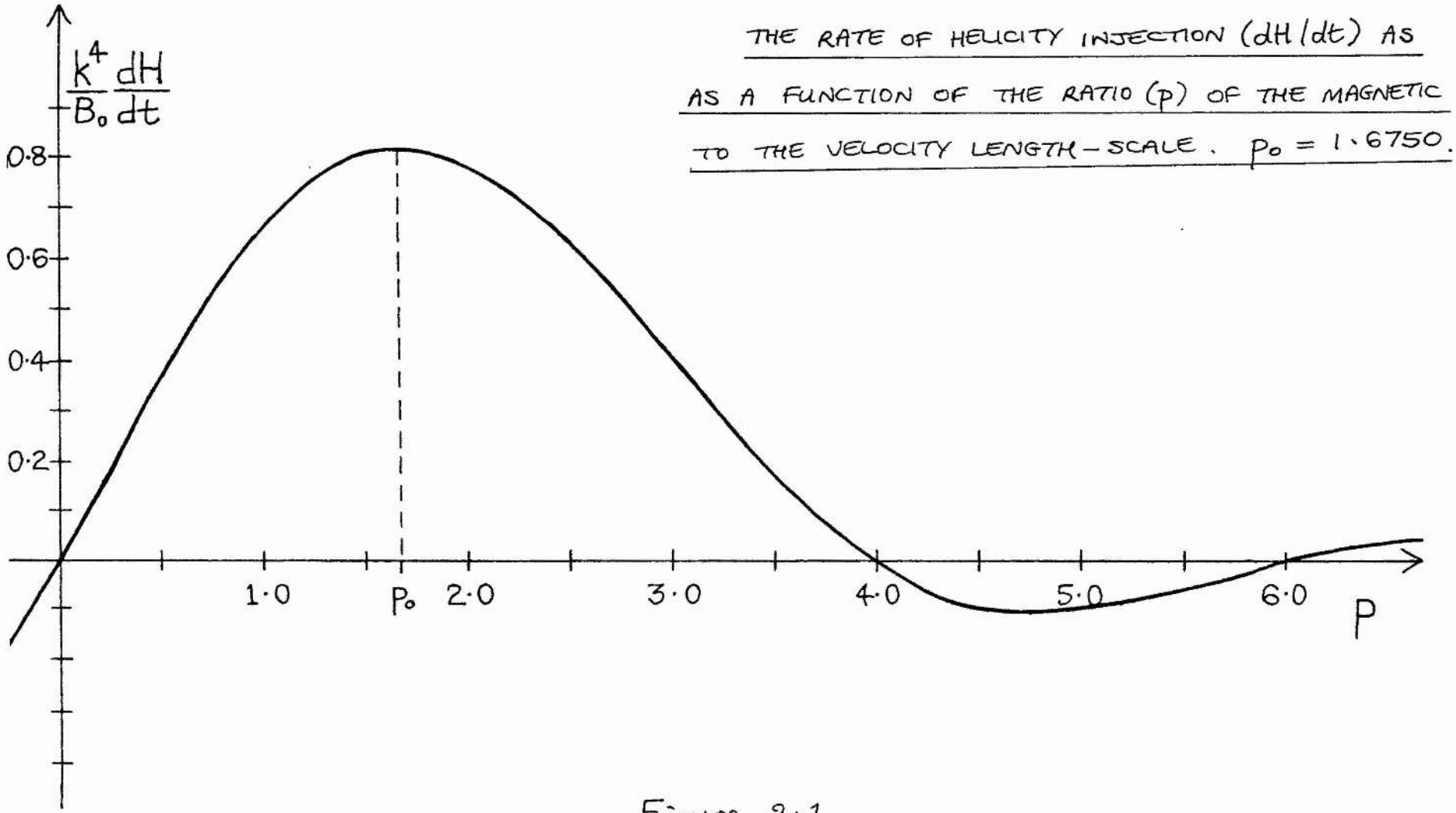

THE RATE OF HELICITY INJECTION (dH/dt) AS AS A FUNCTION OF THE RATIO (p) OF THE MAGNETIC TO THE VELOCITY LENGTH-SCALE. $p_0 = 1{\cdot}6750$.

Figure 2·1

$$\lambda(x,t) \equiv \int_0^t v(x,t)\,dt . \tag{2.14}$$

The helicity evolves according to Equation (2.5).

Let us now assume that $\lambda(x,t)$ is given by the more general form

$$k\lambda(x,t) \equiv f(t)g(p)\sin pkx \tag{2.15}$$

where f and g are arbitrary functions. Then the three expressions (2.12), (2.13) and (2.5) become respectively

$$F(p,t) = \frac{B_0^2(k^2-l^2)^{1/2}}{\mu_0 k^3} g(p)I(p)f'(t) \tag{2.16}$$

$$\frac{1}{4}\pi(k^2-l^2)^{1/2} = f(t)g(p)I(p) \tag{2.17}$$

and

$$\frac{dH}{dt} = \frac{B_0^2}{k^3} g(p)I(p)f'(t) \tag{2.18}$$

where

$$I(p) \equiv \int_0^{\pi/2} \sin p\theta \sin 2\theta\, d\theta . \tag{2.19}$$

The time rate of change of helicity given by (2.18) subject to the condition that the Poynting flux (2.16) remain constant (at F_0, say) in both p and t can then be derived as follows.

From (2.18) we have

$$(k^2-l^2)^{1/2} = \frac{k f(t)h(p)}{\left[f^2(t)h^2(p) + \left(\frac{1}{4}\pi\right)^2\right]^{1/2}} \tag{2.20}$$

where h(p)≡g(p)I(p). This is substituted in Equation (2.16) to give

$$\frac{B_0^2 f(t) f'(t) h^2(p)}{\mu_0 k^2 \left[f^2(t) h^2(p) + \left(\frac{1}{4\pi}\right)^2\right]^{1/2}} = F_0 \tag{2.21}$$

where

$$h^2(p) = c_0 , \text{ say} , \tag{2.22}$$

a constant, for which the helicity evolution equation (2.18) reads

$$\frac{dH}{dt} = \frac{B_0^2}{k^3} c_0^{1/2} f'(t) . \tag{2.23}$$

Integrating (2.21) to find f(t) and substituting in (2.23) yields

$$\frac{dH}{dt} = \frac{\mu_0 F_0}{k} \frac{(1+N_0 t)}{\left[(1+N_0 t)^2 - 1\right]^{1/2}} , \tag{2.24}$$

which determines completely the time-evolution of dH/dt, independently of p. The corresponding result for H(t) is

$$H(t) = \frac{\mu_0 F_0}{k} \frac{\left[(1+N_0 t)^2 - 1\right]^{1/2}}{N_0} \tag{2.25}$$

as shown in Figure 2.2. In particular, it can be seen that for $N_0 t \ll 1$,

$$\frac{dH}{dt} \approx \frac{\mu_0 F_0}{k} \left(\frac{1}{2 N_0 t}\right)^{1/2} \tag{2.26}$$

and

$$H \sim \frac{\mu_0 F_0}{k} \left(\frac{2t}{N_0}\right)^{1/2} \tag{2.27}$$

and that as $N_0 t \to \infty$

$$\frac{dH}{dt} \longrightarrow \frac{\mu_0 F_0}{k} \tag{2.28}$$

THE DIMENSIONLESS HELICITY $\bar{H} = H k N_0 / \mu_0 F_0$ AS A FUNCTION OF TIME FOR CONSTANT POYNTING FLUX F_0, WHERE $N_0 = (4\mu_0 k^2 / \pi B_0^2) F_0$.

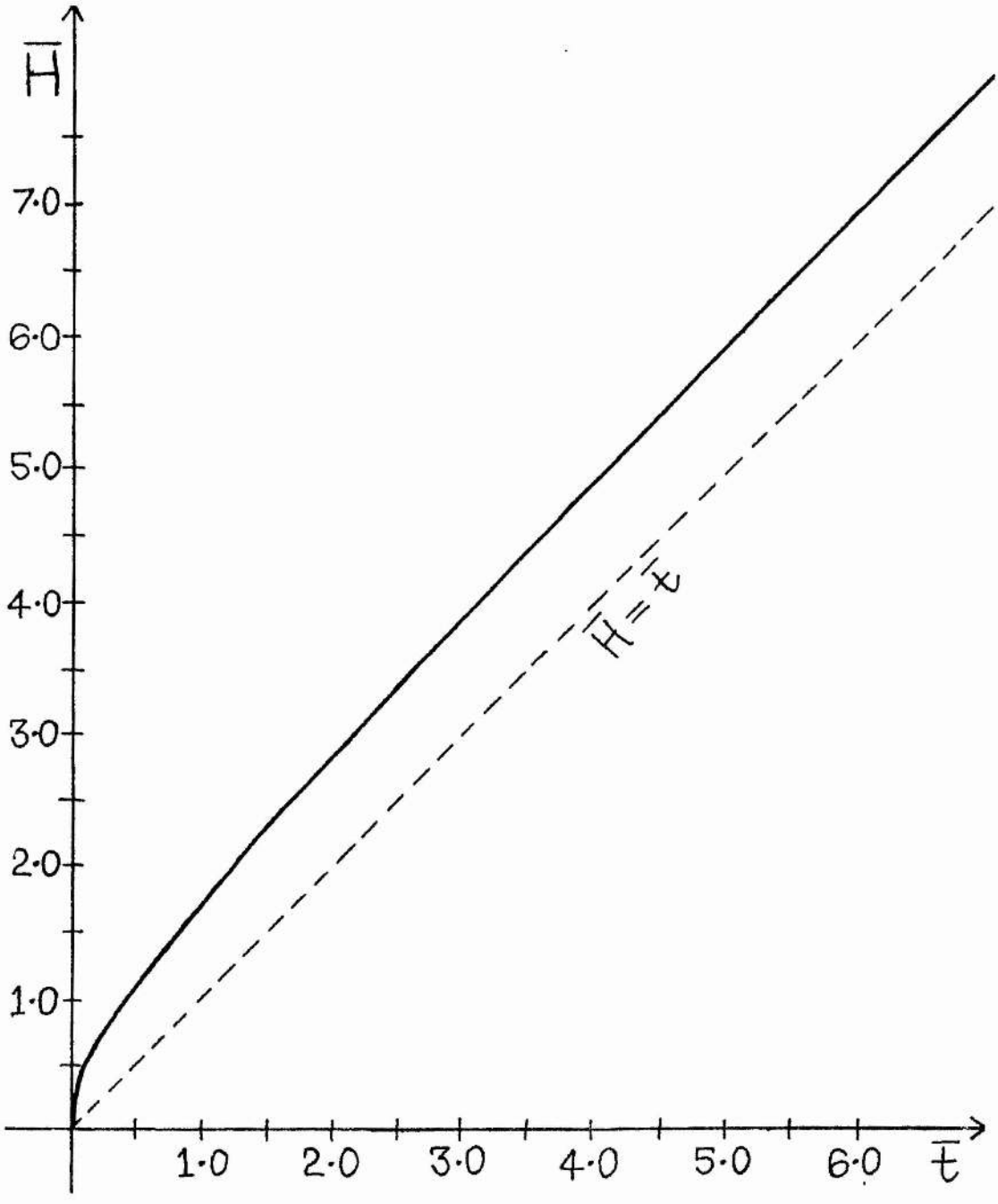

Figure 2·2

and

$$H(t) \sim \frac{\mu_0 F_0}{k} t \,, \tag{2.29}$$

the latter increasing without bound.

Equation (2.25) shows that the helicity injection rate is proportional to the Poynting flux and is independent of the length-scale ratio (p) for flows of the form (2.14). In particular, if we seek to maximise the helicity injection rate subject to the constraint of fixed F (replacing the fixed maximum velocity constraint of the previous section), we observe that there is in fact no maximum. Notice, however, that the time-dependence of dH/dt is somewhat different from that of the Poynting flux, especially at early times. At large times, (2.29) shows that H simply increases linearly in time at a rate proportional to F.

2.2.3 Why g(a) may not have a Quadratic Term.

Heyvaerts and Priest (1984), in choosing a form for g(a), discard certain possibilities. In particular, they do not allow g(a) to have a quadratic term. To investigate their reasons for doing this, let us make the choice

$$g(a) = B_0 \left(\frac{ka}{B_0} + \frac{4\gamma}{3} \frac{k^2 a^2}{B_0^2} \right), \tag{2.30}$$

a quadratic, where

$$a_0 = - \frac{B_0}{k} \cos kx \, e^{-lz} \,. \tag{2.31}$$

The perturbed part a_1 of the flux function expanded as

$$a = a_0 + \varepsilon a_1 \tag{2.32}$$

satisfies the partial differential equation

$$-(\nabla^2 + \alpha^2) a_1 = \alpha \{ g(a_0) + a_0 g'(a_0) \} \tag{2.33}$$

Then, given (2.30) and (2.31), (2.33) becomes

$$-(\nabla^2+\alpha^2)a_1 = 2\alpha B_0\{\gamma e^{-2lz} - \cos kx\, e^{-lz} + \gamma\cos 2kx\, e^{-2lz}\} \quad (2.34)$$

which is to be solved for a_1 subject to the boundary conditions

(i) $a_1=0$ on $z=0$, (ii) $a_1\to 0$ as $z\to\infty$,

(iii) a_1 remains finite on $x=0$, (iv) $a_1=0$ on $x=\pm\pi/2k$. (2.35)

The particular integrals corresponding to the three terms on the right-hand side of Equation (2.34) are, respectively,

$$a_{1\,P.I.(1)} = -\frac{2\alpha B_0\gamma}{(k^2+3l^2)}e^{-2lz}, \quad (2.36)$$

$$a_{1\,P.I.(2)} = -\frac{\alpha}{l}B_0\cos kx\; ze^{-lz} \quad (2.37)$$

and

$$a_{1\,P.I.(3)} = \frac{2B_0\gamma}{3\alpha}\cos 2kx\, e^{-2lz}. \quad (2.38)$$

The general form of the complementary function associated with (2.34) may be written in terms of a parameter β. There are two main cases, as follows:

(a) If $\beta^2\geq\alpha^2$, then we may write the complementary function as

$$a_{1\,C.F.} = \sum_{\beta}\{A_1(\beta)\cos\beta x + A_2(\beta)\sin\beta x\}\times \times\{A_3(\beta)e^{\sqrt{\beta^2-\alpha^2}\,z} + A_4(\beta)e^{-\sqrt{\beta^2-\alpha^2}\,z}\} \quad (2.39)$$

(b) If $\beta^2 < \alpha^2$, then we write instead

$$a_{1\,c.f.} = \sum_{\beta} \{B_1(\beta)\cos\beta x + B_2(\beta)\sin\beta x\} \times$$
$$\times \{B_3(\beta)\cos(\sqrt{\alpha^2-\beta^2}\,z) + B_4(\beta)\sin(\sqrt{\alpha^2-\beta^2}\,z)\}. \tag{2.40}$$

(Note that the summations will in general be integrals.) Hence the "general solution" to Equation (2.34) is the sum of (2.36), (2.37) and (2.38) with one of (2.39) and (2.40). This is now required to satisfy the boundary conditions (2.35). We shall now demonstrate that this is in fact not possible.

We note first of all that (2.40) is not an acceptable form for the complementary function because the terms do not decay to zero as z tends to infinity, thus violating condition (2.35)(ii). We therefore deduce that (2.39) is the correct form, with $\beta^2 \geq \alpha^2$. By the same criterion, we must have

$$A_3(\beta) \equiv 0 \tag{2.41}$$

since otherwise we would have terms which *increase* exponentially as z tends to infinity.

Next, condition (2.35)(iv) implies that

$$A_2(\beta) \equiv 0 \tag{2.42}$$

since a_1 must be even in x about the origin.

We are now required to satisfy the boundary condition (2.35)(i). To do this, we must select the values $\beta=0$ and $\beta=2k$ in the summation in order to balance the x-dependent terms in the particular integral. It is now apparent that choosing $\beta=0$ introduces an unwanted oscillatory term in z from the complementary function, except when $\alpha=0$, and that there is a term in the "solution" which does not satisfy (2.35)(iv). In fact we find that the final expression for a_1 is

$$a_1(x,z) = \frac{2\alpha B_0 \gamma}{(k^2+3l^2)}\left(\cos\alpha z - e^{-2lz}\right)$$

$$- \frac{\alpha}{l} B_0 \cos kx \, z e^{-lz} + \frac{2B_0\gamma}{2\alpha}\left\{e^{-2lz} - e^{-\sqrt{4k^2-\alpha^2}\,z}\right\}. \qquad (2.43)$$

Thus the expression (2.43) is inadmissible because it does not satisfy all the boundary conditions (2.35) and has properties which are also not acceptable on physical grounds. Hence we have shown that Heyvaerts and Priest (1984) were justified in rejecting the quadratic term in g(a).

2.3 The Sunspot Field and the Immediate Relaxation Limit

2.3.1 Introduction

An appropriate two-dimensional constant-α force-free solution in cylindrical polars (R,ϕ,z) is (Schatzman, 1965)

$$\left.\begin{aligned} B_R &= \frac{l}{k} B_0 J_1(kR) e^{-lz} \\ B_\phi &= \frac{\alpha}{k} B_0 J_1(kR) e^{-lz} \\ B_z &= B_0 J_0(kR) e^{-lz} \end{aligned}\right\} \qquad (2.44)$$

where $\alpha = (k^2-l^2)^{1/2}$. If we restrict the solution to the region for which $z \geq 0$ and $0 \leq kR \leq X_1$, where X_1 is the first positive zero of $J_1(X)$, it may be used to model the magnetic field above a single sunspot (see Figure 2.3).

Figure (2.3) shows magnetic flux coming through the plane z=0 (the photosphere) near the axis (R=0) and going back down through z=0 in a ring near the edge ($kR=X_1$).

From Faraday's equation (1.18) and Ohm's law (1.19) it is easily shown that the time-evolution of a vector potential $\underline{A}$ which satisfies $\nabla \times \underline{A} = \underline{B}$ is given by

THE EQUILIBRIUM FIELD (2.44)

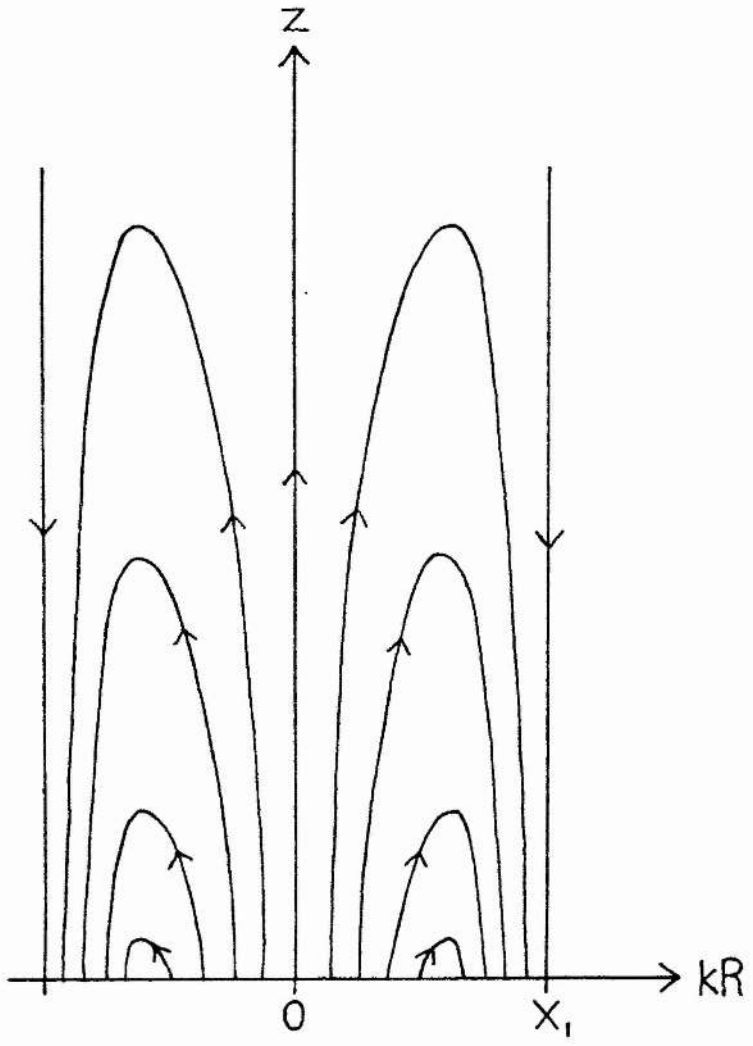

(a) VERTICAL CROSS-SECTION.

(b) HORIZONTAL CROSS-SECTION.

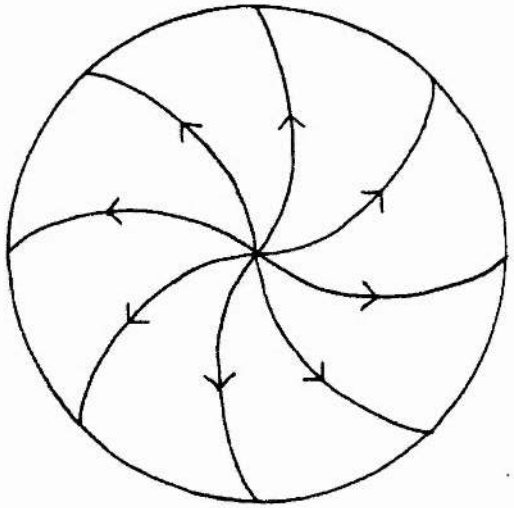

Figure 2·3

$$\frac{\partial \underline{A}}{\partial t} = \underline{v} \times \underline{B} - \frac{\underline{j}}{\sigma} + \nabla g \tag{2.45}$$

where g is related directly to the gauge G_2^1 in Equation (2.3). As has already been noted in Section 2.1, the particular choice of g will not affect the outcome of the evolution of the helicity integral, so without loss of generality we choose

$$\nabla g = \underline{0} \tag{2.46}$$

in which case (1.6) becomes

$$\frac{DH}{Dt} = \int_S (\underline{A} \cdot \underline{v} \times \underline{B} \cdot d\underline{S}_{out}) + \int_S \frac{(\underline{A} \times \underline{j}) \cdot d\underline{S}}{\sigma} - 2 \int \frac{(\underline{B} \cdot \underline{j})}{\sigma} dV \tag{2.47}$$

where S is the boundary of V. In this same gauge, if we let the electrical conductivity (σ) approach infinity on the boundary, (2.45) reduces to (2.2); this is sufficient because only gauge changes on the boundary affect the value of the helicity, as shown by Equation (2.3). Further, neglecting dissipative terms in (2.47) gives (2.1), which together with (2.2) forms the basis of the analysis which we present below.

2.3.2 The Immediate Relaxation Limit

Let us assume motions at the photospheric boundary to be of the general form

$$\underline{v}(R,0,t) = v(R,t)\,\hat{\underline{\phi}} \tag{2.48}$$

where there is no dependence upon ϕ, in keeping with (2.44). A possible vector potential for the field (2.44) that is non-singular in the limit of a potential field (α=0) is

$$A^* = \frac{B_0}{\alpha} J_1(kR) \left\{ \frac{l}{k} e^{-lz} - e^{-kz} \right\} \hat{\underline{R}} + \frac{B_0}{k} J_1(kR) e^{-lz} \hat{\underline{\phi}} + \frac{B_0}{\alpha} J_0(kR) \{ e^{-lz} - e^{-kz} \} \hat{\underline{z}}, \tag{2.49}$$

but in general this will not satisfy the condition (2.46). The aim of this section is to calculate the helicity H in the gauge (2.46) and to find an expression for the energy of the initial force-free field (2.44). In order to do this, the gauge function connecting the two vector potentials must be found, remembering from the relation (2.3) that differences in helicity caused by differences in gauge arise solely from gauge differences on the boundary.

First of all, the helicity H* of the configuration (2.44) for the vector potential $\underline{A}^*$ as given by (2.49) is

$$H^* = \frac{B_0 \pi}{k^3 \ell} \left(\frac{k-\ell}{k+\ell} \right)^{1/2} X_1^2 J_0^2(X_1) \tag{2.50}$$

where X_1 is the first positive zero of J_1 and $X_1^2 J_0^2(X_1) \approx 2.382$. The helicity (H) in the gauge (2.46) is, from (2.3),

$$H = H^* + \int_S G (\underline{B} \cdot d\underline{S}) \tag{2.51}$$

where

$$A = A^* + \nabla G . \tag{2.52}$$

To find G on the boundary, note first that with (2.48) the R-component of (2.2) integrated in time gives

$$A_R(R,0,t) = B_0 J_0(kR) \lambda(R,t) \tag{2.53}$$

where

$$\lambda(R,t) = \int_0^t v(R,t)\, dt \tag{2.54}$$

is the total displacement of fluid at radius R since the time t=0. By comparison, the

R-component of (2.49) on the boundary z=0 is

$$A_R^* = -B_0 \frac{(k-l)}{\alpha k} J_1(kR) , \tag{2.55}$$

which vanishes at t=0 if there is initially an untwisted potential field with l=k. Substituting (2.53) and (2.55) into the R-component of (2.52) and integrating with respect to R gives

$$G(R,0,t) = \frac{B_0}{k^2}\left(\frac{k-l}{k+l}\right)^2 \{1 - J_0(kR)\} + B_0 \int_0^R J_0(kR')\,\lambda(R',t)\,dR' , \tag{2.56}$$

which is the required gauge on the boundary, and which we assume (arbitrarily) to vanish on R=0, since adding a constant to G does not affect (2.51).

Hence from (2.51) using the results (2.50) and (2.56), the helicity in the preferred gauge used in the solution of Equation (2.1) is

$$H = \frac{B_0^2}{k^2}\pi\frac{\alpha}{l}X_1^2 J_0^2(X_1) + \frac{2B_0^2\pi}{k^4}\int_0^{X_1}\theta J_0(\theta)J_1(\theta)k\lambda\left(\frac{\theta}{k},t\right)d\theta \tag{2.57}$$

This result depends on the total displacement of fluid at the boundary, and changes with time. Finally, the magnetic energy of the linear force-free field (2.44) is

$$W_{fff}(l) = \int_V \frac{B^2}{2\mu_0}\,dV = \frac{B_0^2}{2\mu_0}\frac{\pi}{k^2}\frac{1}{l}X_1^2 J_0^2(X_1) . \tag{2.58}$$

2.3.3 Evolution of the Configuration in the Immediate Relaxation Limit

Noting from (2.45) that A_ϕ does not change in time on the boundary and hence that we may use the ϕ-component of (2.49), evaluating the expression (2.1) for (2.44) and (2.48) and integrating it with respect to time gives

$$H = -\frac{2\pi B_0^2}{k^4}\int_0^{X_1} k\,\lambda\left(\frac{\theta}{k},t\right)\theta J_0(\theta)J_1(\theta)\,d\theta \qquad (2.59)$$

which has H=0 at t=0 in agreement with (2.57). [The appearance of this integral in (2.57) but with opposite sign is also a feature of the analysis of Heyvaerts and Priest (1984).] Now (2.57) holds for linear force-free configurations (2.44), whereas (2.59) is the result of applying the Taylor-Heyvaerts hypothesis (2.1). Thus if in addition to Taylor's hypothesis holding we assume that stresses relax by reconnection *instantaneously* towards the appropriate linear force-free field, then at any time the coronal configuration actually realized will be one of the configurations (2.44), whose helicity is given by (2.57). Hence, for instantaneous reconnection, (2.57) can be equated to give

$$\frac{(k^2-l^2)^{1/2}}{l}\frac{1}{4}X_1^2 J_0^2(X_1) = -\int_0^{X_1}\theta J_0(\theta)J_1(\theta)k\,\lambda\left(\frac{\theta}{k},t\right)d\theta \qquad (2.60)$$

for the time-evolution of the parameter l(t) in terms of the fluid motion at the boundary. This implies that, although arbitrary forms for the footpoint velocity are allowed, the resulting configuration depends on them only in the integral sense according to (2.54).

Eliminating l from (2.58) using (2.60) and differentiating with respect to time produces

$$\frac{dW_{fff}}{dt} = -\frac{2\pi B_0^2}{\mu_0 k^4}(k^2-l^2)^{1/2}\int_0^{X_1}\theta J_0(\theta)J_1(\theta)k\,v\left(\frac{\theta}{k},t\right)d\theta \qquad (2.61)$$

which shows how the energy stored in the field changes in time. On the other hand, the rate of change of energy flowing into the coronal volume is given by the Poynting flux through the boundary:

$$\frac{dW_{TOTAL}}{dt} = \int_S \frac{(\underline{E}\times\underline{B})}{\mu_0}\cdot d\underline{S}_{IN} = \int_S \frac{(\underline{v}\cdot\underline{B})(\underline{B}\cdot d\underline{S}_{OUT})}{\mu_0} \qquad (2.62)$$

where "in" refers to the direction upwards through the photosphere into the corona. In the case of (2.44) and (2.48) this reduces to

$$\frac{dW_{TOTAL}}{dt} = -\frac{2\pi B_0^2 (k^2-l^2)^{1/2}}{\mu_0 k^4} \int_0^{X_1} \theta J_0(\theta) J_1(\theta) kV\left(\frac{\theta}{k}, t\right) d\theta \qquad (2.63)$$

which is identical to (2.61). Hence in the limit of infinitely fast reconnection there is no energy available for heating.

2.4 Calculation of the Heating Rate

Now the null heating result of the preceding section occurs when

$$\varepsilon = \tau_R / \tau_V \rightarrow 0. \qquad (2.64)$$

Hence to calculate the heating rate higher-order terms in the parameter ε must be taken. We shall adopt the following procedure. Starting with a force-free linear field, this will be perturbed quasi-statically by an ideal displacement $\underline{\xi}$ to produce a slightly non-linear but force-free field of a different helicity and energy. This field is then allowed to reconnect to the linear force-free field having the same helicity, releasing energy as heat in the process. Such an idealized two-stage process is represented schematically in Figure 2.4.

The heat generated in the above process is then given by

$$\delta W_{HEAT} = \delta W_{MHD} - \delta W_{fff} \qquad (2.65)$$

and the evolution as a whole may be regarded as a repetition of such elementary steps. The ideal displacement in Figure 2.4 lasts one reconnection time (τ_R) and is small compared with the time-scale of the boundary motions (τ_V).

Starting with the initial linear force-free field $\underline{B}_0$, which has magnetic energy

$$W = \frac{1}{2\mu_0} \int_V \underline{B}_0 \cdot \underline{B}_0 \, dV, \qquad (2.66)$$

SCHEMATIC REPRESENTATION OF THE ELEMENTARY HEAT-GENERATING PROCESS

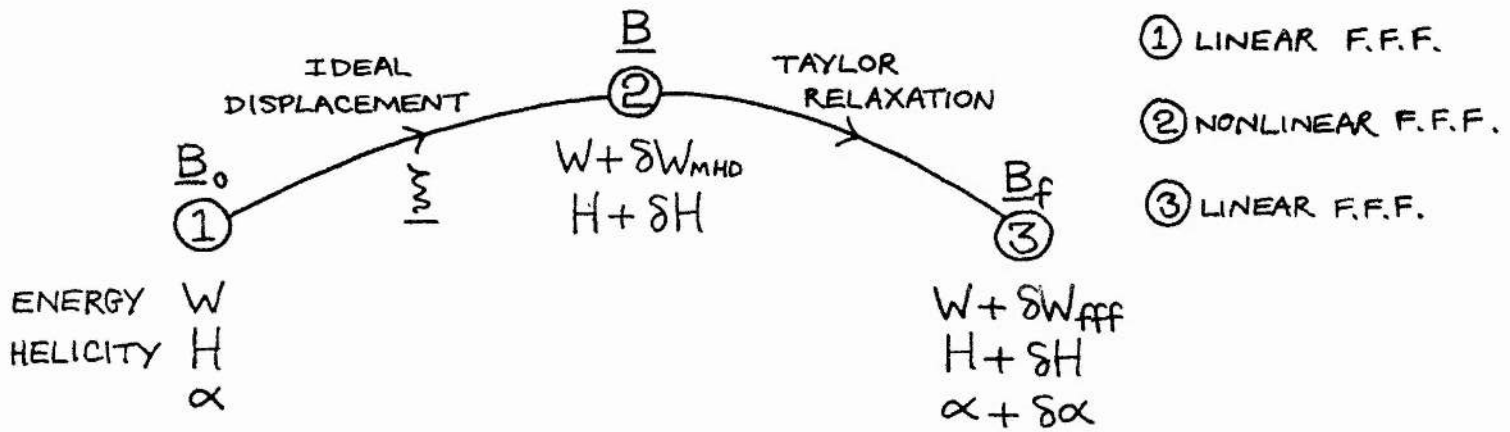

Figure 2.4

it can be shown that (see, for example, Browning and Priest, 1986) a small displacement field $\underline{\xi}$ changes the energy (2.66) by an amount

$$\delta W = \frac{1}{\mu_0}\left\{ \int_S (\underline{\xi}\cdot\underline{B}_0)(\underline{B}_0\cdot d\underline{S}) + \frac{1}{2}\int_V \left[\nabla\times(\underline{\xi}\times\underline{B}_0)\right]^2 dV \right.$$
$$\left. - \frac{1}{2}\int_V \alpha\,\underline{B}_0\times\left[\nabla\times(\underline{\xi}\times\underline{B}_0)\right]\cdot\underline{\xi}\,dV \right\} \qquad (2.67)$$

up to and including terms of order ξ^2. From the helicity evolution equation (2.1) , one can show in a similar way that a displacement field $\underline{\xi}$ produces a helicity change given by

$$\delta H = \int_S (\underline{\xi}\cdot\underline{A}_0)(\underline{B}_0\cdot d\underline{S}) + O(\xi^3)\,, \qquad (2.68)$$

where $\underline{A}_0$ is the initial value of the vector potential in the gauge $\nabla g=0$. Hence, once ξ is determined, (2.67) and (2.68) give us δW_{MHD} and δH.

2.5 Calculation of the Quasi-Static Displacement Field ξ

A general ϕ-independent force-free configuration may be expressed in terms of a flux-function a(R,z) as (e.g. Priest, 1982)

$$B_R = \frac{1}{kR}\frac{\partial a}{\partial z}\,,\quad B_\phi = \frac{1}{kR}f(a)\,,\quad B_z = \frac{1}{kR}\frac{\partial a}{\partial R} \qquad (2.69)$$

where *a* satisfies a Grad-Shafranov equation

$$\Delta_1 a + f(a)\frac{df}{da} = 0 \qquad (2.70)$$

where

$$\Delta_1 \equiv \frac{\partial^2}{\partial R^2} - \frac{1}{R}\frac{\partial}{\partial R} + \frac{\partial^2}{\partial z^2}\,. \qquad (2.71)$$

Thus for the equilibrium configuration (2.44) we have the flux function

$$a_0 = B_0 R J_1(kR) e^{-lz} \tag{2.72}$$

with

$$f_0(a_0) = \alpha a_0 \ . \tag{2.73}$$

If this equilibrium is perturbed, the resulting flux function may be written

$$a(R,z) = a_0(R,z) + \varepsilon a_1(R,z) \tag{2.74}$$

and the new f-function as

$$f(a) = f_0(a) + \varepsilon g(a) \ . \tag{2.75}$$

We require the new configuration to be force-free, and so, after linearizing about a_0, (2.70) becomes

$$\begin{aligned} -\Delta_1 a_1 = {} & a_1 \{ f_0(a_0) f_0''(a_0) + f_0'^2(a_0) \} \\ & + f_0(a_0) g'(a_0) + f_0'(a_0) g(a_0) \end{aligned} \tag{2.76}$$

which by (2.73) reduces to

$$-(\Delta_1 + \alpha^2) a_1 = \alpha \{ g(a_0) + a_0 g'(a_0) \} \ . \tag{2.77}$$

Thus, knowing the function g we have an equation for a_1, subject to the boundary condition

$$a_1(R,0) = 0 \tag{2.78}$$

which expresses line-tying at the photosphere.

The next step is to calculate the displacement field ξ that transforms the variables (a_0, f_0) into $(a_0 + \varepsilon a_1, f_0 + \varepsilon g)$. Such a displacement we shall assume to be of the general

form

$$\underline{\xi} = \xi_\phi(R,z)\,\hat{\underline{\phi}} + \xi_z(R,z)\,\hat{\underline{z}} \,. \qquad (2.79)$$

On a given field-line, a(R,z) is a constant ($\bar{a}$, say), so that if R is fixed we may write

$$a(R,z) = (a_0 + \varepsilon a_1)(R, z + \xi_z)$$

$$= a_0(R,z) + \xi_z \frac{\partial a_0}{\partial z} + \varepsilon a_1(R,z) + \cdots \qquad (2.80)$$

which implies, since $a(R,z)=a_0(R,z)=\bar{a}$, that

$$\xi_z = - \frac{\varepsilon a_1(R,z)}{\left\{\frac{\partial a_0(R,z)}{\partial z}\right\}} \qquad (2.81)$$

is the z-component of the quasi-static displacement.

The determination of ξ_ϕ is more involved. From the equation of the field-lines we know that

$$f(a)\,dR + \frac{\partial a}{\partial z} R\,d\phi = 0 \,. \qquad (2.82)$$

On a given field-line,

$$a_0(x,z) \equiv \frac{B_0}{k} \propto J_1(x) e^{-lz} = \bar{a} \,, \qquad (2.83)$$

where x=kR. The appearance of the projection of a typical field-line onto the x-z plane is shown in Figure 2.5. From above, the field-lines are curved when $\alpha \neq 0$. Also, different field-lines peak at different heights, but these maxima are located on the cylinder $x=\hat{x}\approx 2.40$.

It was shown in Dixon, Browning and Priest (1988) that, because of the cylindrical symmetry imposed on the equilibrium field, ξ_ϕ cannot be determined uniquely without imposing some extra condition. The one which most closely corresponds to the Heyvaerts

PROJECTION OF A TYPICAL EQUILIBRIUM FIELD-LINE IN THE VERTICAL x-z PLANE ($x = kR$).

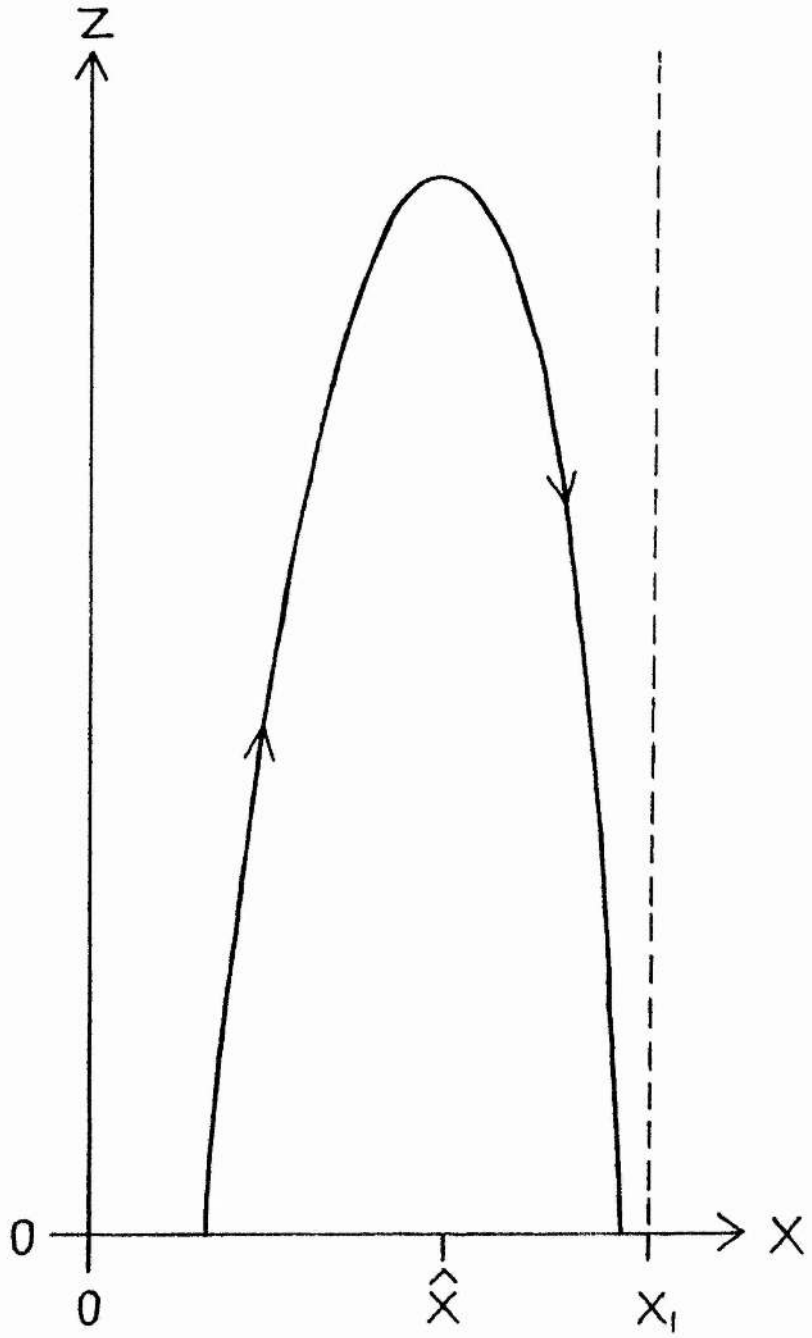

Figure 2·5

and Priest arcade problem is to assume that

$$\xi_\phi(\hat{x}, z) = 0 \tag{2.84}$$

so the peaks do not move in the ϕ-direction during the perturbation. This is the choice we shall make here, but Dixon, Browning and Priest (1988) have shown that the results for δH and δW_{MHD} do not depend on the particular selection made.

From (2.82) we have

$$d\phi = -\frac{f(a)\,dx}{x\,\partial a/\partial z}, \tag{2.85}$$

which may be integrated along both the equilibrium field-line $a_0=\bar{a}$ and the perturbed field-line $a=\bar{a}$ under the condition (2.84). The difference gives the change in displacement between the summit and a footpoint of the field-line produced by the displacement as

$$\begin{aligned}\xi_\phi(x,z) &= \frac{x}{k}\,\delta\phi(x,z) \\ &= -\frac{x}{k}\int_{\hat{x}}^{x}\frac{f(a)\,dx}{x\,\frac{\partial a}{\partial z}} + \frac{x}{k}\int_{\hat{x}}^{x}\frac{f_0(a_0)\,dx}{x\,\frac{\partial a_0}{\partial z}}\,,\end{aligned} \tag{2.86}$$

$[a=\bar{a}]$ $\qquad$ $[a_0=\bar{a}]$

After linearizing this last result about $a_0=\bar{a}$ and using (2.73) and (2.83) we obtain

$$\xi_\phi(x,z) = \frac{\varepsilon x}{k\ell a_0}\left\{g(a_0)\int_{\hat{x}}^{x}\frac{dx}{x} + \frac{\alpha}{\ell}\int_{\hat{x}}^{x}\frac{1}{x}\left(\frac{\partial a_1}{\partial z}+\ell a_1\right)dx\right\}, \tag{2.87}$$

$[a_0=\bar{a}]$ $\qquad$ $[a_0=\bar{a}]$

We now have expressions for both components of the displacement field ξ. Following Heyvaerts and Priest (1984), we shall proceed by selecting a simple, non-linear form for g(a). The simplest physically- meaningful form to take in our case is a quadratic, namely

$$g(a) = \frac{2\gamma}{B_0}k^2a^2 \tag{2.88}$$

where γ is some constant of order unity, a measure of the non-linearity in g(a). We have excluded a term linear in a because it does not produce any heating. Also, we are assuming that a displacement can indeed be found to transfer the force-free field into a neighbouring one.

We note at this point that the quadratic form (2.88) is in fact physically acceptable in the case of the sunspot field, but that this was not the case for the arcade problem of Heyvaerts and Priest (1984), as discussed in detail in Section 2.2.3. The legitimacy of (2.88) as a form will become apparent in due course.

Given g(a) in the form (2.88), Equation (2.77) reduces to an equation for $a_1(x,z)$, namely

$$-(\Delta_1+\alpha^2)a_1 = 6\alpha\gamma B_0 x^2 J_1^2(x)\, e^{-2lz}, \qquad (2.89)$$

which is to be solved subject to the boundary conditions

$$(i)\ a_1 = 0 \text{ on } z=0 \quad (ii)\ a_1 \to 0 \text{ as } z\to\infty$$

$$(iii)\ a_1 \text{ finite on } x=0 \quad (iv)\ a_1 = 0 \text{ on } x = X_1 . \qquad (2.90)$$

The appropriate solution to (2.89) which satisfies the conditions (2.90) may be written in the form

$$a_1(x,z) = \frac{6\gamma\alpha B_0}{k^2}\sum_{n=1}^{\infty} A_n x J_1\left(\frac{X_n}{X_1}x\right)\left\{e^{-P_n z} - e^{-2lz}\right\} \qquad (2.91)$$

where the A_n are the coefficients of the expansion of the function f(x) in the form

$$f(x) = \sum_{n=1}^{\infty} A_n x J_1\left(\frac{X_n}{X_1}x\right) \qquad (2.92)$$

and in turn f(x) is the particular integral of

$$x\frac{d}{dx}\left(\frac{1}{x}\frac{dy}{dx}\right)+\left(1+\frac{3l^2}{k^2}\right)y=-x^2J_1^2(x), \quad (2.93)$$

Using the orthogonality property of Bessel functions, the constants A_n are found from (2.92) to be

$$A_n=\frac{2}{X_1^2J_2^2(X_n)}\int_0^{X_1}f(x)J_1\left(\frac{X_n}{X_1}x\right)dx. \quad (2.94)$$

The X_n are the nth positive zeros of J_1 and

$$p_n\equiv\left(k^2\frac{X_n^2}{X_1^2}-\alpha^2\right)^{1/2}. \quad (2.95)$$

The expansion (2.91) does indeed converge in the double interval $\{0\le x\le X_1,\ 0\le z<\infty\}$, as required.

With our solution (2.91), the two expressions for the components of the ideal displacement ξ given by (2.81) and (2.87) become, after noting (2.83) and (2.88),

$$\xi_z(x,z)=\frac{6\gamma\varepsilon\alpha}{kl\,J_1(x)}\sum_{n=1}^{\infty}A_nJ_1\left(\frac{X_n}{X_1}x\right)\left\{e^{-(p_n-1)^2}-e^{-lz}\right\} \quad (2.96)$$

and

$$\xi_\phi(x,z)=\frac{2\varepsilon\gamma x^2}{l}\log\left(\frac{x}{\hat{x}}\right)J_1(x)e^{-lz}+O(\alpha^2) \quad (2.97)$$

respectively. For reasons of tractibility in subsequent expansions in subsequent calculations, we shall now assume that α is small, so that the configuration is close to potential. Hence, reduced to first order in α, the two components of the ideal displacement are

$$\xi_\phi(x,z)=\frac{2\gamma\varepsilon x^2}{k}\log\left(\frac{x}{\hat{x}}\right)J_1(x)e^{-kz} \quad (2.98)$$

and

$$\xi_z(x,z) = \frac{6\gamma\varepsilon\alpha}{k^2}\sum_{n=1}^{\infty} A_n \frac{J_1\left(\frac{X_n}{X_1}x\right)}{J_1(x)}\left\{e^{-\left(\frac{X_n}{X_1}-1\right)kx} - e^{-kx}\right\} \quad (2.99)$$

We note in passing that ξ_ϕ=O(1) whereas ξ_z=O(α). This completes the calculation of the displacement field.

2.6 Changes in Helicity and Energy in the Ideal Phase

From Equation (2.68), after substituting for ξ_ϕ, A_ϕ and $\underline{B}_0$ from (2.98), (2.49) and (2.44) respectively, we obtain for δH the expression

$$\delta H = \frac{\varepsilon\pi B_0^2}{k^4}(1.60\gamma) + O(\varepsilon^3). \quad (2.100)$$

The corresponding change in energy can be calculated from (2.67) using (2.44) and the results (2.98) and (2.99). In doing this, it is useful to know that, to first order in α, (2.67) simplifies considerably to

$$\delta W_{MHD} = \frac{\alpha}{\mu_0}\delta H + \frac{\pi}{\mu_0 k^2}\int_0^{X_1}\int_0^{\infty}\left\{\frac{\partial\xi_\phi}{\partial R}B_R + \frac{\partial\xi_\phi}{\partial z}B_z - \frac{\xi_\phi B_R}{R}\right\}^2 x\,dx\,dz \quad (2.101)$$

which is of the form

$$\delta W_{MHD} = \varepsilon\,\delta W^{(1)} + \varepsilon^2\,\delta W^{(2)}. \quad (2.102)$$

By comparing the first term in (2.101) with (2.100) and calculating the integrals in the second term on the right-hand side of (2.101), we find

$$\delta W_{MHD} = \frac{\varepsilon\pi B_0^2}{\mu_0 k^4}\{\alpha(1.60\gamma) + \varepsilon k(1.60\gamma + 1.29\gamma^2)\} \quad (2.103)$$

which is a valid expansion provided $O(\varepsilon) < O(\alpha/k)$.

2.7 Calculation of the next Linear Force-Free Field

We have now completed the process of perturbing the original field $\underline{B}_0$ into the non-linear field $\underline{B}$ (Figure 2.4). The energy of the field has increased from W into $W+\delta W_{MHD}$, and its helicity from H to $H+\delta H$. The second stage involves a release of heat energy due to a decrease in potential energy, which we shall now calculate. The helicity does not change during the second stage, and the final field is linear and force-free with parameter $\alpha+\delta\alpha$, compared with the initial field whose parameter was α. Equivalently, comparing positions (1) and (3) in Figure 2.4, overall the parameter l has changed from l_0 to $l_0+\delta l$, say.

Let the initial equilibrium have energy $W_{fff}(l_0)$, and the final linear force-free field have energy $W_{fff}(l_0+\delta l)$. The intermediate non-linear field has energy $W_{fff}(l_0)+\delta W_{MHD}$ and so

$$\delta W_{HEAT} = \{W_{fff}(l_0)+\delta W_{MHD}\} - W_{fff}(l_0+\delta l) \quad (2.104)$$

$$= \delta W_{MHD} - \delta W_{fff} \,. \quad (2.105)$$

This is the required heating rate. (Dixon, Browning and Priest show that this quantity cannot be negative.) To find δl, we deduce first from Equation (2.57) that

$$\delta H = \frac{\pi B_0^2}{k^4}\left\{2\cdot 38\,\delta\left(\frac{\alpha}{l}\right) + 2\int_0^{X_1} \theta J_0(\theta)\overline{J_1}(\theta) k^3 \xi_\phi\left(\frac{\theta}{k},t\right) dt\right\} \quad (2.106)$$

where ξ_ϕ is evaluated on z=0. Hence from the result (2.98) the expression (2.106) reduces to

$$\delta H = \frac{\pi B_0^2}{k^4}\left\{2\cdot 38\,\delta\left(\frac{\alpha}{l}\right) - (1\cdot 60\gamma)\varepsilon\right\} \quad (2.107)$$

in the gauge $\nabla g=\underline{0}$. This expresses the change in H in terms of the corresponding change

in l or vice versa. Equally, the same helicity change is expressed by (2.100). Hence by equating (2.100) and (2.107) we deduce that

$$\delta\left(\frac{\alpha}{l}\right) = (1.34\gamma)\varepsilon + O(\varepsilon^3). \tag{2.108}$$

Expanding l in powers of ε as

$$l = l_0 + \varepsilon l_1 + \varepsilon^2 l_2 + O(\varepsilon^3) \tag{2.109}$$

we can write

$$\delta\left(\frac{\alpha}{l}\right) = \frac{\{k^2 - (l_0+\varepsilon l_1+\varepsilon^2 l_2)^2\}^{1/2}}{(l_0+\varepsilon l_1+\varepsilon^2 l_2)} - \frac{(k^2-l_0^2)^{1/2}}{l_0}. \tag{2.110}$$

Equating first-order and second-order terms in turn in (2.108) and (2.110) gives

$$\delta l = \varepsilon l_1 + \varepsilon^2 l_2$$

$$= -\frac{\varepsilon(1.34\gamma) l_0^2 \alpha_0}{k^2} - \frac{\varepsilon^2(1.34\gamma)^2 l_0^3 (3l_0^2-2k^2)}{2k^4}. \tag{2.111}$$

To first order in α (i.e. α_0), this reduces to

$$\delta l = -(1.34\gamma)\alpha\varepsilon - \frac{1}{2}(2.68\gamma+1.80\gamma^2)k\varepsilon^2. \tag{2.112}$$

To calculate W_{fff}, note first from (2.58) that

$$W_{fff}(l) = 1.19\frac{\pi B_0^2}{\mu_0 k^2 l} \tag{2.113}$$

is the energy of a linear force-free field as a function of the parameter l. It follows that

$$\delta W_{fff}(l_0) = 1.19\frac{\pi B_0^2}{\mu_0 k^2}\frac{1}{l_0}\left\{-\frac{\delta l}{l_0} + \left(\frac{\delta l}{l_0}\right)^2 - \ldots\right\} \tag{2.114}$$

and therefore, with δl given by (2.112), the difference in energy between the initial and final force-free fields is, to first order in α,

$$\delta W_{fff} = \frac{\pi B_0^2}{\mu_0 k^4}\{(1\cdot 60\gamma)\alpha\varepsilon + (1\cdot 60\gamma + 1\cdot 07\gamma^2)k\varepsilon^2\}, \quad (2.115)$$

Again we require $O(\varepsilon) < O(\alpha/k)$ for the expansion to be valid. Comparing (2.115) with (2.103) shows firstly that the terms of first order in ε are the same. This confirms the result at the end of Section 2.3.3 that to first order in τ_R there is no energy released as heat. Secondly, the first-order terms in γ are the same, i.e. heating is an effect of order γ^2. In addition, $\delta W_{HEAT}(\gamma) = \delta W_{HEAT}(-\gamma)$, a consequence of the quadratic and non-negative nature of the heating-rate (Dixon, Browning and Priest, 1988).

Finally, then, substituting the results (2.103) and (2.115) into the formula (2.65), the heating-rate for our sunspot field is

$$\delta W_{HEAT} = 0\cdot 22\varepsilon^2\gamma^2\frac{\pi B_0^2}{\mu_0 k^3} \quad (2.116)$$

in the small α approximation. As might be predicted on dimensional grounds, (2.116) is similar to the expression for the heating rate obtained for the arcade in Heyvaerts and Priest (1984). Hence the results obtained in the present chapter have confirmed the assertions of Heyvaerts and Priest (1984) and Browning and Priest (1986) that tearing turbulence is indeed a viable mechanism for heating the corona.

CHAPTER THREE : HELICAL MODES IN THE SUNSPOT EQUILIBRIUM

3.1 Equilibrium Fields in a Cylinder

We begin this chapter with a comparatively detailed account of the theory of relaxed states in a straight circular cylinder geometry, based on the work summarised in the paper by Taylor (1986). The aim of the remainder of the chapter is to determine whether corresponding results hold in the case of the sunspot field equilibrium which was considered in Chapter 2.

We wish to construct the most general solution, subject to $\nabla.\underline{B} = 0$, of the linear force-free equation, namely

$$(\nabla^2 + \alpha^2)\,\underline{B} = \underline{0}\,, \tag{3.1}$$

in a cylindrical container having perfectly-conducting walls (Figure 3.1). In general, we search for an equilibrium configuration that depends on all three coordinates.

Written out in full, the components of Equation (3.1) are

$$\left(\nabla^2 - \frac{1}{R^2} + \alpha^2\right) B_R - \frac{2}{R^2}\frac{\partial B_\phi}{\partial \phi} = 0\,, \tag{3.2}$$

$$\left(\nabla^2 - \frac{1}{R^2} + \alpha^2\right) B_\phi + \frac{2}{R^2}\frac{\partial B_R}{\partial \phi} = 0 \tag{3.3}$$

and

$$(\nabla^2 + \alpha^2)\,B_z = 0 \tag{3.4}$$

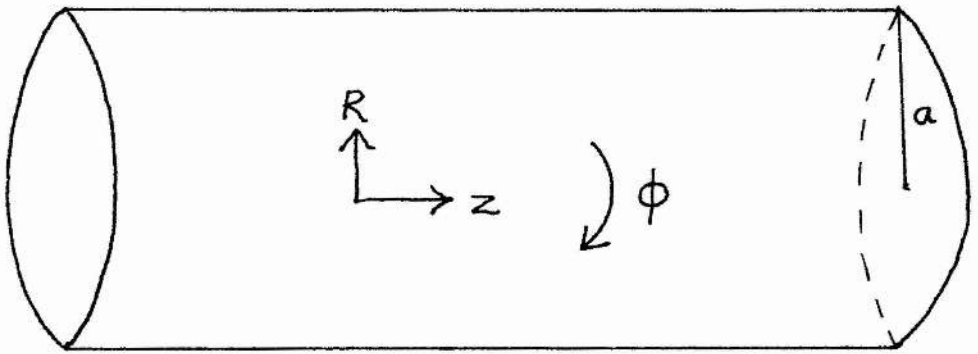

STRAIGHT CIRCULAR CYLINDER WITH PERFECTLY - CONDUCTING WALLS.

Figure 3.1

where

$$\nabla^2 = \frac{\partial^2}{\partial R^2} + \frac{1}{R}\frac{\partial}{\partial R} + \frac{1}{R^2}\frac{\partial^2}{\partial \phi^2} + \frac{\partial^2}{\partial z^2} \tag{3.5}$$

and we have used $\nabla.\underline{B} = 0$. From (3.4) we obtain the result

$$B_z^{mk} = J_m(y)\cos(m\phi + kz) \tag{3.6}$$

for the z-component of the field, where

$$y \equiv R(\alpha^2 - k^2)^{1/2} \tag{3.7}$$

and we have used superscripts as a reminder that the solution depends on the two parameters m and k.

Now the three components of $\nabla\times\underline{B}=\alpha\underline{B}$ are

$$\frac{1}{R}\frac{\partial B_z}{\partial \phi} - \frac{\partial B_\phi}{\partial z} = \alpha B_R , \tag{3.8}$$

$$\frac{\partial B_R}{\partial z} - \frac{\partial B_z}{\partial R} = \alpha B_\phi \tag{3.9}$$

and

$$\frac{1}{R}\frac{\partial}{\partial R}(RB_\phi) - \frac{1}{R}\frac{\partial B_R}{\partial \phi} = \alpha B_z . \tag{3.10}$$

If we now assume that the R- and ϕ-components of the field may be written in the form

$$B_R^{mk} = B_R(R)\sin(m\phi + kz) \tag{3.11}$$

and

$$B_\phi^{mk} = B_\phi(R)\cos(m\phi + kz) , \tag{3.12}$$

then (3.8), (3.9) and (3.10) become

$$-m\frac{J_m(y)}{R} + k B_\phi(R) = \alpha B_R(R) \tag{3.13}$$

$$k B_R(R) - (\alpha^2 - k^2)^{1/2} J_m'(y) = \alpha B_\phi(R) \tag{3.14}$$

and

$$\frac{1}{R}\frac{\partial}{\partial R}\{R B_\phi(R)\} - m\frac{B_R(R)}{R} = \alpha J_m(y) \tag{3.15}$$

respectively. (3.13) and (3.14) may now be solved algebraically to give the ϕ- and z-components of the field, which are found to be

$$B_\phi^{mk} = \frac{-1}{(\alpha^2-k^2)^{1/2}}\left\{\alpha J_m'(y) + mk\frac{J_m(y)}{y}\right\}\cos(m\phi + kz) \tag{3.16}$$

and

$$B_R^{mk} = \frac{-1}{(\alpha^2-k^2)^{1/2}}\left\{k J_m'(y) + m\alpha\frac{J_m(y)}{y}\right\}\sin(m\phi + kz). \tag{3.17}$$

Hence the general solution of (3.1) finite on the axis is of the form

$$\underline{B} = \sum_{m,k} a_{mk}\,(B_R^{mk}, B_\phi^{mk}, B_z^{mk}) \tag{3.18}$$

where the R-, ϕ- and z-components of the field are given by (3.17), (3.16) and (3.6) respectively. Note that we have chosen solutions which are periodic in ϕ and z. In particular, we have disregarded those solutions which behave in an exponential fashion at large z. Thus we may use our solutions to model a torus of *large aspect ratio* , namely one for which $R_0/a_0 \gg 1$, where R_0 and a_0 represent the major and minor radii of the torus respectively.

The relevant boundary condition to take is to have the radial component of the field vanish at the wall, i.e. we must have

$$B_R \ (R=a) \ = \ 0 \ . \qquad (3.19)$$

This corresponds to the condition that the surface of the cylinder is a perfect conductor.

Associated with the cylinder are two invariants. One of these is taken to be the magnetic helicity H, defined by (1.6) and (1.7), and the other is the *toroidal flux* , which is given by the double integral

$$\psi \ = \ \int_0^a \int_0^{2\pi} B_z \, R \, dR \, d\phi \ . \qquad (3.20)$$

Now the m=0, k=0 term of the solution (3.18) clearly satisfies the boundary condition (3.19) for any value of α, and in addition has a non-vanishing toroidal flux. For all other values of the parameters the boundary condition is satisfied only for certain special values of α. From (3.17) set to zero at R=a we see that the governing equation for these eigenvalues is

$$ka\{(\alpha^2-k^2)^{1/2}a\}J_m'\{(\alpha^2-k^2)^{1/2}a\} + m\alpha a J_m\{(\alpha^2-k^2)^{1/2}a\} = 0 \ . \qquad (3.21)$$

Solutions for which m and k are not both zero contribute nothing to the toroidal flux.

It follows that there are two types of solution to $\nabla\times\underline{B}=\alpha\underline{B}$ in the cylinder which could satisfy the boundary condition and correspond to the same given toroidal flux. They are as follows:

(i) The "*symmetric* " m=0,k=0 solution, which exists for any value of α. In the case of such a solution, the appropriate value of α is determined by the value of the ratio H/ψ^2.

(ii) The "*mixed* " solution, consisting of the m=0,k=0 term (to give the reqired toroidal flux) together with one (and only one) of the other terms, thus giving a solution of the form

$$\underline{B} = a_{00}\,\underline{B}^{00} + a_{mk}\,\underline{B}^{mk} . \qquad (3.22)$$

This mixed solution exists only for fixed, discrete values of α, and H/ψ^2 no longer determines α but instead fixes the ratio a_{mk}/a_{00}.

Both of the above types of solution are completely determined by the two invariants H and ψ, but which one has the lower energy, and therefore would be the one we would expect to observe in practice?

To answer this question, we must make use of a result given by Taylor (1986), although not rigorously proved in his paper. It can be demonstrated that, of many possible solutions to $\nabla\times\underline{B}=\alpha\underline{B}$, the one that has the lowest energy is the one with the lowest value of α, under the same boundary conditions and the same value of H. Thus, if $\underline{B}_1$ and $\underline{B}_2$ are two magnetic fields each of helicity H, with energies W_1 and W_2 and force-free constants α_1 and α_2 respectively, then

$$W_2 - W_1 = \left(\frac{\alpha_2-\alpha_1}{\alpha_2+\alpha_1}\right)\int_V \frac{(\underline{B}_2-\underline{B}_1)^2}{2\mu_0}\,dV . \qquad (3.23)$$

Thus the only solution of type (ii) above which can be of interest is that corresponding to the smallest root α of (3.21). According to Taylor (1986), the smallest root occurs when m=1 and $k \approx 1.25$, giving for the lowest eigenvalue $\alpha a = 3.11$. [In verifying these results, we found slightly different values, as shown later.]

The selection of the appropriate solution can now be made. The first symmetric solution is the minimum-energy state for all values of H/ψ^2 which correspond to values of α such that $\alpha a < 3.11$. For any larger value of H/ψ^2 the lowest-energy state is a mixed solution with $\alpha a = 3.11$ and $ka \approx 1.25$.

3.2 Mathematical Details

We now give details of the actual solution of the above minimum energy problem.

(i) Symmetric Solution.

From (3.6), (3.16) and (3.17) we find that the solution with m = 0 and k = 0 has components

$$B_R = 0\,, \quad B_\phi = a_{00} J_1(\alpha R)\,, \quad B_z = a_{00} J_0(\alpha R)\,, \tag{3.24}$$

The boundary condition (3.19) is satisfied automatically. The toroidal flux associated with the configuration (3.24) is from (3.20) found to be

$$\psi_{SYM} = 2\pi a_{00} a^2 \frac{J_1(\alpha a)}{\alpha a} \tag{3.25}$$

and the magnetic energy (per unit length in the z-direction) is

$$W_{SYM} = \frac{\pi a^2 a_{00}^2}{\mu_0 \alpha a}\left\{\alpha a J_0^2(\alpha a) - J_0(\alpha a) J_1(\alpha a) + \alpha a J_1^2(\alpha a)\right\}. \tag{3.26}$$

If we choose the magnetic vector potential $\underline{A}$ to have components

$$A_R = 0\,, \quad A_\phi = a_{00}\frac{J_1(\alpha R)}{\alpha}\,, \quad A_z = \frac{a_{00}}{\alpha}\left\{J_0(\alpha R) - J_0(\alpha a)\right\} \tag{3.27}$$

(so that A_z=0 on the wall for all values of α) then the magnetic helicity of the field (3.24) per unit length in the z-direction is

$$H_{SYM} = \frac{2\pi a^3 a_{00}^2}{(\alpha a)^2}\left\{\alpha a J_0^2(\alpha a) - 2 J_0(\alpha a) J_1(\alpha a) + \alpha a J_1^2(\alpha a)\right\}. \tag{3.28}$$

The helicity (3.28) is seen to vanish in the case of the potential field (α=0), and is in fact a

gauge-invariant form.

We note that the quantity aH/ψ^2 is a function of αa alone, and so determines it implicitly. The coefficient a_{00} is then given in terms of the flux ψ by Equation (3.25).

(ii) Mixed Solution.

From (3.6), (3.16) and (3.17) we deduce that the components of the mixed field having both an m=0, k=0 term and an m=1 term are

$$B_R = -\frac{a_1}{(\alpha^2 - k^2)^{1/2}}\left\{kJ_0(y) + \frac{(\alpha-k)J_1(y)}{y}\right\}\sin(\phi+kz) \quad (3.29)$$

$$B_\phi = a_{00}J_1(\alpha R) - \frac{a_1}{(\alpha^2-k^2)^{1/2}}\left\{\alpha J_0(y) - \frac{(\alpha-k)J_1(y)}{y}\right\}\cos(\phi+kz) \quad (3.30)$$

and

$$B_z = a_{00}J_0(\alpha R) + a_1 J_1(y)\cos(\phi+kz), \quad (3.31)$$

The boundary condition $B_R=0$ on R=a has the effect of fixing the value of αa at one of a number of eigenvalues. The lowest of these may be found from the boundary condition (3.21) by means of a scheme based on the Newton-Raphson method. The results for the eigenvalues of αa and k were found by us to be

$$\alpha a = 3.112, \quad ka = 1.23. \quad (3.32)$$

These values correspond to the lowest energy of the mixed states.

As mentioned previously, the contribution to the toroidal flux of the helical components of the field described by (3.29), (3.30) and (3.31) is zero. We find that the expression for the toroidal flux of the mixed state with $\alpha a = 3.11$ is

$$\psi_{MIXED} = 0.1904\pi a_{00}a^2 \quad (3.33)$$

and the magnetic energy per unit length in the z-direction is given by

$$W_{MIXED} = \frac{\pi a^2}{\mu_0}\left(0.2033 a_{00}^2 + 0.05434 a_1^2\right), \quad (3.34)$$

Finally, the magnetic helicity of the mixed solution with $\alpha a = 3.11$ when the vector potential is given by

$$\underline{A} = \frac{\underline{B}}{\alpha} - a_{00}\frac{J_0(\alpha a)}{\alpha}\hat{\underline{z}} \quad (3.35)$$

is found to be

$$H_{MIXED} = \pi a^3\left(0.1487 a_{00}^2 + 0.03492 a_1^2\right) \quad (3.36)$$

per unit length in the toroidal direction.

We shall now investigate the conditions under which the two kinds of solution exist, and determine which of these should be observed in practice. In the following we shall use the defining notation

$$\alpha_0 a = 3.112 \quad (3.37)$$

for the lowest eigenvalue of the mixed states. We expect (3.37) to be the "critical value" of αa at which the solution type is expected to change.

Case 1 : H/ψ^2 is such that the purely symmetric solution has $0 \le \alpha a < \alpha_0 a$.

In this case the purely symmetric state (3.24) is the minimum energy solution because all the values of αa in the above range are lower than the lowest eigenvalue (3.37) of the mixed state and so have lower energy than it.

From (3.25) and (3.28) we form the quantity

$$\frac{2\pi a H_{SYM}}{\psi^2_{SYM}} = \frac{\alpha a J_0^2(\alpha a) - 2J_0(\alpha a)J_1(\alpha a) + \alpha a J_1^2(\alpha a)}{J_1^2(\alpha a)} \quad (3.38)$$

$$\equiv \overline{H}_{SYM} . \quad (3.39)$$

Similarly, from (3.25) and (3.26) we have the dimensionless parameter

$$\frac{4\pi\mu_0 a^2 W_{SYM}}{\psi^2_{SYM}} = \frac{\alpha a\{\alpha a J_0^2(\alpha a) - J_0(\alpha a)J_1(\alpha a) + \alpha a J_1^2(\alpha a)\}}{J_1^2(\alpha a)} \quad (3.40)$$

$$\equiv \overline{W}_{SYM} . \quad (3.41)$$

The above then represents the lowest available energy states for the case when the expression (3.38) defines implicitly a value of αa which is smaller in magnitude than 3.11.

Case 2 : H/ψ^2 is such that the purely symmetric solution has $\alpha a \geq \alpha_0 a$.

In this particular case we expect the observed configuration to be of the mixed type because (except in the special case when $\alpha a = \alpha_0 a$) this solution type has the lower value of αa and therefore the lower energy.

From (3.33) and (3.36) we deduce that

$$\frac{a_1^2}{a_{00}^2} = \left(\frac{\overline{H}_{MIXED} - 8.2036}{1.9265}\right) \quad (3.42)$$

where

$$\overline{H}_{MIXED} \equiv 2\pi a \frac{H_{MIXED}}{\psi^2_{MIXED}} , \quad (3.43)$$

Similarly, from (3.33) and (3.34) we obtain the expression

$$\overline{W}_{MIXED} \equiv 4\pi\mu_0 a^2 \frac{W_{MIXED}}{\psi^2_{MIXED}} \quad (3.44)$$

$$= \frac{4\left(0.2033 + 0.05434\dfrac{a_1^2}{a_{00}^2}\right)}{(0.1904)^2} . \qquad (3.45)$$

Hence, upon substitution of the ratio a_1^2/a_{00}^2 from (3.42) into (3.45), we find that the non-dimensional forms of the helicity and the energy are related by the simple formula

$$\overline{W}_{MIXED} = 3.112\ \overline{H}_{MIXED} - 3.100 . \qquad (3.46)$$

We note from (3.42) that if a_1 is to be real then the helicity must attain a minimum value of about 8.2, which is the lowest value that the helicity may take if the mixed state is to exist.

We have used the above results to produce graphs of the force-free parameter, the helicity and the energy in the two cases.

Figure (3.2) shows a plot of the variation of helicity with αa for purely symmetric fields, showing also with a dotted line the location of the first mixed solution which occurs at the first eigenvalue $\alpha a = 3.11 = \alpha_0 a$. Notice that there are locations where the helicity becomes infinite, that is, there exist certain "singular" or "resonant" values of αa.

In Figure (3.3) we have the graph of the energy of the symmetric state against αa. This plot is qualitatively very similar in appearance to Figure (3.2), with one difference being that the curve does not pass through the origin. Thus at $\alpha a = 0$ the helicity vanishes but the energy has a finite, non-zero value.

Figure (3.4) is the most informative graph of the three. It shows the energy of the symmetric state and the energy of the first helical (mixed) state against helicity. From this plot we verify that for values of the dimensionless helicity greater than about 8.2 the mixed state has a lower energy than the symmetric state.

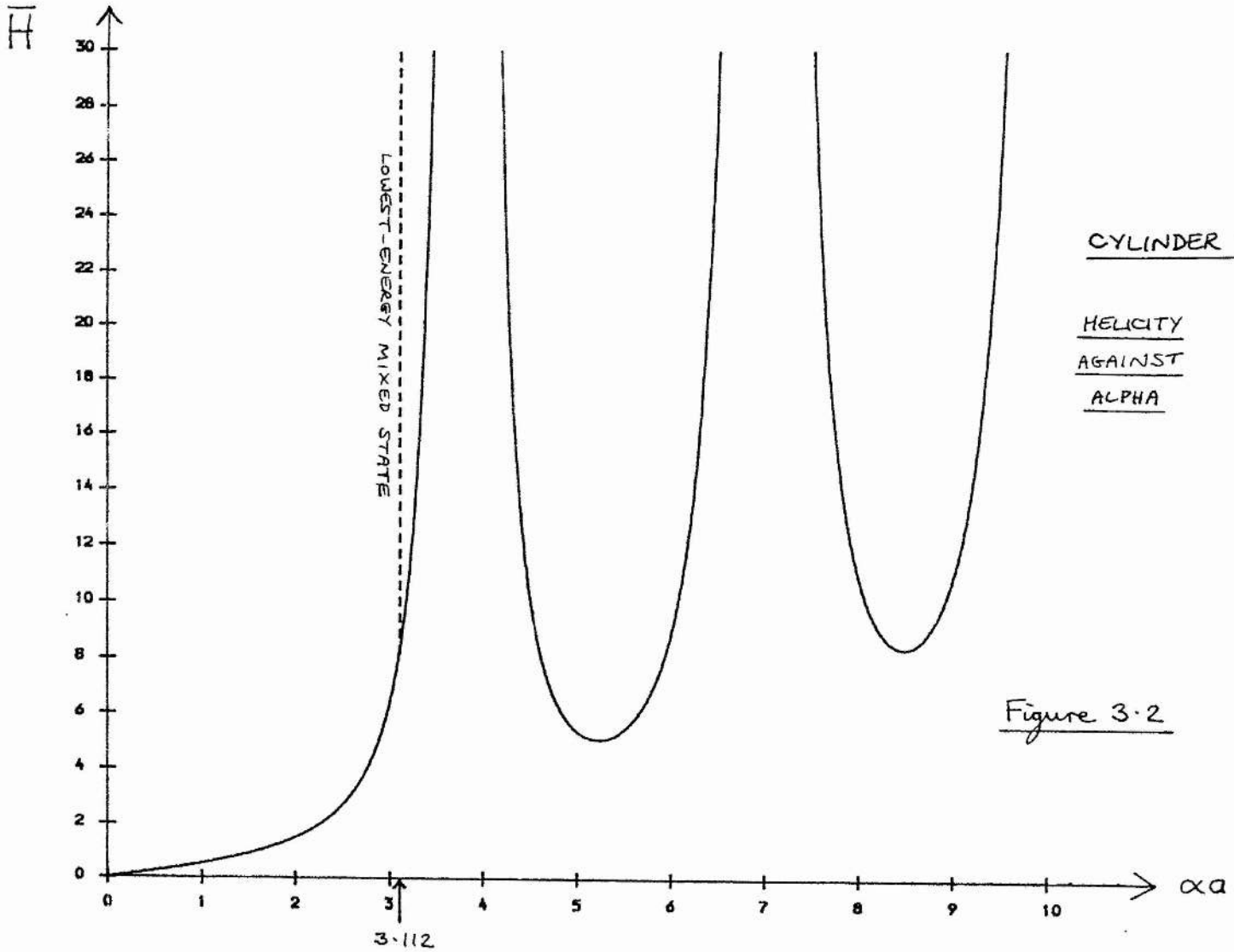

CYLINDER PROBLEM:

HELICITY AGAINST ALPHA

Figure 3.2

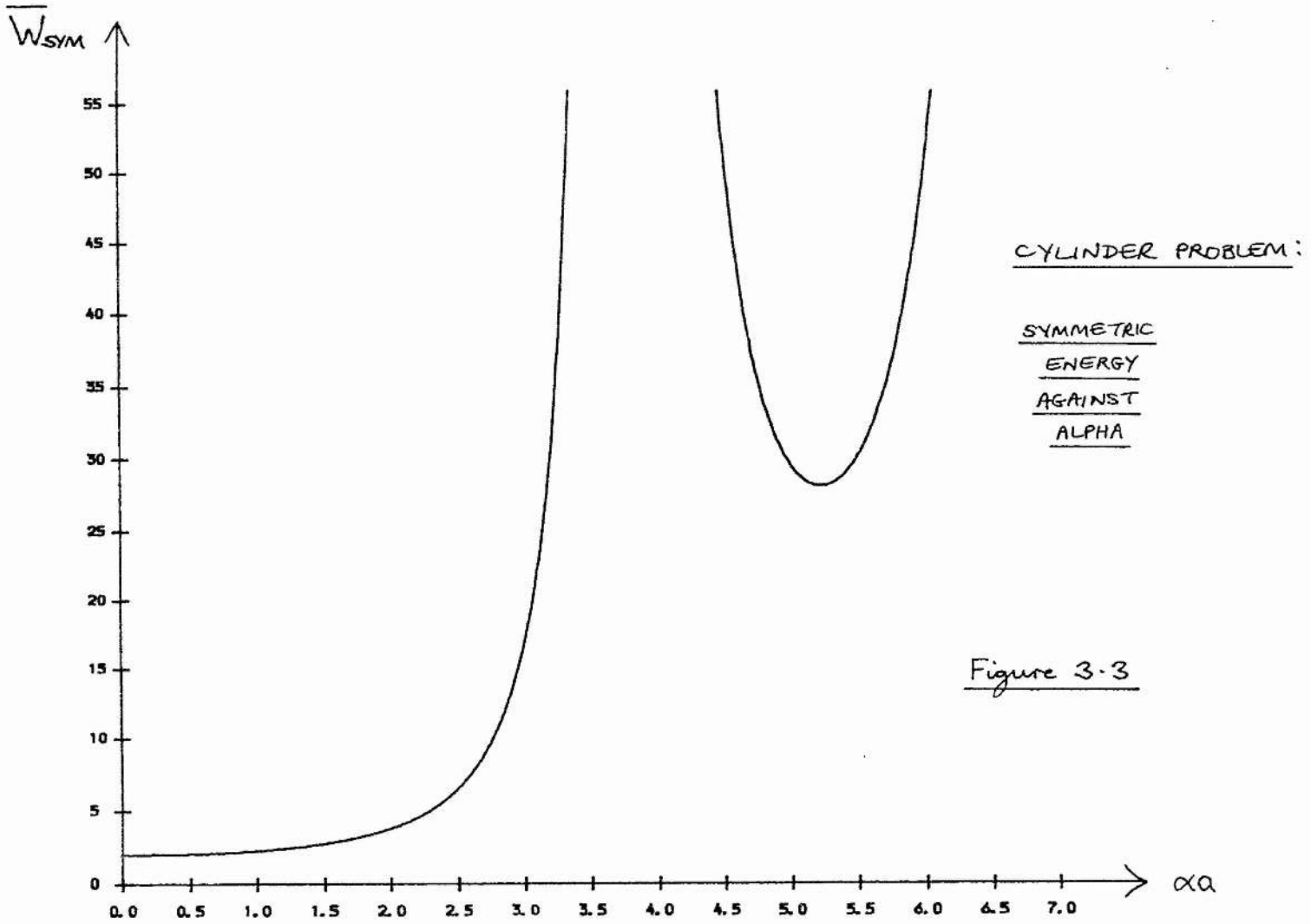

CYLINDER PROBLEM:

SYMMETRIC ENERGY AGAINST ALPHA

Figure 3·3

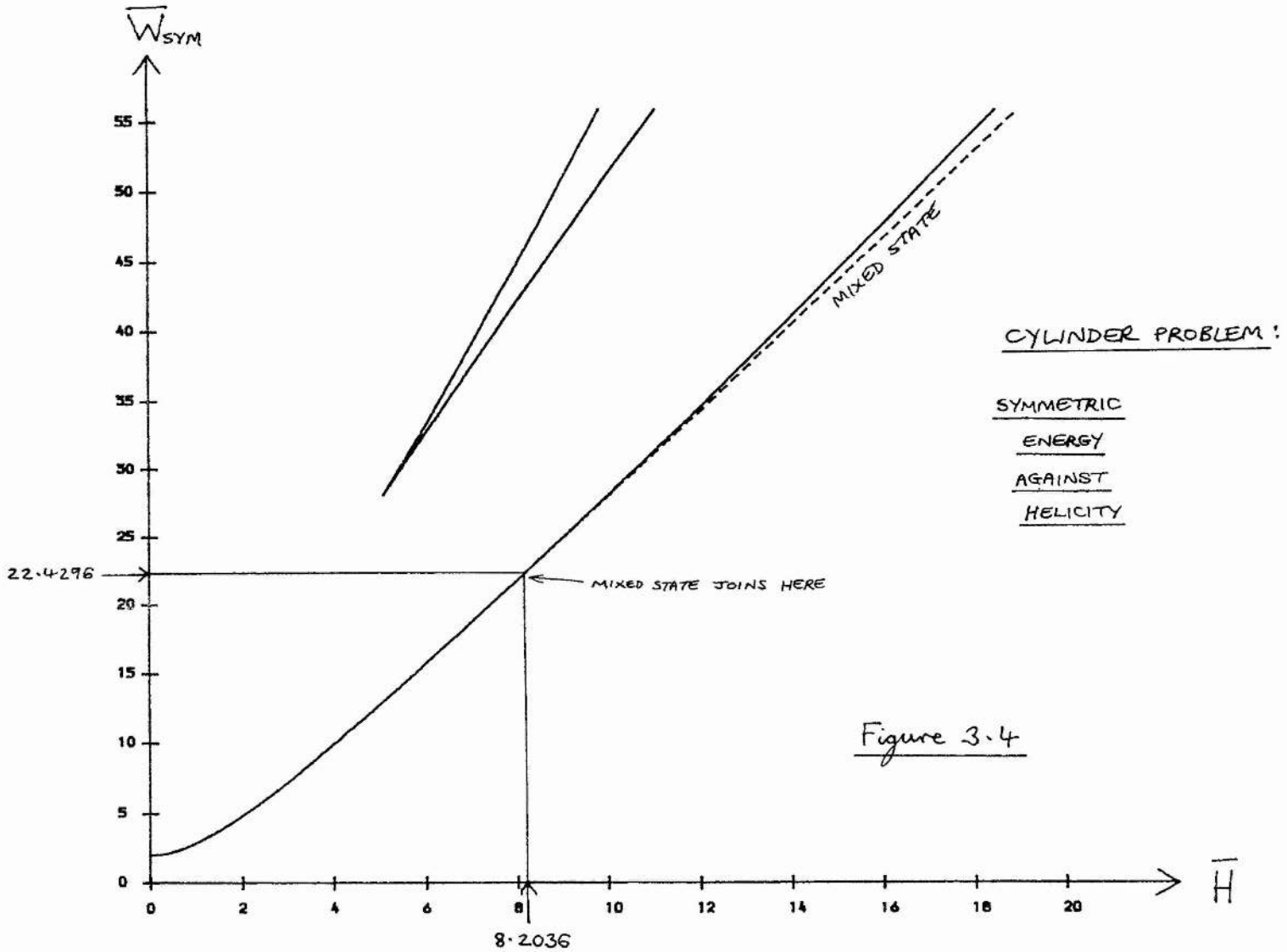
$\overline{W}_{SYM}$
55
50
45
40
35
30
25
22·4296
20
15
10
5
0
0
2
4
6
8
10
12
14
16
18
20
8·2036
$\overline{H}$
MIXED STATE
MIXED STATE JOINS HERE
CYLINDER PROBLEM :
SYMMETRIC
ENERGY
AGAINST
HELICITY

Figure 3.4

It will become apparent in Chapters 4, 5 and 6 that the three diagrams (3.2), (3.3) and (3.4) are, far from being unique special cases, typical of the graphs obtained from theoretical minimum-energy force-free fields in different geometries under a variety of boundary conditions.

To end this section on the theory of relaxed states in a nearly cylindrical geometry, we remark that the onset of helical fields in a large-aspect-ratio torus has been reasonably well confirmed in the laboratory (e.g. Bodin and Newton, 1980), and remains one of the most impressive predictions of Taylor's theory.

3.3 Application to the Sunspot Equilibrium

Consider the "sunspot equilibrium" described by Equation (2.44) and sketched in Figure 2.3. It is the axi-symmetric (ϕ-independent) solution of $\nabla \times \underline{B} = \alpha \underline{B}$ which decays to zero as $z \to \infty$ and also has the property that the R-component vanishes at $kR = 3.82$, the first positive zero of $J_1(x)$. It represents only a single value of the parameter k if the structure has a fixed radius ($=R_0$, say), and so an extreme special case of a much more general solution.

What is the solution of the force-free equation in the sunspot geometry if we retain the property that the field decays to zero with height z, but also allow a variation with ϕ in the solution ?

To investigate this question, we again consider the three components (3.2), (3.3) and (3.4) of the force-free equation (3.1). Substituting a separable form for B_z, we obtain the expression

$$B_z^{mk} = J_m(kR) \cos m\phi \, e^{-lz} . \qquad (3.47)$$

The remaining field components may, in a similar fashion to before, be deduced from Equations 3.8 and 3.9 using (3.47) and assuming that B_R and B_ϕ behave as e^{-lz}. The

results are found to be

$$B_\phi^{mk} = \left\{ \frac{ml}{k^2} \frac{J_m(kR)}{R} \sin m\phi - \frac{\alpha}{k} J_m'(kR) \cos m\phi \right\} e^{-lz} \quad (3.48)$$

and

$$B_R^{mk} = \left\{ -\frac{m\alpha}{k^2} \frac{J_m(kR)}{R} \sin m\phi - \frac{l}{k} J_m'(kR) \cos m\phi \right\} e^{-lz} \quad (3.49)$$

Hence we may write the 'general' solution of (3.1) for the sunspot field in the form

$$\underline{B} = \sum_{m=0}^{\infty} \int_{k=0}^{\infty} C_m(k) \left(B_R^{mk}, B_\phi^{mk}, B_z^{mk} \right) dk \quad (3.50)$$

where the components are given by the expressions (3.49), (3.48) and (3.47) and the $C_m(k)$ are constants. Again we have $\alpha = (k^2 - l^2)^{1/2}$. As suggested by the form of (3.50), the parameter k has (at present) a continuous spectrum, whereas the parameter m can assume only integer values in order to satisfy periodicity in the ϕ-direction. Note that the solution (2.44) is obtained from (3.47), (3.48) and (3.49) by choosing only the m = 0 term and taking $C_0(k) = B_0$.

From (3.49) and (3.50) we observe that the general expression for the radial component of the equilibrium field is

$$B_R = - \sum_{m=0}^{\infty} \int_{k=0}^{\infty} C_m(k) \left\{ \frac{m\alpha}{k^2} \frac{J_m(kR)}{R} \sin m\phi + \frac{l}{k} J_m'(kR) \cos m\phi \right\} e^{-lz}, \quad (3.51)$$

The question we should like to ask is the following : can we, by a judicious choice of values for the constants k, maintain the condition $B_R = 0$ on $R = R_0$ for all values of m ? The answer to this question is that we cannot, as demonstrated by the following argument. In order that the expression (3.51) is zero at $R = R_0$, it is clear that the 'sin mϕ' series and the 'cos mϕ' series must vanish separately, since one consists only of odd functions and

the other only of even functions. Suppose that we choose for k a set of values which we denote by k_m, so that $J_m(k_m R_0) = 0$ for each m. This is easily done using zeros of the Bessel functions $J_m(x)$. However, this means that $J_m'(k_m R_0) \neq 0$ for the same k_m, since the zeros of $J_m(x)$ are distinct from those of $J_m'(x)$ for each m. Thus if the series in $\cos m\phi$ is to vanish, then $C_m(k) = 0$ (from the properties of the Fourier series in $\cos m\phi$) except for $m = 0$, in which case the field is axi-symmetric. Hence we conclude that a general non-axisymmetric equilibrium is not possible if we demand that the R-component vanishes on the cylinder $R = R_0$.

It is apparent at this stage that our sunspot field problem is substantially different from the cylinder problem discussed in Sections 3.1 and 3.2. In particular, we cannot isolate two m-modes by imposing $B_R = 0$ on some cylindrical surface as we could before. We must therefore look for some alternative form for the boundary condition.

Let us instead consider the z-component of the magnetic field on the photosphere, i.e. on $z = 0$. We would like to know if it is possible to calculate the equilibrium field in the region $z > 0$ if the form of B_z is prescribed on $z = 0$.

From (3.47) and (3.50) we have

$$B_z = \sum_{m=0}^{\infty} \int_{k=0}^{\infty} C_m(k) J_m(kR) \cos m\phi \, e^{-(k^2-\alpha^2)^{1/2} z} \, dk \quad (3.52)$$

Let the z-component of the field on $z = 0$ be written in the form

$$B_z(z=0) = f(R, \phi). \quad (3.53)$$

Thus, equating (3.52) evaluated on $z = 0$ with (3.53), we deduce that

$$f(R,\phi) = \sum_{m=0}^{\infty} \int_{k=0}^{\infty} C_m(k) J_m(kR) \cos m\phi \, dk \, . \quad (3.54)$$

Further, if (3.54) is multiplied on both sides by $\cos n\phi$, where n is an integer, and we

integrate with respect to ϕ from 0 to 2π, we obtain the expression

$$\int_0^{2\pi} f(R,\phi')\cos m\phi' d\phi' = \pi \int_0^{\infty} C_m(k) J_m(kR)\, dk \,. \quad (3.55)$$

Consider next the case where k takes on the discrete set of values given by

$$k_{m,n} = \frac{j_{m,n}}{R_0} \,, \quad n = 1, 2, \ldots, \infty \quad (3.56)$$

where $j_{m,n}$ is the n^{th} positive zero of $J_m(x)$ and R_0 is the radius of the structure depicted in Figure 2.3. Then, instead of (3.55), we should write

$$\int_0^{2\pi} f(R,\phi')\cos m\phi' d\phi' = \pi \sum_{n=1}^{\infty} C_{mn} J_m\left(j_{m,n}\frac{R}{R_0}\right) . \quad (3.57)$$

Now, multiplying both sides of (3.57) by the quantity

$$R\, J_m\left(j_{m,p}\frac{R}{R_0}\right) \quad (3.58)$$

where p indicates the p^{th} positive zero of $J_m(x)$, and integrating with respect to R between the limits 0 and R_0 gives the expression

$$\int_0^{R_0} R' J_m\left(j_{m,p}\frac{R'}{R_0}\right)\left\{\int_0^{2\pi} f(R',\phi')\cos m\phi' d\phi'\right\} dR'$$
$$= \pi \sum_{n=1}^{\infty} C_{mn} \int_0^{R_0} R' J_m\left(j_{m,p}\frac{R'}{R_0}\right) J_m\left(j_{m,n}\frac{R'}{R_0}\right) dR' \,. \quad (3.59)$$

Now the integral on the right-hand side of (3.59) is equal to zero when $n \neq p$, and equal to

$$\frac{R_0^2\left\{J_{m+1}(j_{m,n})\right\}^2}{2} \quad (3.60)$$

if $n = p$. We therefore deduce from (3.59) that

$$\int_0^{R_0} R' J_m\left(j_{m,n}\frac{R'}{R_0}\right)\left\{\int_0^{2\pi} f(R',\phi')\cos m\phi' d\phi'\right\} dR'$$

$$= \frac{R_0^2 \{J_{m+1}(j_{m,n})\}^2 \pi}{2} C_{mn}, \qquad (3.61)$$

which determines the coefficients C_{mn} in terms of the boundary field $f(R,\phi)$.

For the special case when the values of k are given by (3.56), we write (3.52) in the form of a double sum, namely

$$B_z = \sum_{m=0}^{\infty} \sum_{n=1}^{\infty} C_{mn} J_m(kR) \cos m\phi \, e^{-(k^2-\alpha^2)^{1/2} z} \qquad (3.62)$$

and similarly for the other two components of the field. What is the physical significance of this solution, which has been obtained by restricting the values of k?

To see this, we first note from (3.53) and (3.62) that

$$f(R,\phi) = \sum_{m=0}^{\infty} \sum_{n=1}^{\infty} C_{mn} J_m(kR) \cos m\phi \, . \qquad (3.63)$$

If we now set $R = R_0$ in (3.63), since by definition (3.56) we know that

$$J_m(kR_0) = J_m(j_{m,n}) \equiv 0 \, , \qquad (3.64)$$

it follows that

$$f(R_0, \phi) = 0 \qquad (3.65)$$

which means that B_z vanishes on the photosphere $z = 0$ at the radial boundary $R = R_0$. Further, (3.62) shows that, for the same reason, the z-component of the field vanishes at $R = R_0$ for all values of z. Neither B_R nor B_ϕ is zero on $R = R_0$, as is apparent from inspection of (3.48) and (3.49). Hence at this cylindrical boundary the magnetic field is purely horizontal.

To summarize, if one chooses for B_z on z=0 a function of R and ϕ, which is zero

on the surface $R=R_0$ but is otherwise arbitrary, then the field everywhere is of the form

$$\underline{B} = \sum_{m=0}^{\infty} \sum_{n=1}^{\infty} C_{mn} \left(B_R^{mn}, B_\phi^{mn}, B_z^{mn} \right) \tag{3.66}$$

with coefficients given by (3.61) as

$$C_{mn} = \frac{2}{\pi R_0^2 \{J_{m+1}(j_{m,n})\}^2} \int_0^{R_0} R' J_m\left(j_{m,n} \frac{R'}{R_0}\right) \left\{ \int_0^{2\pi} f(R',\phi') \cos m\phi' \, d\phi' \right\} dR' \tag{3.67}$$

by analogy with (3.50), and field components given by (3.49), (3.48) and (3.47).

The above, then, forms a prescription for determining the structure of fully three-dimensional fields for the case where the field is horizontal at some fixed radius and one knows the vertical component of the field everywhere on the photosphere within that fixed radius. In the final section of this chapter we propose an alternative formulation for relaxed fields which are axi-symmetric.

3.4 General Axi-Symmetric Equilibrium

Consider the special case when in the general solution (3.50) with (3.49), (3.48) and (3.47) only the m = 0 terms are present, corresponding to fields which are axi-symmetric. These solutions are thus of the form

$$\underline{B} = \int_0^{\infty} C(k) \left(B_R^k, B_\phi^k, B_z^k \right) dk \tag{3.68}$$

with components

$$B_R^k = \frac{l(k)}{k} J_1(kR) e^{-l(k)z} \tag{3.69}$$

$$B_\phi^k = \frac{\alpha}{k} J_1(kR) e^{-l(k)z} \tag{3.70}$$

and

$$B_z^k = J_0(kR)\, e^{-l(k)z} \tag{3.71}$$

with obvious notation.

We are now able to impose the boundary condition that the radial component B_R of the field vanishes at some fixed radius $R = R_0$ provided that we choose the values of k to be the zeros of $J_1(x)$ divided by R_0. Thus we write the radial component of the field as

$$B_R(R,z) = \sum_{n=1}^{\infty} C_n \frac{l_n(k_n)}{k_n} J_1(k_n R)\, e^{-l_n(k_n)z} \tag{3.72}$$

where

$$k_n = j_{1,n} R_0^{-1} . \tag{3.73}$$

Let us now prescribe the functional form of the normal component B_z of the field on the photosphere, i.e. we have

$$B_z(R,0) = g(R) \tag{3.74}$$

where g is some function. Comparing (3.74) with (3.71) evaluated on $z = 0$ and using (3.73) we deduce that

$$g(R) = \sum_{n=1}^{\infty} C_n J_0\left(j_{1,n} \frac{R}{R_0}\right) . \tag{3.75}$$

The problem now is to calculate the coefficients C_n.

Taking the derivative with respect to R of both sides of (3.75), we obtain

$$g'(R) = -\sum_{n=1}^{\infty} C_n \frac{j_{1,n}}{R_0} J_1\left(j_{1,n} \frac{R}{R_0}\right) . \tag{3.76}$$

Multiplying both sides of (3.76) by the quantity

$$R\,J_1\left(j_{1,p}\frac{R}{R_0}\right) \tag{3.77}$$

and integrating with respect to R from 0 to R_0, we have

$$\int_0^{R_0} R' J_1\left(j_{1,p}\frac{R'}{R_0}\right) g'(R')\,dR'$$

$$= \sum_{n=1}^{\infty} C_n \frac{j_{1,n}}{R_0} \int_0^{R_0} R' J_1\left(j_{1,n}\frac{R'}{R_0}\right) J_1\left(j_{1,p}\frac{R'}{R_0}\right) dR' \tag{3.78}$$

Therefore, by the appropriate orthogonality relation of Bessel functions, we deduce that

$$C_n = -\frac{2}{j_{1,n} R_0 J_2^2(j_{1,n})} \int_0^{R_0} R' J_1\left(j_{1,n}\frac{R'}{R_0}\right) g'(R')\,dR' \tag{3.79}$$

is the required expression for the coefficients of the field. In fact (3.79) may be integrated by parts to give an expression for the C_n in terms of g(R) itself, namely

$$C_n = \frac{2}{R_0^2\{J_2(j_{1,n})\}^2} \int_0^{R_0} R' J_0\left(j_{1,n}\frac{R'}{R_0}\right) g(R')\,dR' . \tag{3.80}$$

Thus, if we know the form (3.74) of the normal field on the photosphere, we are then able to calculate the relaxed field in the entire region above the photosphere within the cylinder $R=R_0$, since from (3.80) we are able to calculate the coefficients directly.

Hence, from (3.69), (3.70) and (3.71), the components of the field are

$$B_R(R,z) = \sum_{n=1}^{\infty} C_n \frac{l_n(k_n)}{k_n} J_1(k_n R) e^{-l_n(k_n) z} \tag{3.81}$$

$$B_\phi(R,z) = \alpha \sum_{n=1}^{\infty} C_n \frac{1}{k_n} J_1(k_n R) e^{-l_n(k_n) z} \tag{3.82}$$

and

$$B_z(R,z) = \sum_{n=1}^{\infty} C_n J_0(k_n R) e^{-l_n(k_n) z} \tag{3.83}$$

with the k_n given by (3.73). In addition, the l_n are related to the k_n by

$$\{l_n(k_n)\}^2 = k_n - \alpha^2 . \qquad (3.84)$$

Note that the definition (3.84) imposes an upper bound on α, since l_n must be real in order that the field is decaying as $z \to \infty$. Thus α must be smaller in magnitude than the smallest member of the set of k_n.

In conclusion, we remark that the formulation developed above might be used to model general axi-symmetric, non-potential fields above mono-polar sunspots, by using data from observations of the normal component of the photospheric magnetic field. In practice, of course, the function g(R) would be replaced by a grid of numerical values and so the coefficients C_n would therefore be determined from (3.80) by numerical means.

CHAPTER FOUR : SPHEROMAK WITH DIPOLE BOUNDARY CONDITION

4.1 Introduction

In the following three chapters we shall be investigating solutions of the linear force-free equation (1.5) in a spherical geometry. In particular, we shall be confining our attention to those relaxed states having a radial field component which does not vanish identically on the boundary. Thus we are considering the case where the boundary condition is "inhomogeneous", that is, magnetic flux crosses the boundary at $r = a$, where a is the radius of the sphere. In this way we hope to produce models of spheromak configurations having boundaries which are not magnetic surfaces. A precursor of our work here is the paper by Turner (1984), who considers force-free solutions in a cylindrical container, with point sources of flux positioned at various places on the boundary (see Chapter 6). As far as spherical geometry is concerned, Rosenbluth and Bussac (1979) described equilibrium fields in a sphere, but for the case in which the boundary is a magnetic surface.

We are justified in approximating spheromak fields by solutions to the force-free equation (1.5), because laboratory experiments have revealed that relaxed states in spheromaks are close to force-free (e.g. Jarboe *et al* ., 1983, Turner *et al* ., 1983). In particular, it is an experimental fact that the final state of a spheromak discharge is independent of the details of the method of its production, with the magnetic field being generated by internal plasma currents. The plasma settles down to a minimum-energy state which is described well by Taylor's theory of relaxation (Taylor, 1974; 1986), that is, the final state may be approximated to a high degree of accuracy by a linear force-free field.

4.2 The General Solution

We start our investigation by noting that the most general solution of the linear force-free equation (1.5) in spherical polar coordinates (r,θ,ϕ) which is well-behaved at the origin has components which may be written (e.g. Chandrasekhar and Kendal, 1957)

$$B_r = \sum_{m=0}^{\infty} \sum_{n \geq m}^{\infty} C_n^m \, n(n+1) \left(\frac{a}{r}\right)^{3/2} J_{n+\frac{1}{2}}(\alpha r) P_n^m(\cos\theta) e^{im\phi} \tag{4.1}$$

$$B_\theta = \sum_{m=0}^{\infty} \sum_{n \geq m}^{\infty} C_n^m \left[\left\{ \alpha a \left(\frac{a}{r}\right)^{1/2} J_{n-\frac{1}{2}}(\alpha r) - n \left(\frac{a}{r}\right)^{3/2} J_{n+\frac{1}{2}}(\alpha r) \right\} \frac{d}{d\theta} P_n^m(\cos\theta) \right.$$
$$\left. + im \, \alpha a \left(\frac{a}{r}\right)^{1/2} J_{n+\frac{1}{2}}(\alpha r) \frac{1}{\sin\theta} P_n^m(\cos\theta) \right] e^{im\phi} \tag{4.2}$$

and

$$B_\phi = \sum_{m=0}^{\infty} \sum_{n \geq m}^{\infty} C_n^m \left[im \left\{ \alpha a \left(\frac{a}{r}\right)^{1/2} J_{n-\frac{1}{2}}(\alpha r) - n \left(\frac{a}{r}\right)^{3/2} J_{n+\frac{1}{2}}(\alpha r) \right\} \frac{P_n^m(\cos\theta)}{\sin\theta} \right.$$
$$\left. - \alpha a \left(\frac{a}{r}\right)^{1/2} J_{n+\frac{1}{2}}(\alpha r) \frac{d}{d\theta} P_n^m(\cos\theta) \right] e^{im\phi} \tag{4.3}$$

where the C_n^m are complex constants and the P_n^m are the associated Legendre functions.

We note here that the class of axi-symmetric solutions to $\nabla \times \underline{B} = \alpha \underline{B}$ is obtained by setting m=0 in (4.2), (4.3) and (4.4). In this case it may be verified that the scalar function

$$A(r,\theta) = \frac{1}{\alpha} r \sin\theta \, B_\phi \tag{4.4}$$

where B_ϕ is given by (4.3) with m=0, is a solution of the equation

$$(\underline{B} \cdot \underline{\nabla}) A = 0 \, , \tag{4.5}$$

and so surfaces of constant A are flux surfaces. In other words, for symmetric fields there exists a flux function of the form (4.4). The ϕ-component of the field is determined directly in terms of this function from (4.4), and the remaining field components are given in terms of A by

$$B_r = \frac{1}{r^2 \sin\theta} \frac{\partial A}{\partial \theta} \tag{4.6}$$

and

$$B_\theta = -\frac{1}{r \sin\theta} \frac{\partial A}{\partial r} . \tag{4.7}$$

We shall use the formulation (4.4) in the present and in the following two chapters as the basis for the calculation of plots of field lines in the case of purely symmetric fields.

4.3 The Boundary Condition

In this chapter we shall be looking for linear force-free solutions in a sphere of radius a subject to the particular boundary condition

$$B_r (r = a) = B_0 P_1 (\cos\theta) = B_0 \cos\theta , \tag{4.8}$$

where P_1 is the Legendre polynomial of the first order. This boundary condition provides a natural match onto an external field which is uniform and parallel to the 'north-south' axis of the sphere, and may be termed the 'dipole boundary condition'. In fact (4.8) corresponds to the term having m=0 and n=1 in the expression (4.1) for the radial field. The magnitude of the field B_0 in (4.8) is thus related by direct proportion to the constant C_1 in (4.1). The above boundary condition may be regarded as the first term in a series involving all orders of the Legendre polynomials in $\cos\theta$, which expresses a generalized boundary condition (see Chapter 6).

4.4 Axi-Symmetric Solution

As noted previously, in the general solution (4.1), (4.2) and (4.3), modes which are independent of the coordinate ϕ have m = 0. The particular axi-symmetric component which satisfies (4.8) for all values of αa , except at certain isolated singular points, we shall write in terms of the flux function A as

$$\underline{B} = D_1^0 \, \underline{B}_1^0 \tag{4.9}$$

where

$$\underline{B}_1^0 = \left(\frac{1}{r^2 \sin\theta} \frac{\partial A}{\partial \theta}, -\frac{1}{r \sin\theta} \frac{\partial A}{\partial r}, \frac{\alpha A}{r \sin\theta} \right) \tag{4.10}$$

$$A(r,\theta) = B_0 a^{3/2} r^{1/2} J_{3/2}(\alpha r) \sin^2\theta \tag{4.11}$$

and

$$D_1^0 = \left\{ 2 J_{3/2}(\alpha a) \right\}^{-1} . \tag{4.12}$$

This solution has n = 1 and is the axi-symmetric state of lowest energy.

4.5 Non-Axi-Symmetric Solutions

Because of the nature of the boundary condition (4.8), ϕ-dependent solutions, for which $m \geq 1$, are admissible only for isolated values of the variable αa, that is, only for a set of discrete *eigenvalues* . All these purely non-axi-symmetric modes have $B_r = 0$ on r = a, and clearly only one of these non-axi-symmetric components may exist at one time, superposed on the axi-symmetric solution.

The lowest-energy eigen-solution has m = 1 and n = 2 with eigenvalue

$$\alpha_0 a = 5.763459 \ldots \quad (4.13)$$

Note that in (4.1),(4.2) and (4.3) the state with m = 1 and n = 1 is disallowed because its eigenvalue coincides with the singular value

$$\alpha_s a = 4.493409 \ldots \quad (4.14)$$

at which the coefficient (4.12) of the symmetric part of the field (4.9) becomes unbounded, since (4.17) is the first zero of $J_{3/2}(x)$. However, it may be verified that the m = 1, n = 1 solution is in fact the m = 0, n = 1 solution rotated by an angle of $\pi/2$ in θ, with a suitable change of origin in ϕ.

4.6 Nature of the Minimum-Energy State

In general, the minimum-energy solution is of the form

$$\underline{B} = D_1^0 \underline{B}_1^0 + D_2^1 \underline{B}_2^1 \quad (4.15)$$

where the m = 0 term is always present in order to satisfy the boundary condition (4.8). We shall demonstrate in what follows that the coefficient D_2^1 is non-zero if the relative helicity H exceeds a certain threshold value. Below this value, only the solution of type (4.9) exists; above this value we have a choice for the minimum-energy state, either type (4.9), or type (4.18) with $D_2^1 \neq 0$. As has been already noted, of two candidate solutions having the same boundary values, the one of lower αa has the lower energy and is therefore the preferred state (Reiman, 1981). We shall now address this problem in detail.

From (4.10) and (4.11) we deduce that

$$\underline{B}^{0}_{1} = B_0 \Big[2\,(a/r)^{3/2} J_{3/2}(\alpha r)\cos\theta\ \hat{\underline{r}} + \{(a/r)^{3/2} J_{3/2}(\alpha r) - \alpha r\,(a/r)^{1/2} J_{1/2}(\alpha r)\}\sin\theta\ \hat{\underline{\theta}} + \alpha a\,(a/r)^{1/2} J_{3/2}(\alpha r)\sin\theta\ \hat{\underline{\phi}} \Big] . \qquad (4.16)$$

With (4.12), this defines completely the axi-symmetric component of (4.15).

From (4.1), (4.2) and (4.3), we find that that the m = 1, m = 2 solution is

$$\underline{B}^{1}_{2} = B_0 \Big[3\,(a/r)^{3/2} J_{5/2}(\alpha r)\sin 2\theta\cos\phi\ \hat{\underline{r}} + \{ (\alpha a\,(a/r)^{1/2} J_{3/2}(\alpha r) - 2\,(a/r)^{3/2} J_{5/2}(\alpha r))\cos 2\theta\cos\phi - \alpha a\,(a/r)^{1/2} J_{5/2}(\alpha r)\cos\theta\sin\phi \}\ \hat{\underline{\theta}} + \{ (2\,(a/r)^{3/2} J_{5/2}(\alpha r) - \alpha a\,(a/r)^{1/2} J_{3/2}(\alpha r))\cos\theta\cos\phi - \alpha a (a/r)^{1/2} J_{5/2}(\alpha r)\cos 2\theta\cos\phi \}\ \hat{\underline{\phi}} \Big] \qquad (4.17)$$

which is determined up to an arbitrary multiplicative constant, effectively taken into D_2^1. It is to be understood throughout that if D_2^1 is non-zero then αa has the value given by (4.13).

To determine D_2^1, (since the boundary is not a flux surface) we must calculate the *relative* helicity H of the field (4.15) contained within the sphere of radius *a* with boundary condition (4.8). For the relative helicity we shall essentially follow the basic definition of Berger and Field (1984); for the details of the method adopted in what follows we refer the reader to the formulation given in the Appendix (Section 4.14).

4.8 Calculation of the Relative Helicity

The potential ('vacuum') field solution of the linear force-free equation (1.5) which satisfies the boundary condition (4.8) is

$$\underline{B}_o = B_o \cos\theta\, \hat{\underline{r}} - B_o \sin\theta\, \hat{\underline{\theta}} \,, \tag{4.18}$$

for which there exists a simple corresponding vector potential given by

$$\underline{A}_o = \frac{1}{2} B_o r \sin\theta\, \hat{\underline{\phi}} \,. \tag{4.19}$$

For the field in which we are interested, defined by (4.15) with (4.16) and (4.17), a vector potential whose tangential components equal those of $\underline{A}_0$ on the boundary is

$$\underline{A} = D^0_1\, \underline{A}^0_1 + D^1_2\, \underline{A}^1_2 \tag{4.20}$$

where

$$\underline{A}^0_1 = \frac{B_o}{\alpha}\Bigg[2\left(\frac{a}{r}\right)^{3/2} J_{3/2}(\alpha r)\cos\theta\, \hat{\underline{r}}$$

$$+ \left\{ \left(\frac{a}{r}\right)\left[\left(\frac{a}{r}\right)^{1/2} J_{3/2}(\alpha r) - J_{3/2}(\alpha a)\right] - \alpha a \left(\frac{a}{r}\right)^{1/2}\left[J_{1/2}(\alpha r) - \left(\frac{a}{r}\right)^{1/2} J_{1/2}(\alpha a)\right]\right\} \sin\theta\, \hat{\underline{\theta}}$$

$$+ \alpha a \left(\frac{a}{r}\right)^{1/2} J_{3/2}(\alpha r)\sin\theta\, \hat{\underline{\phi}} \Bigg] \tag{4.21}$$

and

$$\underline{A}^1_2 = \frac{B_o}{\alpha}\Bigg[3\left(\frac{a}{r}\right)^{3/2} J_{5/2}(\alpha r)\sin 2\theta \cos\phi\, \hat{\underline{r}}$$

$$+ \Bigg\{ \Bigg(\alpha a \left(\frac{a}{r}\right)^{1/2}\left[J_{3/2}(\alpha r) - \left(\frac{a}{r}\right)^{1/2} J_{3/2}(\alpha a)\right]$$

$$- 2\left(\frac{a}{r}\right)^{3/2} J_{5/2}(\alpha r)\Bigg)\cos 2\theta \cos\phi - \alpha a \left(\frac{a}{r}\right)^{1/2} J_{5/2}(\alpha r)\cos\theta \sin\phi \Bigg\} \hat{\underline{\theta}}$$

$$+\left\{\left(2\left(\frac{a}{r}\right)^{3/2}J_{5/2}(\alpha r)-\alpha a\left(\frac{a}{r}\right)^{1/2}\left[J_{3/2}(\alpha r)-\left(\frac{a}{r}\right)^{1/2}J_{3/2}(\alpha a)\right]\right)\cos\theta\sin\phi\right.$$

$$\left.-\alpha a\left(\frac{a}{r}\right)^{1/2}J_{5/2}(\alpha r)\cos 2\theta\cos\phi\right\}\hat{\underline{\phi}}\Bigg]\,. \qquad (4.22)$$

The relative helicity of the field (4.15) with (4.16) and (4.17) is thus

$$H = \int_V \underline{A}\cdot\underline{B}\,dV - \int_V \underline{A}_0\cdot\underline{B}_0\,dV \qquad (4.23)$$

where V denotes the volume enclosed by the spherical boundary located at r = a.

From (4.18) and (4.19) we deduce that the second of the integrals in (4.23) vanishes. Also, we have

$$\int_V \underline{A}\cdot\underline{B}\,dV = (D_1^0)^2\int_V \underline{A}_1^0\cdot\underline{B}_1^0\,dV + (D_2^1)^2\int_V \underline{A}_2^1\cdot\underline{B}_2^1\,dV \qquad (4.24)$$

since the cross terms vanish by orthogonality.

Using (4.23) and (4.24) and performing the space integrals with (4.16), (4.17), (4.21) and (4.22), we find that the relative helicity is of the form

$$H = (D_1^0)^2 H_1^0 + (D_2^1)^2 H_2^1 \qquad (4.25)$$

where

$$H_1^0 = \frac{16B_0^2a^4}{3}\left\{1+\frac{\sin(2\alpha a)}{2(\alpha a)}-\frac{1}{(\alpha a)^2}+\frac{\cos(2\alpha a)}{(\alpha a)^2}\right\} \qquad (4.26)$$

which is the helicity of the ϕ-independent part of the field, and

$$H_2^1 = \frac{16 B_0^2 a^4}{5}\left\{1 - \frac{\sin(2\alpha a)}{2(\alpha a)} - \frac{4}{(\alpha a)^2}\right.$$

$$- \frac{2\cos(2\alpha a)}{(\alpha a)^2} - \frac{6}{(\alpha a)^4} - \frac{12\cos(2\alpha a)}{(\alpha a)^4}$$

$$\left. + \frac{18\sin(2\alpha a)}{(\alpha a)^5} - \frac{9}{(\alpha a)^6} + \frac{9\cos(2\alpha a)}{(\alpha a)^6}\right\} \qquad (4.27)$$

which is the component of the relative helicity due to the ϕ-dependent part of the equilibrium field.

4.9 Calculation of the Magnetic Field Energy

In a similar way, the magnetic energy stored in the field (4.15) is of the form

$$W = (D_1^0)^2 W_1^0 + (D_2^1)^2 W_2^1 \qquad (4.28)$$

where

$$W_1^0 = \frac{1}{2\mu_0}\int_V \underline{B}_1^0 \cdot \underline{B}_1^0 \, dV \qquad (4.29)$$

and

$$W_2^1 = \frac{1}{2\mu_0}\int_V \underline{B}_2^1 \cdot \underline{B}_2^1 \, dV . \qquad (4.30)$$

From (4.16) and (4.29) we find that

$$W_1^0 = \frac{8 B_0^2 a^3 (\alpha a)}{3\mu_0}\left[1 - \frac{1}{(\alpha a)^2} + \frac{\sin(2\alpha a)}{(\alpha a)^3}\right.$$

$$\left. - \frac{1}{2(\alpha a)^4} + \frac{\cos(2\alpha a)}{2(\alpha a)^4}\right] , \qquad (4.31)$$

which is the magnetic energy due to the symmetric part of the field, and similarly from (4.17) and (4.30) that

$$W_2^1 = \frac{8B_0^2 a^3(\alpha a)}{5\mu_0}\left[1 - \frac{3}{(\alpha a)^2} - \frac{3\sin(2\alpha a)}{(\alpha a)^3} - \frac{27\cos(2\alpha a)}{2(\alpha a)^4} - \frac{9}{2(\alpha a)^4} + \frac{18\sin(2\alpha a)}{(\alpha a)^5} - \frac{9}{(\alpha a)^6} + \frac{9\cos(2\alpha a)}{(\alpha a)^6}\right] \quad (4.32)$$

which is the energy associated with the ϕ-dependent part of the field (4.15).

4.10 Comments

We now have expressions for the magnetic field (4.15), its relative helicity (4.25) and its magnetic energy (4.28).

Note that as αa increases in value from zero, the symmetric coefficient D_1^o, as given by (4.12), becomes unbounded as the first zero of $J_{3/2}(x)$ is approached. This is the first 'resonance' value of αa for the symmetric field, that is, the lowest value of αa at which the field would naturally exist if the boundary condition were $B_r(r=a) = 0$. This value, given by (4.14), we shall term the lowest *singular* value, and shall hereafter denote it by the symbol $\alpha_S a$. It is a property of the symmetric field alone. On the other hand, we shall use the term lowest *eigenvalue* for the lowest value of αa for which the ϕ-dependent part of the field (4.15) is non-zero. This value is given by (4.13) and is represented by the symbol $\alpha_0 a$ in what follows.

The values of the two constants $\alpha_S a$ and $\alpha_0 a$ are in fact fundamental in determining the nature of of the relaxed configuration in a spherical container. The quantity $\alpha_S a$, given numerically by (4.14), is quoted by Rosenbluth and Bussac (1979) in their theoretical determination of the radius of the 'classical' spheromak configuration.

4.11 Predicted States

The nature of the theoretically preferred minimum-energy state depends on the value of the relative helicity. There are two cases (c.f. the cylinder problem in Chapter 3):

(i) H has a value admitting a purely symmetric field with $0 \le \alpha a < \alpha_0 a$

In this case the purely symmetric field has the lower value of αa and therefore is the state of minimum energy. The helicity and the energy are not high enough to reach a 'mixed' state, for which we must have $\alpha a = \alpha_0 a$, and thus $D_2^1 = 0$ in this range. Hence from the definition (4.25) with (4.12) and (4.26) we have

$$H = \frac{2\pi B_0^2 a^4 (\alpha a)}{3\left(\frac{\sin \alpha a}{\alpha a} - \cos \alpha a\right)^2}\left\{1 - \frac{\sin(2\alpha a)}{2(\alpha a)} - \frac{1}{(\alpha a)^2} + \frac{\cos(2\alpha a)}{(\alpha a)^2}\right\}. \tag{4.33}$$

In a similar way, from (4.28) with (4.12) and (4.31) we have

$$W_{SYM} = \frac{\pi B_0^2 a^3 (\alpha a)^2}{3\mu_0\left(\frac{\sin \alpha a}{\alpha a} - \cos \alpha a\right)^2}\left\{1 - \frac{1}{(\alpha a)^2} + \frac{\sin(2\alpha a)}{(\alpha a)^3} - \frac{1}{2(\alpha a)^4} + \frac{\cos(2\alpha a)}{2(\alpha a)^4}\right\}. \tag{4.34}$$

(ii) H has a value such that the purely symmetric field has $\alpha a \ge \alpha_0 a$

In this case the mixed field solution with $\alpha a = \alpha_0 a$ is the predicted minimum-energy state, since this minimizes αa. From (4.12), (4.25), (4.26) and (4.27) evaluated at $\alpha a = \alpha_0 a$, we find that the helicity in the mixed state is given by

$$H = 3.842306\,\pi B_0^2 a^4 + 2.913141\,(D_2^1)^2 B_0^2 a^4, \tag{4.35}$$

This last equation effectively determines the coefficient D_2^1 if the relative helicity is given. We also see from (4.35) that there is a lower bound set on H so that D_2^1 is real as required.

From (4.12), (4.28), (4.31) and (4.32) evaluated at $\alpha a = \alpha_0 a$ and taking $D_2^{\frac{1}{2}}$ from (4.35) in terms of H, we obtain the result

$$W_{MIX} = \pi B_0^2 a^3 \left\{ 2.881729 \frac{H}{\pi B_0^2 a^4} + 0.666667 \right\} \qquad (4.36)$$

for the energy of the mixed (axi-symmetric plus asymmetric) state. We shall use the suffices 'SYM' and 'MIX' to denote symmetric and mixed states respectively.

Now the results (4.33), (4.34), (4.35) and (4.36) above may be studied by plotting graphs involving the four quantities αa, H, W_{SYM} and W_{MIX}. This we have done, and we now describe the results.

Figure 4.1 shows how the relative helicity H varies with the force-free parameter αa in the symmetric state. We have marked the position at $\alpha a = \alpha_0 a$ of the first asymmetric solution : here increasing H does not change αa but instead increases $(D_2^{\frac{1}{2}})^2$ according to Equation (4.35). Thus the lowest of the mixed states appears on the graph as a vertical straight line. Note that the relative helicity H is zero when αa is zero, but is unbounded as αa approaches any positive zero of $J_{3/2}(x)$. Also, H increases monotonically with αa when the latter falls between 0 and $\alpha_S a$, but not so between any pair of positive zeros of $J_{3/2}(x)$, that is, whenever αa lies to the right of $\alpha_S a$ on the graph.

In Figure 4.2 we have plotted the magnetic energy of the symmetric field against the relative helicity. The first mixed state is also indicated. From this important graph it is possible to tell at a glance which candidate minimum-energy state, symmetric or mixed, has in fact the lower energy for any given value of the relative helicity. Thus it is clear from Figure 4.2 that a selection of any value for H predicts a minimum-energy state of the 'purely symmetric' kind.

We may remark on the similarity in the general appearance of Figures 4.1 and 4.2 with Figures 3.2 and 3.4 respectively, the main difference between the two sets of graphs being the position of the lowest-energy mixed state, a significant feature.

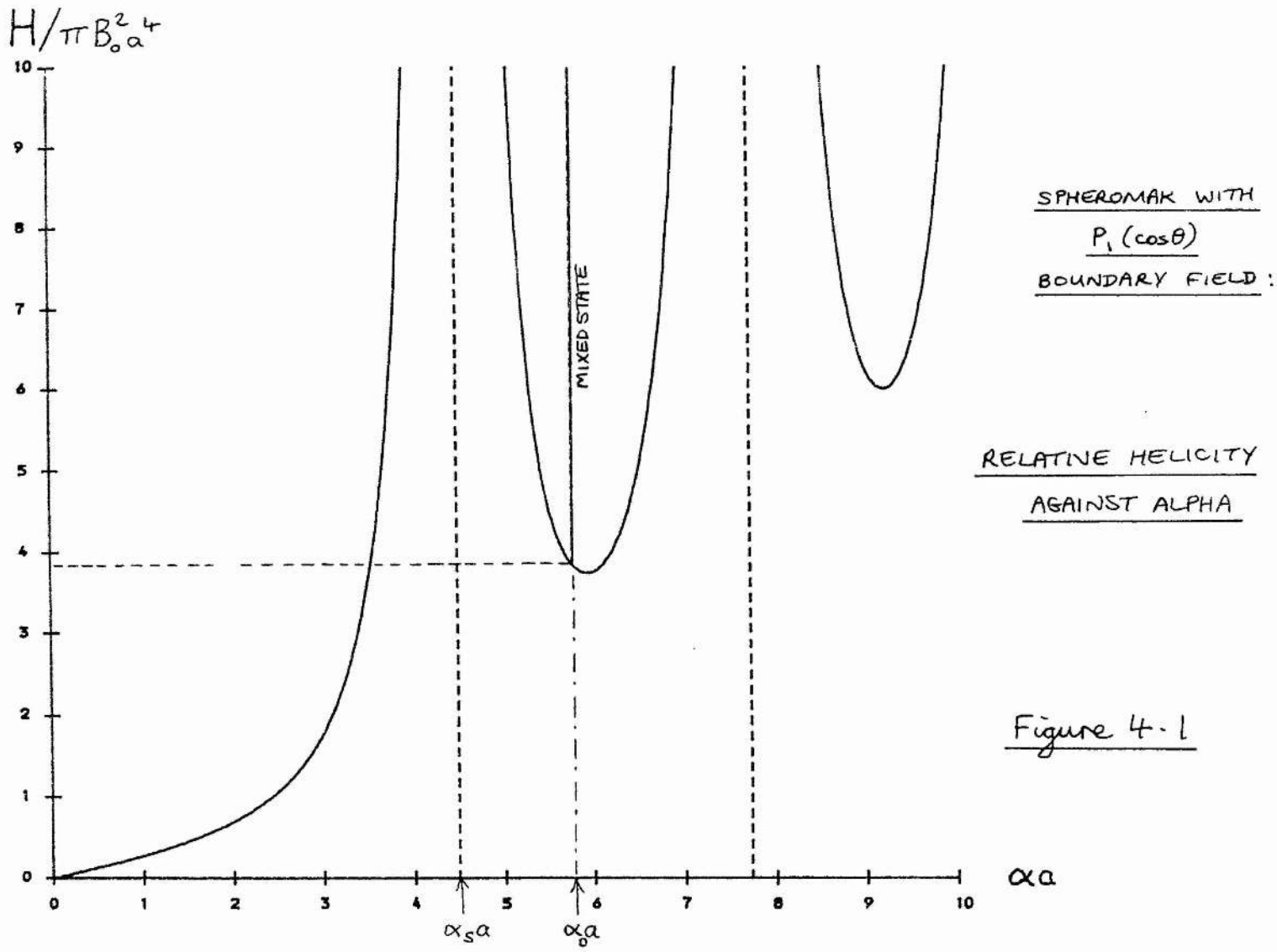

SPHEROMAK WITH $P_1(\cos\theta)$ BOUNDARY FIELD :

RELATIVE HELICITY AGAINST ALPHA

Figure 4.1

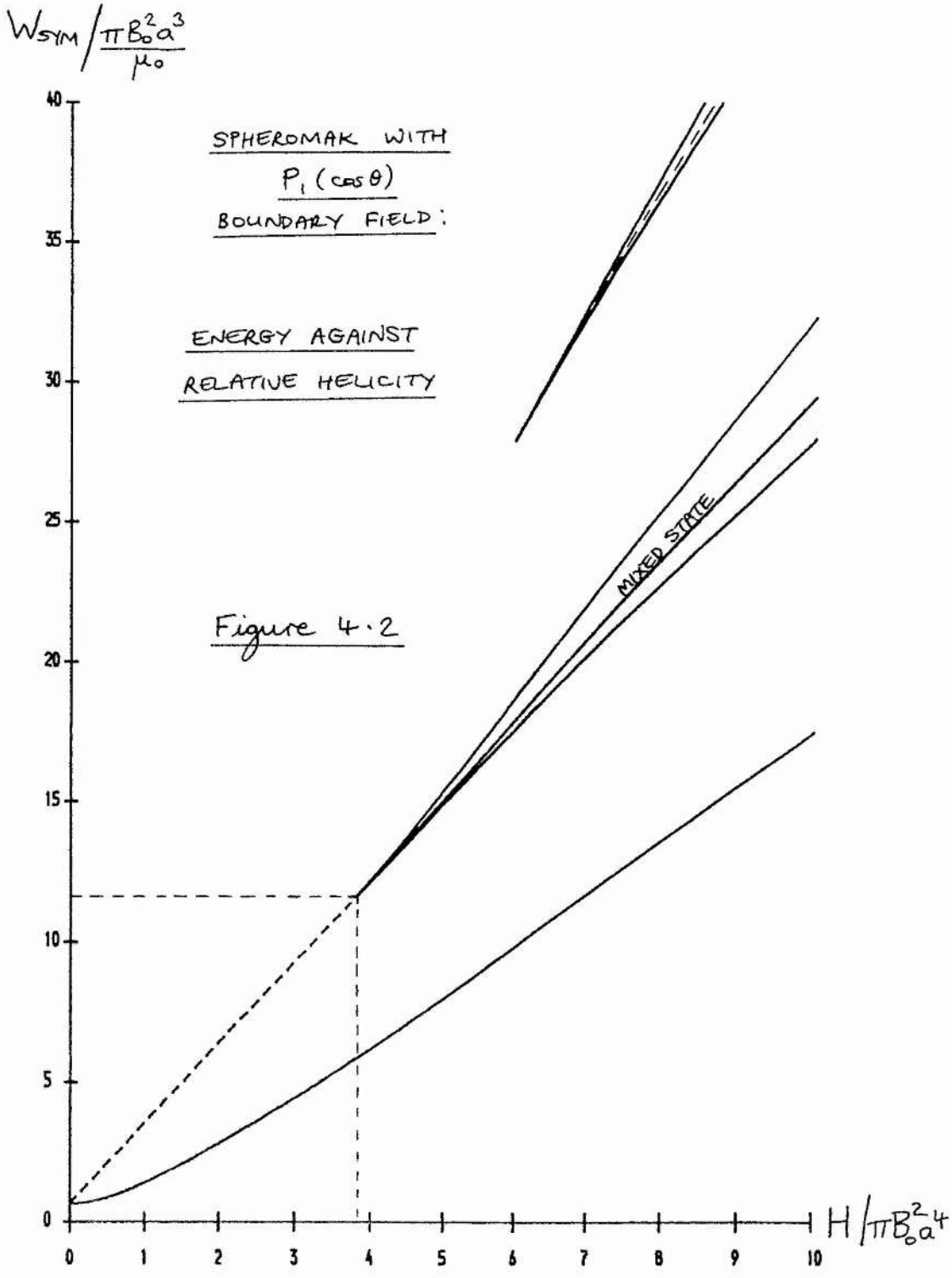
$W_{SYM} / \frac{\pi B_0^2 a^3}{\mu_0}$
SPHEROMAK WITH
$P_1(\cos\theta)$
BOUNDARY FIELD:
ENERGY AGAINST
RELATIVE HELICITY
MIXED STATE
$H / \pi B_0^2 a^4$
0
5
10
15
20
25
30
35
40
0
1
2
3
4
5
6
7
8
9
10

Figure 4.2

4.12 Conclusion for a Uniform External Field

Subject to the uniform external field (4.8), for all values of H our theory predicts that the system should in all cases relax towards a minimum-energy configuration which is an axi-symmetric , linear, force-free field. This is because the singular value ($\alpha_S a$), at which the helicity of the symmetric state becomes infinite, is lower than the eigenvalue ($\alpha_0 a$) at which an asymmetric state is admissible.

4.13 Appearance of the Relaxed Configuration

Using the flux-function defined by (4.11), one can map the field-lines of the relaxed states. Figures 4.3 to 4.9 inclusive show a selection of such plots, for various different values of αa (or, equivalently, H). The range of values represented is between 0 and $\alpha_S a$. In Figure 4.3 αa is small, and the relaxed state inside the sphere almost matches the uniform field outside. As the value of αa is increased, we note the formation of an island structure, and the increase in field strength as the singular value $\alpha_S a$ is approached. To attain this value of αa requires infinite energy input, so this represents a natural barrier to any further increase in αa.

4.14 Appendix : Relative Helicity in a Spheromak

Let V_a represent the volume inside a sphere of radius a , and V_b that of the rest of space, that is, the volume exterior to the sphere. Let $\underline{B}$ and $\underline{B}'$ be two magnetic fields which differ in V_a but are the same in V_b, and let $\underline{A}$ and $\underline{A}'$ be the respective vector potentials which generate these fields. Then

$$H_R = \int_{V_a+V_b} \underline{A} \cdot \underline{B} \, dV - \int_{V_a+V_b} \underline{A}' \cdot \underline{B}' \, dV \qquad (4.37)$$

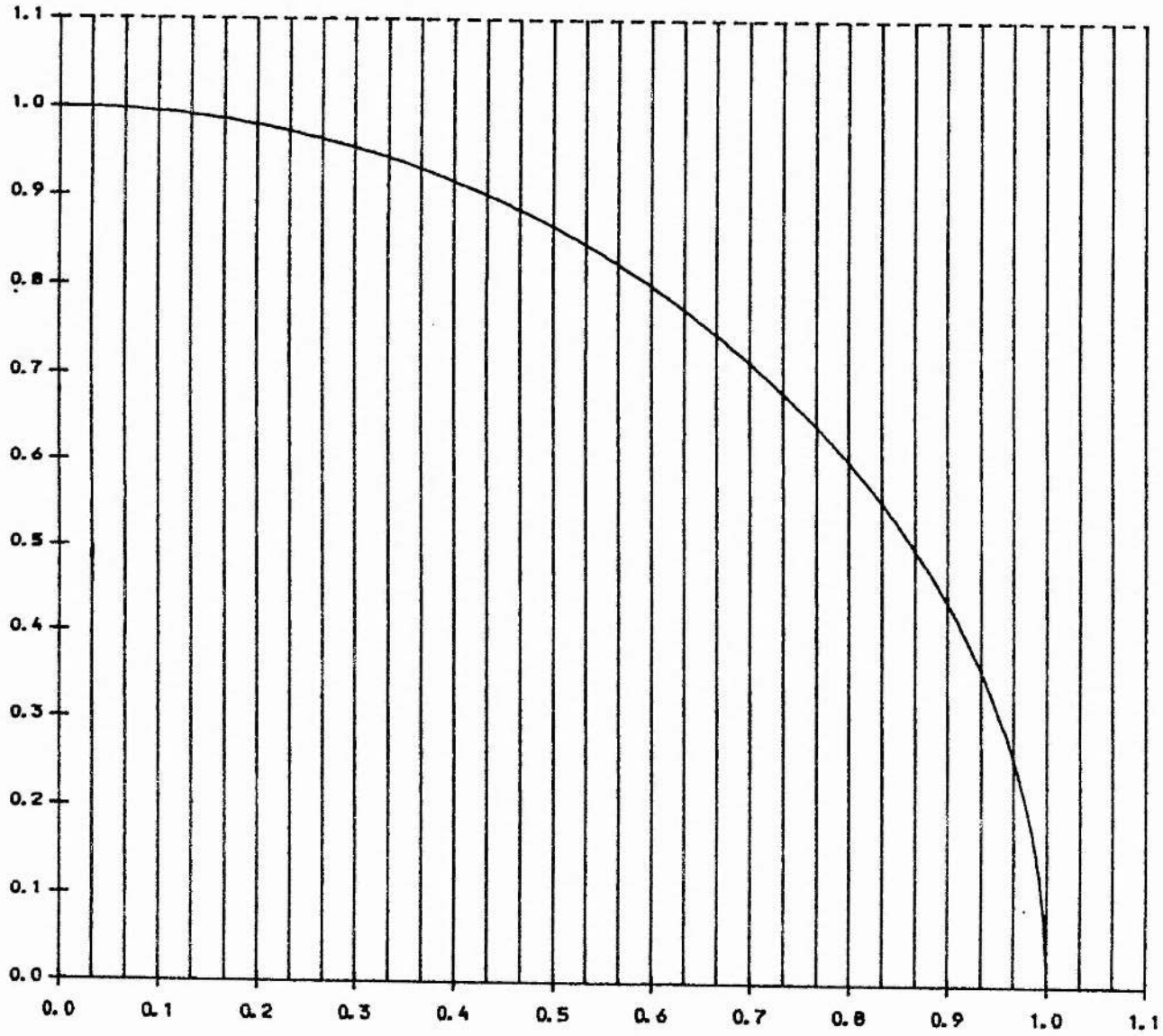

SPHEROMAK WITH

$P_1(\cos\theta)$

BOUNDARY FIELD:

SET OF SEVEN

SYMMETRIC

FIELD PLOTS.

$$\frac{H}{\pi B_o^2 a^4} = 0.03$$

$$\alpha a = 0.1$$

Figure 4.3

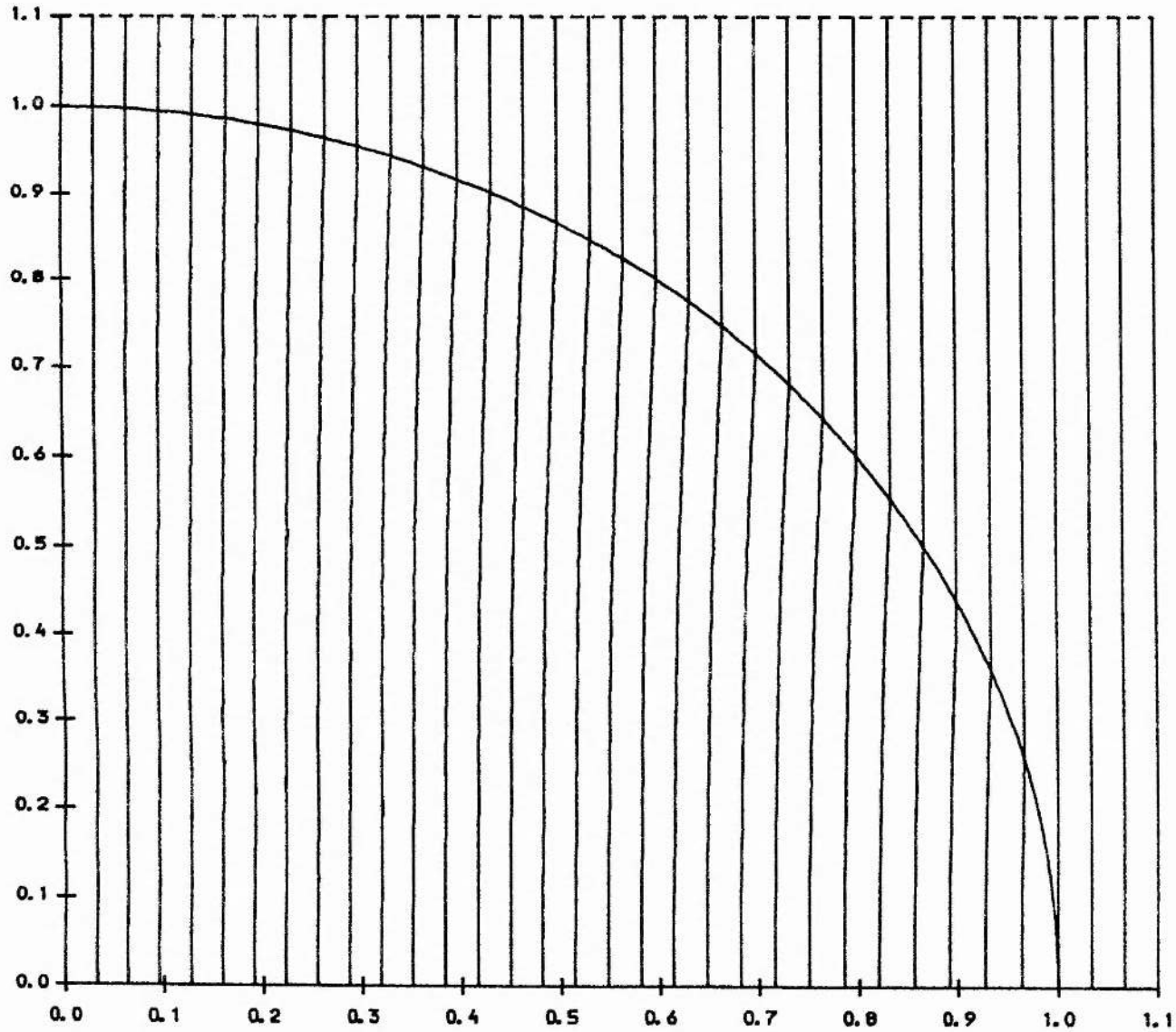

$$\frac{H}{\pi B_o^2 a^4} = \underline{0.28}$$

$$\alpha a = \underline{1.0}$$

Figure 4.4

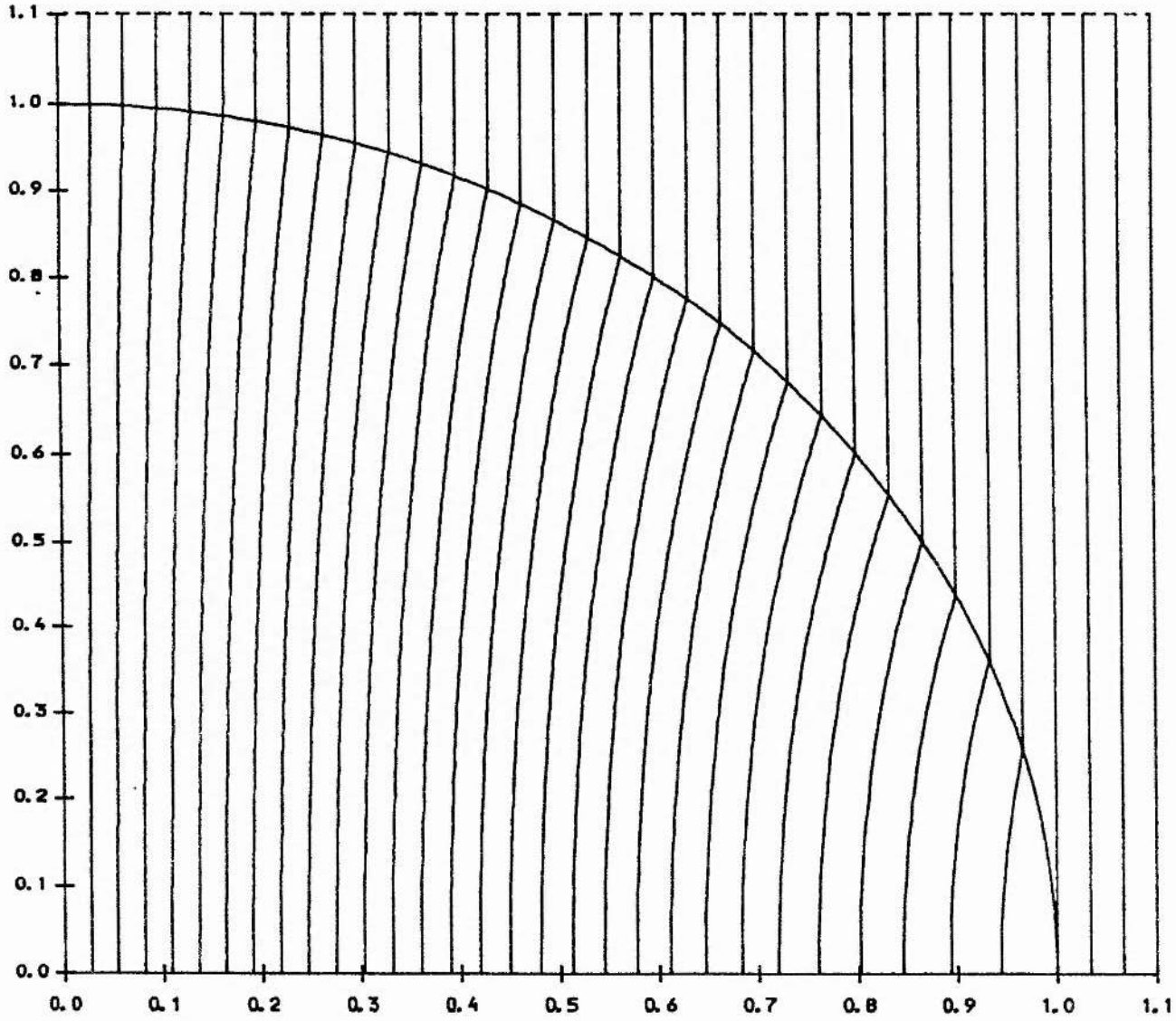

$$\frac{H}{\pi B_o^2 a^4} = \underline{0.70}$$

$$\alpha a = \underline{2.0}$$

Figure 4.5

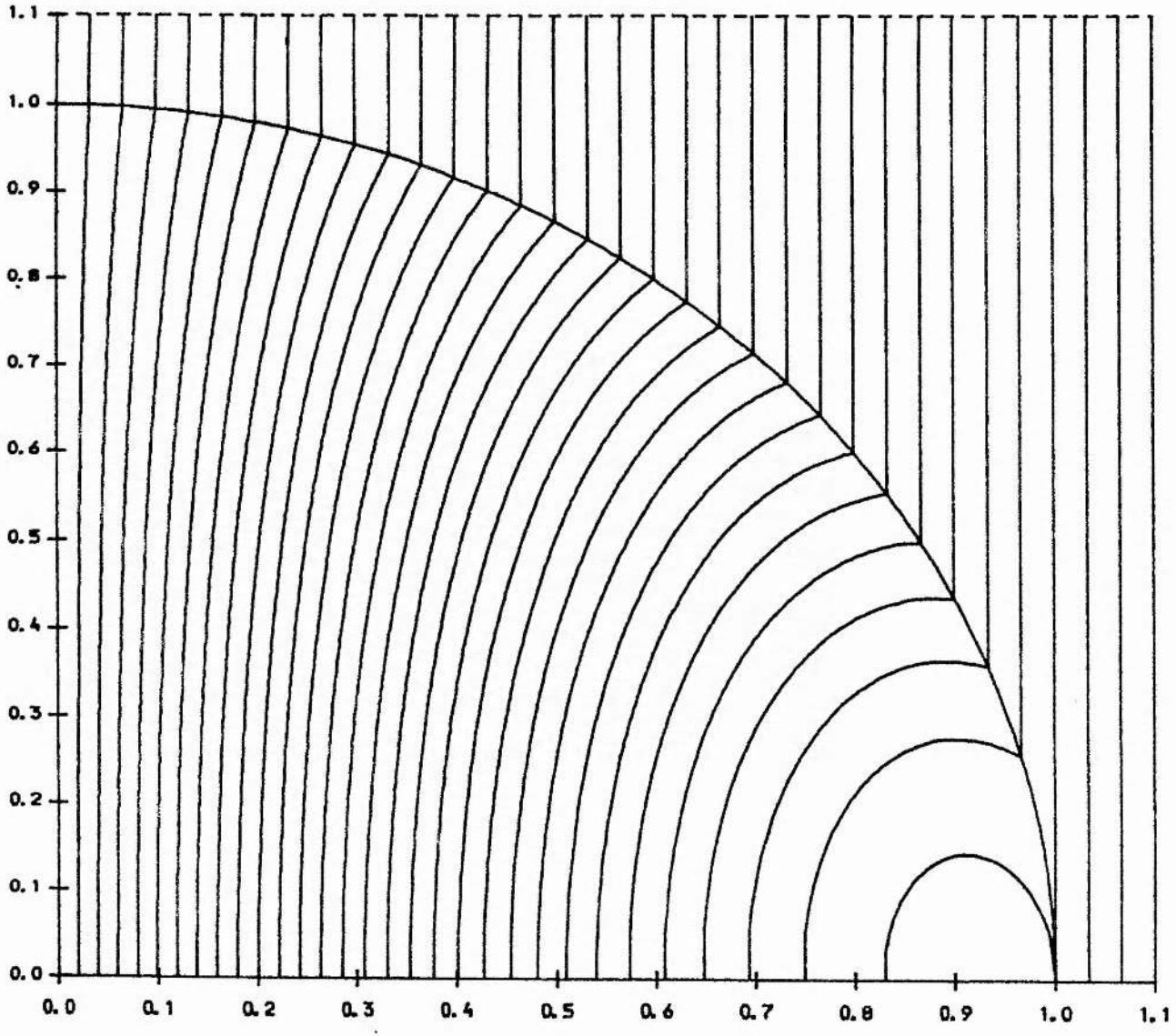

$$\frac{H}{\pi B_0^2 a^4} = \underline{1.76}$$

$$\alpha a = \underline{3.0}$$

Figure 4.6

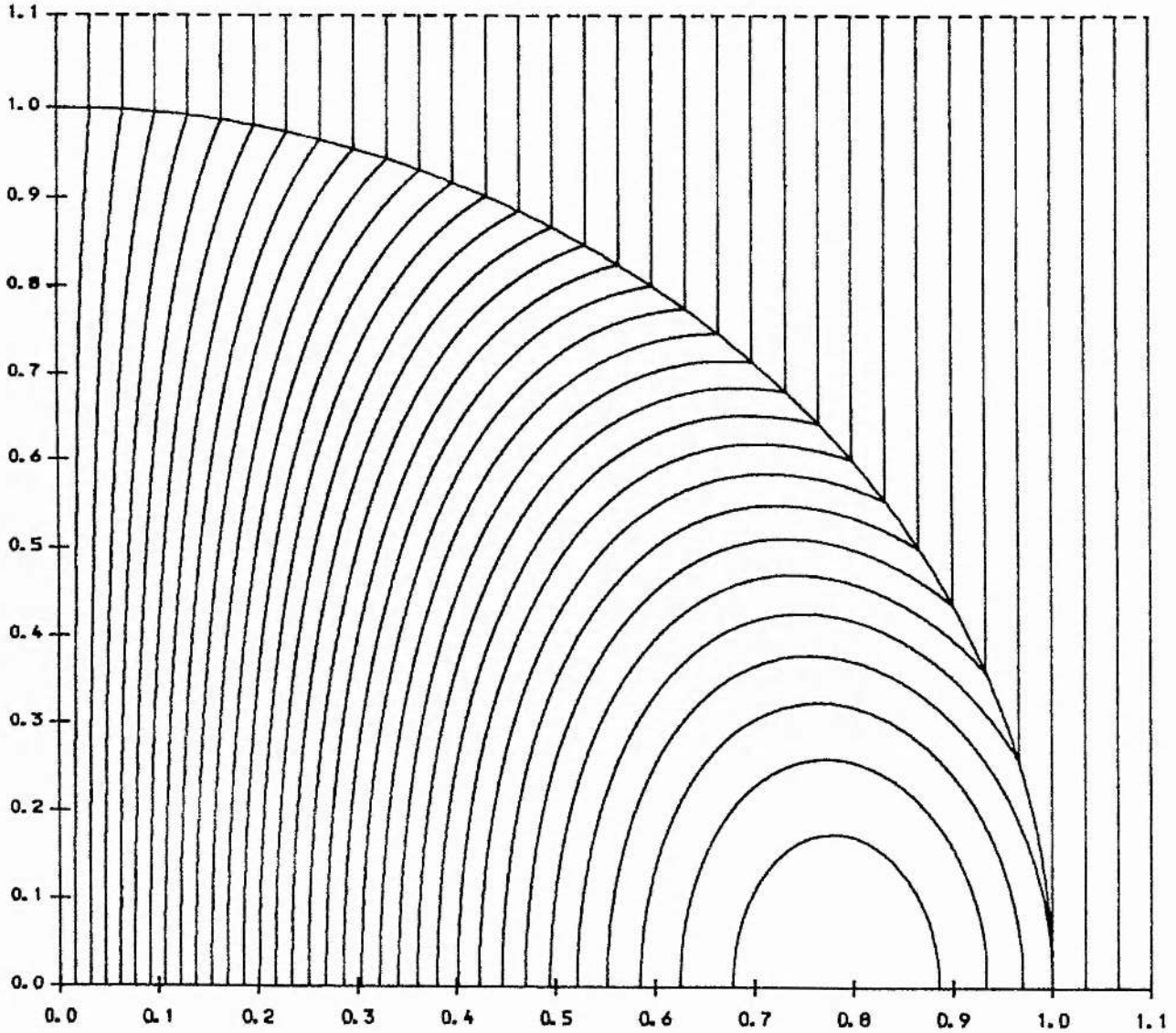

$$\frac{H}{\pi B_0^2 a^4} = \underline{3.58}$$

$$\alpha a = \underline{3.5}$$

Figure 4.7

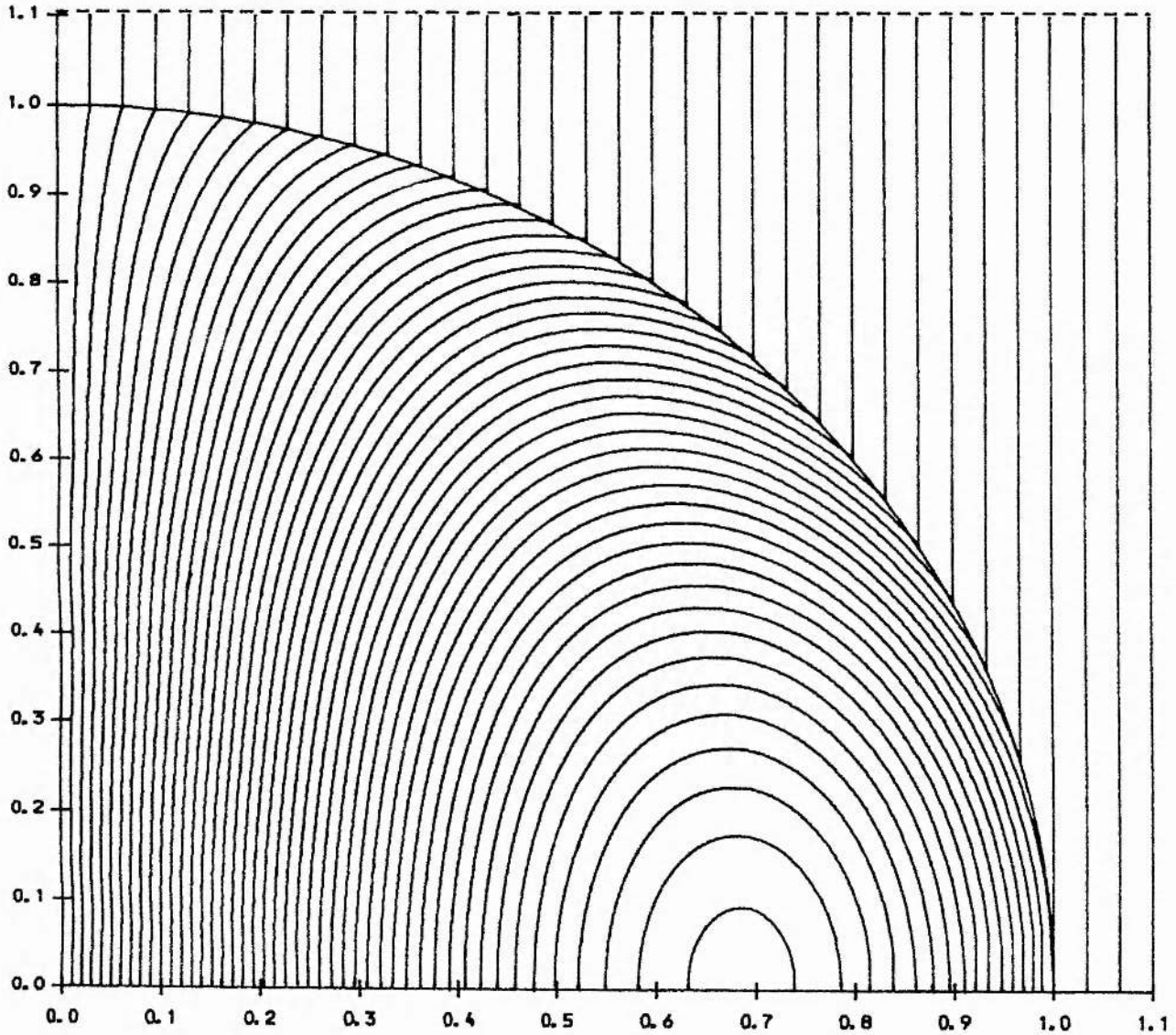

$$\frac{H}{\pi B_o^2 a^4} = \underline{13.0}$$

$$\alpha a = \underline{4.0}$$

Figure 4.8

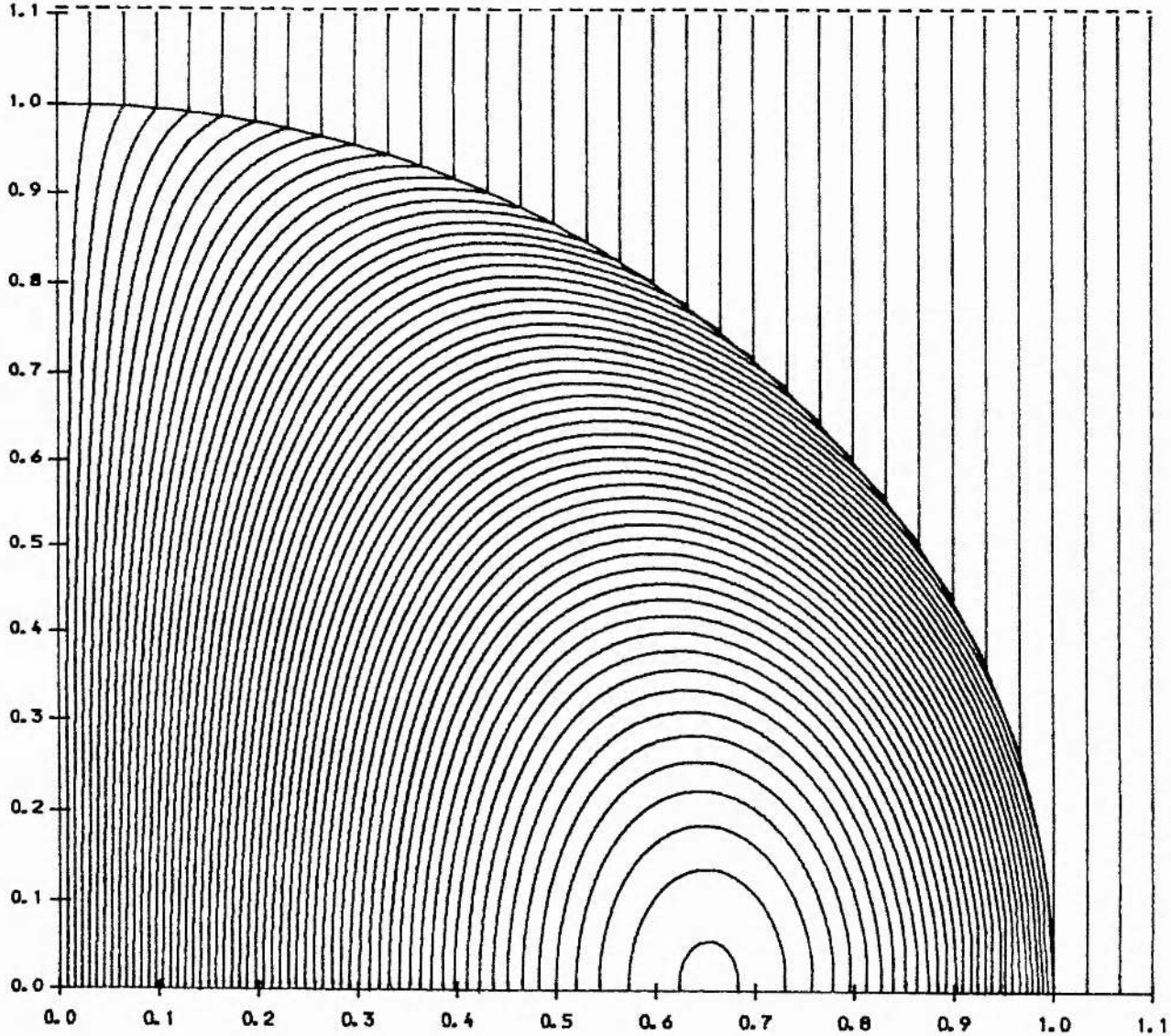

$$\frac{H}{\pi B_o^2 a^4} = \underline{35.6}$$

$$\alpha a = \underline{4.2}$$

Figure 4.9

is the *relative helicity* of the two fields $\underline{B}$ and $\underline{B}'$ as defined by Berger and Field (1984). The quantity (4.37) has the very desirable property that it is independent of the common extension of $\underline{B}$ and $\underline{B}'$ to V_b.

Specifically, if $\underline{B}'$ is a vacuum field, that is, we have

$$\nabla \times \underline{B}' = 0 \,, \tag{4.38}$$

(except possibly at $r = a$), and in addition

$$\underline{B}' \cdot \hat{\underline{n}} = \underline{B} \cdot \hat{\underline{n}} \quad \text{on } r = a \,, \tag{4.39}$$

then (4.37) is a property of the field $\underline{B}$ alone. The above prescription demands nothing regarding the gauges of $\underline{A}$ and $\underline{A}'$, except that it is assumed that for each of the fields the gauge of the vector potential is the same in V_a as in V_b (Finn and Antonsen, 1985).

If in the outer region we have

$$\underline{A}' = \underline{A} + \nabla \beta \tag{4.40}$$

where β is a single-valued function of position, then (4.37) becomes

$$H_R = \int_{V_a} \underline{A} \cdot \underline{B} \, dV - \int_{V_a} \underline{A}' \cdot \underline{B}' \, dV + \int_{r=a} \beta \, \underline{B} \cdot d\underline{S} \tag{4.41}$$

where $d\underline{S}$ points out of V_a. Now the three components of (4.40) are

$$\left.\begin{aligned} \frac{\partial \beta}{\partial r} &= (\underline{A}' - \underline{A})_r \\ \frac{1}{r} \frac{\partial \beta}{\partial \theta} &= (\underline{A}' - \underline{A})_\theta \\ \frac{1}{r \sin\theta} \frac{\partial \beta}{\partial \phi} &= (\underline{A}' - \underline{A})_\phi \end{aligned}\right\} \,. \tag{4.42}$$

Clearly, if $(\underline{A}'-\underline{A})_\theta = 0$ and $(\underline{A}'-\underline{A})_\phi = 0$ on $r = a$, then β is a constant there and as a result the surface integral in (4.41) vanishes.

Hence a *sufficient* condition that the 'Berger and Field' relative helicity take the simplified form

$$H_R = \int_{V_a} \underline{A} \cdot \underline{B}\, dV - \int_{V_a} \underline{A}' \cdot \underline{B}'\, dV , \tag{4.43}$$

which involves only integrals over the field of interest, is that

$$\underline{B} \cdot \hat{\underline{n}} = \underline{B}' \cdot \hat{\underline{n}} \quad \text{on } r = a \tag{4.44}$$

and

$$\underline{A}_{tgt} = \underline{A}'_{tgt} \quad \text{on } r = a , \tag{4.45}$$

[In fact (4.45) implies (4.44).]

Hence (4.43) is a convenient, gauge-invariant quantity if the tangential components of the two vector potentials match at the boundary.

We shall speak of *the* relative helicity of a field $\underline{B}$ when $\underline{B}'$ is a potential field $\underline{B}_0$. Hence we write

$$H_R = \int_V \underline{A} \cdot \underline{B}\, dV - \int_V \underline{A}_0 \cdot \underline{B}_0\, dV \tag{4.46}$$

where $\underline{A}_0$ is the vector potential for $\underline{B}_0$ and V denotes the volume enclosed by the sphere.

CHAPTER FIVE : SPHEROMAK WITH QUADRUPOLE BOUNDARY FIELD

5.1 Boundary Condition

In this chapter we shall carry through the same kind of analysis as in Chapter 4, but for the new boundary condition

$$B_r(r=a) = B_0 P_2(\cos\theta) = \frac{1}{4} B_0 (1+3\cos 2\theta) \quad (5.1)$$

which employs the next member of the sequence of Legendre polynomials in $\cos\theta$. This represents an external field with quadrupolar form.

5.2 Axi-Symmetric Field

In the general solution (4.1), (4.2) and (4.3), the $m = 0$ component which matches the boundary distribution (5.1) for all values of θ has $n = 2$. Hence the symmetric field on this occasion has the general form

$$\underline{B} = D^{\circ}_2 \underline{B}^{\circ}_2 \quad (5.2)$$

with corresponding flux-function

$$A(r,\theta) = 2B_0 a^{3/2} r^{1/2} J_{5/2}(\alpha r) \sin^2\theta \cos\theta \quad (5.3)$$

such that

$$\underline{B}^{\circ}_2 = \left(\frac{1}{r^2 \sin\theta} \frac{\partial A}{\partial \theta}, -\frac{1}{r\sin\theta} \frac{\partial A}{\partial r}, \frac{\alpha A}{r\sin\theta} \right) \quad (5.4)$$

and the coefficient is

$$D_2^{\circ} = \{4 J_{5/2}(\alpha a)\}^{-1} \qquad (5.5)$$

We see from (5.5) that the singular values of αa are the zeros of $J_{5/2}(x)$.

5.3 Non-Axi-Symmetric Field

The lowest-energy, ϕ-independent component of (4.1), (4.2) and (4.3) which vanishes on $r = a$ has $m = n = 1$, with eigenvalue

$$\alpha_0 a = 4.493409 \qquad (5.6)$$

which is the first zero of $J_{3/2}(x)$.

5.4 Lowest-Energy State

The situation with the '$P_2(\cos\theta)$' boundary condition is fundamentally different from that with '$P_1(\cos\theta)$' since the lowest eigenvalue (5.6) of the helical part of the field is now *smaller* than the first singular value of the symmetric field, which is

$$\alpha_s a = 5.763459 \qquad (5.7)$$

[c.f. (4.13) and (4.14)]. This leads us to expect that the minimum-energy configuration may, for sufficiently high values of the relative helicity H, be the combined symmetric plus asymmetric solution.

From the above, and from the experience gained in Chapter 4, we predict that :

(i) The minimum-energy state will have a value of αa in the range from 0 to 5.76;

(ii) If αa is between 0 and 4.49, the purely symmetric solution will have the lower energy;

(iii) If αa lies between 4.49 and 5.76, then the mixed state, consisting of both axi-symmetric and ϕ-dependent components, will be the lower-energy state.

5.5 Mathematical Analysis

In the present case the minimum-energy configuration may be written

$$\underline{B} = D_2^0 \underline{B}_2^0 + D_1^1 \underline{B}_1^1 \tag{5.8}$$

where D_2^0 is given by (5.5),

$$\begin{aligned}\underline{B}_2^0 = B_0 \Bigg[& \left(\frac{a}{r}\right)^{3/2} J_{5/2}(\alpha r)(1+3\cos 2\theta)\,\hat{\underline{r}} \\ & + \left\{2\left(\frac{a}{r}\right)^{3/2} J_{5/2}(\alpha r) - \alpha a \left(\frac{a}{r}\right)^{1/2} J_{3/2}(\alpha r)\right\} \sin 2\theta\,\hat{\underline{\theta}} \\ & + \alpha a \left(\frac{a}{r}\right)^{1/2} J_{5/2}(\alpha r) \sin 2\theta\,\hat{\underline{\phi}}\Bigg]\end{aligned} \tag{5.9}$$

and

$$\begin{aligned}\underline{B}_1^1 = B_0 \Bigg[& 2\left(\frac{a}{r}\right)^{3/2} J_{3/2}(\alpha r) \sin\theta\cos\phi\,\hat{\underline{r}} \\ & + \left\{\left(\alpha a \left(\frac{a}{r}\right)^{1/2} J_{1/2}(\alpha r) - \left(\frac{a}{r}\right)^{3/2} J_{3/2}(\alpha r)\right)\cos\theta\cos\phi \right. \\ & \left. - \alpha a \left(\frac{a}{r}\right)^{1/2} J_{3/2}(\alpha r)\sin\phi\right\}\hat{\underline{\theta}} \\ & + \left\{\left(\left(\frac{a}{r}\right)^{3/2} J_{3/2}(\alpha r) - \alpha a \left(\frac{a}{r}\right)^{1/2} J_{1/2}(\alpha r)\right)\sin\phi \right. \\ & \left. - \alpha a \left(\frac{a}{r}\right)^{1/2} J_{3/2}(\alpha r)\cos\theta\cos\phi\right\}\hat{\underline{\phi}}\Bigg].\end{aligned} \tag{5.10}$$

In a similar way to before, if $D_1^1 \neq 0$, then αa is understood to assume the eigenvalue (5.6).

5.6 Relative Helicity

We now proceed to calculate the relative helicity (following Section 4.14) of the field (5.8) whose components are (5.9) and (5.10), subject to the boundary condition (5.1).

The potential field solution satisfying (5.1) is found to be

$$\underline{B}_0 = \frac{B_0}{4}\frac{r}{a}(1+3\cos 2\theta)\hat{\underline{r}} - \frac{3}{4}B_0\frac{r}{a}\sin 2\theta\,\hat{\underline{\theta}} \qquad (5.11)$$

for which there is a corresponding vector potential

$$\underline{A}_0 = \frac{1}{4}\frac{B_0}{a}r^2\sin 2\theta\,\hat{\underline{\phi}} \qquad (5.12)$$

such that $\underline{B}_0 = \nabla \times \underline{A}_0$. A vector potential for the field (5.8) with (5.9) and (5.10) whose tangential components equal those of $\underline{A}_0$ on the boundary $r = a$ is of the form

$$\underline{A} = D_2^0\,\underline{A}_2^0 + D_1^1\,\underline{A}_1^1 \qquad (5.13)$$

where

$$\underline{A}_2^0 = \frac{B_0}{\alpha}\Big[\left(\frac{a}{r}\right)^{3/2}J_{5/2}(\alpha r)(1+3\cos 2\theta)\hat{\underline{r}}$$
$$+\Big\{2\left(\frac{a}{r}\right)\Big[\left(\frac{a}{r}\right)^{1/2}J_{5/2}(\alpha r) - J_{5/2}(\alpha a)\Big]$$
$$-\alpha a\left(\frac{a}{r}\right)^{1/2}\Big[J_{3/2}(\alpha r) - \left(\frac{a}{r}\right)^{1/2}J_{3/2}(\alpha a)\Big]\Big\}\sin 2\theta\,\hat{\underline{\theta}}$$
$$+\alpha a\left(\frac{a}{r}\right)^{1/2}J_{5/2}(\alpha r)\sin 2\theta\,\hat{\underline{\phi}}\Big] \qquad (5.14)$$

and

$$\underline{A}_1^1 = \frac{B_0}{\alpha}\left[2\left(\frac{a}{r}\right)^{3/2} J_{3/2}(\alpha r)\sin\theta\cos\phi\,\hat{\underline{r}}\right.$$

$$+\left\{\left(\alpha a\left(\frac{a}{r}\right)^{1/2}\left[J_{1/2}(\alpha r) - \left(\frac{a}{r}\right)^{1/2} J_{1/2}(\alpha a)\right]\right.\right.$$

$$\left.\left. - \left(\frac{a}{r}\right)^{3/2} J_{3/2}(\alpha r)\right)\cos\theta\cos\phi - \alpha a\left(\frac{a}{r}\right)^{1/2} J_{3/2}(\alpha r)\sin\phi\right\}\hat{\underline{\theta}}$$

$$+\left\{\left(\left(\frac{a}{r}\right)^{3/2} J_{3/2}(\alpha r) - \alpha a\left(\frac{a}{r}\right)^{1/2}\left[J_{1/2}(\alpha r) - \left(\frac{a}{r}\right)^{1/2} J_{1/2}(\alpha a)\right]\right)\sin\phi\right.$$

$$\left. - \alpha a\left(\frac{a}{r}\right)^{1/2} J_{3/2}(\alpha r)\cos\theta\cos\phi\right\}\hat{\underline{\phi}}\,\Big] \,. \qquad (5.15)$$

In a similar manner to Chapter 4, we find that the relative helicity takes the form

$$H = (D_2^0)^2 H_2^0 + (D_1^1)^2 H_1^1 \qquad (5.16)$$

where

$$H_2^0 = \frac{64}{15} B_0^2 a^4 \left\{1 - \frac{1}{2}\frac{\sin 2\alpha a}{\alpha a} - \frac{3}{(\alpha a)^2}\right.$$

$$\left. - 3\frac{\cos 2\alpha a}{(\alpha a)^2} + \frac{6\sin 2\alpha a}{(\alpha a)^3} - \frac{3}{(\alpha a)^4} + 3\frac{\cos 2\alpha a}{(\alpha a)^4}\right\} \qquad (5.17)$$

and

$$H_1^1 = \frac{16}{3} B_0^2 a^4 \left\{1 + \frac{1}{2}\frac{\sin 2\alpha a}{\alpha a} - \frac{3}{2}\frac{1}{(\alpha a)^2}\right.$$

$$\left. + \frac{1}{2}\frac{\cos 2\alpha a}{(\alpha a)^2} + \frac{\sin 2\alpha a}{(\alpha a)^3} - \frac{1}{2}\frac{1}{(\alpha a)^4} + \frac{1}{2}\frac{\cos 2\alpha a}{(\alpha a)^4}\right\} \qquad (5.18)$$

Again, we remind the reader that if $D_1^1 \neq 0$ then it is understood that $\alpha a = \alpha_0 a$.

5.7 Magnetic Energy

In a similar way to before, the magnetic energy of the field (5.8), (5.9) and (5.10), with the condition (5.1), may be written as

$$W = (D_2^0)^2 W_2^0 + (D_1^1)^2 W_1^1 \qquad (5.19)$$

and the components are found after some calculation to be

$$W_2^0 = \frac{32 B_0^2 a^3 (\alpha a)}{15\mu_0}\left\{1 - \frac{3}{(\alpha a)^2} - \frac{3\sin 2\alpha a}{(\alpha a)^3} - \frac{9}{2}\frac{1}{(\alpha a)^4} - \frac{27}{2}\frac{\cos 2\alpha a}{(\alpha a)^4} + 18\frac{\sin 2\alpha a}{(\alpha a)^5} - \frac{9}{(\alpha a)^6} + 9\frac{\cos 2\alpha a}{(\alpha a)^6}\right\} \qquad (5.20)$$

and

$$W_1^1 = \frac{8 B_0^2 a^3 (\alpha a)}{3\mu_0}\left\{1 - \frac{1}{(\alpha a)^2} + \frac{\sin 2\alpha a}{(\alpha a)^3} - \frac{1}{2}\frac{1}{(\alpha a)^4} + \frac{\cos 2\alpha a}{2(\alpha a)^4}\right\}. \qquad (5.21)$$

5.8 Predicted States

(i) <u>H has a value admitting a purely symmetric field with $0 \le \alpha a \le \alpha_0 a$</u>

In this case the purely symmetric field is the minimum-energy state. The relative helicity as a function of αa is, from (5.5), (5.16) and (5.17) with $D_1^1 = 0$,

$$H = \frac{2\pi B_0^2 a^4 (\alpha a)}{15\left\{\left(\frac{3}{(\alpha a)^2} - 1\right)\sin\alpha a - \frac{3}{\alpha a}\cos\alpha a\right\}^2}\left\{1 - \frac{1}{2}\frac{\sin 2\alpha a}{\alpha a} - \frac{3}{(\alpha a)^2} - \frac{3\cos 2\alpha a}{(\alpha a)^2} + \frac{6\sin 2\alpha a}{(\alpha a)^3} - \frac{3}{(\alpha a)^4} + \frac{3\cos 2\alpha a}{(\alpha a)^4}\right\}, \qquad (5.22)$$

From (5.5), (5.19) and (5.20) with $D_1^! = 0$, the corresponding magnetic energy is

$$W_{SYM} = \frac{}{15\mu_0\left\{\left(\frac{3}{(\alpha a)^2}-1\right)\sin\alpha a - \frac{3\cos\alpha a}{\alpha a}\right\}^2}\left\{1 - \frac{3}{(\alpha a)^2}\right.$$

$$- \frac{3\sin 2\alpha a}{(\alpha a)^3} - \frac{9}{2}\frac{1}{(\alpha a)^4} - \frac{27}{2}\frac{\cos 2\alpha a}{(\alpha a)^4}$$

$$\left. + 18\frac{\sin 2\alpha a}{(\alpha a)^5} - \frac{9}{(\alpha a)^6} + 9\frac{\cos 2\alpha a}{(\alpha a)^5}\right\}. \quad (5.23)$$

(ii) H is such that the purely symmetric field has $\alpha a \geq \alpha_0 a$

The mixed state with $\alpha a = \alpha_0 a$ is the minimum-energy solution. From (5.5), (5.6), (5.16), (5.17) and (5.18) we find that

$$H = 0.599121\,\pi B_0^2 a^4 + 5.081651\,(D_1^!)^2 B_0^2 a^4 \quad (5.24)$$

which determines $D_1^!$ if H is specified. In a similar way, from (5.5), (5.6), (5.19), (5.20) and (5.21) and substituting for $(D_1^!)^2$ from (5.24), we obtain the result

$$W_{MIX} = \frac{\pi B_0^2 a^3}{\mu_0}\left\{2.246704\,\frac{H}{\pi B_0^2 a^4} - 0.133333\right\}. \quad (5.25)$$

It is interesting to compare (5.24) and (5.25) with (4.35) and (4.36).

5.9 Remarks on the Results

Again, we have plotted graphs involving the quantities αa, H, W_{SYM} and W_{MIX}.

Figure 5.2 shows that, for values of H greater than approximately 0.6, a *mixed* state is predicted, in direct contrast with Figure 4.2, which indicates for that case that the

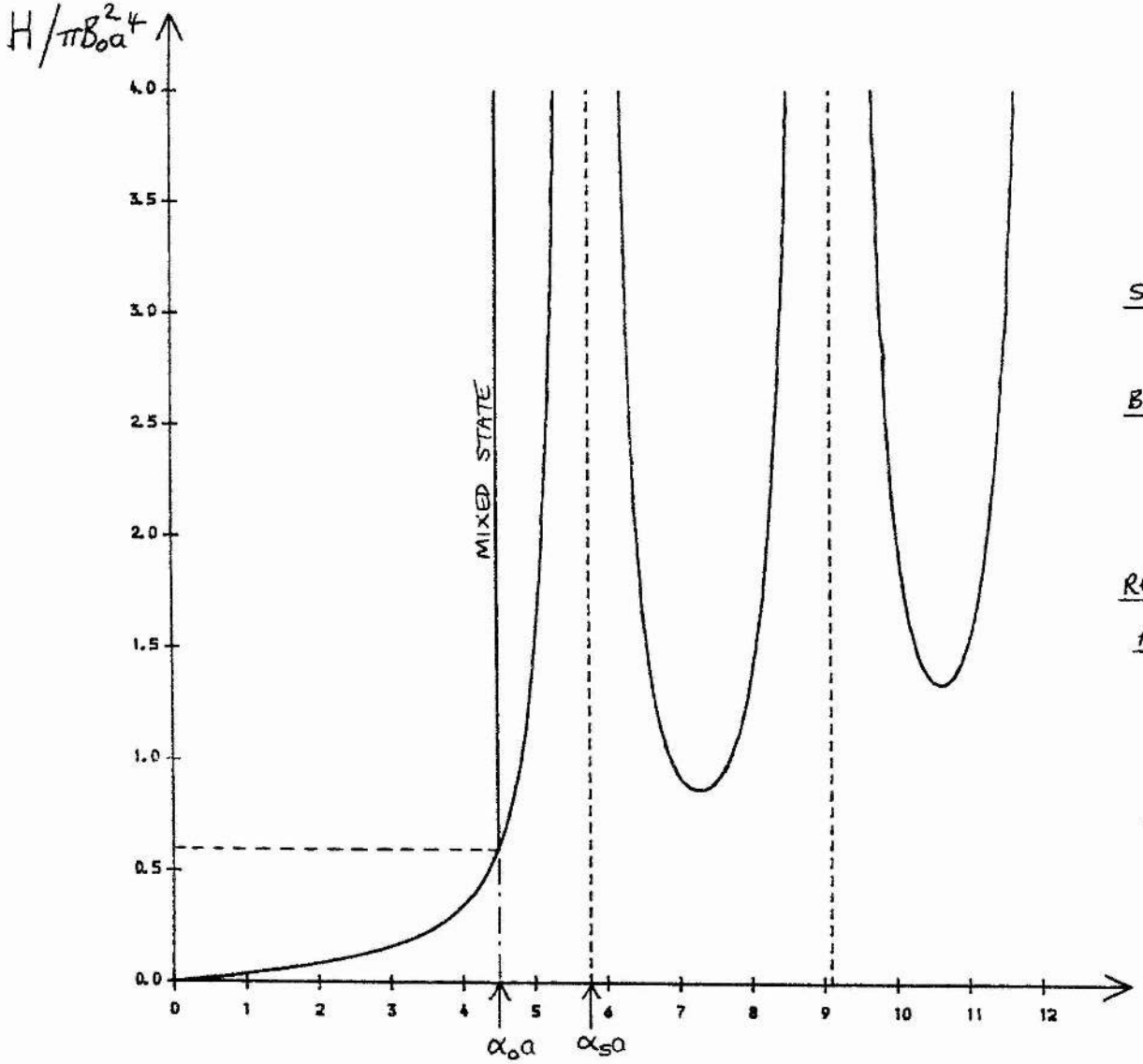

SPHEROMAK WITH

$P_2(\cos\theta)$

BOUNDARY FIELD:

RELATIVE HELICITY

AGAINST ALPHA

Figure 5·1

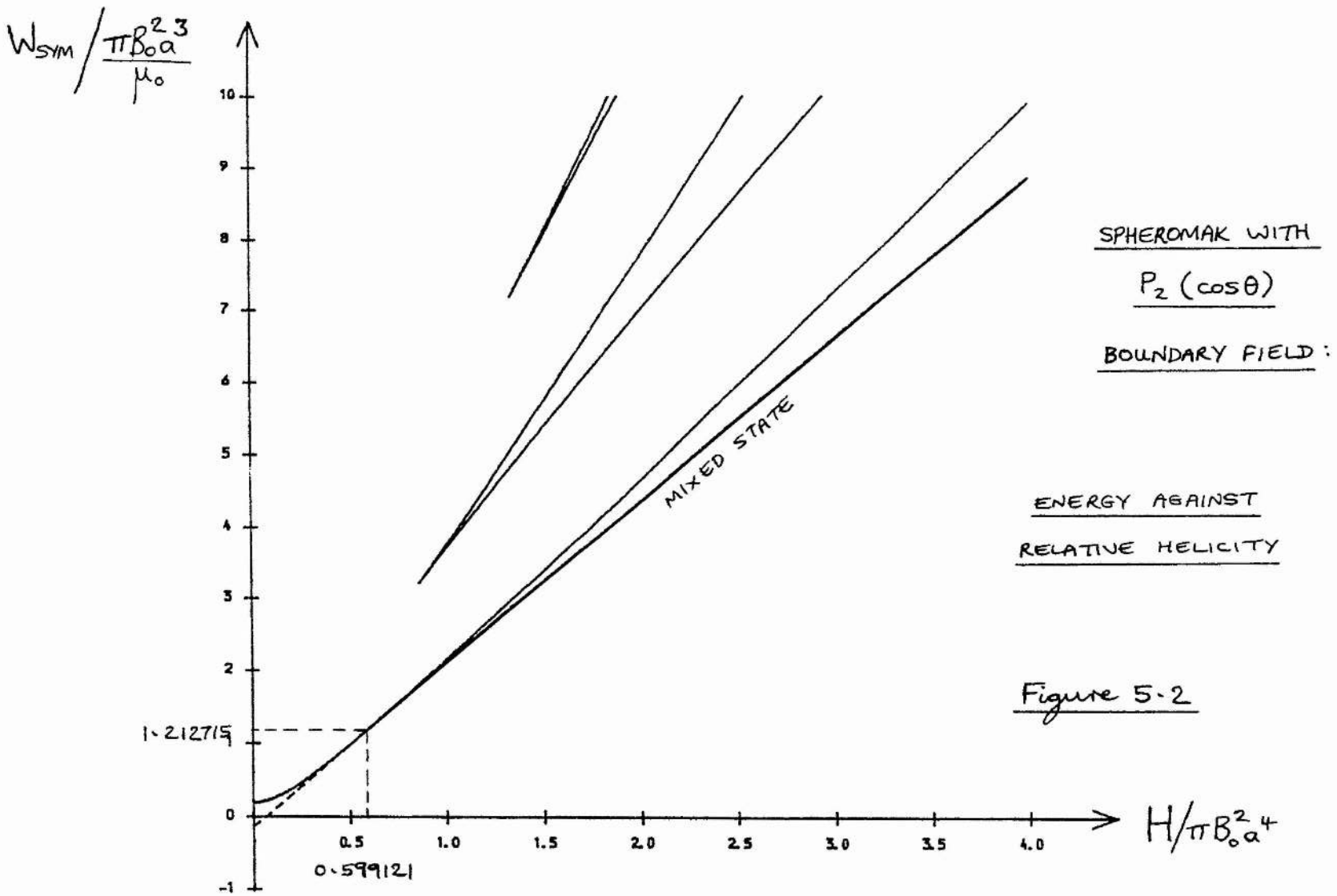
$W_{SYM} / \frac{\pi B_0^2 a^3}{\mu_0}$
10
9
8
7
6
5
4
3
2
1·212715
0
-1
0·5
0·599121
1.0
1.5
2.0
2.5
3.0
3.5
4.0
$H/\pi B_0^2 a^4$
MIXED STATE
SPHEROMAK WITH
$P_2(\cos\theta)$
BOUNDARY FIELD:
ENERGY AGAINST
RELATIVE HELICITY

Figure 5·2

minimum-energy state must always be purely symmetric.

The difference between Figure 5.1 and Figure 4.1 clearly demonstrates how changing the imposed boundary field distribution has altered the nature of the relaxed state. The decisive factor is seen to be the ordering of $\alpha_0 a$ and $\alpha_S a$. If $\alpha_0 a < \alpha_S a$, as in Figure 5.1, then for sufficiently large values of H the lowest-energy state is fully three-dimensional. If $\alpha_0 a > \alpha_S a$, as in Figure 4.1, then the relaxed state is always axi-symmetric, regardless of the value of H.

5.10 Appearance of the Relaxed Configuration

We should like to be able to see what the minimum-energy configuration looks like, that is, to produce field-line plots for a number of different values of the relative helicity. Now the relaxed configuration (5.8) is of the form

$$\underline{B} = D_2^0(\alpha)\,\underline{B}_2^0(r,\theta) + D_1^1(\alpha)\,\underline{B}_1^1(r,\theta,\phi) \qquad (5.26)$$

$$= B_r\,\hat{\underline{r}} + B_\theta\,\hat{\underline{\theta}} + B_\phi\,\hat{\underline{\phi}}\,, \qquad (5.27)$$

and in principle the equation of the field-lines is determinable from the standard formula, namely

$$\frac{dr}{B_r} = \frac{r\,d\theta}{B_\theta} = \frac{r\sin\theta\,d\phi}{B_\phi}\,. \qquad (5.28)$$

However, with the components of the field obtained from (5.9) and (5.10), there arise certain difficulties.

The first problem encountered is that, if $D_1^1 \neq 0$, then (5.28) is an 'inseparable form' and cannot be integrated analytically ; there is no flux function representation for the field. Therefore for mixed-field solutions it is necessary to integrate the field-line equations

numerically. This was indeed attempted using a computer program package for solving ordinary differential equations.

The approach adopted was to solve (5.28) in the (r,θ) plane, that is, for a fixed value of ϕ. It was at this stage that the second difficulty arose. It was found for mixed fields that the field-lines did not form closed patterns in the plane. A possible explanation accounting for this behaviour is that the field-lines may be *ergodic* , in which case the field is no longer describable in terms of field-lines. A method which could possibly be tried is to produce so-called *puncture plots* . These consist of diagrams of the intersections in a plane of a chosen 'field-line' as it journeys endlessly round the container. If one is fortunate, a definite pattern may emerge.

Because of the above setbacks, it was necessary to abandon any attempts to plot the non-axi-symmetric fields, and instead to devote all our attention to the mapping of purely symmetric states. This will be described in the remaining sections of this chapter.

5.11 Exterior Potential Field

5.11.1 Potential Field

Consider the '$\alpha a = 0$' solution within the sphere, subject to the boundary condition (5.1), which is given by (5.11). Taking the limit as $\alpha a \to 0$ of the flux-function (5.3), one finds that the equation governing the field-lines of the potential field is

$$r^3 \sin^2\theta \cos\theta = \text{CONSTANT} \tag{5.29}$$

in spherical polar notation. Defining cartesian co-ordinates

$$x \equiv r\sin\theta \tag{5.30}$$

and

$$y \equiv r\cos\theta \tag{5.31}$$

(5.29) may be re-written in the form

$$x^2 y = \text{CONSTANT} \tag{5.32}$$

which shows clearly that the potential-field solution corresponding to the boundary condition (5.1) has field-lines which are hyperbolae. In the (x,y) system defined by (5.30) and (5.31), the two components of the field (5.11) are

$$B_x = -\frac{1}{2} B_0 \left(\frac{x}{a}\right) \tag{5.33}$$

and

$$B_y = B_0 \left(\frac{y}{a}\right) . \tag{5.34}$$

5.11.2 Exterior Field

We shall assume that the relaxed field outside the sphere is a continuation of the internal potential field described by (5.11). In Figure 5.3 we have sketched a few typical field-lines for the case where both interior and exterior fields are potential. The dotted line, lying at $\theta = (1/2)\cos^{-1}(-1/3)$, has the property that the field at any point on it has no radial component. This line also divides the curved boundary into two distinct regions : below the line flux is entering the sphere, whereas above the line flux is leaving. Using the r-component of (5.11), we find that the amount of magnetic flux crossing the boundary in Figure 5.3 between the dotted line and $\theta = \pi/2$ per unit angle ϕ is given by

$$F = \frac{B_0 a^2}{3\sqrt{3}} . \tag{5.35}$$

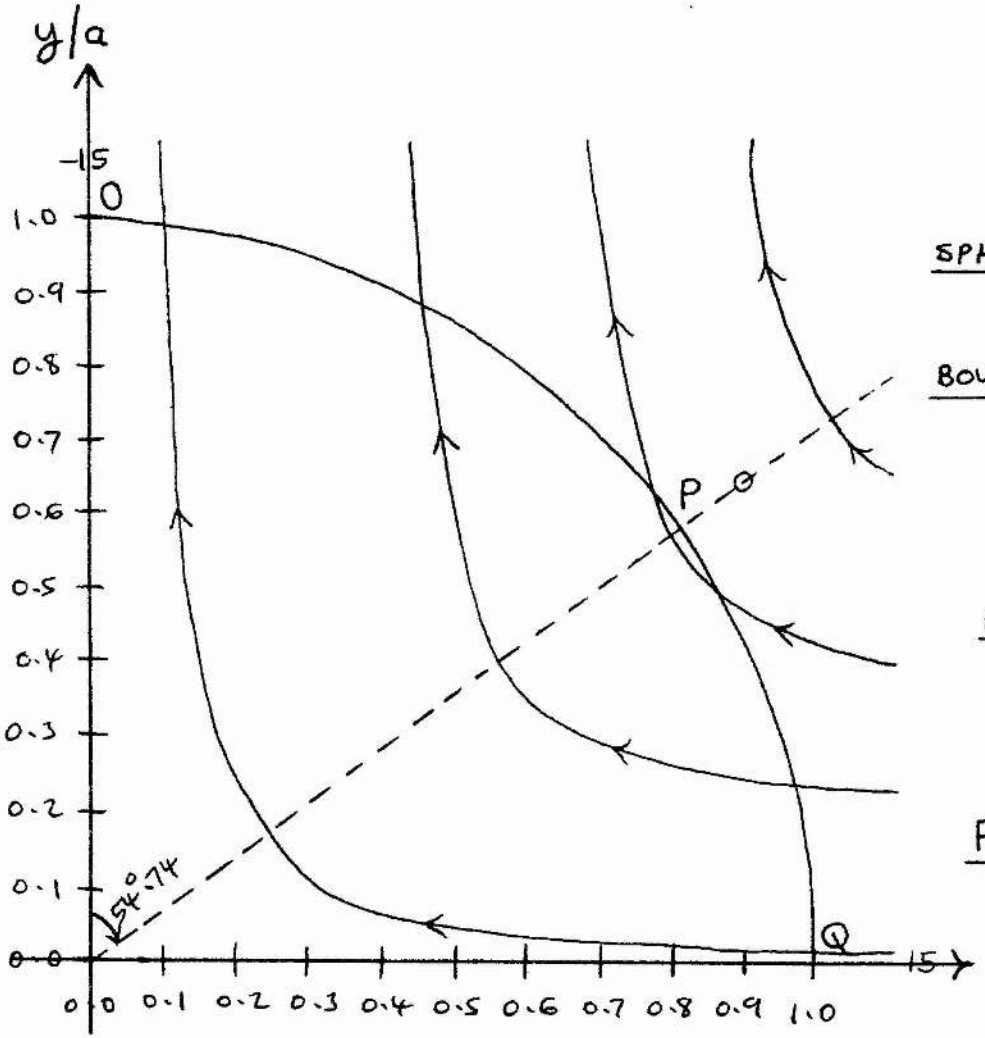

SPHEROMAK WITH $P_2(\cos\theta)$ BOUNDARY CONDITION:

SKETCH OF POTENTIAL FIELD.

Figure 5.3

We shall divide the flux entering the region between P and Q in Figure 5.3 into equal parts, so that the points of division are the positions of intersection of field-lines with the boundary. A summary of the method is as follows.

Let the arc PQ be divided into 15 segments, and the separation points in θ be defined as $\theta_0, \theta_1, ..., \theta_{14}$ and θ_{15}, where θ_0 represents P and θ_{15} represents Q. Using (5.11), we find that the magnetic flux *entering* the sphere between the points θ_n and θ_{n+1} is

$$\Delta F_n^{n+1} = \frac{1}{2} B_0^2 a^2 \left(\sin^2\theta_n \cos\theta_n - \sin^2\theta_{n+1} \cos\theta_{n+1} \right) \quad (5.36)$$

which is by definition equal to one fifteenth of F, given in turn by (5.35). We therefore deduce that

$$\sin^2\theta_{n+1} \cos\theta_{n+1} = \sin^2\theta_n \cos\theta_n - \frac{2}{45\sqrt{3}} \quad (5.37)$$

and hence that

$$\cos^3\theta_n - \cos\theta_n + \frac{2}{3\sqrt{3}} \left(1 - \frac{n}{15} \right) = 0 . \quad (5.38)$$

Writing $z = \cos\theta_n$, for each n the three candidate roots of (5.38) may be written

$$z_1 = \frac{2}{\sqrt{3}} \left(\frac{1}{3} \psi \right) \quad (5.39)$$

$$z_2 = \frac{2}{\sqrt{3}} \cos\left\{ \frac{1}{3} (\psi + 2\pi) \right\} \quad (5.40)$$

and

$$z_3 = \frac{2}{\sqrt{3}} \cos\left\{ \frac{1}{3} (\psi + 4\pi) \right\} \quad (5.41)$$

where

$$\cos\psi = -\left(1 - \frac{n}{15}\right). \qquad (5.42)$$

Only one of the above three roots (5.39), (5.40) and (5.41) in each case corresponds to a value of θ_n lying between P and Q, for which we require

$$0 \leqslant z \leqslant 0.577 \quad . \qquad (5.43)$$

It turns out that the significant root is always given by (5.41) for points on PQ.

A similar analysis may be performed to determine the positions of boundary field-lines lying on the arc OP, which we label with values of n from -15 (point O, $\theta = 0$) to 0 (point P, $\theta = \theta_0$). In this case we require the root z to lie in the range

$$0.577 \leqslant z \leqslant 1 \qquad (5.44)$$

and the appropriate roots for OP are given by (5.39) with n in (5.42) replaced by (-n).

The values of intersection in θ for the whole arc OQ are tabulated in Figure 5.4, and the positions on the boundary shown in Figure 5.5.

5.12 Plotting Symmetric Fields

From (5.28), the standard equation describing field-lines in the r-θ plane is

$$\frac{dr}{d\theta} = \frac{r B_r}{B_\theta} \quad . \qquad (5.45)$$

In the case of axi-symmetric fields we have from (5.2) and (5.9) that

$$B_r = D_2^0 B_0 \left(\frac{a}{r}\right)^{3/2} J_{5/2}(\alpha r)(1 + 3\cos 2\theta) \qquad (5.46)$$

n	θ_n
-15	0·000 000 000 (Q)
-14	0·161 952 955
-13	0·231 695 465
-12	0·287 251 890
-11	0·336 014 696
-10	0·380 904 022
-9	0·423 494 860
-8	0·464 820 784
-7	0·505 682 206
-6	0·546 808 165
-5	0·588 981 817
-4	0·633 196 171
-3	0·680 944 732
-2	0·734 973 451
-1	0·802 198 568
0	0·955 316 618 (P)

SPHEROMAK WITH

$P_2(\cos\theta)$

BOUNDARY FIELD:

TABLE OF

POSITIONS OF

BOUNDARY

FIELD-LINES.

Figure 5.4

n	θ_n
0	0·955 316 618 (P)
1	1·102 985 548
2	1·164 298 256
3	1·211 880 041
4	1·252 558 888
5	1·288 969 610
6	1·322 463 038
7	1·353 844 721
8	1·383 644 409
9	1·412 236 110
10	1·439 899 127
11	1·466 852 206
12	1·493 274 182
13	1·519 317 325
14	1·545 116 564
15	1·570 796 327 (Q)

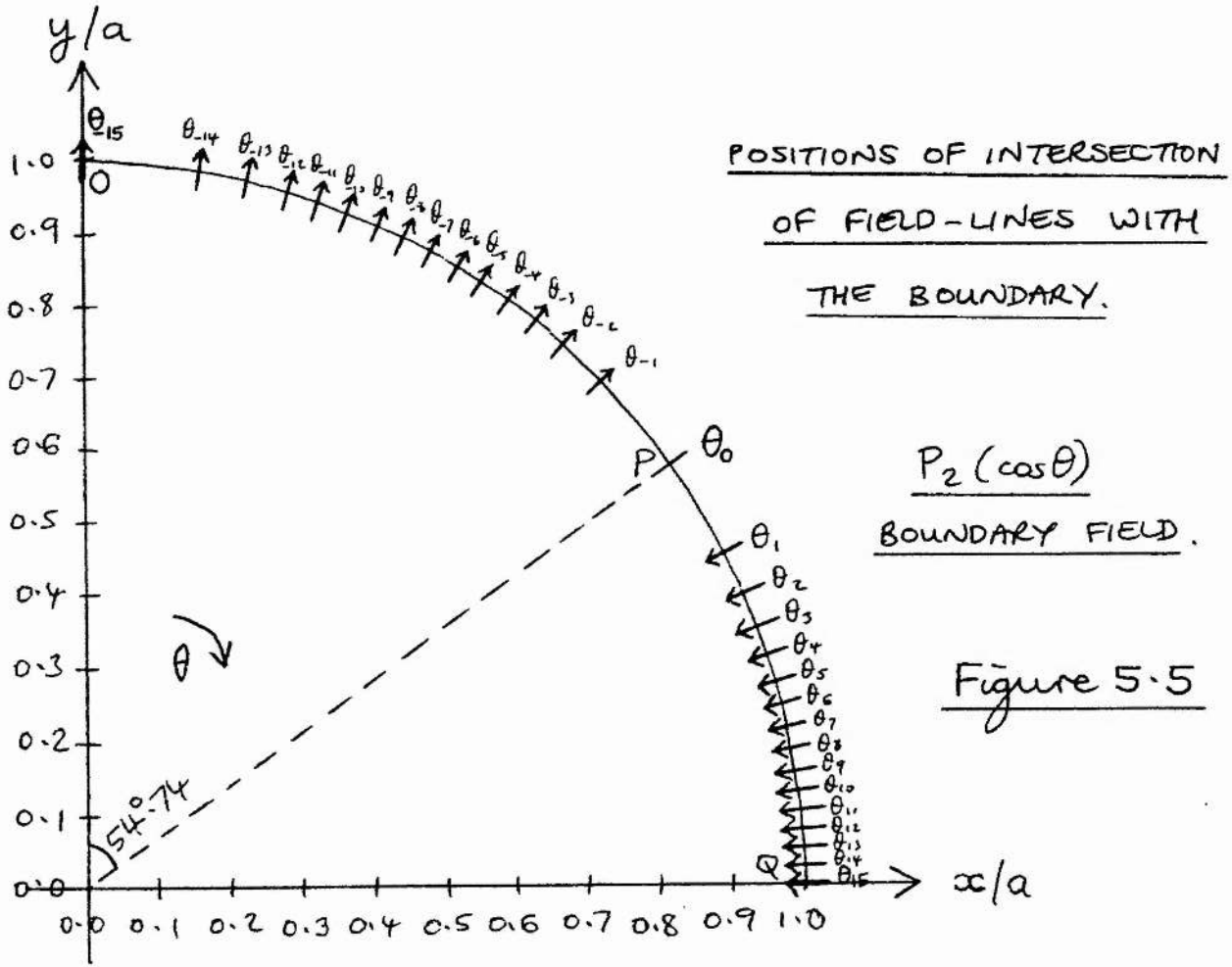

POSITIONS OF INTERSECTION OF FIELD-LINES WITH THE BOUNDARY.

$P_2(\cos\theta)$ BOUNDARY FIELD.

Figure 5·5

and

$$B_\theta = D_2^\circ B_\circ \left\{ 2\left(\frac{a}{r}\right)^{3/2} J_{5/2}(\alpha r) - (\alpha a)\left(\frac{a}{r}\right)^{1/2} J_{3/2}(\alpha r) \right\} \sin 2\theta \quad (5.47)$$

Substituting (5.46) and (5.47) into (5.45), this may be rearranged into the separable form

$$-\int \frac{\frac{d}{du}\left\{u^{1/2} J_{5/2}(u)\right\} du}{u^{1/2} J_{5/2}(u)} = \int \left(\frac{1+3\cos 2\theta}{\sin 2\theta}\right) d\theta \quad (5.48)$$

where $u = \alpha r$. Performing the integration, we obtain the result

$$u^{1/2} J_{5/2}(u) \sin^2\theta \cos\theta = \text{CONSTANT} \quad (5.49)$$

for the equation of the field-lines, which we compare with (5.3).

In order to plot field-lines in the r-θ plane we must determine the values taken by the constant on the right-hand side of (5.49). For field-lines which cross the boundary at r = a between P and Q in Figure 5.5, this is done by substituting boundary values of $\sin^2\theta_n \cos\theta_n$ from (5.38) into (5.49), in which case we find that

$$\text{CONSTANT} = (\alpha a)^{1/2} J_{5/2}(\alpha a) \frac{2}{3\sqrt{3}} \left(1 - \frac{n}{15}\right) \quad (5.50)$$

where n = 1, 2, ..., 14, 15. In the case of 'island' field-lines, that is, those which do not cross the boundary at r = a , it can be shown that $n \leq 0$ in (5.50), that is, n = 0, -1, -2, -3, ... with the actual number of islands present depending on αa.

The number of islands may be determined as follows. Consider the line $\theta = \theta_0$ in Figure 5.5. From (5.38) we have that

$$\sin^2\theta_0 \cos\theta_0 = \frac{2}{3\sqrt{3}} \,. \quad (5.51)$$

Hence, combining (5.49) and (5.50) at $\theta = \theta_0$, using (5.51) and converting the Bessel functions into trigonometric functions, we obtain the equation

$$\frac{\left\{\left(\frac{3}{(\alpha r)^2} - 1\right)\sin\alpha r - \frac{3}{\alpha r}\cos\alpha r\right\}}{\left\{\left(\frac{3}{(\alpha a)^2} - 1\right)\sin\alpha a - \frac{3}{\alpha a}\cos\alpha a\right\}} = 1 - \frac{n}{15}, \quad (5.52)$$

from which may be found the two values of r for each value of αa at which closed field-lines intersect the line $\theta = \theta_0$.

The values of αa used for the field-line plots were 0.25, 2.20, 3.30, 3.85, 4.15 and 4.35, giving corresponding values for the relative helicity of about 0.01, 0.10, 0.20, 0.30, 0.40 and 0.50 respectively. It was found that islands were visible only for the cases $\alpha a = 4.15$ and $\alpha a = 4.35$. The graphs of (5.52) for these two values of αa given in Figures 5.6 and 5.7 show that the islands number one and two respectively.

Thus, using the foregoing information, it was possible to determine an initial pair of values (r_0,θ_0) for each field-line to be plotted, enabling the trajectories of the field-lines to be found using a program for solving initial-value problems.

The resulting field-line plots for symmetric fields are shown as Figures 5.8 to 5.13 inclusive. Figure 5.8 shows a state close to the potential field configuration, and so the field-lines are nearly hyperbolic. As the dimensionless relative helicity $H / \pi B_0{}^2 a^4$ is increased by steps of about 0.1, the appearance of the field at first changes only slightly, but the noticeable trend is that field-lines are increasingly bowed towards the centre of the sphere. At $H \approx 0.30$ for the particular values chosen for the flux-function we begin to see the emergence of island structures. Close to the eigenvalue $\alpha_0 a = 4.49$ the magnetic field has a finite helicity and energy, as we should expect. Thus if the boundary condition is *purely* $P_2(\cos\theta)$, there appears to be no problem in attaining the value of αa required for the appearance of a mixed state. However, this is in general not true, as we shall discuss in the next chapter.

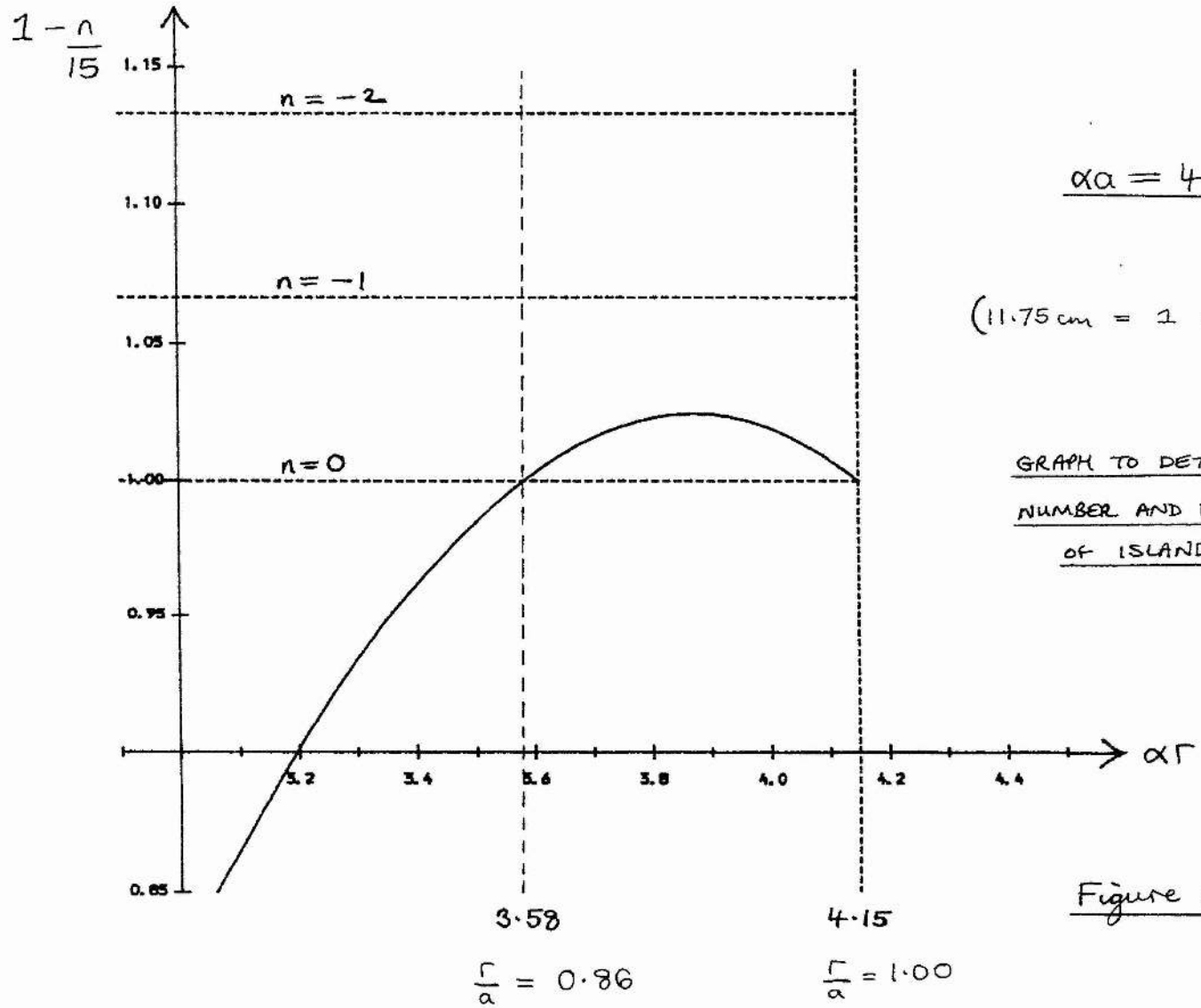

αa = 4·15

(11·75 cm = 1 unit of αr)

GRAPH TO DETERMINE NUMBER AND POSITIONS OF ISLANDS.

Figure 5·6

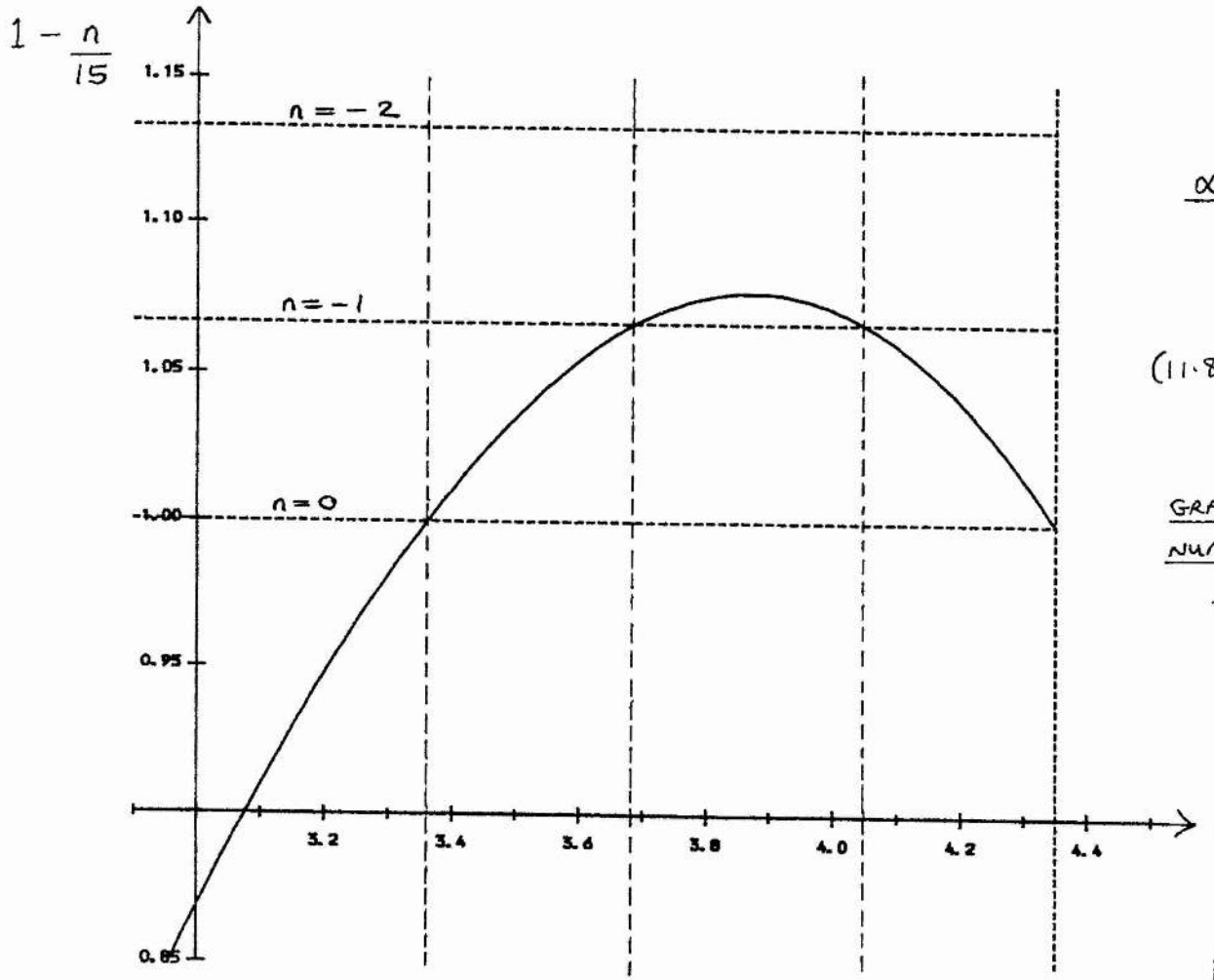

$\alpha a = 4.35$

(11.8 cm = 1 unit of αr)

GRAPH TO DETERMINE NUMBER AND POSITIONS OF ISLANDS.

Figure 5.7

3.36 3.69 4.05 4.35

$\frac{r}{a} = 0.77$ $\frac{r}{a} = 0.85$ $\frac{r}{a} = 0.93$ $\frac{r}{a} = 1.00$

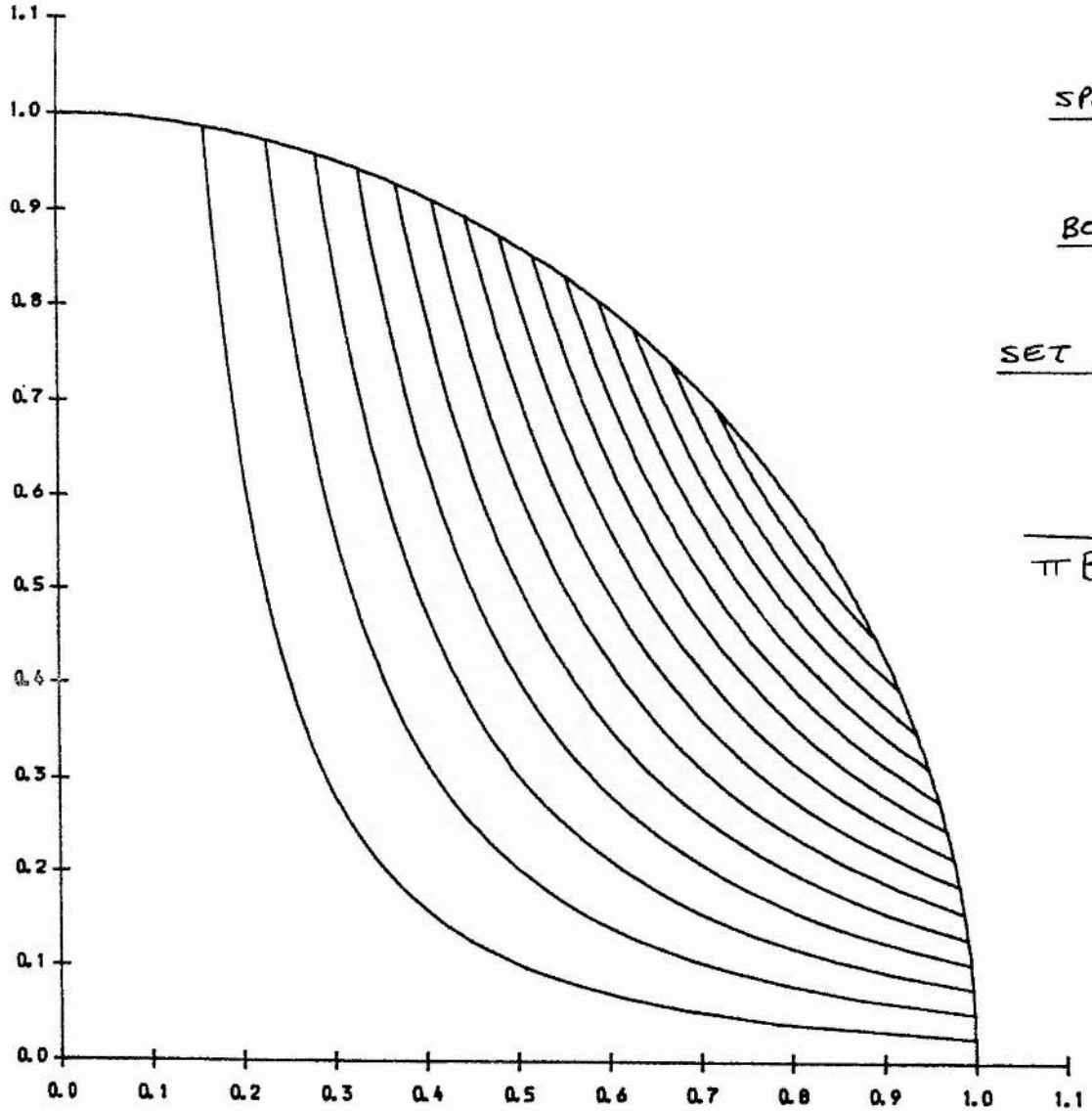

SPHEROMAK WITH

$P_2(\cos\theta)$

BOUNDARY FIELD:

SET OF SIX SYMMETRIC FIELD PLOTS.

$$\frac{H}{\pi B_0^2 a^4} = 0.01$$

$$\alpha a = 0.25$$

Figure 5.8

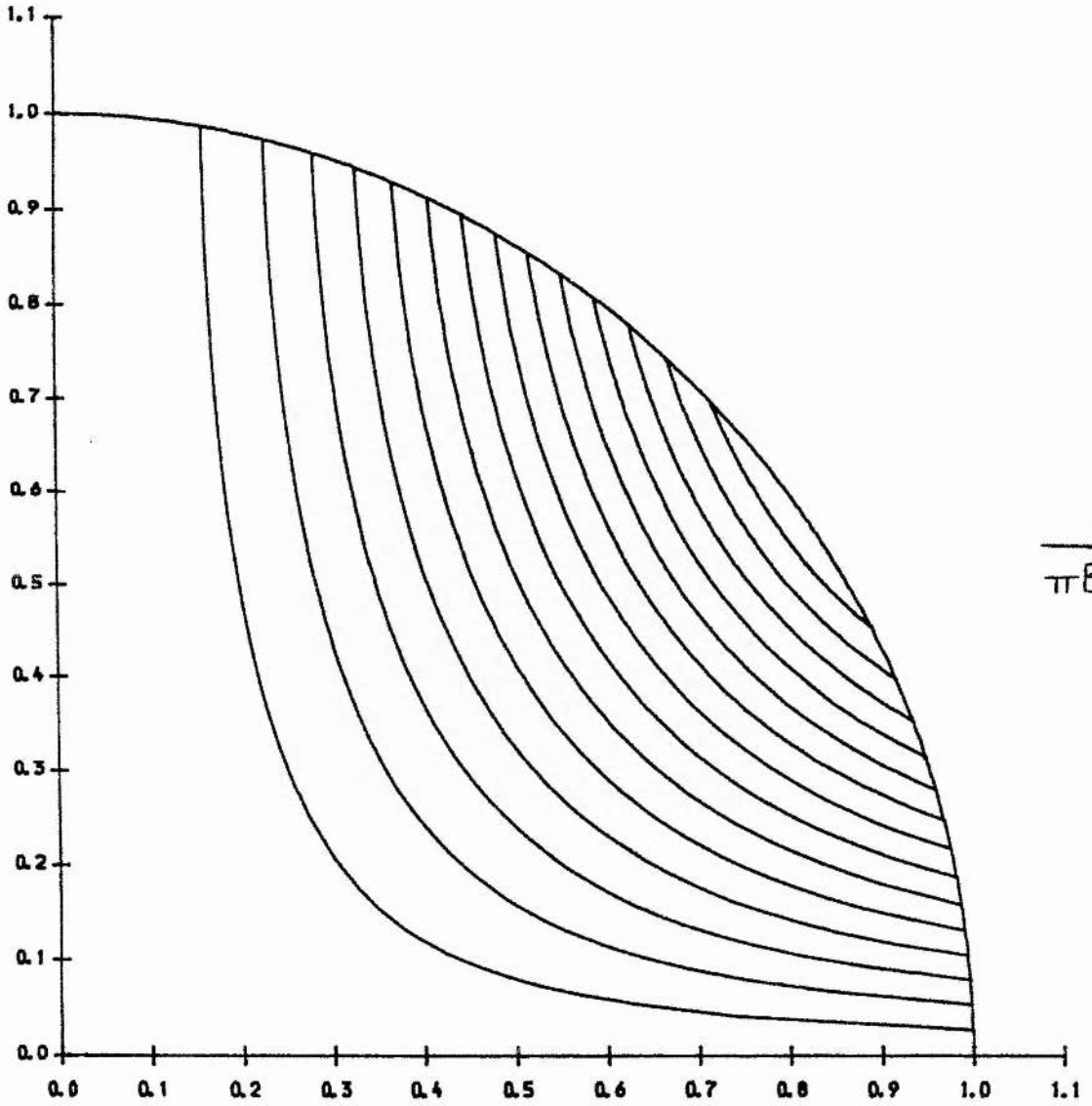

$$\frac{H}{\pi B_0^2 a^4} = \underline{0.10}$$

$$\alpha a = \underline{2.20}$$

Figure 5.9

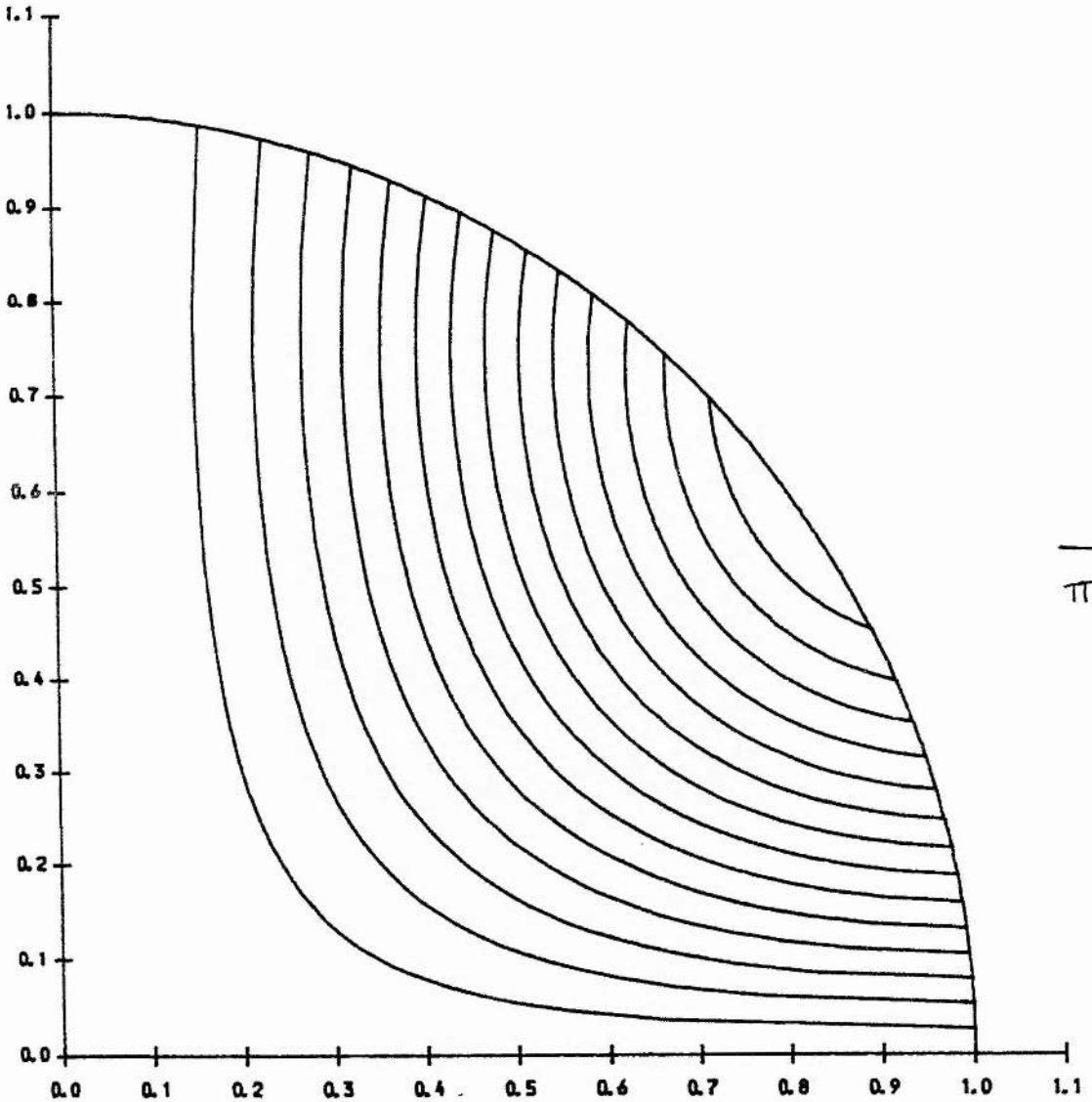

$$\frac{H}{\pi B_o^2 a^4} = \underline{0.20}$$

$$\alpha a = \underline{3.30}$$

Figure 5.10

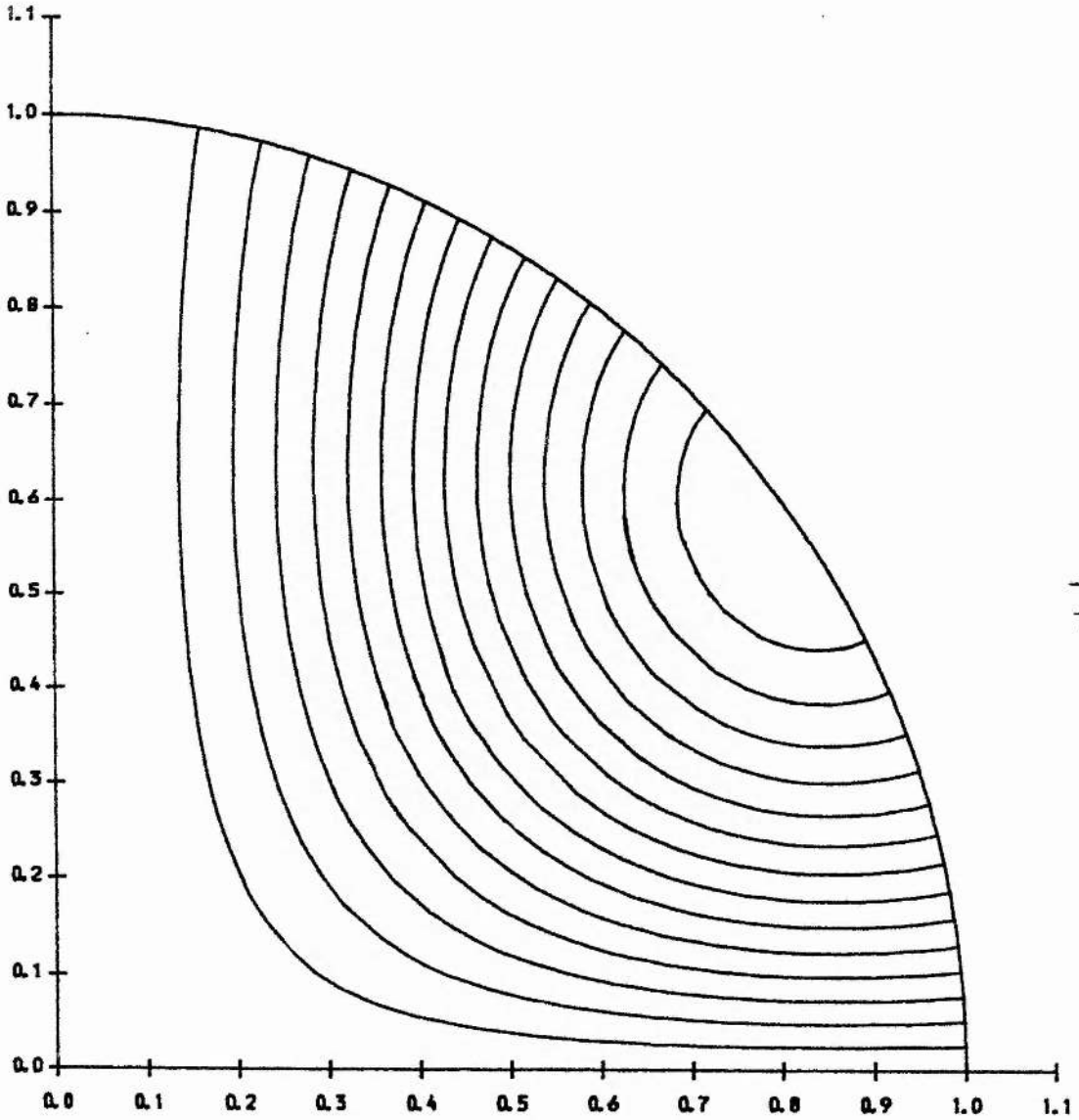

$$\frac{H}{\pi B_0^2 a^4} = \underline{0.30}$$

$$\alpha a = \underline{3.85}$$

Figure 5.11

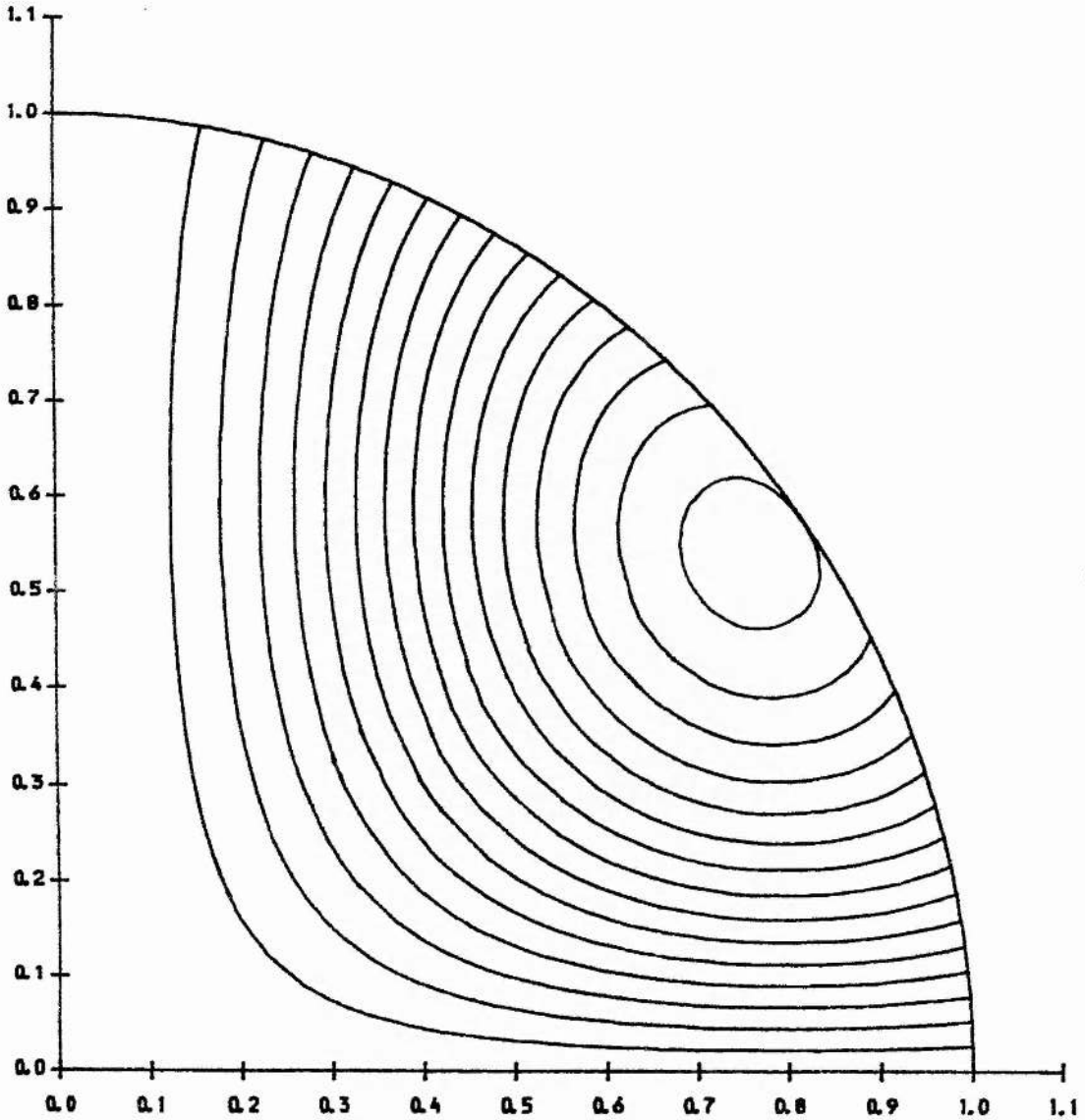

$$\frac{H}{\pi B_o^2 a^4} = \underline{0.40}$$

$$\alpha a = \underline{4.15}$$

Figure 5.12

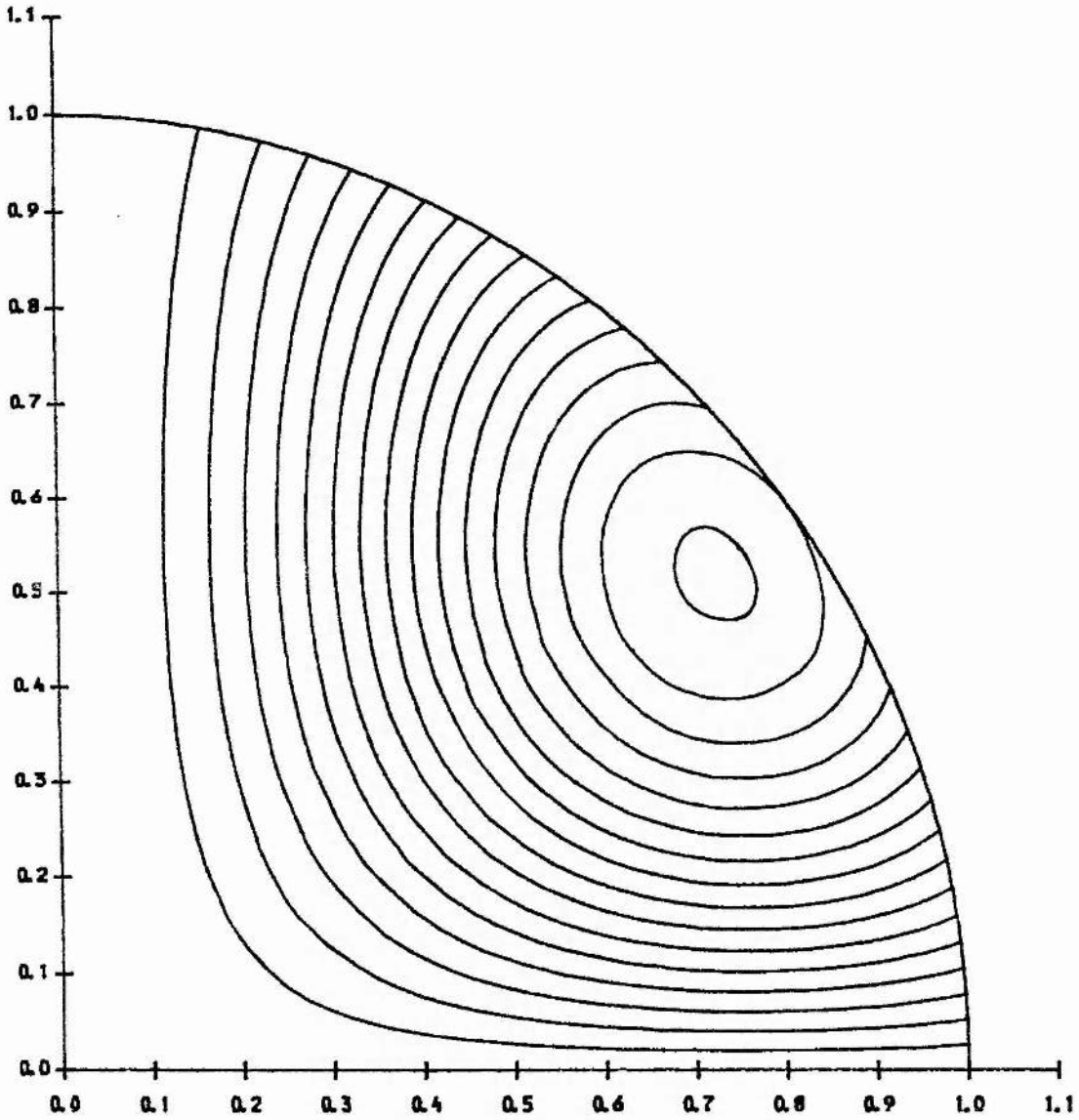

$$\frac{H}{\pi B_0^2 a^4} = \underline{0.50}$$

$$\alpha a = \underline{4.35}$$

Figure 5.13

CHAPTER SIX : SPHEROMAK WITH BOUNDARY POINT SOURCES

6.1 General Boundary Fields

We can in principle express a general axi-symmetric boundary field as a linear combination of Legendre polynomials in $\cos\theta$ of the form

$$B_r(a) = c_1 P_1(\cos\theta) + c_2 P_2(\cos\theta) + c_3 P_3(\cos\theta) + \ldots \quad (6.1)$$

where the c_n , n = 1, 2, 3, ... are constants.

Now such a boundary condition would be expected to introduce 'resonance' behaviour into the general solution (4.1), (4.2) and (4.3). This would occur at values of αa which are zeros of $J_{3/2}(x)$, $J_{5/2}(x)$, $J_{7/2}(x)$, ... In general, if $c_n \neq 0$ in (6.1) then zeros of $J_{n+1/2}(x)$ will be singular values characteristic of the relaxed state. It follows in particular that if $c_1 \neq 0$ then the first resonance encountered will occur at the lowest positive zero of $J_{3/2}(x)$, that is, when $\alpha a = 4.49$. Thus the behaviour of the field as this value is approached is qualitatively the same as was found in Chapter 4, where the boundary condition was purely $P_1(\cos\theta)$.

We conclude that if a boundary field has a non-zero amount of P_1 present, then the corresponding field within the sphere will 'resonate' at the value of αa given by (4.14). As a result, all minimum-energy states will be axi-symmetric, as in Chapter 4. The behaviour found in Chapter 5 where the relaxed state could be asymmetric is thus rather pathological.

We shall now go on to describe fields more general than in Chapters 4 and 5. In particular, we shall consider fields generated by boundary point sources.

6.2 General Axi-Symmetric Fields : Boundary Point Sources

We are interested in solutions of the linear force-free equation (1.5) in a sphere which has localized sources and sinks of magnetic flux on the boundary. We shall consider first the case in which there is a 'point source' located at $\theta = \pi$ and a 'point sink' at $\theta = 0$. This may be regarded as an idealization of a PS-1 type spheromak (Figure 6.1).

Later in this chapter, we shall consider the more general case where the 'point sink' becomes a 'ring sink' positioned at some latitude $\theta = \theta^*$. For values of θ^* sufficiently close to π , the boundary distribution may model the concentric cylindrical electrodes of spheromaks of the 'gun-injection' type, such as described by Hammer (1984).

For solutions of the linear force-free equation in cylindrical polar geometry we refer the reader to the paper by Turner (1984), who solved the point source problem by means of a Green's function method. Here we employ a more direct approach, as follows.

6.3 Mathematical Solution

We consider general axi-symmetric solutions of (1.5), given by setting $m = 0$ in the general solution (4.1), (4.2) and (4.3) and summing over all n , namely

$$B_r = \sum_{n=0}^{\infty} C_n \, n(n+1) \left(\frac{a}{r}\right)^{3/2} J_{n+\frac{1}{2}}(\alpha r) \, P_n(\cos\theta) \qquad (6.2)$$

$$B_\theta = \sum_{n=0}^{\infty} C_n \left\{ \alpha a \left(\frac{a}{r}\right)^{1/2} J_{n-\frac{1}{2}}(\alpha r) - n \left(\frac{a}{r}\right)^{3/2} J_{n+\frac{1}{2}}(\alpha r) \right\} \frac{d}{d\theta} P_n(\cos\theta) \qquad (6.3)$$

and

$$B_\phi = \sum_{n=0}^{\infty} C_n \left\{ - \alpha a \left(\frac{a}{r}\right)^{1/2} J_{n+\frac{1}{2}}(\alpha r) \frac{d}{d\theta} P_n(\cos\theta) \right\} \qquad (6.4)$$

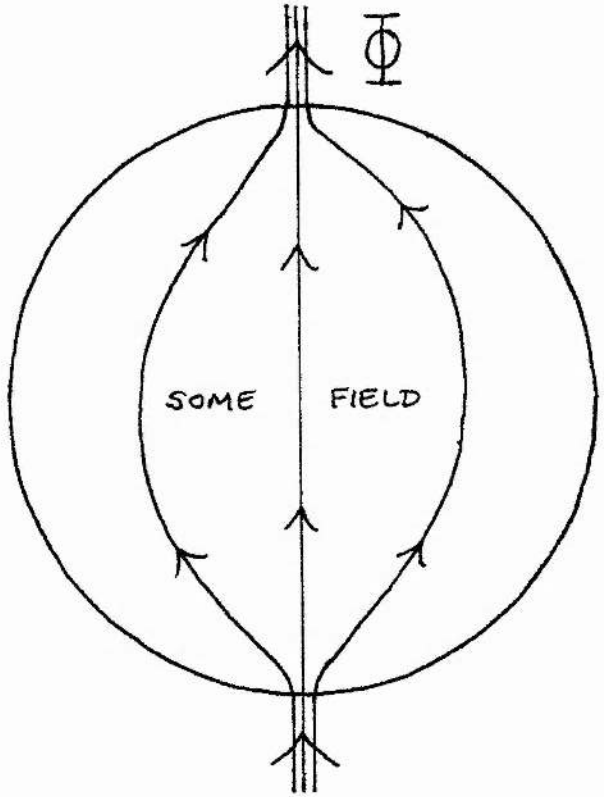

(r, θ, ϕ)

SPHERE
RADIUS a

SPHEROMAK WITH
AXIAL FLUX
INJECTION.

Figure 6·1

where the P_n are the Legendre polynomials and the C_n are constants, to be determined.

For an injected axial flux Φ, the boundary radial magnetic field shown in Figure 6.1 may be written in terms of delta functions as

$$B_r(a) = \frac{\Phi}{2\pi a^2}\{\delta(s-1) - \delta(s+1)\} \tag{6.5}$$

where $s \equiv \cos\theta$ and a is the radius of the sphere. Equating (6.5) with (6.2) evaluated on $r = a$, we produce the relation

$$\sum_{n=0}^{\infty} C_n\, n(n+1)\, J_{n+\frac{1}{2}}(\alpha a)\, P_n(s) = \frac{\Phi}{2\pi a^2}\{\delta(s-1) - \delta(s+1)\}. \tag{6.6}$$

The coefficients C_n may be determined from (6.6) using the orthogonality property of the Legendre polynomials, namely

$$\int_{-1}^{1} P_m(s) P_n(s)\, ds = \begin{cases} 0, & m \neq n \\ \dfrac{2}{2n+1}, & m = n \end{cases}. \tag{6.7}$$

We find that

$$C_n = \frac{(2n+1)\,\Phi\,\{P_n(1) - P_n(-1)\}}{4\pi a^2\, n(n+1)\, J_{n+\frac{1}{2}}(\alpha a)}. \tag{6.8}$$

Since $P_n(-x) = P_n(x)$ for all x and $P_n(1) = 1$ for all n, the expression (6.8) simplifies to

$$C_n = \begin{cases} \dfrac{(2n+1)\,\Phi}{2\pi a^2\, n(n+1)\, J_{n+\frac{1}{2}}(\alpha a)}, & n \text{ odd} \\ 0, & n \text{ even}. \end{cases} \tag{6.9}$$

Thus (6.2), (6.3) and (6.4) with coefficients given by (6.9) constitute a formal series solution of $\nabla \times \underline{B} = \alpha \underline{B}$ where α is uniform, subject to the boundary distribution (6.5).

6.4 Flux Function Representation of the Field

It is desirable in order to plot flux surfaces of the field (6.2), (6.3) and (6.4) to be able to calculate the corresponding flux function. [We mention at this point that it is a general result for any system of co-ordinates (u_1, u_2, u_3) with scale factors (h_1, h_2, h_3) and corresponding field components (B_1, B_2, B_3) that if u_3 is an ignorable co-ordinate then the flux function $A \propto h_3 B_3$.] Using (6.4) and (4.4) we therefore find that an appropriate expression for the flux function in this case is

$$A = \sum_{n=0}^{\infty} C_n a^2 \left(\frac{r}{a}\right)^{1/2} J_{n+\frac{1}{2}}(\alpha r) \sin^2\theta P_n'(\cos\theta) \qquad (6.10)$$

in which the prime denotes differentiation with respect to the argument.

The formula (6.10) may be re-written in terms of the spherical Bessel functions, which are defined as

$$j_n(\alpha r) \equiv \left(\frac{\pi}{2\alpha r}\right)^{1/2} J_{n+\frac{1}{2}}(\alpha r) \qquad (6.11)$$

by use of the identity

$$(\cos^2\theta - 1) P_n'(\cos\theta) = n \cos\theta P_n(\cos\theta) - n P_{n-1}(\cos\theta) \qquad (6.12)$$

and by substitution of C_n from (6.9). Doing all this, we write the result in the form

$$\bar{A} \equiv \frac{2\pi A}{\Phi} = \sum_{\substack{n=1 \\ (\text{ODD})}}^{\infty} \left(\frac{2n+1}{n+1}\right)\left(\frac{r}{a}\right) \frac{j_n(\alpha r)}{j_n(\alpha a)} \{P_{n-1}(\cos\theta) - \cos\theta P_n(\cos\theta)\}. \qquad (6.13)$$

6.5 Boundary Values of A

Setting r = a in (6.13) and reverting to the 'derivative form' using (6.12), we have

$$\bar{A}(a) = -\sin\theta \frac{d}{d\theta}\left\{ \sum_{\substack{n=1 \\ (\text{ODD})}}^{\infty} \left(\frac{1}{n} + \frac{1}{n+1}\right) P_n(\cos\theta) \right\} \tag{6.14}$$

$$= -\frac{\sin\theta}{2} \frac{d}{d\theta}\left\{ \sum_{n=1}^{\infty} \left(\frac{1}{n} + \frac{1}{n+1}\right) P_n(\cos\theta) - \sum_{n=1}^{\infty} (-1)^n \left(\frac{1}{n} + \frac{1}{n+1}\right) P_n(\cos\theta) \right\} \tag{6.15}$$

$$= -\frac{\sin\theta}{2} \frac{d}{d\theta}\left\{ \sum_{n=1}^{\infty} \frac{1}{n} P_n(\cos\theta) - \sum_{n=1}^{\infty} \frac{(-1)^n}{n} P_n(\cos\theta) + \sum_{n=0}^{\infty} \frac{1}{(n+1)} P_n(\cos\theta) - \sum_{n=0}^{\infty} \frac{(-1)^n}{(n+1)} P_n(\cos\theta) \right\}. \tag{6.16}$$

All the series in (6.16) may be summed using directly or adapting results given by Mangulis (1965), pp. 124-125 to give

$$\bar{A}(a) = -\frac{\sin\theta}{2} \frac{d}{d\theta}\left\{ -\log\left[\sin\left(\frac{\theta}{2}\right)\left(\sin\left(\frac{\theta}{2}\right)+1\right)\right] + \log\left[\cos\left(\frac{\theta}{2}\right)\left(\cos\left(\frac{\theta}{2}\right)+1\right)\right] + \log\left[1+\operatorname{cosec}\left(\frac{\theta}{2}\right)\right] - \log\left[1+\sec\left(\frac{\theta}{2}\right)\right] \right\}, \quad 0 < \theta < \pi, \tag{6.17}$$

$$= -\frac{\sin\theta}{2} \frac{d}{d\theta}\left\{ \log\left[\frac{\cos\left(\frac{\theta}{2}\right)\left(\cos\left(\frac{\theta}{2}\right)+1\right)\cos\left(\frac{\theta}{2}\right)\left(1+\sin\left(\frac{\theta}{2}\right)\right)}{\sin\left(\frac{\theta}{2}\right)\left(\sin\left(\frac{\theta}{2}\right)+1\right)\sin\left(\frac{\theta}{2}\right)\left(1+\cos\left(\frac{\theta}{2}\right)\right)} \right] \right\} \tag{6.18}$$

$$= -\sin\theta \frac{d}{d\theta}\left\{ \log\left[\cot\left(\frac{\theta}{2}\right)\right] \right. \tag{6.19}$$

$$= -\sin\theta \cdot \frac{1}{\cot\left(\frac{\theta}{2}\right)} \left\{ -\frac{1}{2} \operatorname{cosec}^2\left(\frac{\theta}{2}\right) \right\} = 1. \tag{6.20}$$

Thus we see that the dimensionless form ($\bar{A}$) of the flux function takes the value unity on the curved part of the boundary of the sphere. The result (6.20) may be verified independently, as follows.

For symmetric fields ($\partial/\partial\phi = 0$), the r-component of $\nabla x\underline{B} = \alpha\underline{B}$ reads

$$\frac{1}{r^2 \sin\theta}\frac{\partial}{\partial\theta}(r\sin\theta\, B_\phi) = \alpha B_r \,, \tag{6.21}$$

which may be alternatively written using the definition (4.4) as

$$\frac{\partial}{\partial\theta} A(r,\theta) = r^2 \sin\theta\, B_r(r,\theta) \,. \tag{6.22}$$

Integrating (6.22) from $\theta = 0$ to $\theta = \pi/2$ and setting $r = a$, we have

$$A(a) = a^2 \int_0^{\pi/2} \sin\theta\, B_r(a,\theta)\, d\theta \,. \tag{6.23}$$

Now the magnetic flux crossing the boundary between $\theta = 0$ and $\theta = \pi/2$ is

$$2\pi a^2 \int_0^{\pi/2} \sin\theta\, B_r(a,\theta)\, d\theta = \Phi \,, \tag{6.24}$$

and so eliminating the integral between (6.23) and (6.24) and noting (6.13) we obtain

$$\bar{A}(a) = 1 \,, \tag{6.25}$$

in agreement with the result (6.20).

The value of $\bar{A}$ on $\theta = 0$ may be determined by substitution of $\cos\theta = 1$ into (6.13). Knowing that $P_n(1) = 1$ for all n, we see easily that

$$\bar{A}(\theta = 0) = 0 \,. \tag{6.26}$$

Thus the line $\theta = 0$ is a 'field-line', as we should expect from considerations of symmetry.

Since we expect the field-line plots to have symmetry about the plane $\theta = \pi/2$, the region of the cross-section of the sphere to which we shall focus our attention is the quarter circle in Figure 6.2, which shows the boundary values of the dimensionless form of the flux function. There is a discontinuity in the value of $\bar{A}$ located at $\theta = 0$, which corresponds to the position of the point source.

6.6 Programming the Contour Plots

In order to produce field-line diagrams for the boundary condition (6.5), we first used the formula (6.13) to calculate values of $\bar{A}$ on a regular grid in r/a and θ. It was found that the convergence of (6.13) was very poor on the boundary at $r = a$. Hence a large number of terms in the series was required to ensure distortion-free plots. In all, 750 terms were taken, counting of course only the odd values of n.

Second, the grid of values of $\bar{A}$ was then used as the data input for a contouring program specially adapted for use with polar co-ordinates. This program generated a set of grid files which were then converted into hard-copy output using GHOST graphics facilities.

6.7 Resonance Values of αa

In common with the problems treated in Chapters 4 and 5, we predict that the relaxed field inside the sphere will resonate for a certain discrete set of values of αa, by which we mean that the intensity of the field will become infinite. Given (6.9), which determines the coefficients C_n, it is clear, noting (6.11), that resonance will occur whenever αa coincides with any of the zeros of the spherical Bessel functions of odd order, that is, if

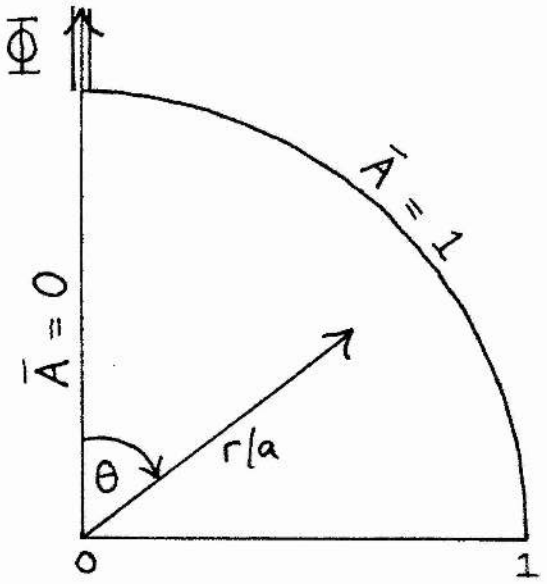

BOUNDARY VALUES OF THE FLUX FUNCTION.

Figure 6.2

$$j_n(\alpha a) = 0, \quad n = 1, 3, 5, \ldots . \tag{6.27}$$

Letting the s^{th} zero of $j_n(x)$ be denoted by $\lambda_{n,s}$, the following is a list of all such zeros smaller than 10.0 in magnitude :

$$\left.\begin{aligned} \lambda_{1,1} &= 4.493 \\ \lambda_{1,2} &= 7.725 \\ \lambda_{3,1} &= 6.988 \\ \lambda_{5,1} &= 9.355 . \end{aligned}\right\} \tag{6.28}$$

Thus if αa were to be increased continuously from 0.0 to 10.0, four resonances would be passed through altogether. The values (6.28) represent values of αa at which individual terms in (6.2) match the 'natural' boundary condition $B_r = 0$ on $r = a$.

6.8 The Relationship Between A and B

The connection between the flux function A and the magnitude $|\underline{B}|$ of the magnetic field in the r-θ plane may be found in the following way.

Now the r- and θ- components of the axi-symmetric fields in which we are interested are given in terms of A by (4.6) and (4.7) respectively. Hence the magnitude of the 'total' field measured in the r-θ plane is given by

$$|\underline{B}| = (B_r^2 + B_\theta^2)^{1/2} = \frac{1}{r\sin\theta}\left\{\left(\frac{1}{r}\frac{\partial A}{\partial \theta}\right)^2 + \left(\frac{\partial A}{\partial r}\right)^2\right\}^{1/2} \tag{6.29}$$

$$= \frac{1}{r\sin\theta}\,|\nabla A| . \tag{6.30}$$

Thus the magnetic field strength at a point (r,θ) in the plane is directly proportional to the magnitude of the gradient of the flux function at that point.

The result (6.30) is reflected in the range of maximum and minimum values of $\overline{A}$ shown in Figures 6.3 to 6.18. Over this set of diagrams the value of αa ranges from 0.0 to 20.0 . We find that whenever αa is not close to one of the singular values, which for $\alpha a \leq 10.0$ are given by (6.28), the range of $\overline{A}$ over the plot is relatively small. For example, for the case $\alpha a = 6.0$ in Figure 6.11 the range of $\overline{A}$ is about 3.2. Conversely, when αa is in relatively close proximity to a singular value, the range of $\overline{A}$ is much greater. Thus for $\alpha a = 9.36$ in Figure 6.16b the range of $\overline{A}$ is about 402.3 , because in this case we are very close to the singular value $\lambda_{5,1} = 9.355$.

6.9 Comments on the Results

One may make a number of observations from the field-line plots.

(i) For values of αa between 0.0 and about 2.5, the diagrams show an absence of magnetic islands : all visible field-lines link directly the poles of the sphere.

(ii) There appears to be a transition point at $\alpha a \approx 2.5$ where an islands seems to be emerging from the point $r = a , \theta = \pi/2$ (see Figure 6.6). In principle, the precise value of αa at which this transition occurs may be deduced from the condition $B_r = B_\theta = 0$ for the centre point of an island. From (6.2) we see that $B_r (r = a, \theta = \pi/2) = 0$. Hence the problem reduces itself to the solution for αa of

$$B_\theta (\alpha a , r = a , \theta = \pi/2) = 0 \qquad (6.31)$$

using (6.3), which could be done numerically.

(iii) For all subsequent plots, that is, for which $\alpha a > 2.5$, our results show that there exist regions of the field consisting of closed magnetic structures. Generally speaking, the higher the value of αa , the more complicated the field structure. Figure 6.18 which has $\alpha a = 20.0$ is thus the most complex of the cases we have calculated.

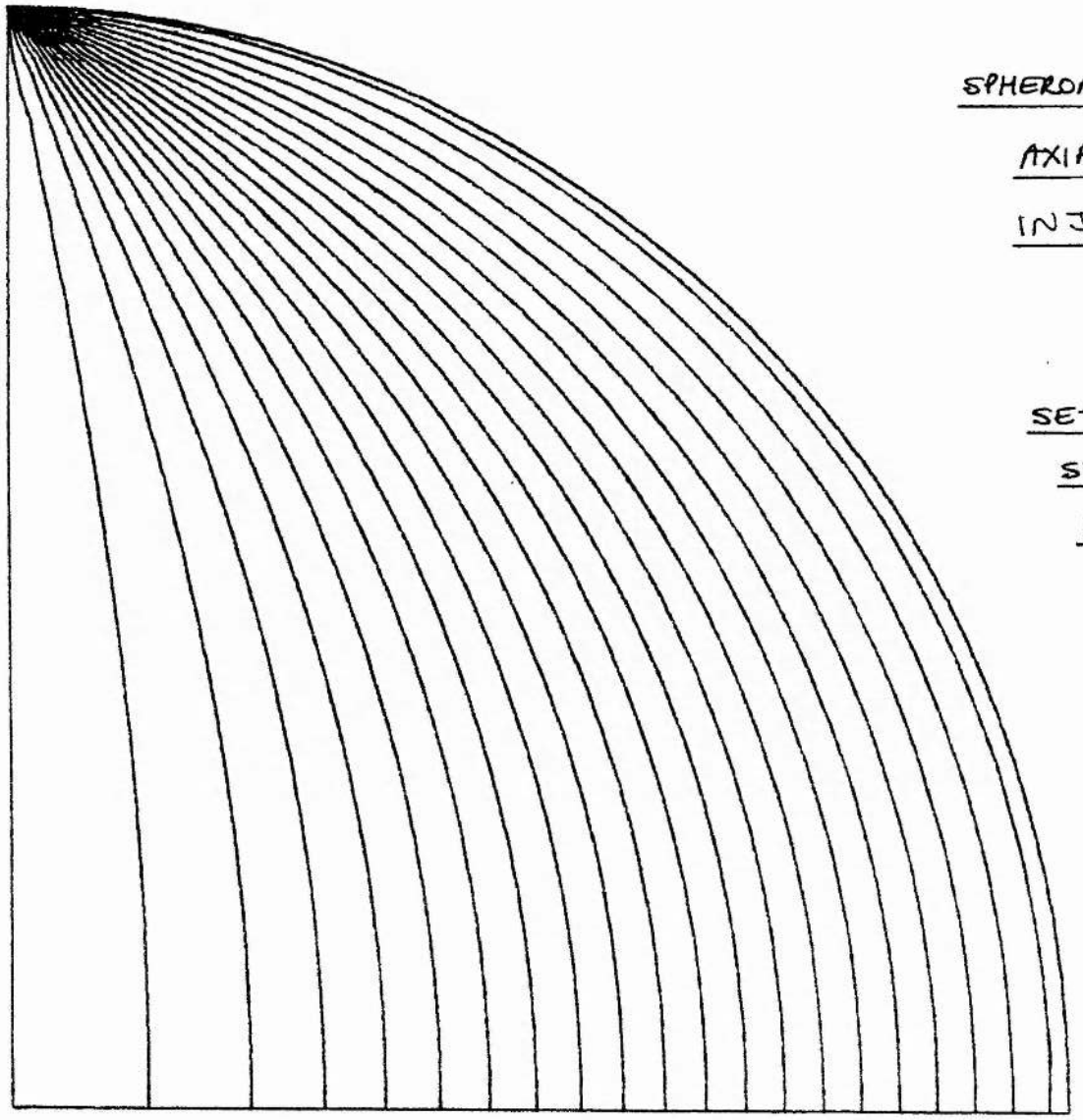

SPHEROMAK WITH AXIAL FLUX INJECTION:

SET OF TWENTY SYMMETRIC FIELD PLOTS.

$\bar{A}_{max} = 1.0000$

$\bar{A}_{min} = 0.0000$

$\alpha a = 0.0000$

Figure 6.3

$\bar{A}_{max} = 1.0000$
$\bar{A}_{min} = 0.0000$
$\alpha_a = 1.0000$

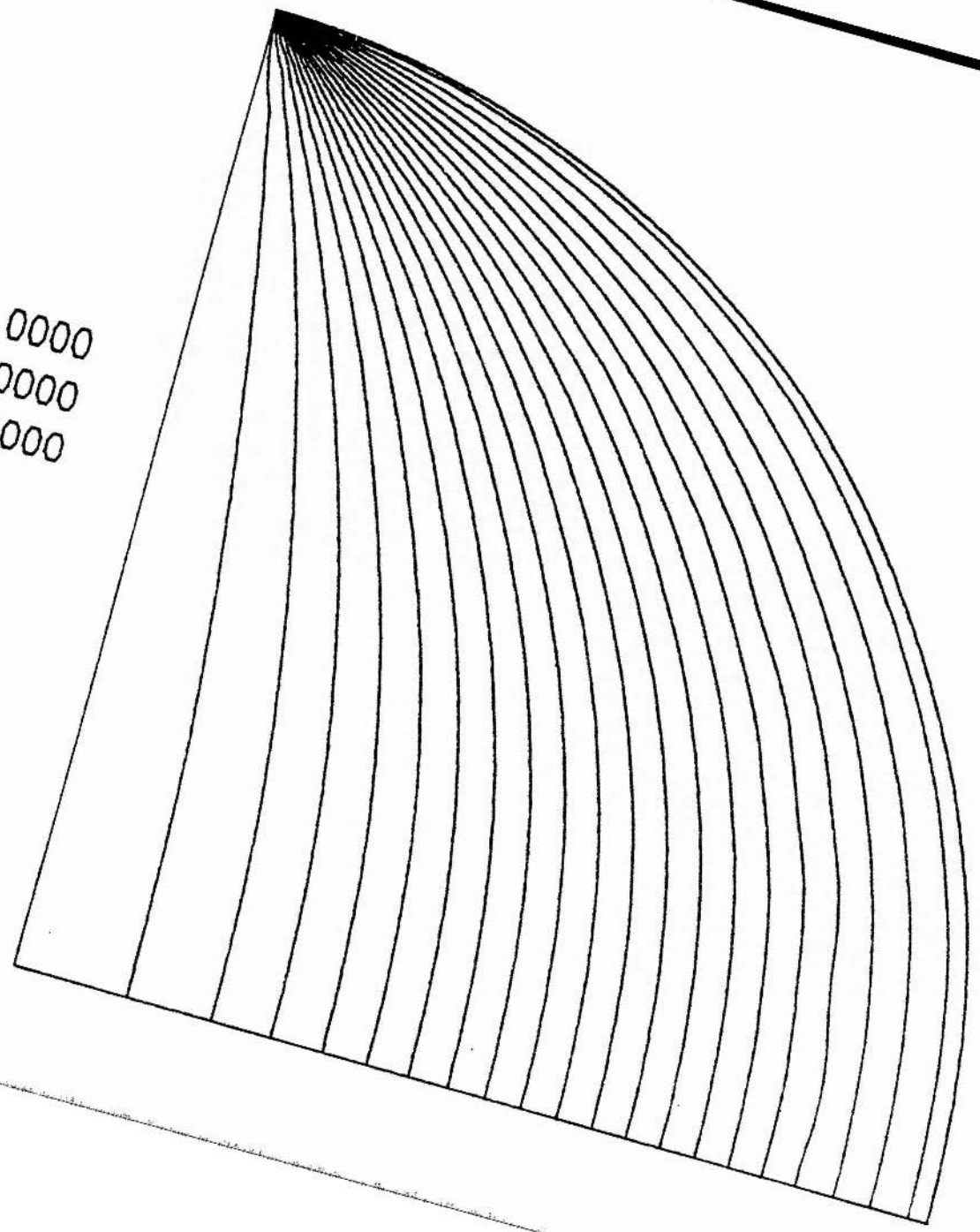

Figure 6.4

$\bar{A}_{max} = 1.0000$
$\bar{A}_{min} = 0.0000$
$\alpha_a = 2.0000$

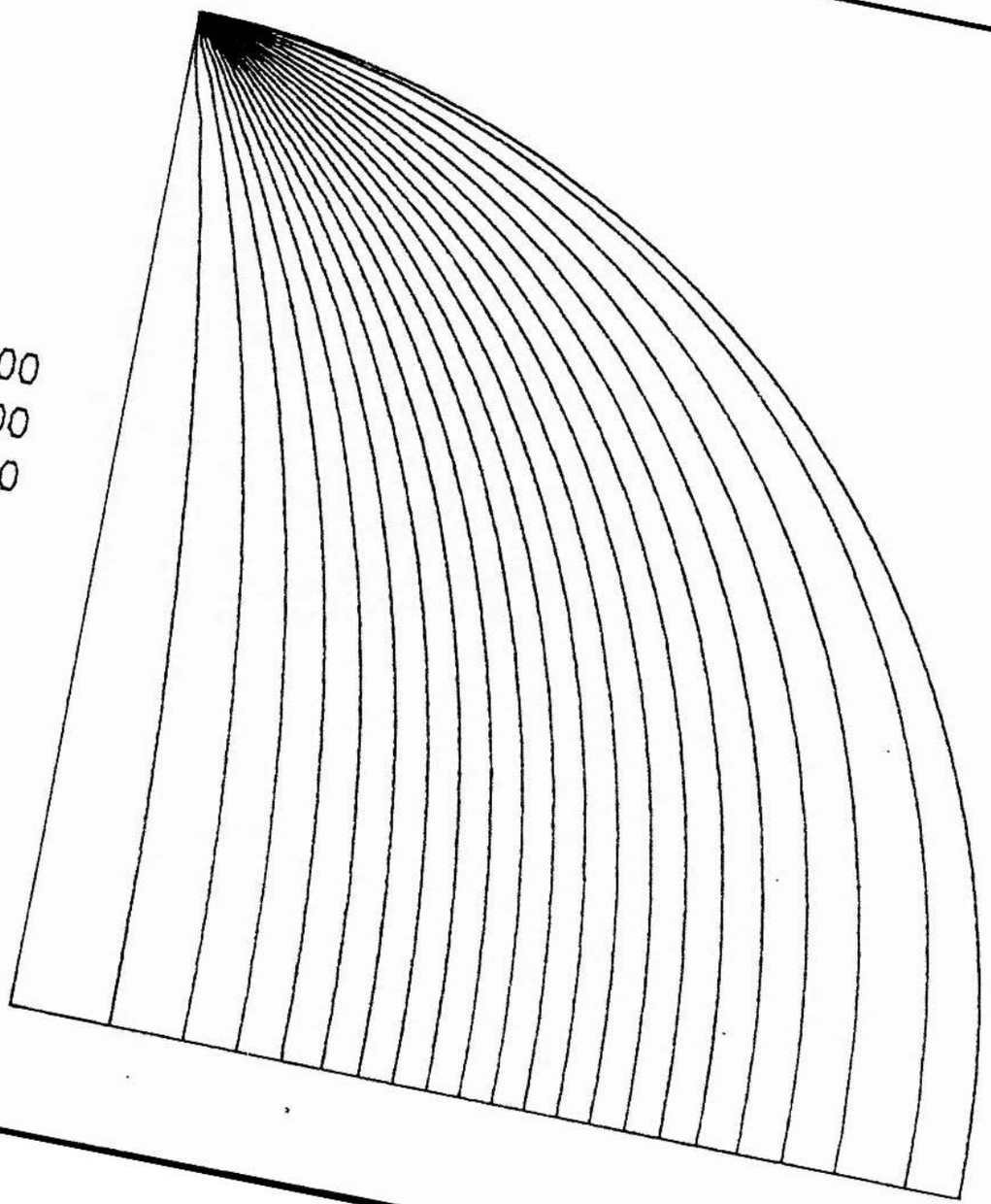

Figure 6.5

$\bar{A}_{max} = 1.0190$
$\bar{A}_{min} = 0.0000$
$\alpha_a = 2.5000$

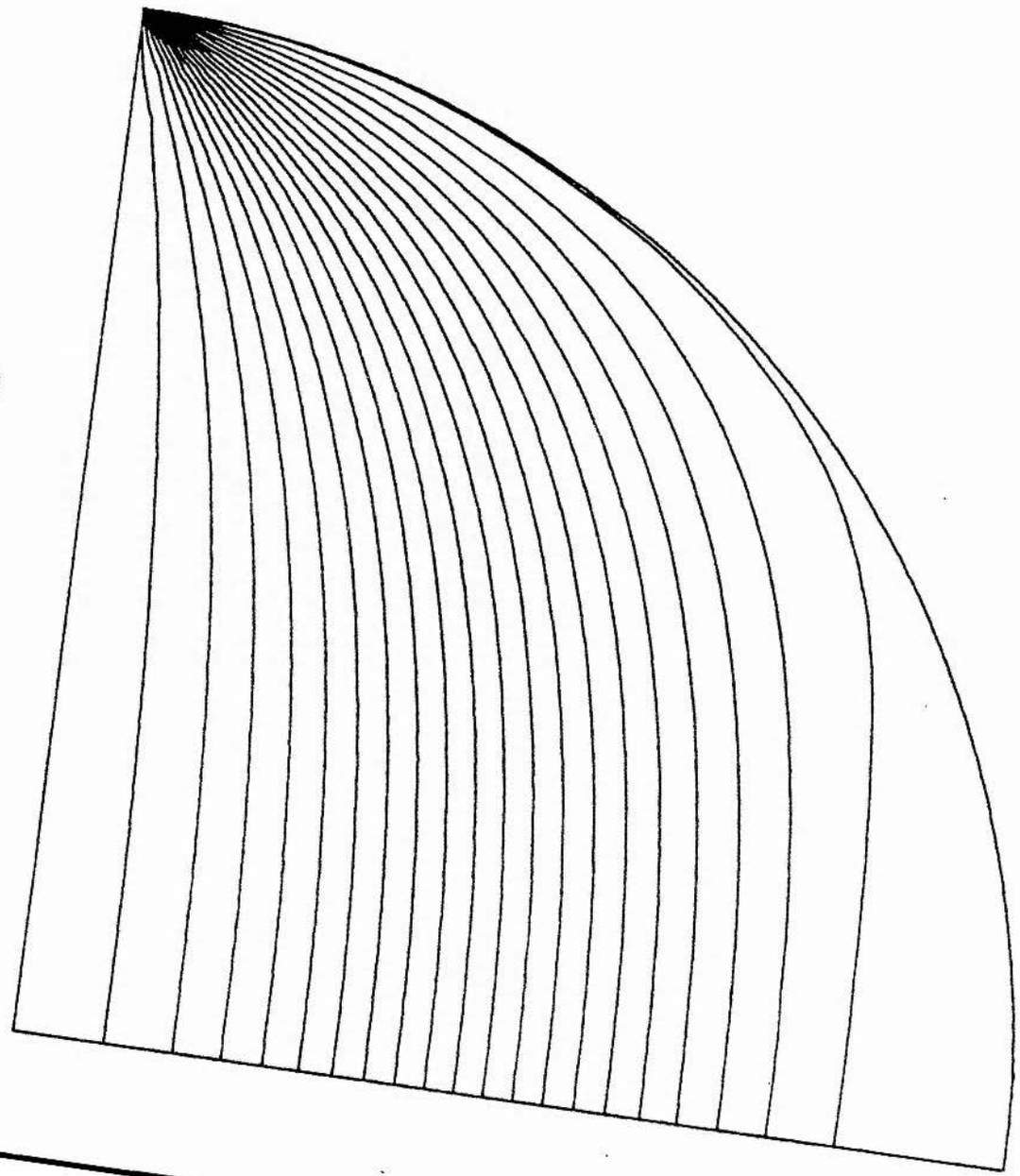

Figure 6-6

$\bar{A}_{max} = 1.1740$

$\bar{A}_{min} = 0.0000$

$\alpha_a = 3.0000$

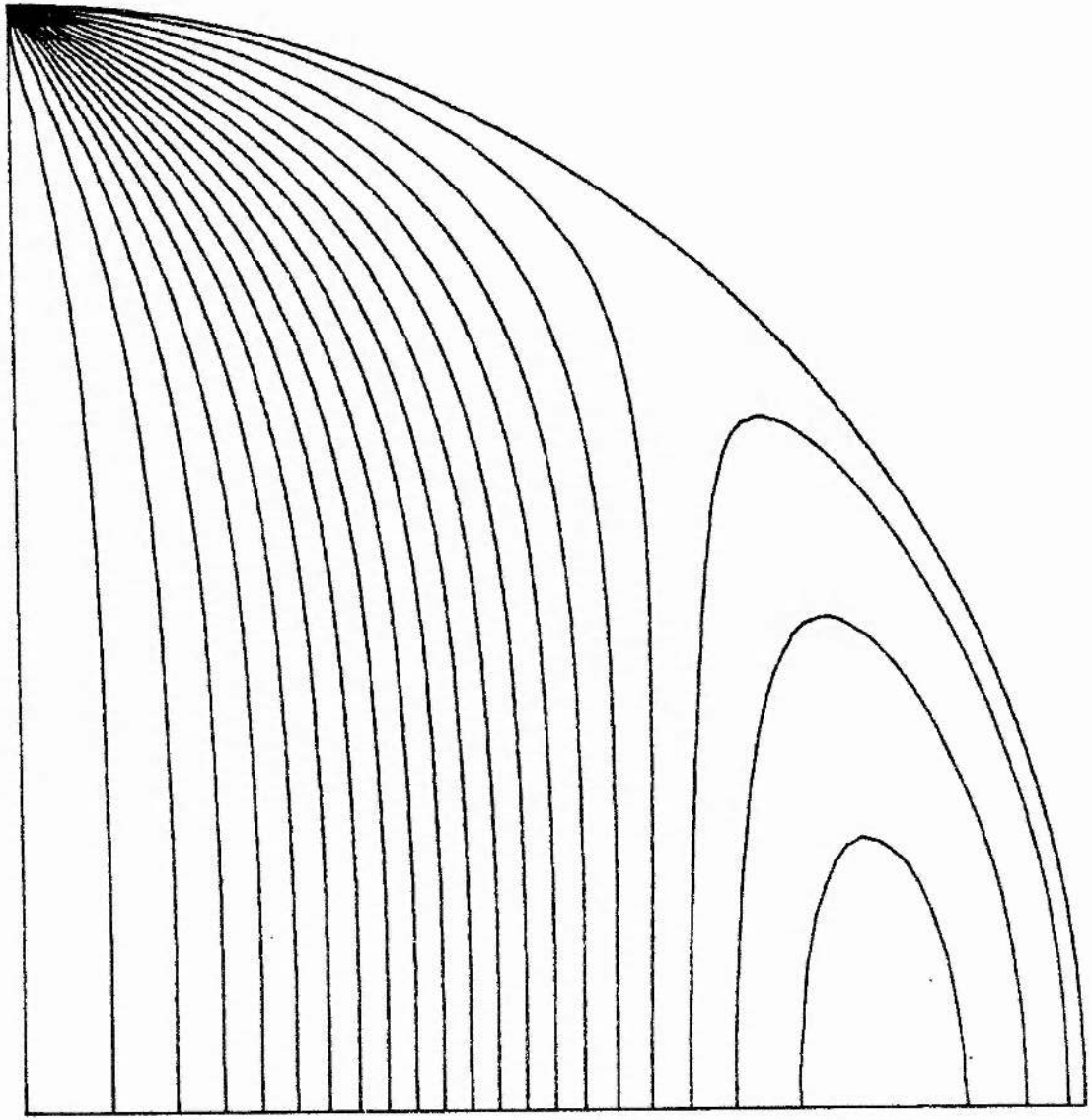

Figure 6-7

$\bar{A}$ max = 3.1860
$\bar{A}$ min = 0.0000
αa = 4.0000

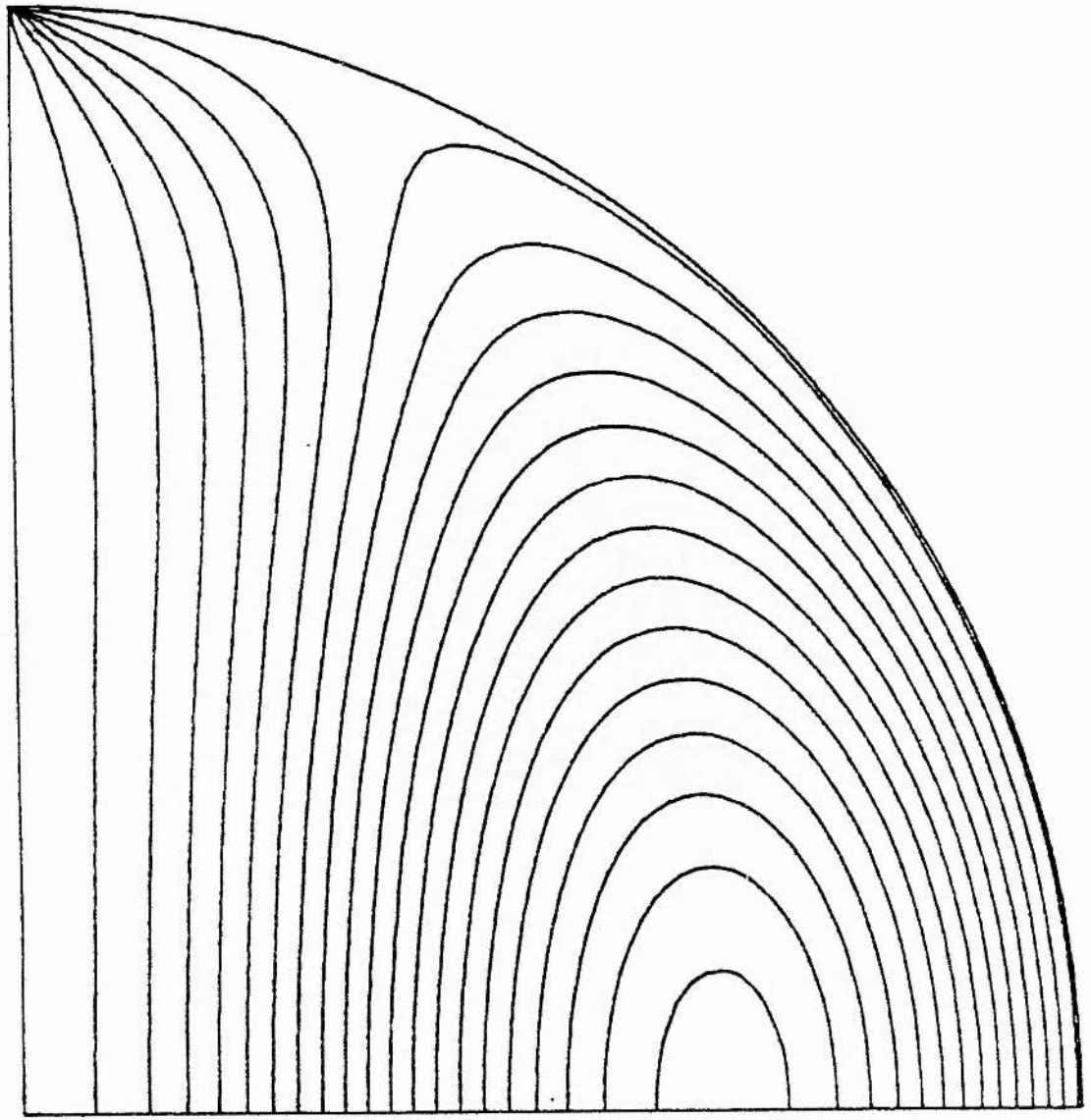

Figure 6.8

$\bar{A}_{max} = 121.6000$

$\bar{A}_{min} = 0.0000$

$\alpha_a = 4.4800$

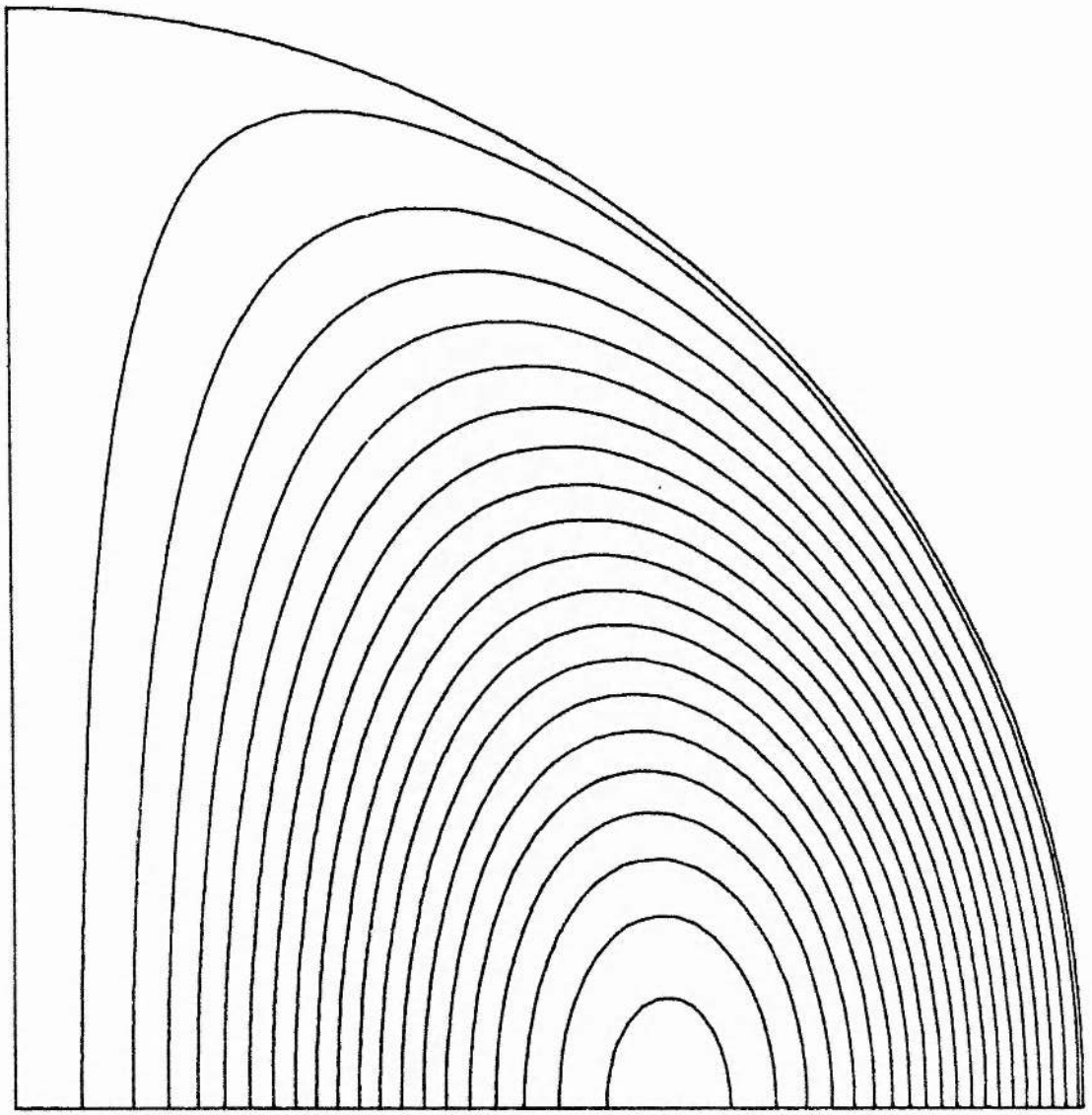

Figure 6-9a

$\bar{A}_{max} = 1.0000$

$\bar{A}_{min} = -248.1000$

$\alpha a = 4.5000$

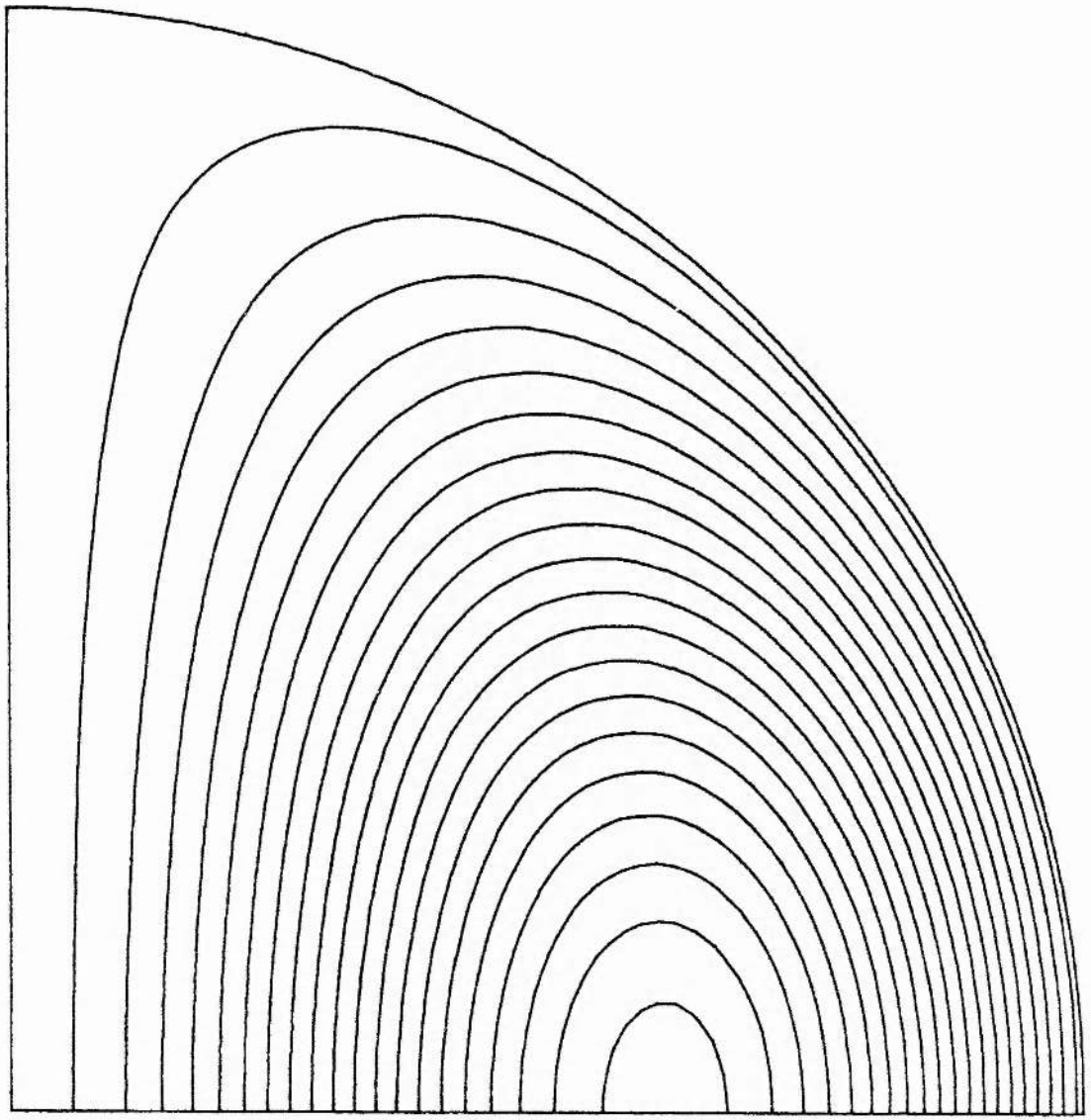

Figure 6.9b

$\bar{A}_{max} = 1.0000$

$\bar{A}_{min} = -3.5980$

$\alpha_a = 5.0000$

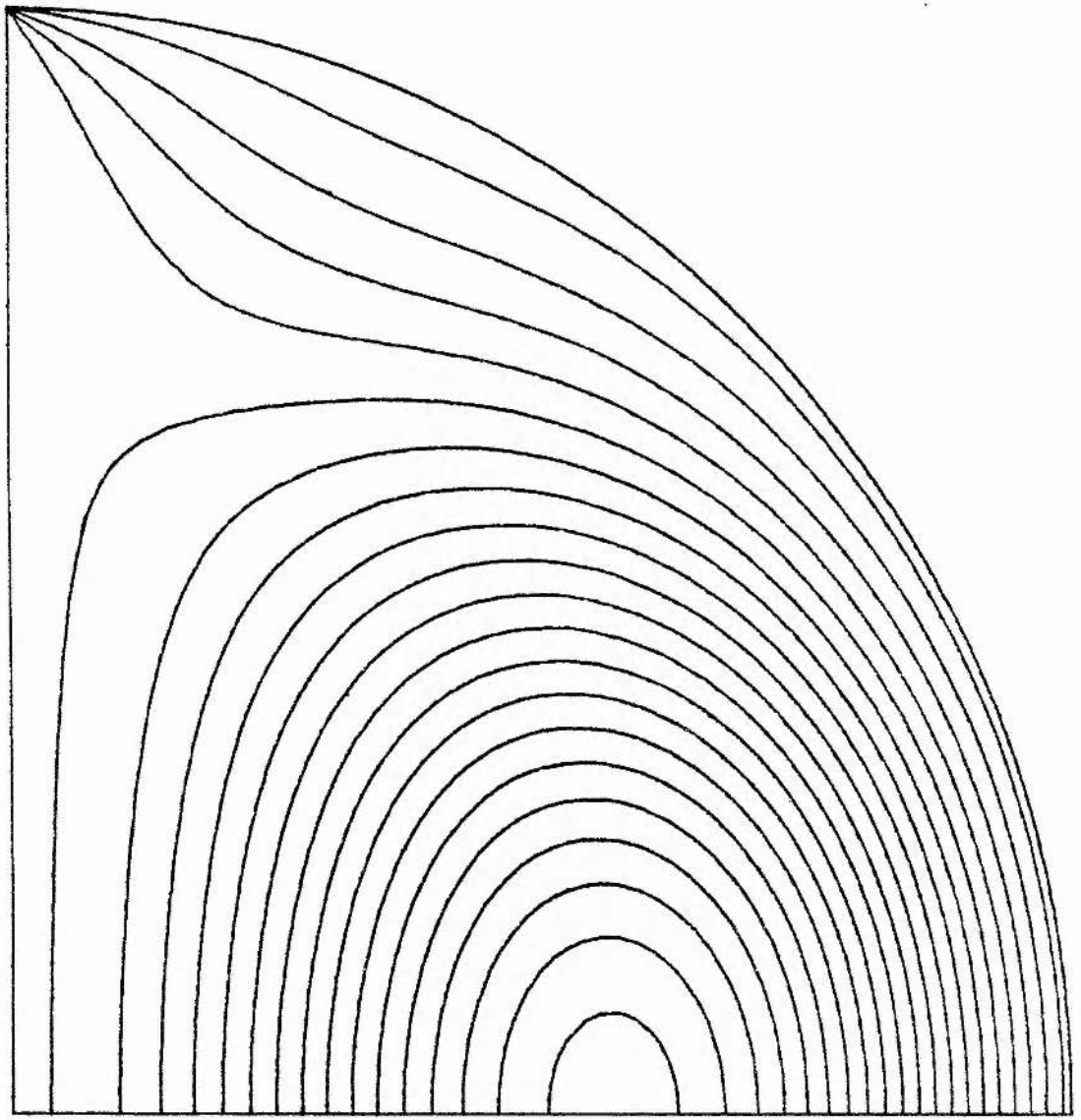

Figure 6-10

$\bar{A}_{max} = 1.2270$

$\bar{A}_{min} = -2.0070$

$\alpha a = 6.0000$

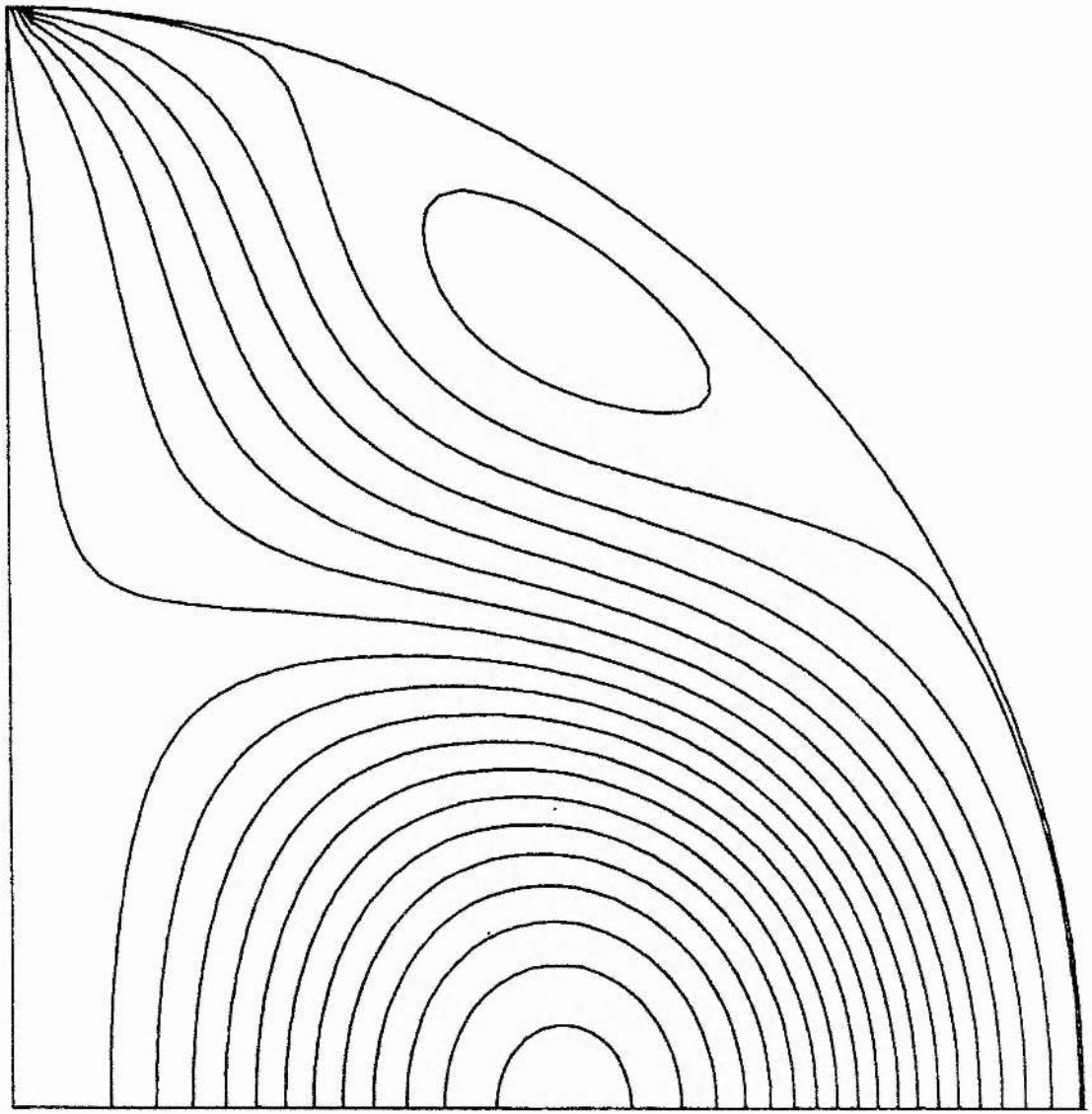

Figure 6.11

$\bar{A}_{max} = 108.7000$

$\bar{A}_{min} = -134.3000$

$\alpha_a = 6.9800$

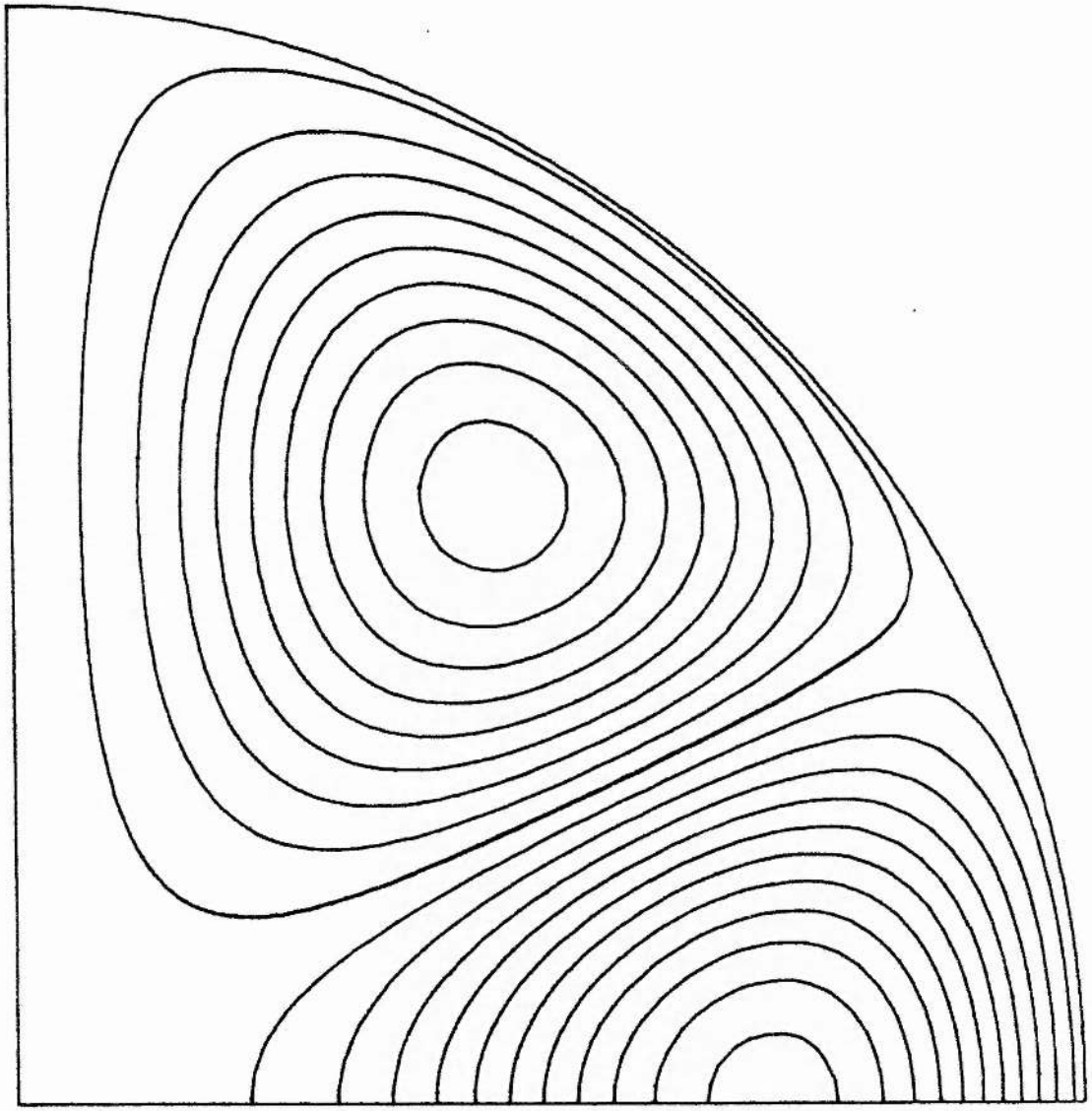

Figure 6-12a

$\bar{A}_{max} = 90.4300$

$\bar{A}_{min} = -70.8600$

$\alpha_a = 7.0000$

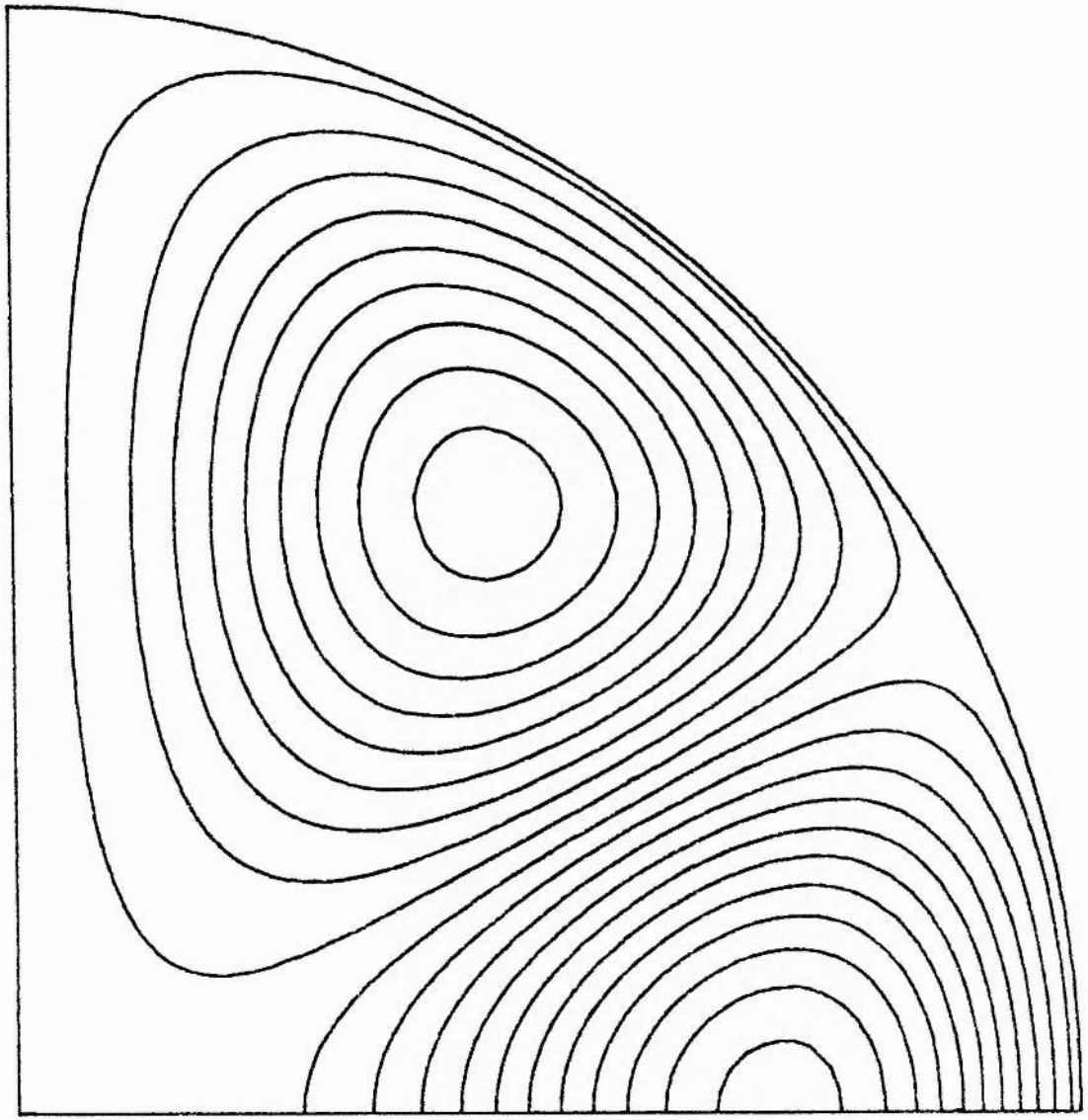

Figure 6-12b

$\bar{A}_{max} = 101.9000$

$\bar{A}_{min} = -104.9000$

$\alpha_a = 7.7100$

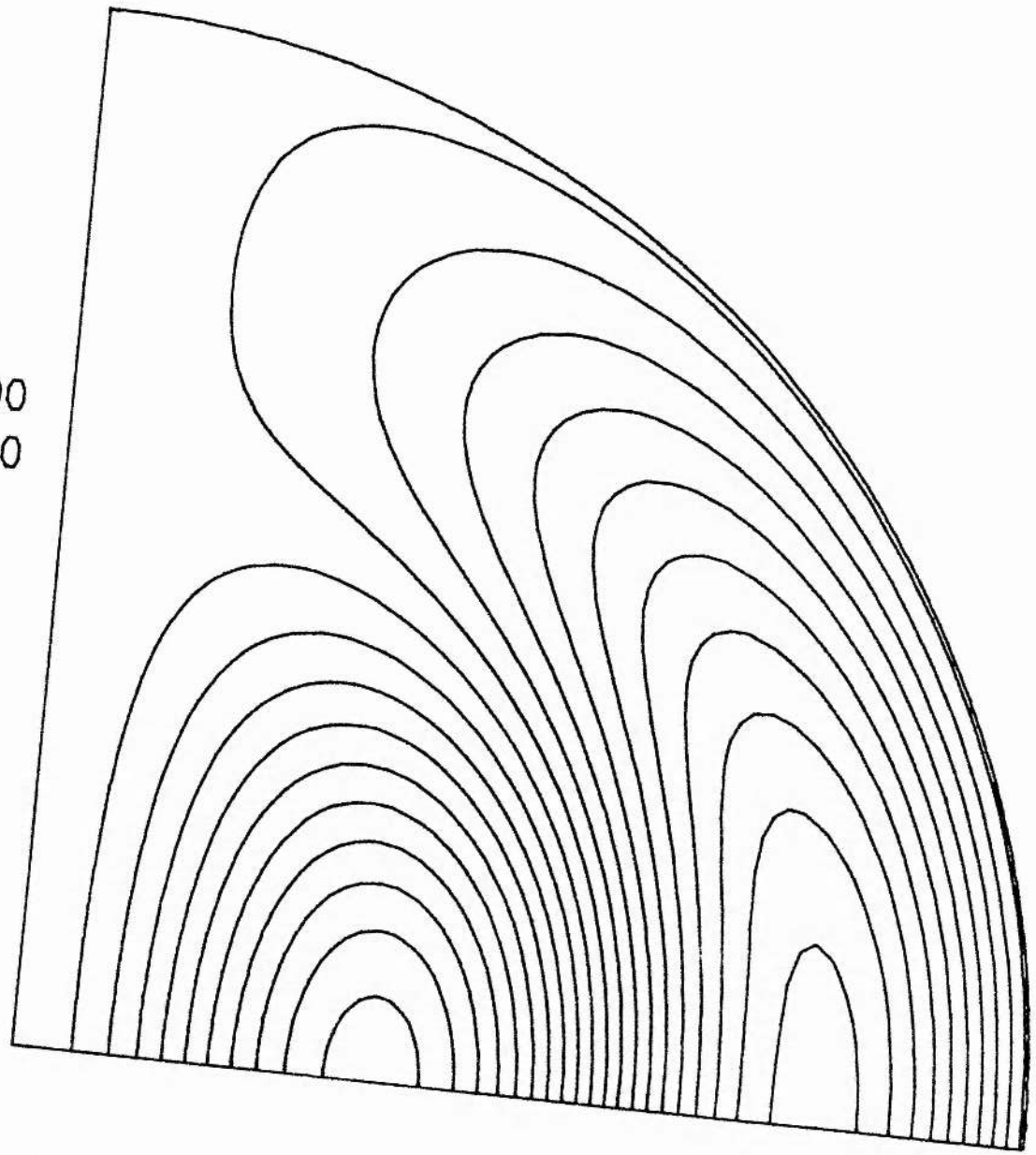

Figure 6-13a

$\bar{A}_{max} = 339.0000$
$\bar{A}_{min} = -321.0000$
$\alpha_a = 7.7300$

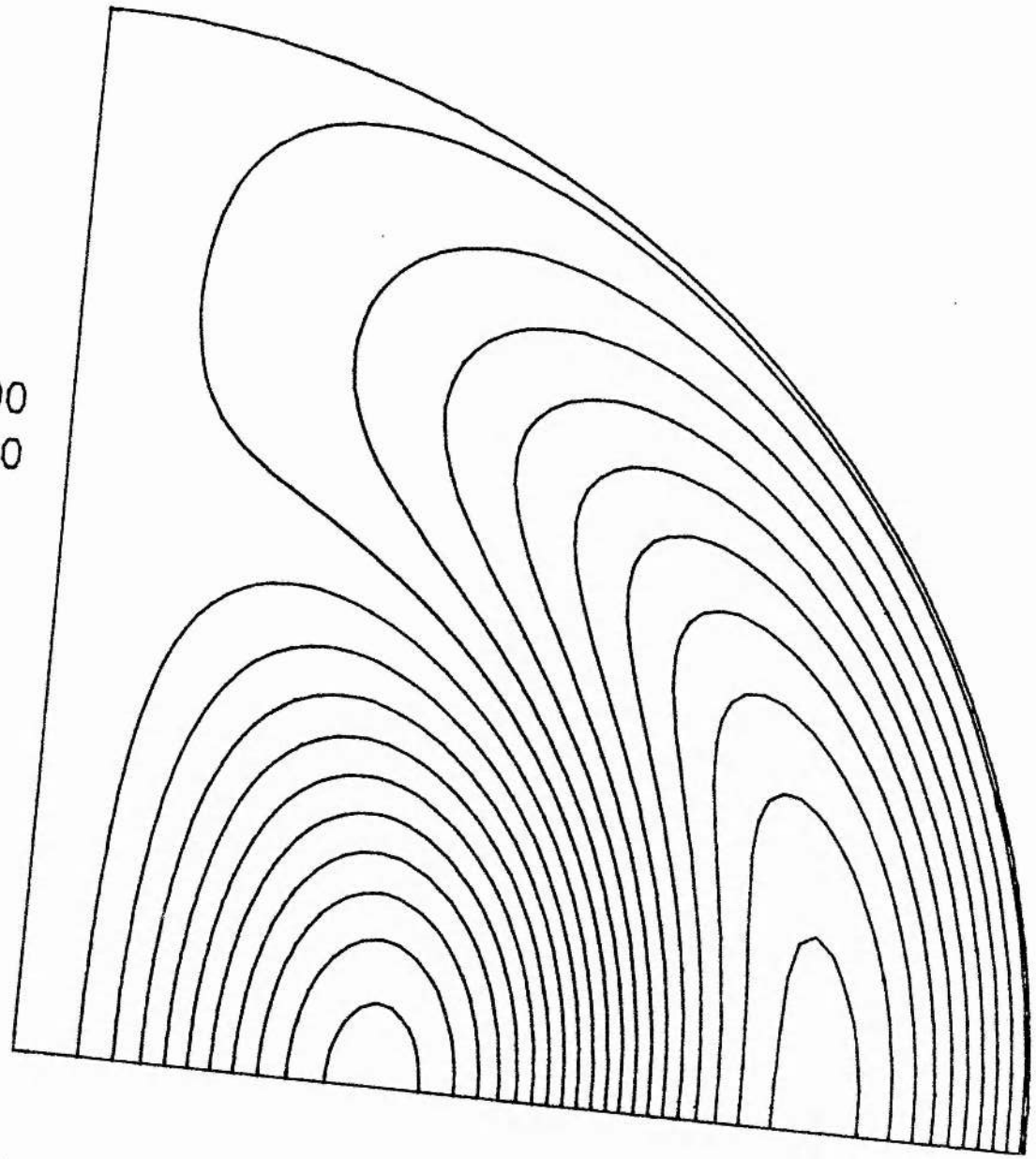

Figure 6-13b

$\bar{A}_{max} = 6.3390$

$\bar{A}_{min} = -4.9040$

$\alpha a = 8.0000$

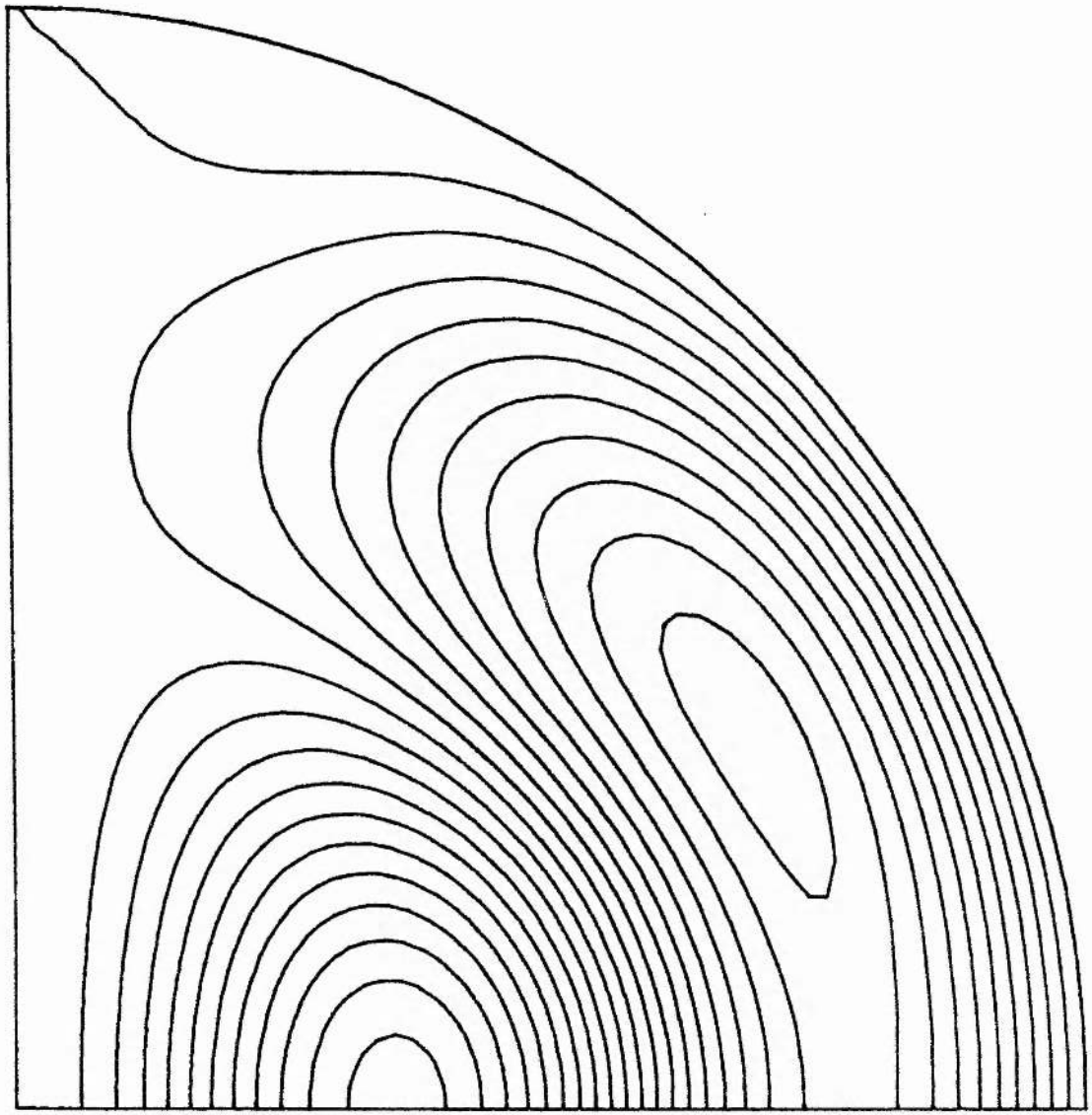

Figure 6-14

$\bar{A}$ max = 2.1600
$\bar{A}$ min = -3.3090
αa = 9.0000

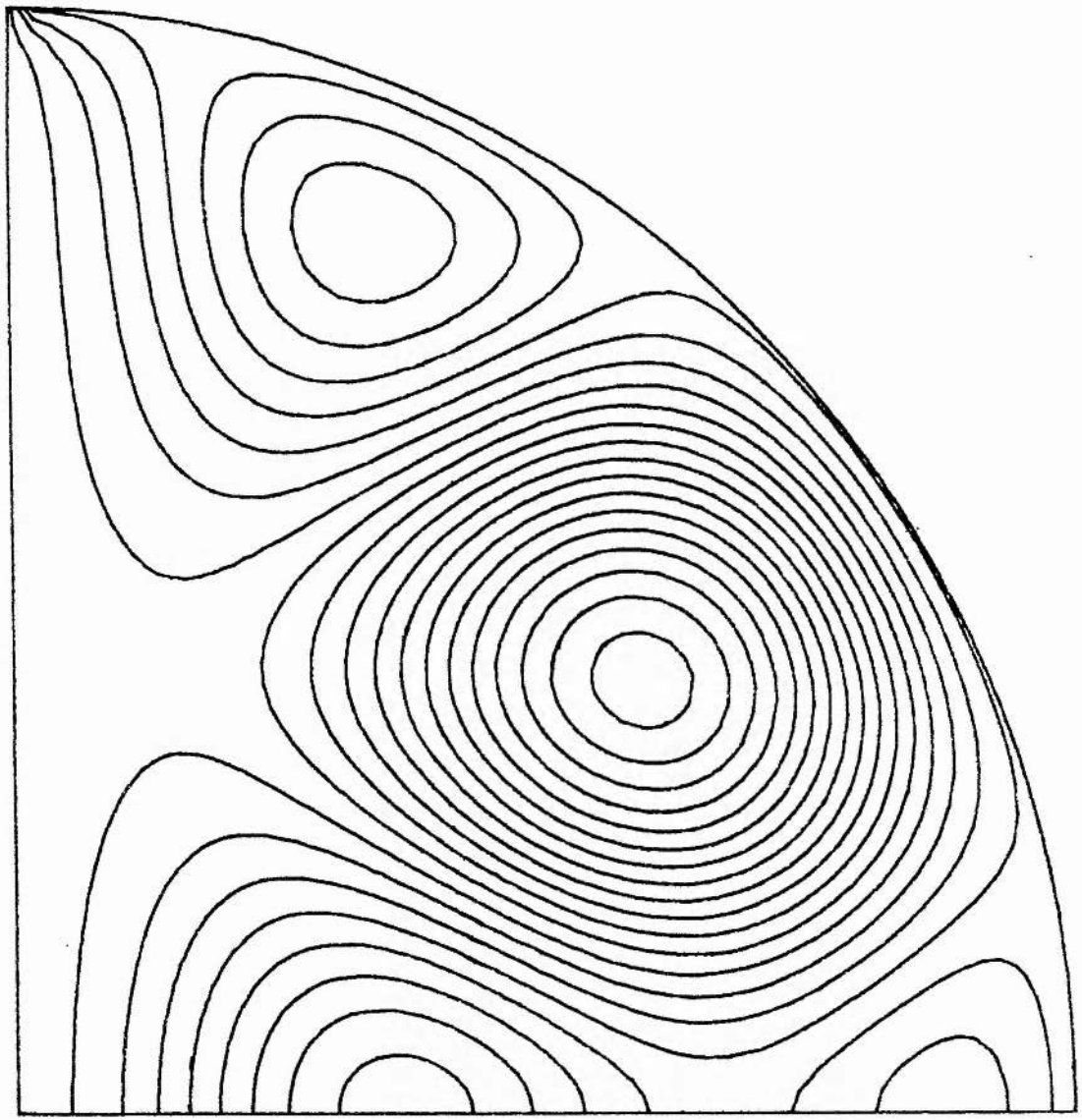

Figure 6-15

$\bar{A}max = 57.0100$

$\bar{A}min = -53.8200$

$\alpha a = 9.3400$

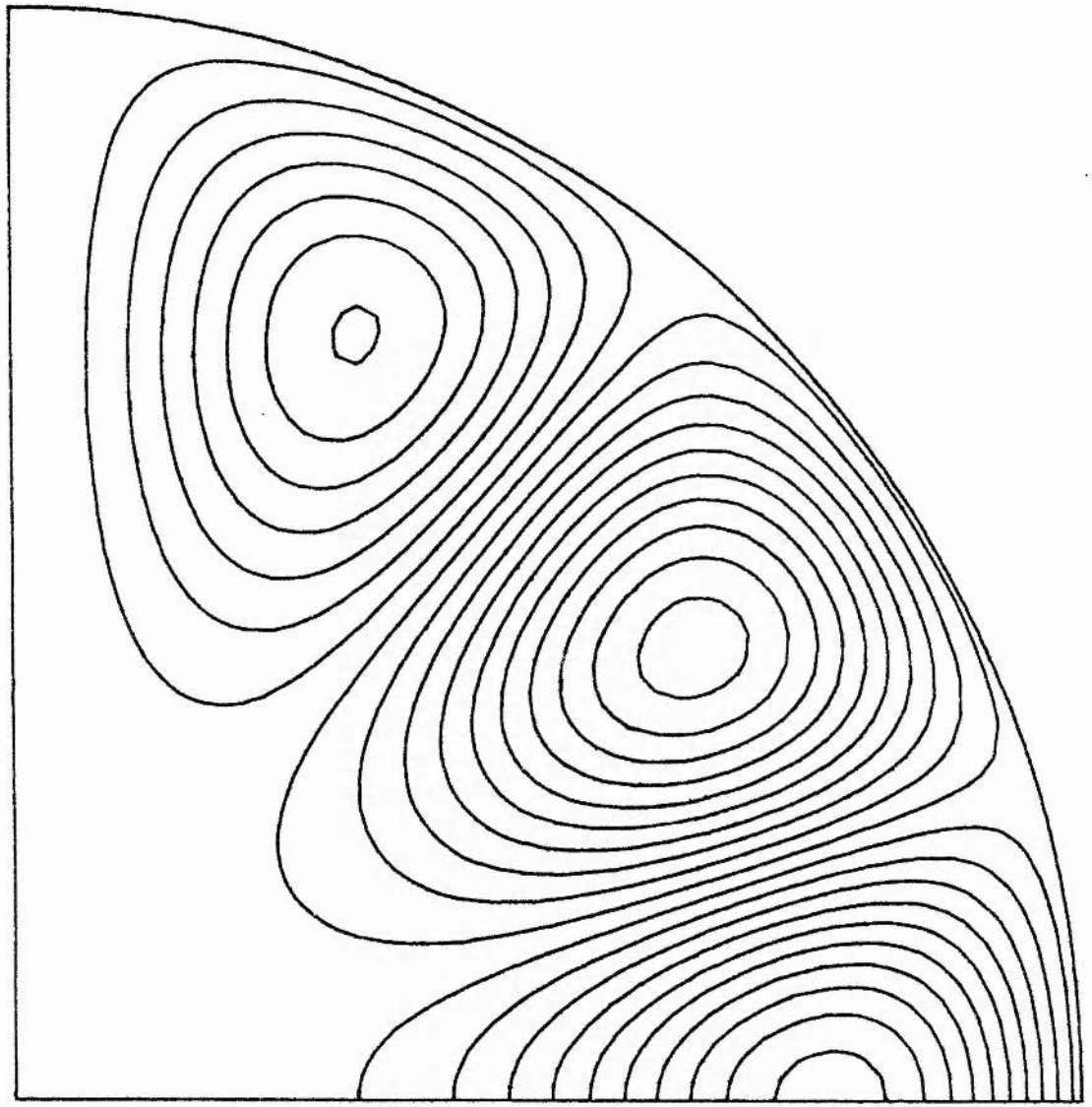

Figure 6.16a

$\bar{A}_{max}$ = 201.4000
$\bar{A}_{min}$ = -220.9000
α_a = 9.3600

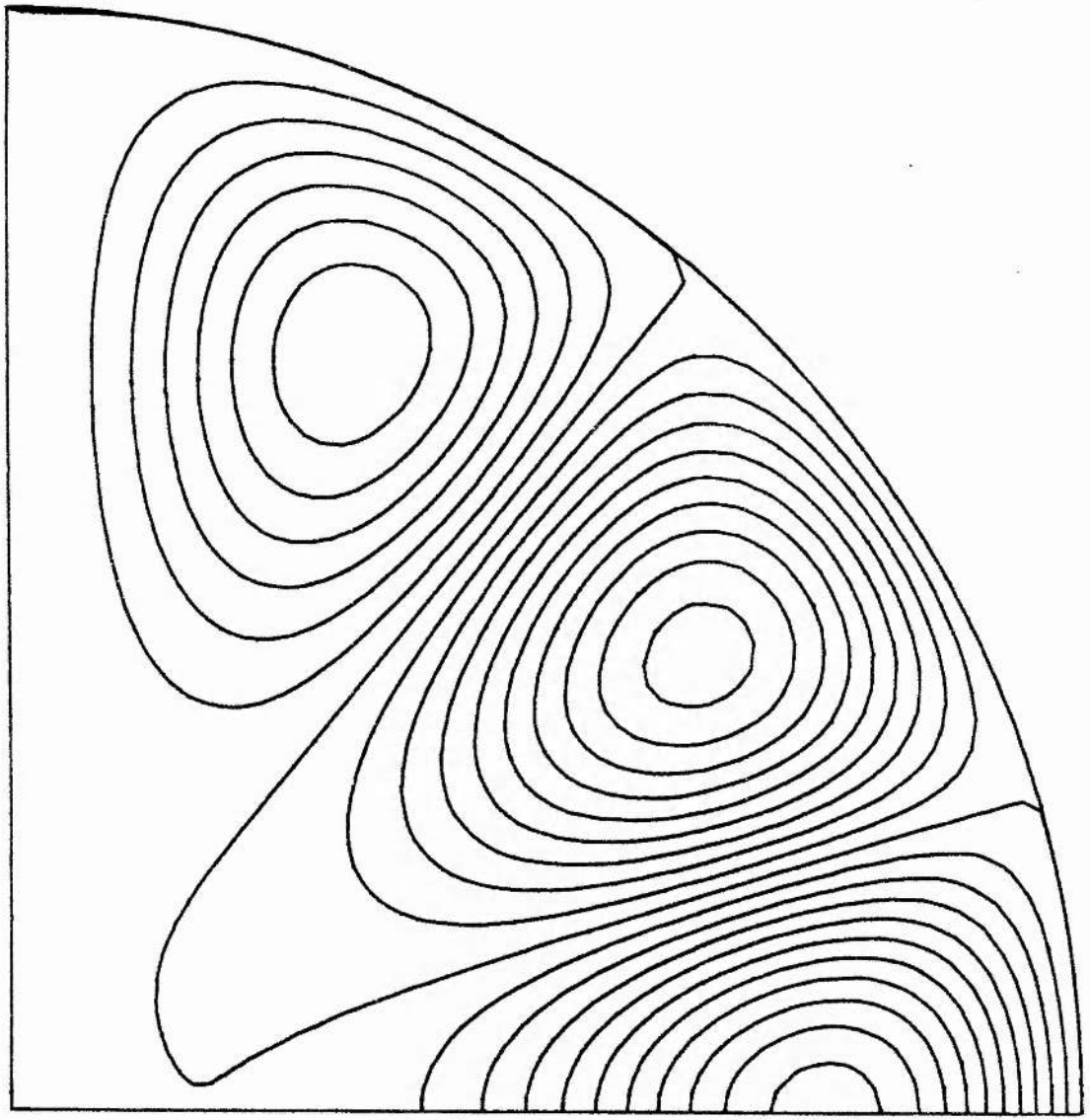

Figure 6.16b

$\bar{A}_{max}$ = 29.9000
$\bar{A}_{min}$ = -30.2900
αa = 14.0000

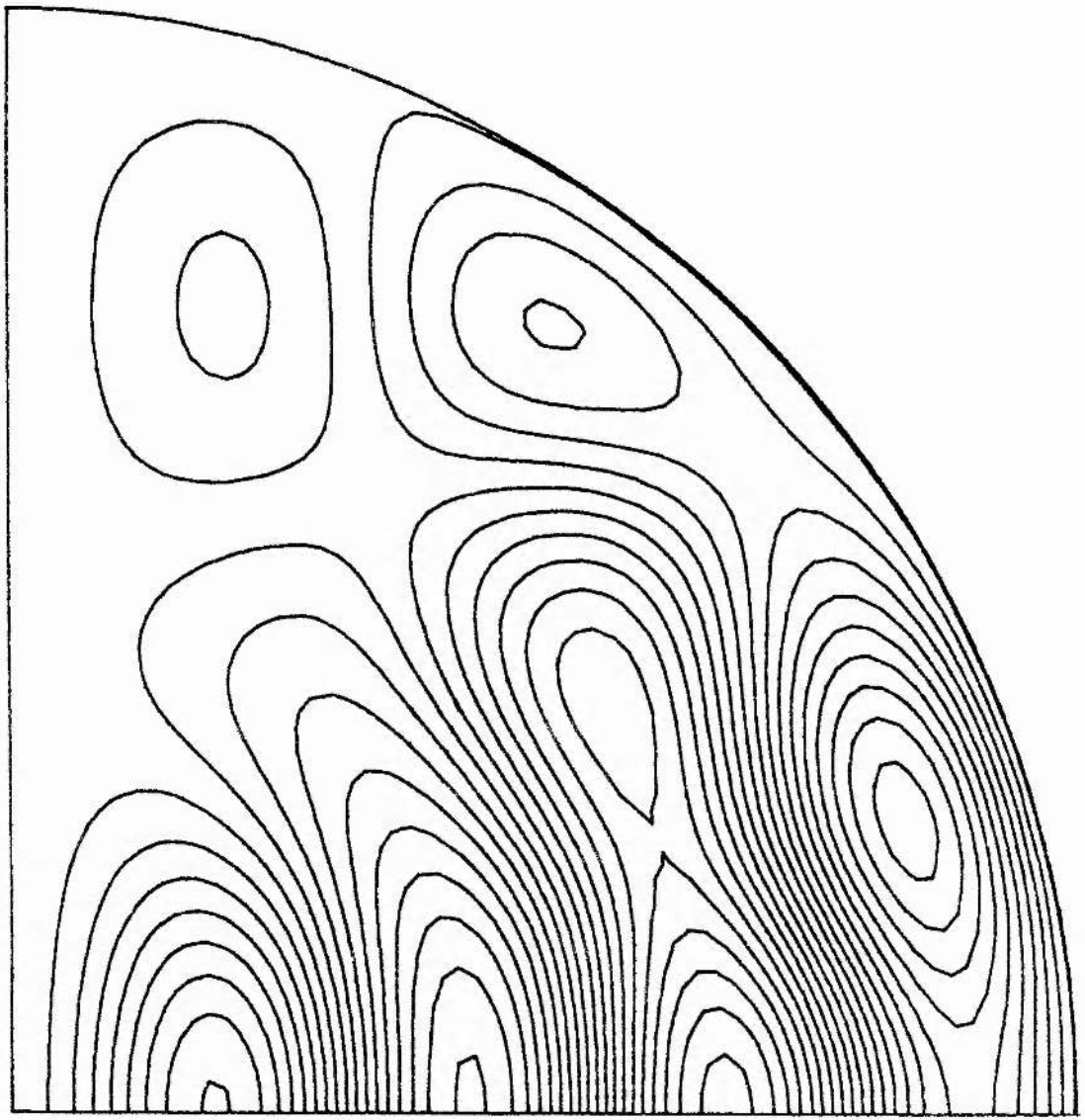

Figure 6.17

$\bar{A}_{max} = 9.9280$

$\bar{A}_{min} = -10.1400$

$\alpha a = 20.0000$

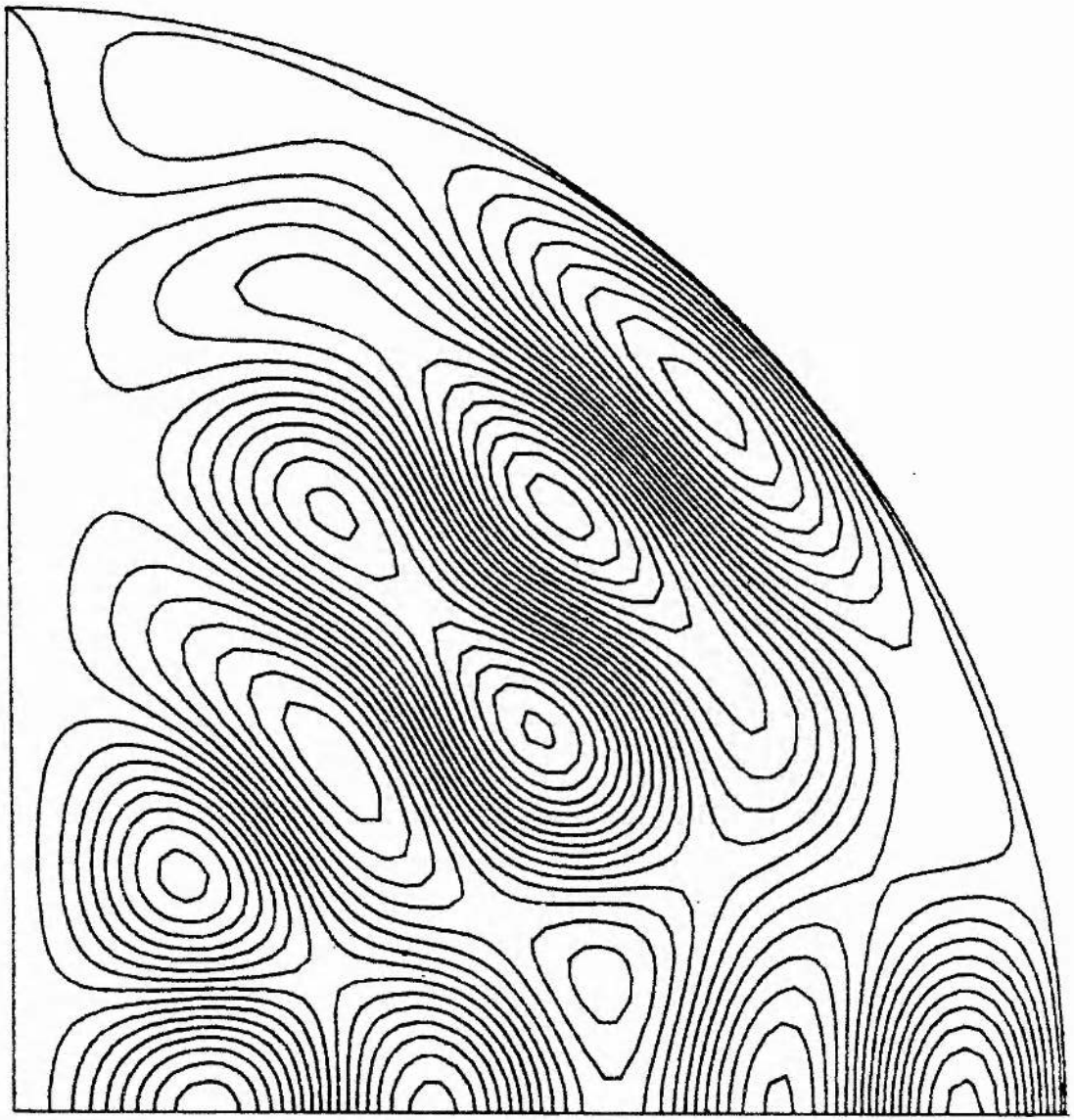

Figure 6-18

(iv) For our plots we have included a number of special pairs of values of αa, consisting of values of αa on either side of all the resonant points in the range 0.0 to 10.0. The diagrams concerned are Figures 6.9a, 6.9b, 6.12a, 6.12b, 6.13a, 6.13b, 6.16a and 6.16b.

From Figures 6.7 and 6.8 we see that there appears to be on the boundary an O-point which moves closer to the 'north pole' of the sphere as the first resonance point ($\alpha a = 4.493$) is approached. At the same time, the maximum value of $\overline{A}$ increases to large, positive values (Figure 6.9a) and the field structure resembles that of the 'classical spheromak' configuration. As αa is increased to a value slightly beyond the first resonance, we see from Figure 6.9b that the minimum value of $\overline{A}$ jumps from zero to a large *negative* value, and the maximum value of $\overline{A}$ drastically falls to the value 1. The implication, using Equation (4.4), is that the field component B_ϕ has reversed sign.

The other resonances shown are less easy to interpret, as both large positive and large negative values of $\overline{A}$ are present on both sides of the resonant points, as, for example in Figures 6.12a and 6.12b. It is notable here that there are*three* island regions in the space $0 \le \theta \le \pi$, compared with *one* at the first resonance, and we conjecture that in Figure 6.12b the sign of B_ϕ associated with each island has changed from what it was in Figure 6.12a.

(v) What can be said about the topology of the relaxed field close to resonance points?

Now the sequence made up from Figures 6.8, 6.9a, 6.9b and 6.10 has a property in common with the sequence made up from Figures 6.15, 6.16a and 6.16b. This is that in the first 'frame' of each sequence, the group of field-lines leaving the sphere at the north pole passes the immediately adjacent island close to the axis (that is, to the *left*) whereas in the last 'frame' of each sequence, the north polar field-lines pass to the *right* of the island. The conclusion, supporting the conjecture in (iv) above, is that in the island structures the toroidal field component reverses direction as αa goes through a singular value, but the overall appearance of the field remains relatively unchanged.

6.10 Helicity and Energy of the Field

We would like to calculate the magnetic energy and the relative helicity of the realaxed field given by (6.2), (6.3) and (6.4) with coefficients (6.9).

(a) Magnetic Energy

The magnetic energy is given for axi-symmetric fields by

$$W = \frac{\pi}{\mu_0} \int_0^a \int_0^\pi (B_r^2 + B_\theta^2 + B_\phi^2) r^2 \sin\theta \, dr \, d\theta \,. \quad (6.32)$$

It is helpful first to note some special integrals, as follows :

(i) $$\int_0^\pi \sin\theta \, P_m(\cos\theta) \, P_n(\cos\theta) \, d\theta \,, \quad m,n \in \mathbb{N}$$

$$= \int_{-1}^{1} P_m(x) \, P_n(x) \, dx$$

$$= \begin{cases} 0 \,, & m \neq n \\ \dfrac{2}{2n+1} \,, & m = n \,. \end{cases} \quad (6.33)$$

(ii) $$\int_0^\pi \sin\theta \, \frac{d}{d\theta}\{P_m(\cos\theta)\} \frac{d}{d\theta}\{P_n(\cos\theta)\} \, d\theta$$

$$= \int_{-1}^{1} (1-x^2) \, P_m'(x) \, P_n'(x) \, dx$$

$$= [(1-x^2) P_m'(x) P_n(x)]_{-1}^{1} - \int_{-1}^{1} P_n(x) \frac{d}{dx}\{(1-x^2) P_n'(x)\} dx$$

$$= - \int_{-1}^{1} P_n(x) \{-2x P_m'(x) + (1-x^2) P_m''(x)\} dx$$

$$= m(m+1) \int_{-1}^{1} P_n(x) \, P_m(x) \, dx \,, \quad (6.34)$$

the last result being obtained using Legendre's equation. Upon applying (6.33) to (6.34) we therefore deduce that

$$\int_0^{\pi} \sin\theta \frac{d}{d\theta}\{P_m(\cos\theta)\}\frac{d}{d\theta}\{P_n(\cos\theta)\}\,d\theta = \begin{cases} 0, & m \neq n \\ \dfrac{2n(n+1)}{2n+1}, & m = n \end{cases} . \qquad (6.35)$$

From (6.33) and (6.35) it is clear that all the cross terms arising from the substitution of (6.2), (6.3) and (6.4) into (6.32) will vanish.

Thus from (6.2), (6.3), (6.4), (6.32), (6.33) and (6.35), performing the integration over θ and substituting spherical Bessel functions from (6.11), we obtain

$$W = \frac{4a^3}{\mu_0}\sum_{n=0}^{\infty} C_n^2 \frac{n(n+1)}{(2n+1)}\left[\int_0^{\alpha a}\left\{(2n^2+n+u^2)j_n^2(u) - 2nu\,j_{n-1}(u)j_n(u) + u^2 j_{n-1}^2(u)\right\}du\right] \qquad (6.36)$$

where $u = \alpha r$. Substituting for C_n from (6.9) in (6.36) and again using (6.11), we get

$$W = \frac{\Phi^2}{2\pi\mu_0\alpha a^2}\sum_{\substack{n=1 \\ (ODD)}}^{\infty}\frac{(2n+1)}{n(n+1)j_n^2(\alpha a)}\int_0^{\alpha a}\left\{(u^2+2n^2+n)j_n^2(u) - 2nu\,j_{n-1}(u)j_n(u) + u^2 j_{n-1}^2(u)\right\}du . \qquad (6.37)$$

It is demonstrated in the Appendix to this chapter (Section 6.14) that (6.37) may be written alternatively in the simplified, dimensionless form

$$\overline{W} = \frac{1}{\alpha a}\sum_{\substack{n=1 \\ (ODD)}}^{\infty}\frac{(2n+1)}{n(n+1)}\left[\int_0^{\alpha a} 2u^2\frac{j_n^2(u)}{j_n^2(\alpha a)}\,du\right.$$

$$+ (\alpha a)^2 \frac{j_{n-1}(\alpha a)}{j_n(\alpha a)} - n(\alpha a)\Big] \qquad (6.38)$$

where

$$\overline{W} = \frac{2\pi\mu_0 a}{\Phi^2} W \,. \qquad (6.39)$$

(b) Relative Helicity

We should now like to calculate the gauge-invariant relative helicity H of the field (6.2), (6.3) and (6.4) with the coefficients (6.9). According to the prescription given in Section 4.14, this means we shall need to calculate vector potentials for the field of interest and for the potential field having the same boundary condition.

From (6.2) and (6.9), taking the limit as $\alpha a \to 0$ and using the result

$$\lim_{\alpha a \to 0} \frac{j_n(\alpha r)}{j_n(\alpha a)} = \frac{r^n}{a^n} \,, \qquad (6.40)$$

we find that the r-component of the potential field is

$$(B_r)_0 = \frac{\Phi}{2\pi a^2} \sum_{\substack{n=1 \\ (\text{ODD})}}^{\infty} (2n+1)\left(\frac{r}{a}\right)^{n-1} P_n(\cos\theta) \,. \qquad (6.41)$$

Finding the θ-component of the potential field is more difficult. Using (6.3), (6.9) and (6.11), the θ-component of the field may be written in the form

$$B_\theta = \frac{\Phi}{2\pi a} \sum_{\substack{n=1 \\ (\text{ODD})}}^{\infty} \frac{(2n+1)}{n(n+1)} \frac{1}{r} \frac{\frac{d}{dr}\{r j_n(\alpha r)\}}{j_n(\alpha a)} \frac{d\{P_n(\cos\theta)\}}{d\theta} \qquad (6.42)$$

Now

$$\frac{1}{r} \lim_{\alpha a \to 0} \frac{\frac{d}{dr}\{r j_n(\alpha r)\}}{j_n(\alpha a)}$$

$$= \frac{1}{r}\frac{d}{dr}\left(\frac{r^{n+1}}{a^n}\right) = (n+1)\frac{r^{n-1}}{a^n} \qquad (6.43)$$

where we have used the result (6.40) and also have assumed the limit and derivative are interchangeable. Hence, upon substitution of (6.43) into (6.42), we have that the θ-component of the potential field is

$$(B_\theta)_0 = \frac{\Phi}{2\pi a^2}\sum_{\substack{n=1\\(ODD)}}^{\infty}\left(\frac{2n+1}{n}\right)\left(\frac{r}{a}\right)^{n-1}\frac{d}{d\theta}\{P_n(\cos\theta)\}, \qquad (6.44)$$

From (6.4) and (6.9) we find that the ϕ-component of the potential field is

$$(B_\phi)_0 = 0 . \qquad (6.45)$$

Thus solving directly the defining equation for the corresponding vector potential $\underline{A}_0$ of the potential field (6.41), (6.44) and (6.46), namely

$$\underline{B}_0 = \nabla \times \underline{A}_0 , \qquad (6.46)$$

we find that a convenient form for the vector potential is

$$\underline{A}_0 = -\frac{\Phi}{2\pi a^2}\sum_{\substack{n=1\\(ODD)}}^{\infty}\frac{(2n+1)}{n(n+1)}r\left(\frac{r}{a}\right)^{n-1}\frac{d}{d\theta}\{P_n(\cos\theta)\}\hat{\underline{\phi}}, \qquad (6.47)$$

This has the property that $\underline{A}_0 \cdot \underline{B}_0 = 0$, where $\underline{B}_0$ represents the potential field.

For a general field $\underline{B}$ ($\alpha a \neq 0$), we must find a corresponding vector potential $\underline{A}$, which in the case of our linear force-free field may be written as

$$\underline{A} = \frac{\underline{B}}{\alpha} + \nabla g \qquad (6.48)$$

where g is some function of r and θ, such that the tangential components of $\underline{A}$ are the same as the tangential components of $\underline{A}_0$ on r = a. The components of (6.48) are

$$A_r = \frac{B_r}{\alpha} + \frac{\partial g(r,\theta)}{\partial r} \,, \tag{6.49}$$

$$A_\theta = \frac{B_\theta}{\alpha} + \frac{1}{r}\frac{\partial g(r,\theta)}{\partial \theta} \tag{6.50}$$

and

$$A_\phi = \frac{B_\phi}{\alpha} \,. \tag{6.51}$$

From (6.4) with (6.9), we see that A_ϕ does indeed match $(\underline{A}_0)_\phi$, given by (6.47), on r = a as required. Since the r-components do not have to match, in (6.49) we may take

$$\frac{\partial g(r,\theta)}{\partial r} = 0 \,, \tag{6.52}$$

as an arbitrary condition. Thus to determine the correct gauge it remains only to solve

$$\frac{B_\theta(r=a)}{\alpha} + \frac{1}{a}\frac{dg}{d\theta} = 0 \tag{6.53}$$

for $dg/d\theta$.

From (6.3) we deduce that

$$B_\theta(r=a) = \sum_{n=0}^{\infty} C_n \left\{ \alpha a \, J_{n-\frac{1}{2}}(\alpha a) - n \, J_{n+\frac{1}{2}}(\alpha a) \right\} \frac{d}{d\theta}\{P_n(\cos\theta)\} \tag{6.54}$$

and hence from (6.53) that

$$\frac{dg}{d\theta} = -\frac{a}{\alpha} \sum_{n=0}^{\infty} C_n \left\{ \alpha a \, J_{n-\frac{1}{2}}(\alpha a) - n \, J_{n+\frac{1}{2}}(\alpha a) \right\} \frac{d}{d\theta}\{P_n(\cos\theta)\} \,. \tag{6.55}$$

Thus using (6.55) with the aid of (6.2), (6.3), (6.9) and (6.11), we find from the definitions (6.49), (6.50) and (6.51) that the components of the vector potential $\underline{A}$ are

$$A_r = \frac{\Phi}{2\pi a(\alpha a)} \sum_{\substack{n=1 \\ (ODD)}}^{\infty} (2n+1)\left(\frac{a}{r}\right)\frac{j_n(\alpha r)}{j_n(\alpha a)} P_n(\cos\theta), \tag{6.56}$$

$$A_\theta = \frac{\Phi}{2\pi a(\alpha a)} \sum_{\substack{n=1 \\ (ODD)}}^{\infty} \frac{(2n+1)}{n(n+1)}\frac{1}{j_n(\alpha a)}\left[\alpha a\left\{j_{n-1}(\alpha r) - \frac{a}{r} j_{n-1}(\alpha a)\right\}\right.$$
$$\left. - n\left(\frac{a}{r}\right)\{j_n(\alpha r) - j_n(\alpha a)\}\right]\frac{d}{d\theta}\{P_n(\cos\theta)\} \tag{6.57}$$

and

$$A_\phi = -\frac{\Phi}{2\pi a(\alpha a)} \sum_{\substack{n=1 \\ (ODD)}}^{\infty} \frac{(2n+1)}{n(n+1)} \alpha a \frac{j_n(\alpha r)}{j_n(\alpha a)} \frac{d}{d\theta}\{P_n(\cos\theta)\} \tag{6.58}$$

The corresponding field components are

$$B_r = \frac{\Phi}{2\pi a^2} \sum_{\substack{n=1 \\ (ODD)}}^{\infty} (2n+1)\left(\frac{a}{r}\right)\frac{j_n(\alpha r)}{j_n(\alpha a)} P_n(\cos\theta) \tag{6.59}$$

$$B_\theta = \frac{\Phi}{2\pi a^2} \sum_{\substack{n=1 \\ (ODD)}}^{\infty} \frac{(2n+1)}{n(n+1)}\frac{1}{j_n(\alpha a)}\{\alpha a\, j_{n-1}(\alpha r)$$
$$- n\left(\frac{a}{r}\right) j_n(\alpha r)\}\frac{d}{d\theta}\{P_n(\cos\theta)\} \tag{6.60}$$

and

$$B_\phi = -\frac{\Phi}{2\pi a^2} \sum_{\substack{n=1 \\ (ODD)}}^{\infty} \frac{(2n+1)}{n(n+1)} \alpha a \frac{j_n(\alpha r)}{j_n(\alpha a)} \frac{d}{d\theta}\{P_n(\cos\theta)\} \tag{6.61}$$

With the above results, from (4.46) the correct expression for the relative helicity is

$$H = \int_V \underline{A}\cdot\underline{B}\, dV \tag{6.62}$$

since $\underline{A}_0\cdot\underline{B}_0 = 0$, where V is the volume of the sphere.

Now we could if we wanted calculate the relative helicity directly from (6.62) using (6.56), (6.57), (6.58), (6.59), (6.60). However, it turns out to be slightly easier in terms of the integration needed to proceed as follows.

From (6.62) we have

$$H = 2\pi \int_0^a \int_0^\pi (A_r B_r + A_\theta B_\theta + A_\phi B_\phi) r^2 \sin\theta \, dr \, d\theta \quad (6.63)$$

which may be re-written using the relations (6.49), (6.50), (6.51) and (6.52) in the form

$$H = \frac{2\pi}{\alpha} \int_0^a \int_0^\pi \underline{B} \cdot \underline{B} \, r^2 \sin\theta \, dr \, d\theta + 2\pi \int_0^a \int_0^\pi B_\theta \frac{dg}{d\theta} r \sin\theta \, dr \, d\theta . \quad (6.64)$$

Hence by (6.32) we deduce that H and W are connected by the formula

$$H = \frac{2\mu_0}{\alpha} W + 2\pi \int_0^a \int_0^\pi B_\theta \frac{dg}{d\theta} r \sin\theta \, dr \, d\theta \quad (6.65)$$

in which $dg/d\theta$, which does not depend on r, is given by (6.55). Using the result (6.42), we can calculate the integral

$$\int_0^a r B_\theta \, dr = \frac{\Phi}{2\pi} \sum_{\substack{n=1 \\ (\text{ODD})}}^{\infty} \frac{(2n+1)}{n(n+1)} \frac{d}{d\theta}\{P_n(\cos\theta)\} \quad (6.66)$$

and hence (6.65) becomes

$$H = \frac{2\mu_0}{\alpha} W + \Phi \int_0^\pi \left\{ \sum_{\substack{n=1 \\ (\text{ODD})}}^{\infty} \frac{(2n+1)}{n(n+1) d\theta} \frac{d}{d\theta}\{P_n(\cos\theta)\} \right\} \frac{dg}{d\theta} \sin\theta \, d\theta . \quad (6.67)$$

Substituting for $dg/d\theta$ from (6.55) into (6.67), using the orthogonality relation (6.35) and

using (6.11), we find that integrating (6.67) produces the result

$$\overline{H} = \frac{1}{(\alpha a)}\left\{\overline{W} - \sum_{\substack{n=1 \\ (ODD)}}^{\infty} \frac{(2n+1)}{n(n+1)} \frac{\{\alpha a j_{n-1}(\alpha a) - n j_n(\alpha a)\}}{j_n(\alpha a)}\right. \tag{6.68}$$

where

$$\overline{H} = \frac{\pi}{\overline{\Phi}^2} H \tag{6.69}$$

is an appropriate non-dimensionalization. Thus (6.68) gives the magnetic helicity of the field whose magnetic energy has been calculated from (6.38).

Alternatively, if (6.38) is substituted into (6.68), we obtain the result

$$\overline{H} = \frac{1}{(\alpha a)^2} \sum_{\substack{n=1 \\ (ODD)}}^{\infty} \frac{(2n+1)}{n(n+1)} \int_0^{\alpha a} \frac{2u^2 j_n^2(u)}{j_n^2(\alpha a)} du \tag{6.70}$$

as a separate expression for the magnetic helicity.

Using the results (6.38) and (6.68) above, we have produced plots of helicity against alpha (Figure 6.19), energy against alpha (Figure 6.20) and energy against helicity (Figure 6.21) using the computer program ' enhel.for', and we notice that the graphs show the same characteristics as those of the same quantities obtained in Chapters 4 and 5.

6.11 Variation of Boundary Source Location

We should now like to investigate the consequences of altering the positions of the boundary point sources. We shall keep the 'south pole' source of Figure 6.1 in the same position as before, whilst moving the source previously at the 'north pole' around the boundary to a position making an angle θ^* with the axis of the sphere (Figure 6.22). If

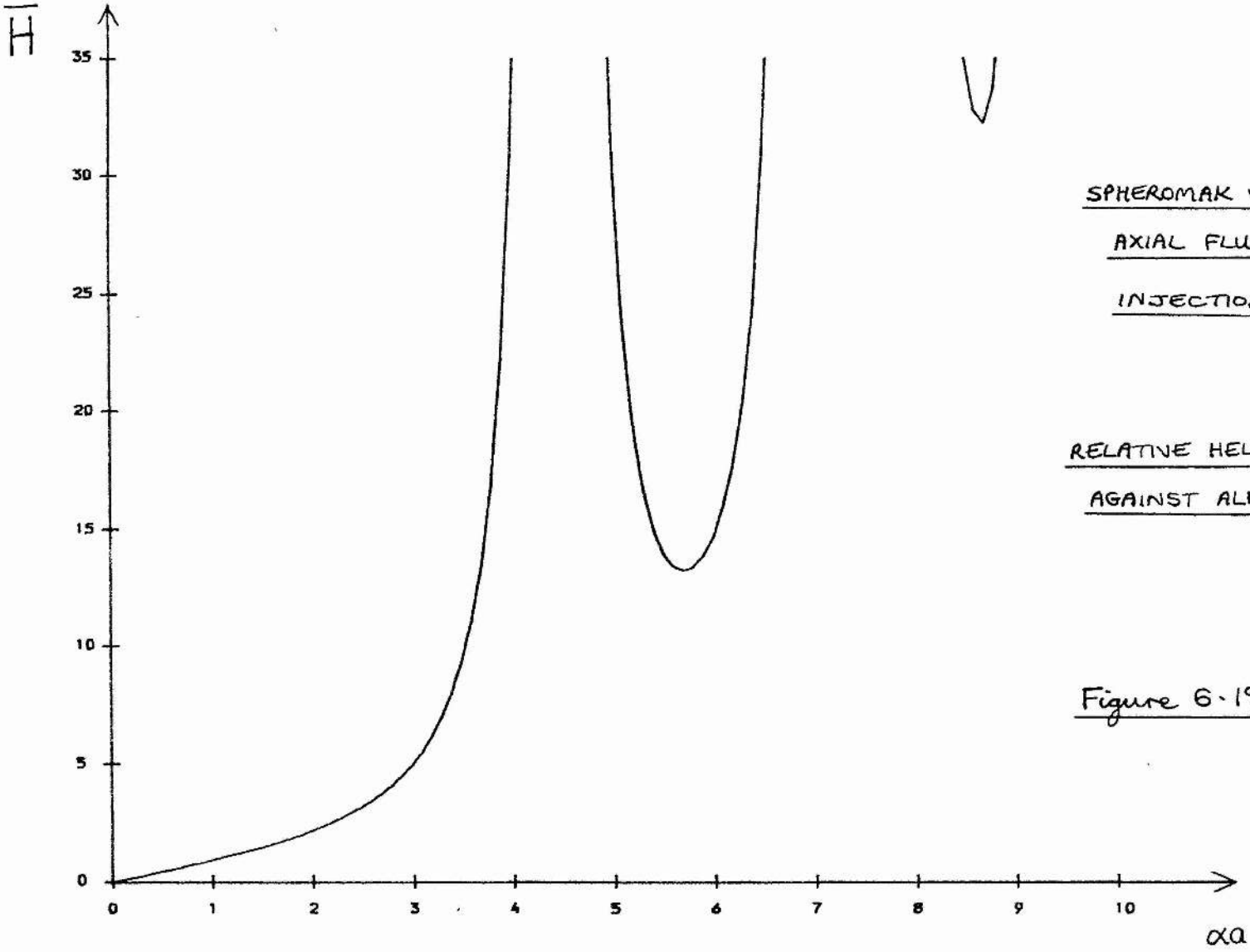

SPHEROMAK WITH AXIAL FLUX INJECTION:

RELATIVE HELICITY AGAINST ALPHA

Figure 6.19

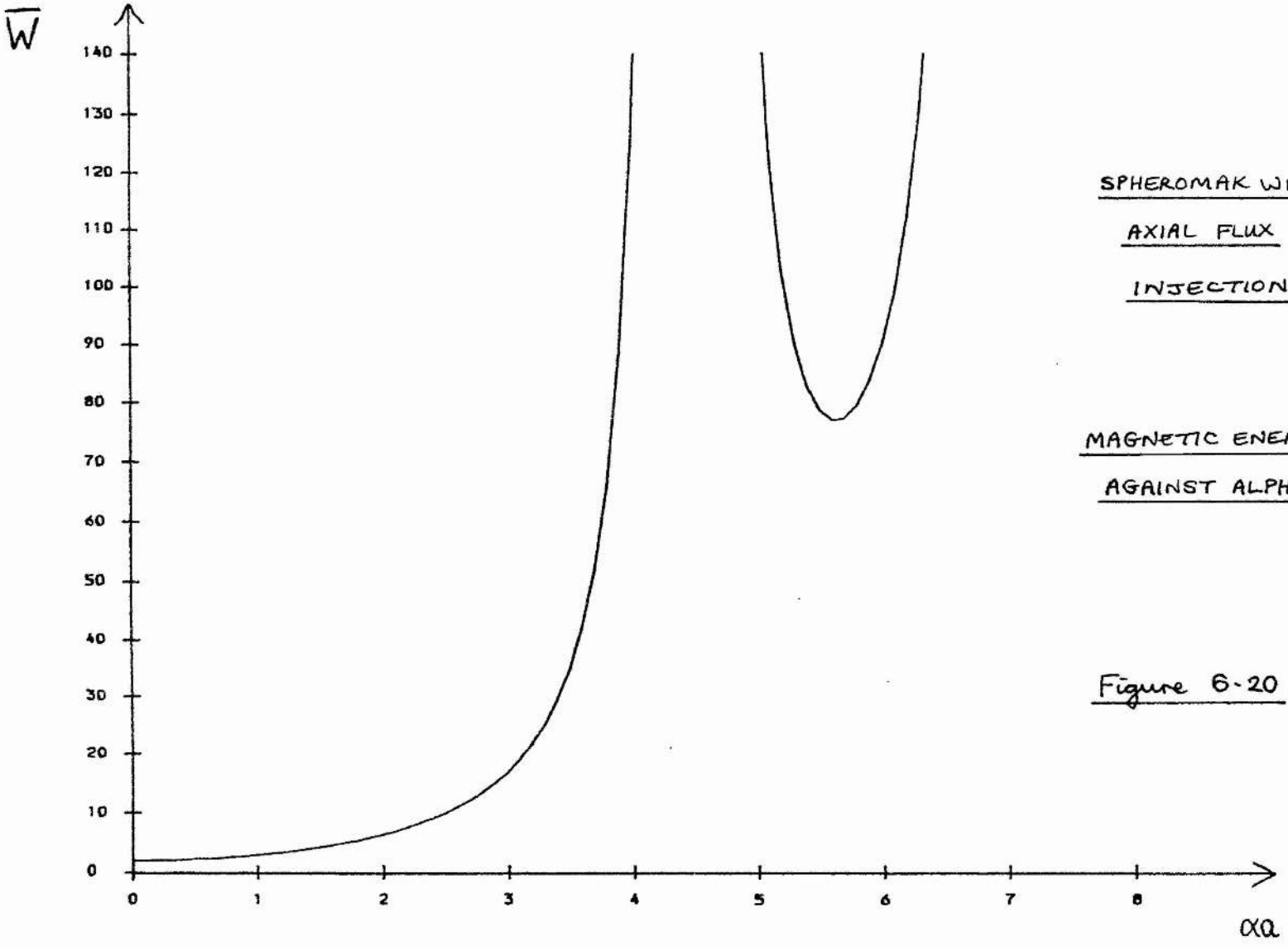

SPHEROMAK WITH AXIAL FLUX INJECTION:

MAGNETIC ENERGY AGAINST ALPHA

Figure 6-20

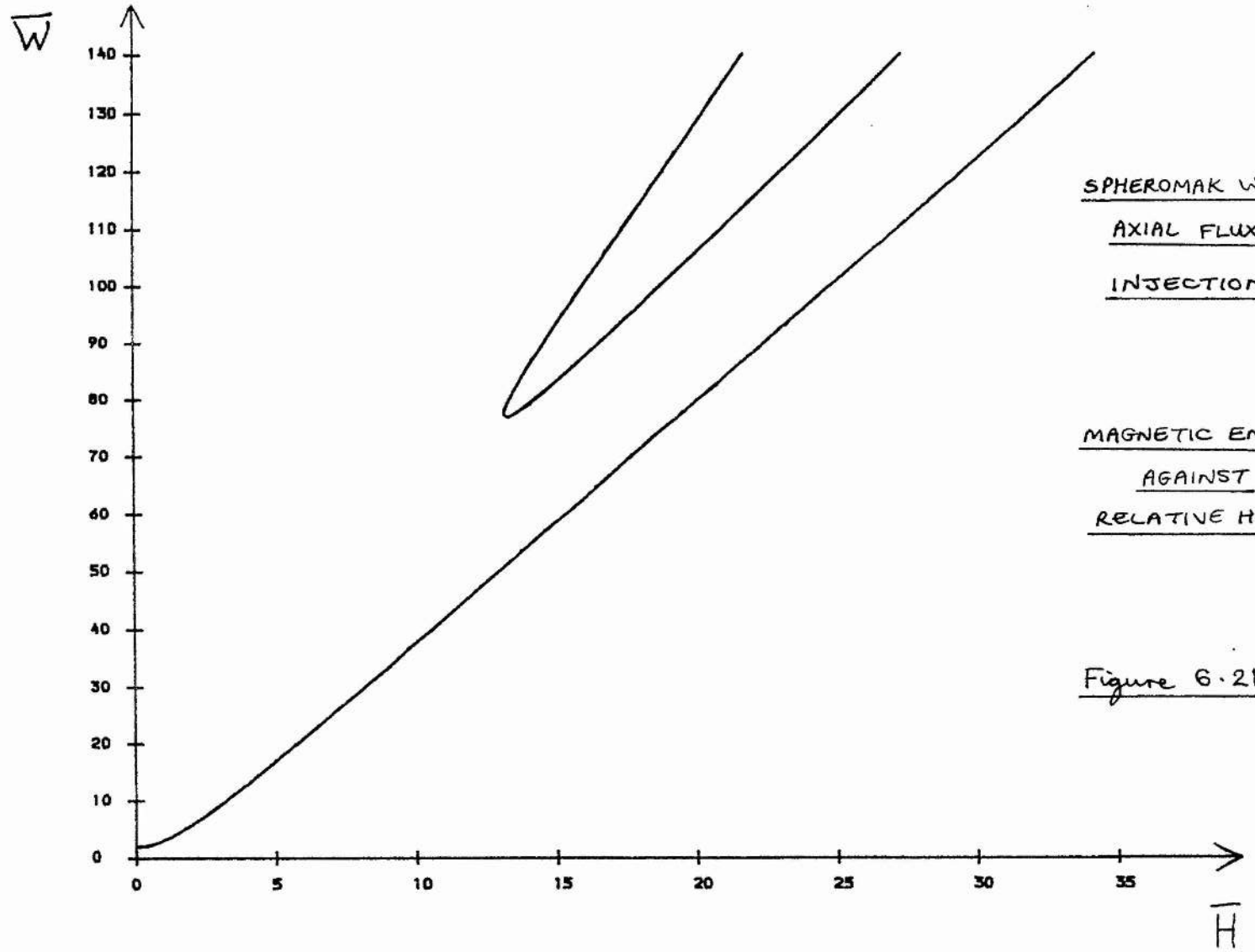

SPHEROMAK WITH AXIAL FLUX INJECTION:

MAGNETIC ENERGY AGAINST RELATIVE HELICITY

Figure 6.21

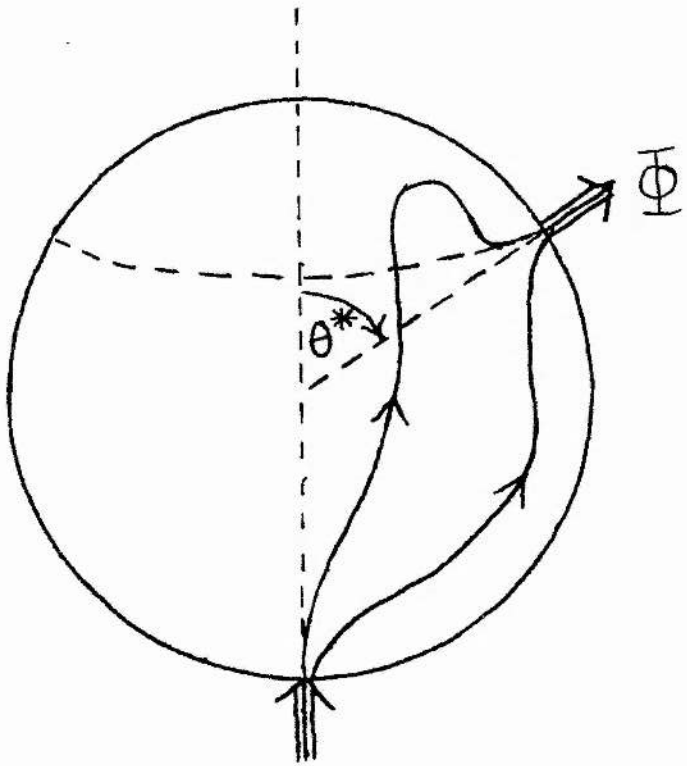

SPHEROMAK WITH POINT SOURCE AND RING SINK.

Figure 6.22

axial symmetry is to be preserved, it is clear that the sink at $\theta = \theta^*$ must necessarily be a circle rather than a point. As mentioned at the beginning of this chapter, for values of θ^* sufficiently close to π, the boundary distribution may model the concentric cylindrical electrodes of spheromaks of the 'gun-injection' type, such as described by Hammer (1984). In this case the source and sink lie close together at the base of the sphere.

6.12 Mathematical Solution

The boundary condition corresponding to the configuration shown in Figure 6.22 is

$$B_r(a) = \frac{\Phi}{2\pi a^2}\{\delta(s-s^*) - \delta(s+1)\} \qquad (6.71)$$

where $s = \cos\theta$ and $s^* = \cos\theta^*$. We note that the expression (6.71) reduces to the form (6.5) when $\theta^* = 0$ as required.

The relaxed solution within the sphere is still given by (6.2), (6.3) and (6.4), but the coefficients are now, by analogy with (6.8),

$$C_n = \frac{(2n+1)\Phi\{P_n(s^*) - P_n(-1)\}}{4\pi n(n+1)a^2 J_{n+\frac{1}{2}}(\alpha a)} \qquad (6.72)$$

Except for the case $n = 0$, all the C_n are in general non-zero.

By comparison with (6.13), we deduce that the dimensionless form of the flux-function for the field with coefficients (6.72) is

$$\bar{A} = \sum_{n=1}^{\infty}\left(\frac{2n+1}{n+1}\right)\frac{\{P_n(\cos\theta^*) - P_n(-1)\}}{2} \times$$

$$\times \left(\frac{r}{a}\right)\frac{j_n(\alpha r)}{j_n(\alpha a)}\{P_{n-1}(\cos\theta) - \cos\theta P_n(\cos\theta)\}, \qquad (6.73)$$

Now the quantity (6.73) vanishes on the axis of the sphere $\theta = 0$ as does its counterpart (6.13). It is not immediately obvious from (6.73) what values are taken by $\overline{A}$ on the curved boundary. However, from our experience of the previous, special case, we should expect a discontinuity in A at the point $r = a, \theta = \theta^*$.

From the computer plots of the field-lines using (6.73), we in fact find the following values of the flux-function on $r = a$:

$$\left.\begin{aligned} \overline{A} &= 0 \quad \text{for} \quad \theta = 0 \ \text{and} \ \theta = \pi ; \\ \overline{A} &= 0 \quad \text{for} \quad 0 < \theta < \theta^* ; \\ \overline{A} &= 1 \quad \text{for} \quad \theta^* < \theta < \pi . \end{aligned}\right\} \tag{6.74}$$

Thus these values confirm our intuition above.

Figures 6.23 to 6.35 inclusive show cross-sections of the field-lines computed using (6.73) for a selection of values of αa and three different values of θ^*, namely 0.0, 1.4 and 2.8. We see a number of features in these plots.

(i) It is apparent at once that in the cases for which $\theta^* \neq 0$ the line $\theta = \pi/2$ is *not* an axis of symmetry, as we should expect from the positioning of the boundary sources and the resulting form of the field-line equation.

(ii) For a fixed value of αa, increasing the angle θ^* seems to have the effect of decreasing the mean field strength, as measured by the difference between the maximum and minimum values of the flux-function. This particular effect is not discernible in the case when $\alpha a = 2.0$, but is clearly present for $\alpha a = 3.0$ and $\alpha a = 4.0$. It is possible to confirm by calculation that for fixed αa the magnetic energy of the configuration decreases monotonically to zero as θ^* increases from 0 to π.

(iii) If instead θ^* is held constant and αa increased, an effect seen with certain values, notably $\theta^* = 0.0$ and 1.4, is that the fraction of the cross-sectional area occupied by island

SPHEROMAK WITH VARYING BOUNDARY SOURCE LOCATIONS:

SET OF THIRTEEN PLOTS.

$\bar{A}max = 1.0000$

$\bar{A}min = 0.0000$

$\alpha a = 2.0000$

$\theta^* = 0.0000$

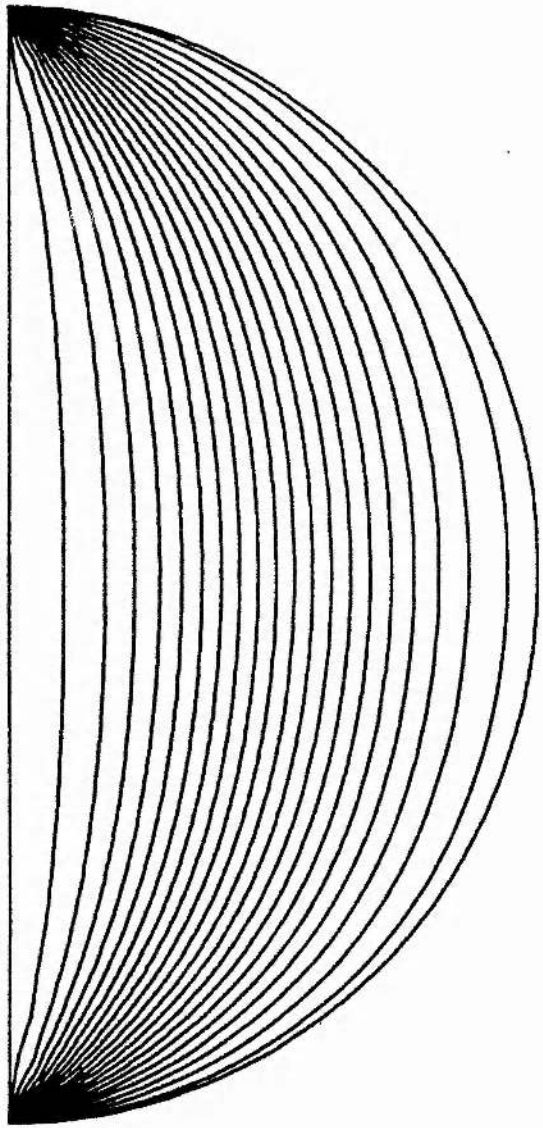

Figure 6.23

$\bar{A}_{max} = 1.0000$

$\bar{A}_{min} = 0.0000$

$\alpha_a = 2.0000$

$\theta^* = 1.4000$

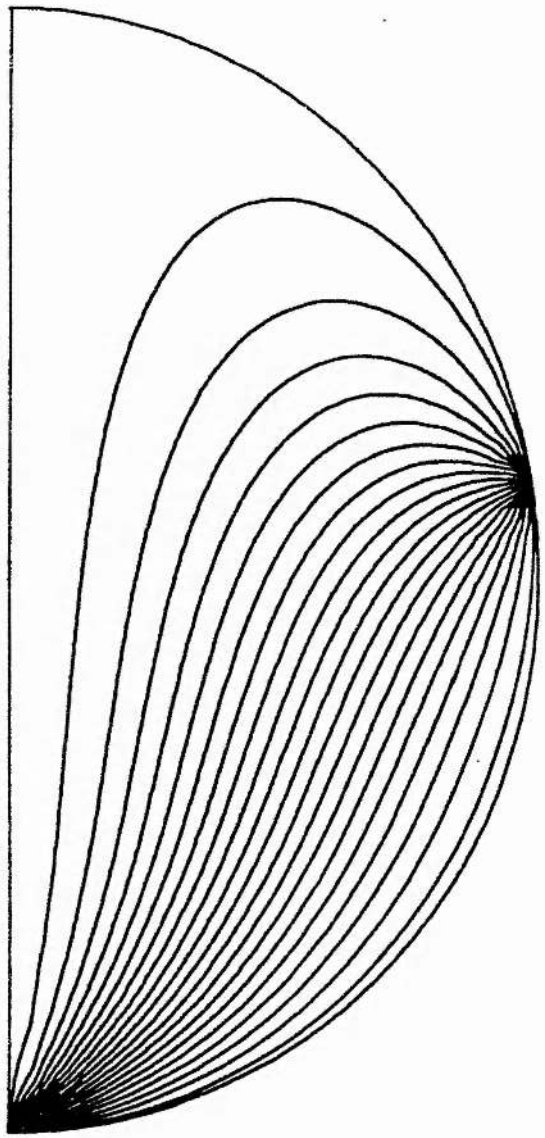

Figure 6.24

$\bar{A}_{max} = 1.0000$

$\bar{A}_{min} = 0.0000$

$\alpha_a = 2.0000$

$\theta^* = 2.8000$

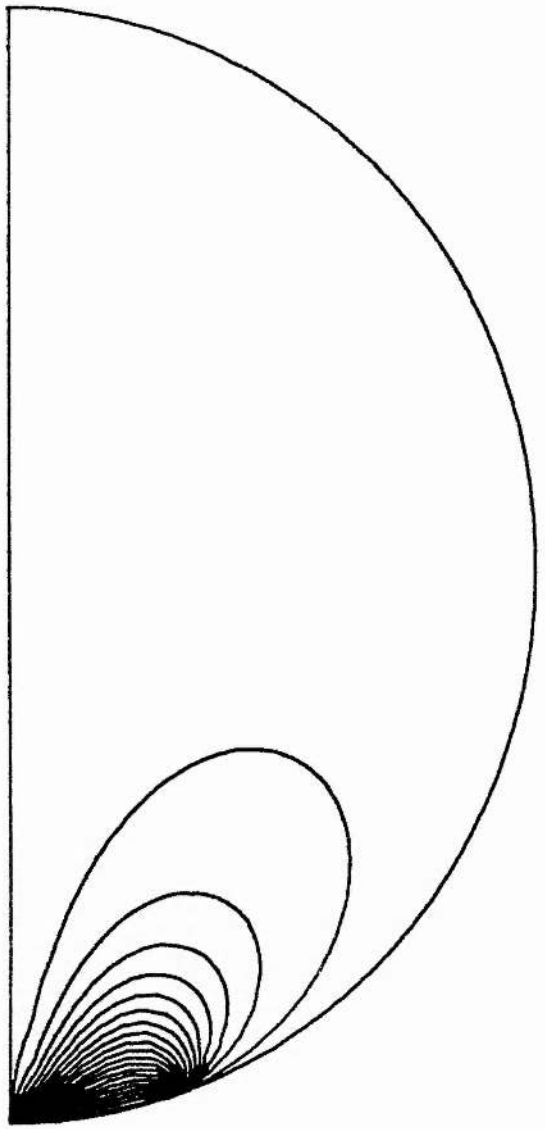

Figure 6-25

$\bar{A}_{max} = 1.1730$

$\bar{A}_{min} = 0.0000$

$\alpha a = 3.0000$

$\theta^* = 0.0000$

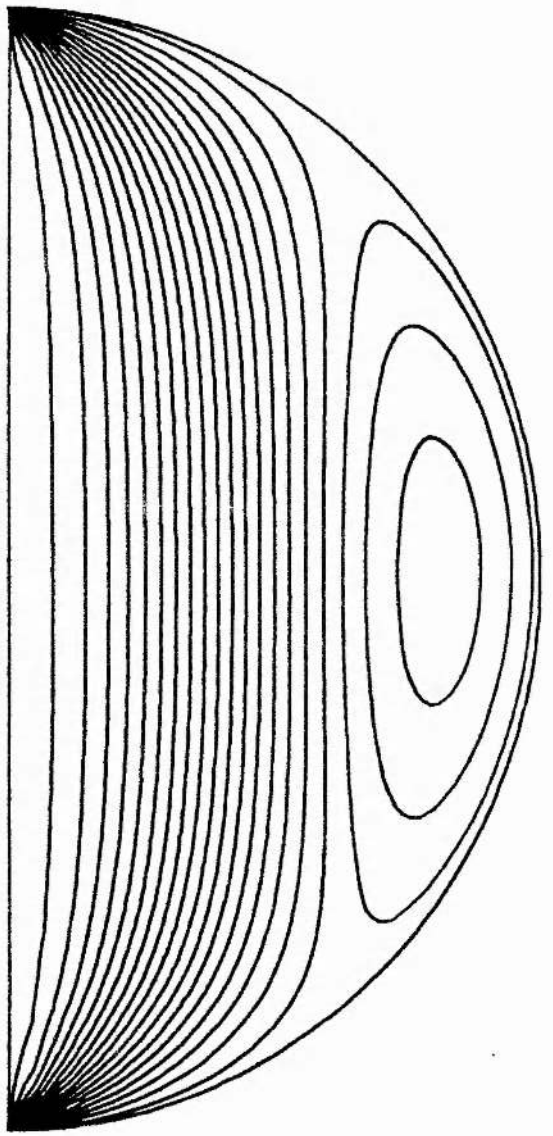

Figure 6.26

$\bar{A}_{max} = 1.0340$

$\bar{A}_{min} = 0.0000$

$\alpha a = 3.0000$

$\theta^* = 1.4000$

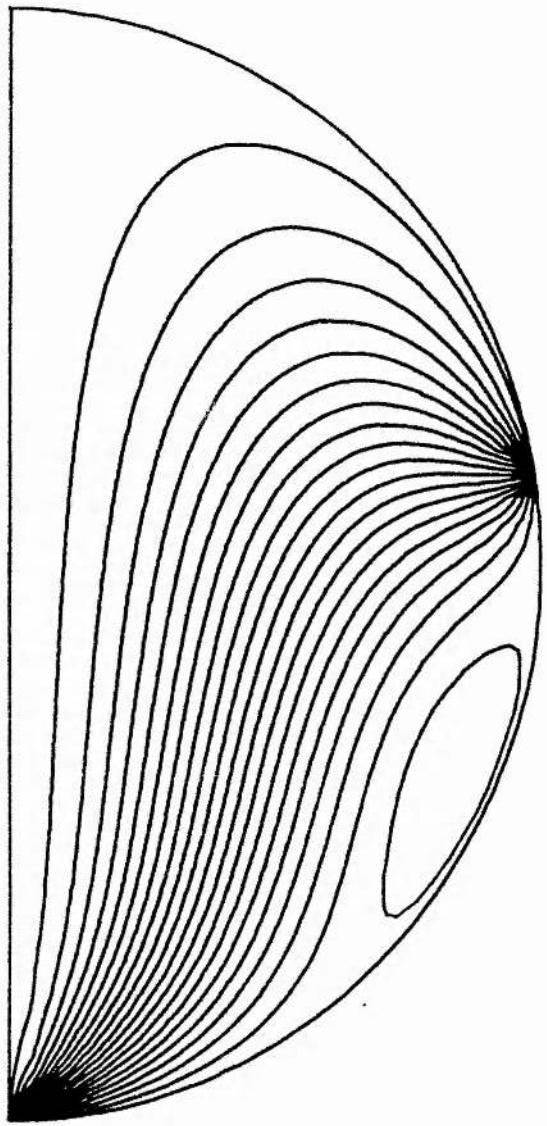

Figure 6.27

$\bar{A}_{max} = 1.0000$

$\bar{A}_{min} = 0.0000$

$\alpha_a = 3.0000$

$\theta^* = 2.8000$

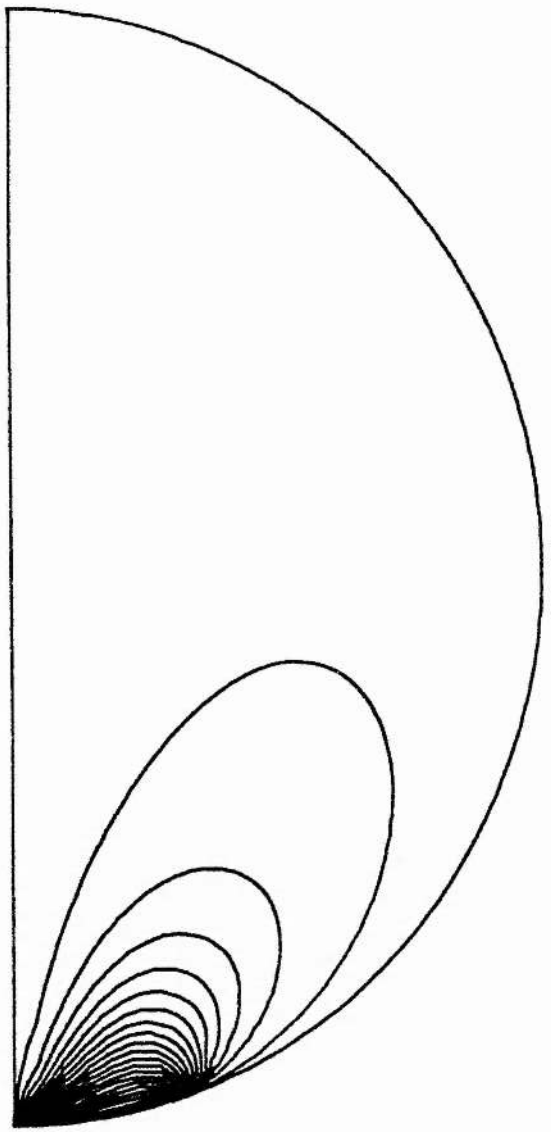

Figure 6-28

$\bar{A}_{max} = 3.1850$

$\bar{A}_{min} = 0.0000$

$\alpha a = 4.0000$

$\theta^* = 0.0000$

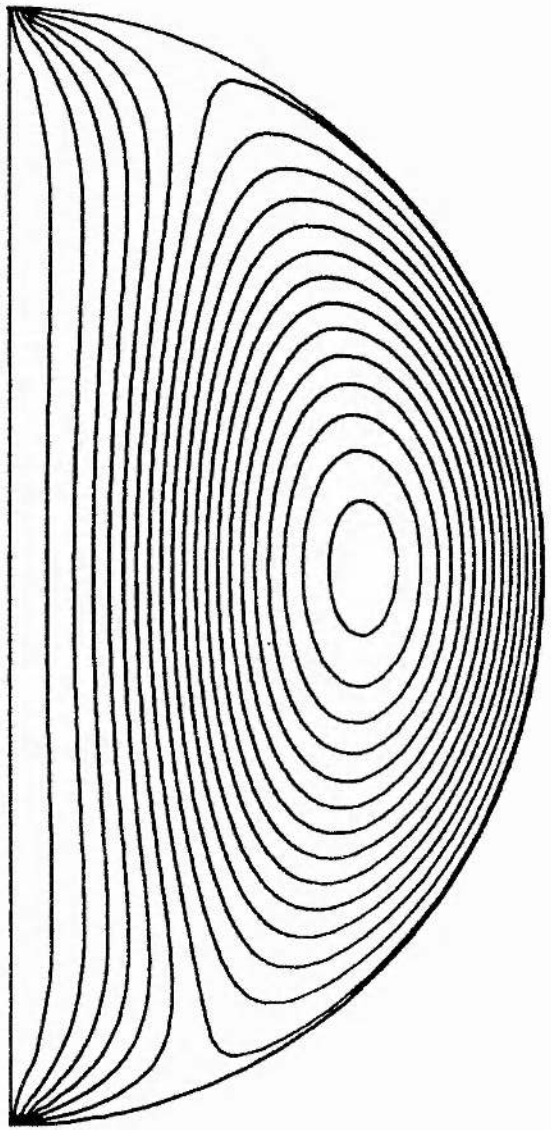

Figure 6.29

$\bar{A}_{max} = 2.0830$

$\bar{A}_{min} = 0.0000$

$\alpha a = 4.0000$

$\theta^* = 1.4000$

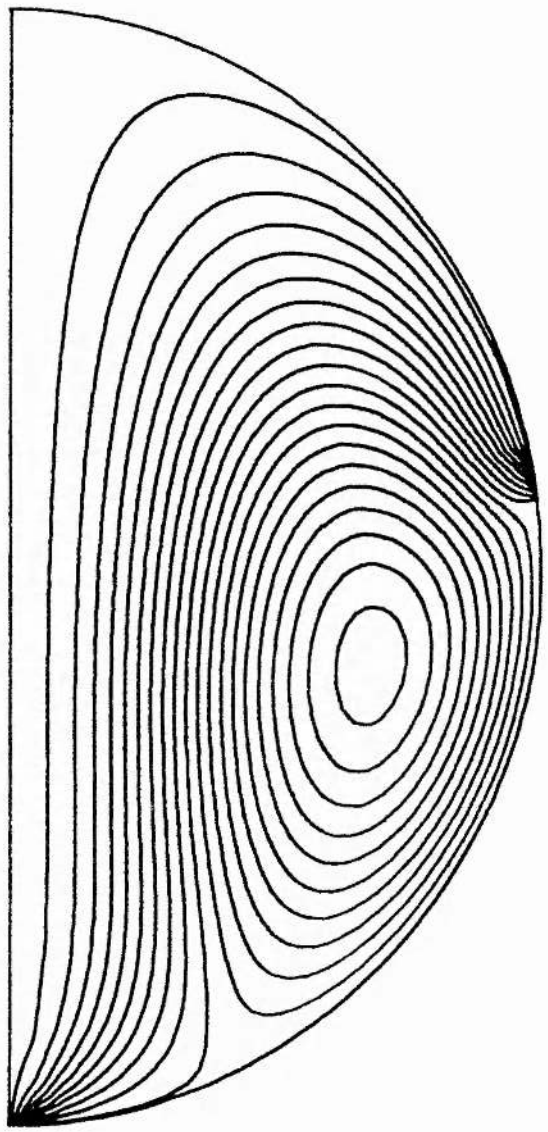

Figure 6.30

$\bar{A}_{max} = 1.0000$

$\bar{A}_{min} = 0.0000$

$\alpha a = 4.0000$

$\theta^* = 2.8000$

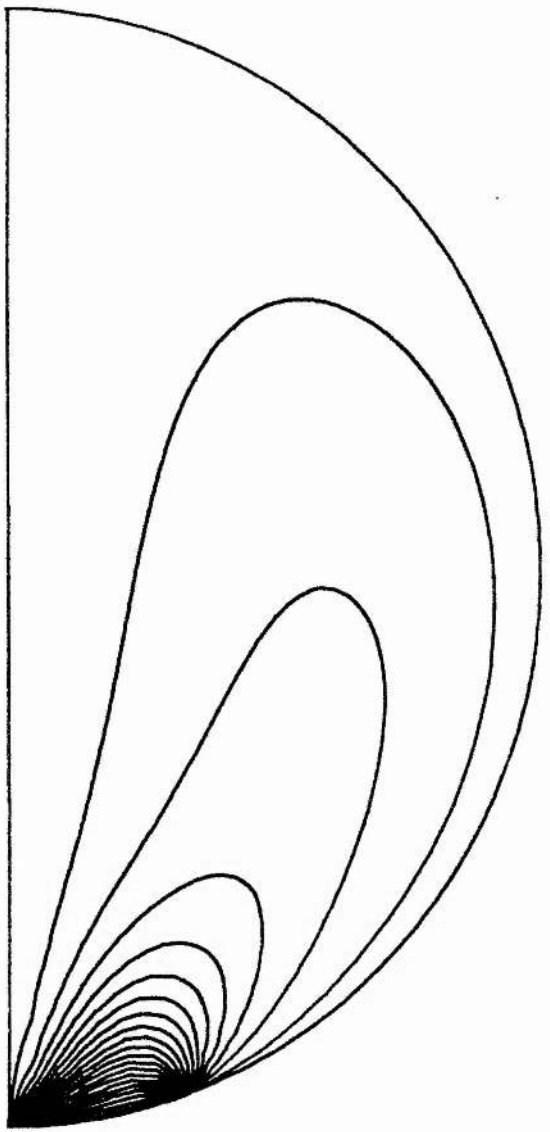

Figure 6-31

$\bar{A}max = 478.6000$

$\bar{A}min = 0.0000$

$\alpha a = 4.4900$

$\theta^* = 0.0000$

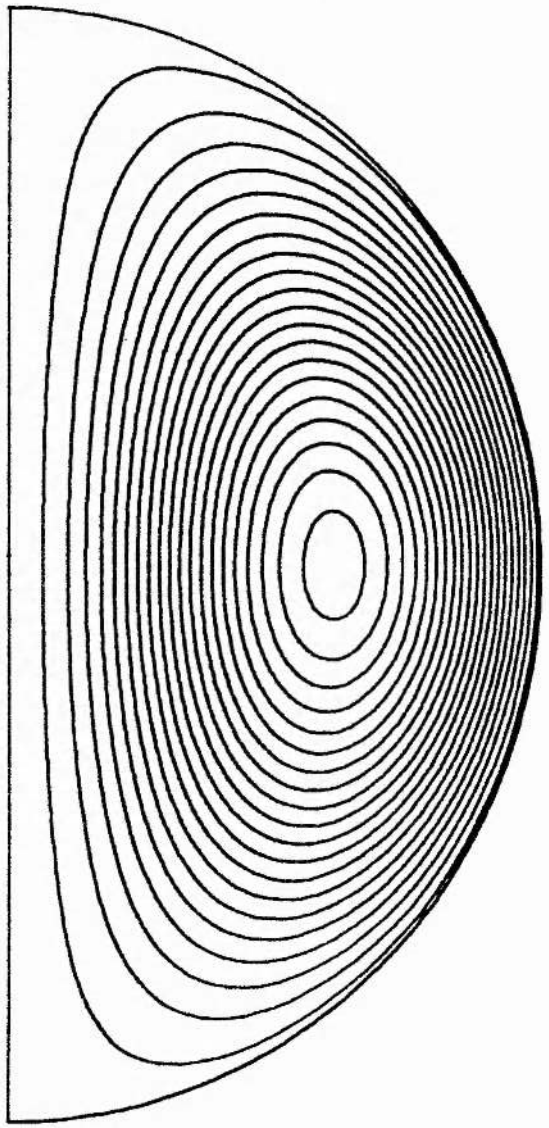

Figure 6-32

$\bar{A}_{max} = 1.0000$

$\bar{A}_{min} = -3.5950$

$\alpha a = 5.0000$

$\theta^* = 0.0000$

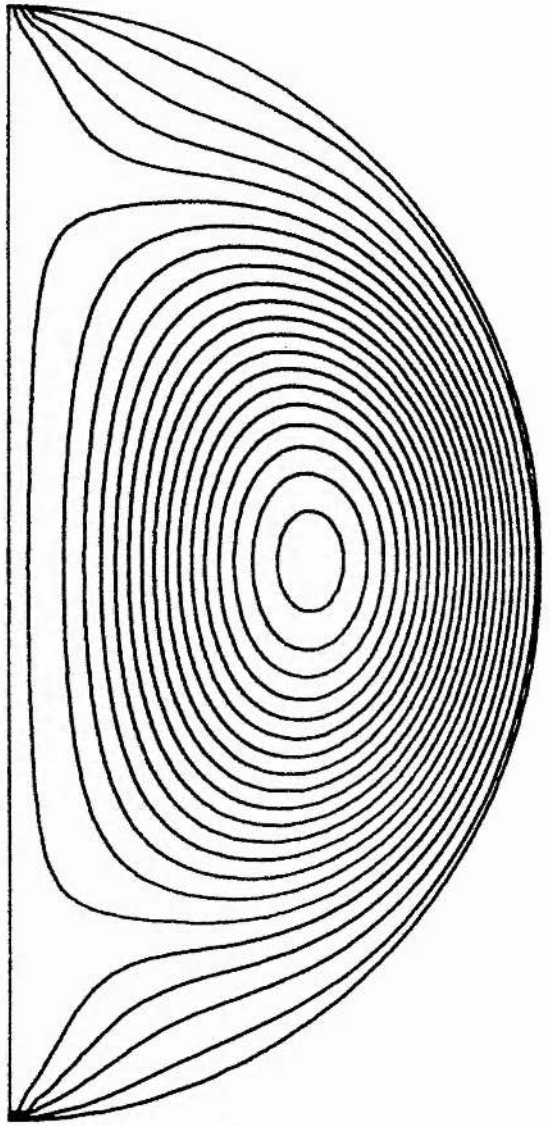

Figure 6-33

$\bar{A}_{max} = 1.0290$

$\bar{A}_{min} = -2.4420$

$\alpha a = 5.0000$

$\theta^* = 1.4000$

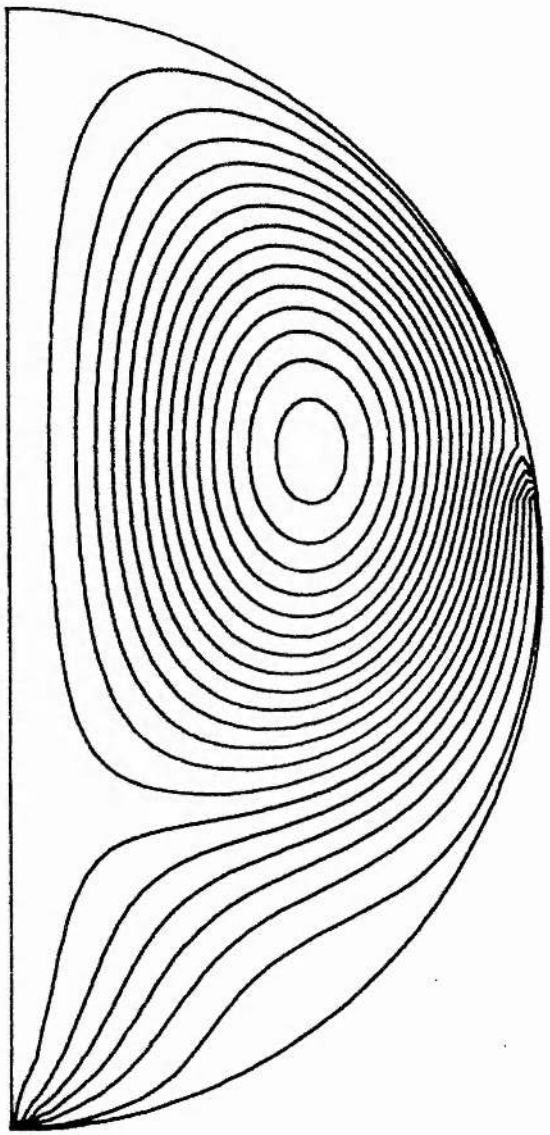

Figure 6.34

$\bar{A}_{max} = 1.0000$

$\bar{A}_{min} = -0.1675$

$\alpha a = 5.0000$

$\theta^* = 2.8000$

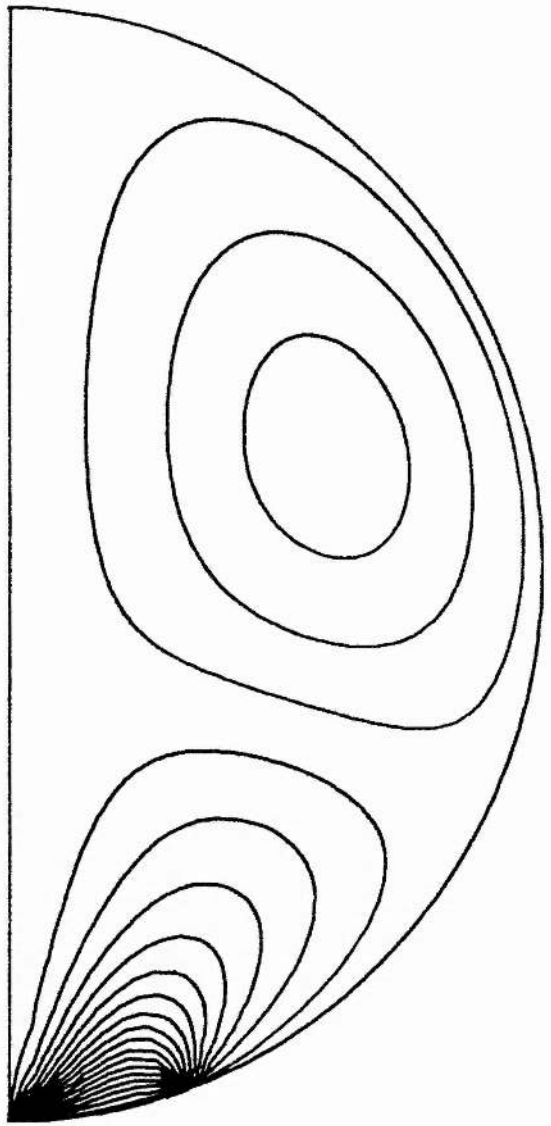

Figure 6.35

regions is increased. This follows the general trend whereby increasing αa increases the topological complexity of the field structure.

(iv) For one plot only, shown in Figure 6.32, we have chosen a value of αa very close to the first zero of $j_1(x)$, that is, the first resonant value of the field. Note the large difference between the maximum and minimum values of the flux-function, indicative of the very high field strength near resonance. Note also that it not possible to tell from the appearance of the field-lines where the boundary sources are; in fact we have shown the case $\theta^* = 0.0$, but the other cases for different values of θ^* are indistinguishable from it.

(v) Although we do not expect these fields to be realised in practice (for reasons that have been discussed earlier) we have included for interest plots of the field for the case $\alpha a = 5.0$ and for the three different values of θ^*, shown in Figures 6.33, 6.34 and 6.35. To see how the topology of the field changes (for fixed θ^*) across the resonance at $\alpha a \approx 4.49$, we compare, for example, Figure 6.30 with Figure 6.34, which suggests the reversal of the ϕ-component of the field as the resonance point is passed through.

6.13 Helicity and Energy of the '$\cos\theta^*$' Field

We wish to modify the results (6.70) and (6.38) in order to find the relevant expressions for the relative helicity and magnetic energy respectively of the fields depicted in Figure 6.22 and described by the flux-function (6.73) . Comparing (6.72) with (6.9) and noting from (5.36) that W (and therefore also H) is proportional to C_n^2 , it is clear that a modifying factor of

$$\left[\frac{1}{2}\left\{P_n(\cos\theta^*) - P_n(-1)\right\}\right]^2 \qquad (6.75)$$

must be introduced into the coefficients of the series for H and W to do this. Hence from the (dimensionless) expressions for the helicity and energy given by (6.70) and (6.38), noting the relations (6.69) and (6.39), we may write the required results as

$$\overline{H}(\theta^*,\alpha a)=\frac{1}{(\alpha a)^2}\sum_{n=1}^{\infty}\left[\frac{1}{2}\{P_n(\cos\theta^*)-P_n(-1)\}\right]^2\frac{(2n+1)}{n(n+1)}\int_0^{\alpha a}\frac{2u^2 j_n^2(u)\,du}{j_n^2(\alpha a)} \tag{6.76}$$

and

$$\overline{W}(\theta^*,\alpha a)=\frac{1}{(\alpha a)}\sum_{n=1}^{\infty}\left[\frac{1}{2}\{P_n(\cos\theta^*)-P_n(-1)\}\right]^2\frac{(2n+1)}{n(n+1)}\left[\int_0^{\alpha a}\frac{2u^2 j_n^2(u)\,du}{j_n^2(\alpha a)}\right.$$
$$\left.+(\alpha a)^2\frac{j_{n-1}(\alpha a)}{j_n(\alpha a)}-n(\alpha a)\right]. \tag{6.77}$$

We have used (6.76) to compute graphs of $\overline{H}$ against θ^* for several different values of αa, the results of which are shown in Figure (6.36). This graph shows that for fixed αa the helicity in each case decreases monotonically to zero with the angle θ^*. Clearly, the case $\theta^* = \pi$ corresponds to the situation where the boundary source and sink of flux coincide and thus annihilate one another : we therefore expect no field within the sphere, with the helicity and energy zero by definition.

The graph of energy against θ^*, obtained using (6.77), is qualitatively very similar to Figure 6.36, with the energy of the field also decreasing monotonically to zero as θ^* increases from 0 to π. For the range of values of αa represented here, the maximum values of $\overline{H}$ and $\overline{W}$ are therefore both attained at $\theta^* = 0.0$.

6.14 Appendix : Some Integration Results and Power Series

A. Simplification of the Result (6.37).

In this section we describe how (6.37) is transformed into (6.38).

Consider then the terms in the integrand of (6.37). First, using the spherical Bessel function identity

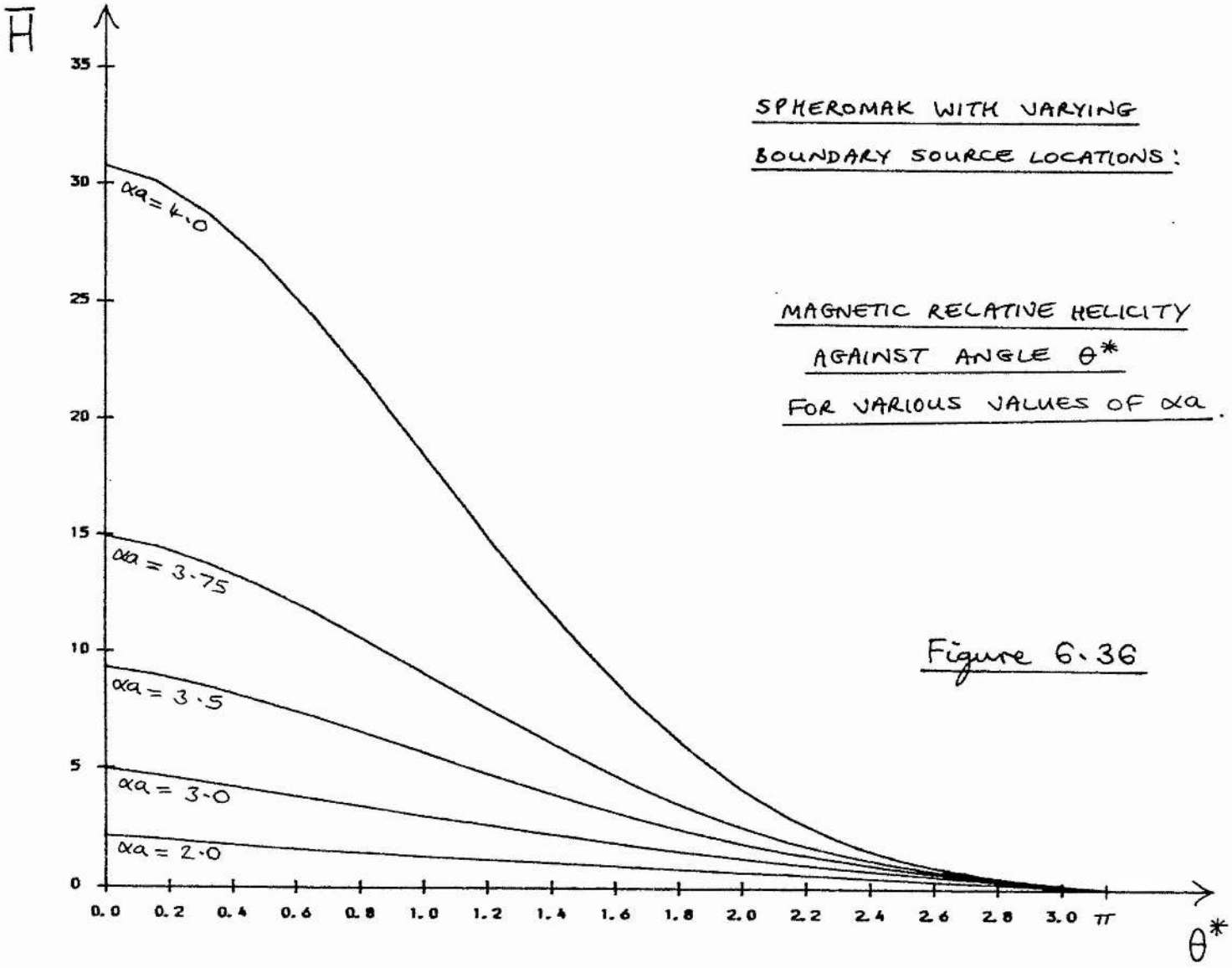

SPHEROMAK WITH VARYING BOUNDARY SOURCE LOCATIONS:

MAGNETIC RELATIVE HELICITY AGAINST ANGLE θ^* FOR VARIOUS VALUES OF αa.

Figure 6.36

$$\bar{j}_{n-1}(x) = \bar{j}_n'(x) + \frac{(n+1)}{x}\bar{j}_n(x) \qquad (6.78)$$

we have

$$\int_0^{\alpha a} u\,\bar{j}_{n-1}(u)\,\bar{j}_n(u)\,du = \int_0^{\alpha a}\left\{(n+1)\bar{j}_n^2(u) + u\bar{j}_n(u)\bar{j}_n'(u)\right\}du$$

$$= \int_0^{\alpha a}\left(n+\tfrac{1}{2}\right)\bar{j}_n^2(u)\,du + \tfrac{1}{2}\alpha a\,\bar{j}_n^2(\alpha a) \qquad (6.79)$$

after integrating by 'parts'.

Again using (6.78), we have

$$\int_0^{\alpha a} u^2\bar{j}_{n-1}^2(u)\,du = \int_0^{\alpha a} u^2\left\{\frac{(n+1)}{u}\bar{j}_n(u) + \bar{j}_n'(u)\right\}^2 du$$

$$= \int_0^{\alpha a}(n+1)^2\bar{j}_n^2(u)\,du + 2(n+1)\int_0^{\alpha a} u\bar{j}_n(u)\bar{j}_n'(u)\,du$$

$$+ \int_0^{\alpha a} u^2\left\{\bar{j}_n'(u)\right\}^2 du$$

$$= \int_0^{\alpha a} n(n+1)\bar{j}_n^2(u)\,du + (n+1)\alpha a\,\bar{j}_n^2(\alpha a)$$

$$+ \int_0^{\alpha a} u^2\left\{\bar{j}_n'(u)\right\}^2 du \qquad (6.80)$$

upon integration of the second term. Taking the third term of (6.80), we find that integrating it by parts gives

$$\int_0^{\alpha a} u^2\left\{\bar{j}_n'(u)\right\}^2 du = \left[u^2\bar{j}_n'(u)\bar{j}_n(u)\right]_0^{\alpha a}$$

$$- \int_0^{\alpha a}\bar{j}_n(u)\left\{2u\bar{j}_n'(u) + u^2\bar{j}_n''(u)\right\}du\,. \qquad (6.81)$$

We now use Bessel's equation for $j_n(x)$, namely

$$x^2 j_n''(x) = -2x j_n'(x) - \{x^2 - n(n+1)\} j_n(x) \quad (6.82)$$

in order to eliminate the double derivative term from (6.81). Thus we find that

$$\int_0^{\alpha a} u^2 \{j_n'(u)\}^2 = \left[u^2 j_n(u)\left\{j_{n-1}(u) - \frac{(n+1)}{u} j_n(u)\right\}\right]_0^{\alpha a} + \int_0^{\alpha a} \{u^2 - n(n+1)\} j_n^2(u)\, du . \quad (6.83)$$

Hence, substituting (6.83) into (6.80) we have

$$\int_0^{\alpha a} u^2 j_{n-1}^2(u)\, du = (\alpha a)^2 j_n(\alpha a) j_{n-1}(\alpha a) + \int_0^{\alpha a} u^2 j_n^2(u)\, du . \quad (6.84)$$

The two results (6.79) and (6.84) may now be substituted into the integrand (6.37), which therefore becomes

$$\int_0^{\alpha a} \{(u^2 + 2n^2 + n) j_n^2(u) - 2nu\, j_{n-1}(u) j_n(u) + u^2 j_{n-1}^2(u)\}\, du$$
$$= \int_0^{\alpha a} 2u^2 j_n^2(u)\, du + (\alpha a)^2 j_n(\alpha a) j_{n-1}(\alpha a) - n(\alpha a) j_n^2(\alpha a) . \quad (6.85)$$

Finally, the expression (6.38) is obtained by substituting (6.85) into (6.37) and using the non-dimensionalizing scaling factor (6.39).

B. Power Series for $j_n(x)$.

It is often convenient and advantageous in the numerical evaluation of spherical Bessel functions to use appropriate power series forms rather than use values output from

standard computer packages. This was found to be the case in evaluating the integrands in (6.38) and (6.70), because for large n the value of $j_n(u)$ was often smaller than 10^{-38} and thus returned as 0 by the VAX.

The power series for $j_n(x)$ is (e.g. Abramowitz and Stegun, p.437)

$$j_n(x) = \frac{x^n}{1.3.5\ldots(2n+1)}\left\{1 - \frac{\frac{1}{2}x^2}{1!(2n+3)} + \frac{(\frac{1}{2}x^2)^2}{2!(2n+3)(2n+5)} - \frac{(\frac{1}{2}x^2)^3}{3!(2n+3)(2n+5)(2n+7)} + \cdots\right\} \quad (6.86)$$

which we shall rewrite in the form

$$j_n(x) = \frac{x^n}{1.3.5\ldots(2n+1)} S_n(x) , \quad (6.87)$$

In particular, therefore, we have the ratio

$$\frac{j_n(\alpha r)}{j_n(\alpha a)} = \left(\frac{r}{a}\right)^n \frac{S_n(\alpha r)}{S_n(\alpha a)} , \quad (6.88)$$

which may be used in the evaluation by numerical integration of (6.38) and (6.70).

Further, we may write

$$S_n(x) = \sum_{k=0}^{\infty} a_k \left(\frac{1}{2}x^2\right)^k \quad (6.89)$$

whose coefficients are then given by the recurrence relation

$$a_k = \frac{-1}{k(2n+2k+1)} a_{k-1} \quad (6.90)$$

with 'starting value' $a_0 = 1$.

In the above formulation, a result also useful in calculating (6.38) is

$$\frac{\bar{j}_{n-1}(x)}{\bar{j}_n(x)} = \frac{(2n+1)}{x} \frac{S_{n-1}(x)}{S_n(x)} , \qquad (6.91)$$

C. Asymptotic Formulae.

As $n \to \infty$, we see from the definition (6.86) that

$$\bar{j}_n(x) \longrightarrow \frac{x^n}{1 \cdot 3 \cdot 5 \ldots (2n+1)} , \qquad (6.92)$$

Thus, in particular,

$$\frac{\bar{j}_{n-1}(x)}{\bar{j}_n(x)} \longrightarrow \frac{(2n+1)}{x} \quad \text{as} \quad n \to \infty , \qquad (6.93)$$

CHAPTER SEVEN : THE GENERALIZATION OF THE WOLTJER MINIMUM-ENERGY PRINCIPLE TO FREE BOUNDARIES

7.1 Introduction

In this chapter we discuss the extension of the theorem of Woltjer (1958) for the minimization of the magnetic energy of a magnetic structure to include the case of a free boundary subjected to external magnetic or plasma pressure forces. We also indicate how to treat the case in which the boundary is not a magnetic surface. To illustrate the theory, we have provided three applications, the first of these to a finite cylindrical flux tube and the remaining two to possible spheromak configurations.

As remarked in Chapter One, Woltjer (1958) showed that for fields confined within a magnetic surface ($\underline{B}\cdot\underline{n} = 0$) with the single constraint of magnetic helicity conservation, the extrema of the magnetic energy are given by linear (constant - α) force-free fields. A tacit assumption here is that the bounding surface of the confined volume is not capable of deformation, that is, it is rigid. Clearly, in an astrophysical context this is inappropriate since there is generally an absence of confining walls such as in the laboratory. Hence a more realistic theory must also take into account the possibility of 'free' boundaries such as exist in a natural environment. The theory which has been developed in the present chapter uses an extension of the variational approach originally employed by Woltjer (1958). A major difference is that, in addition to the constraint that the magnetic helicity be held constant, we must incorporate the condition that the pressure forces at the boundary balance at the energy extrema. We assume that the pressure within the volume of interest is purely magnetic in origin, but in the external region we allow for either an ideal gas pressure or a pressure produced by a magnetic field.

7.2 Setting-up of the Minimization Problem

7.2.1 Basic Ideas

Consider plasma occupying a simply-connected volume V of space, separated from the rest of space by a magnetic surface S, as depicted in Figure 7.1. Multiply-connected regions can be accommodated by a straightforward extension of the basic theory. The extension to allow magnetic flux to cross the boundary S will be outlined later.

Within the region V we assume there exists a non-zero magnetic field $\underline{B}$ which dominates the gas pressure, that is, we adopt the 'low beta' approximation. Associated with this field are the field energy W and the magnetic relative helicity H. The region V' is characterized in the first instance by having no magnetic field but a finite, non-zero plasma pressure p which depends on position. The analysis should also hold if we include a potential field in V'.

The important new feature is that S is allowed to be a *free boundary* , which may change its spatial configuration due to the balance of pressure across it.

Treating the magnetic relative helicity H of the system as a global invariant in the manner of Taylor (1974), we minimize the magnetic energy W of the system subject to the additional constraint that there is a pressure balance at the free boundary. In this way we discover the nature of the field $\underline{B}$ which minimizes the energy.

7.2.2 Physical Quantities

In the usual manner, we define the magnetic field $\underline{B}$ in terms of the magnetic vector potential $\underline{A}$ by

$$\underline{B} = \nabla \times \underline{A} \quad . \tag{7.1}$$

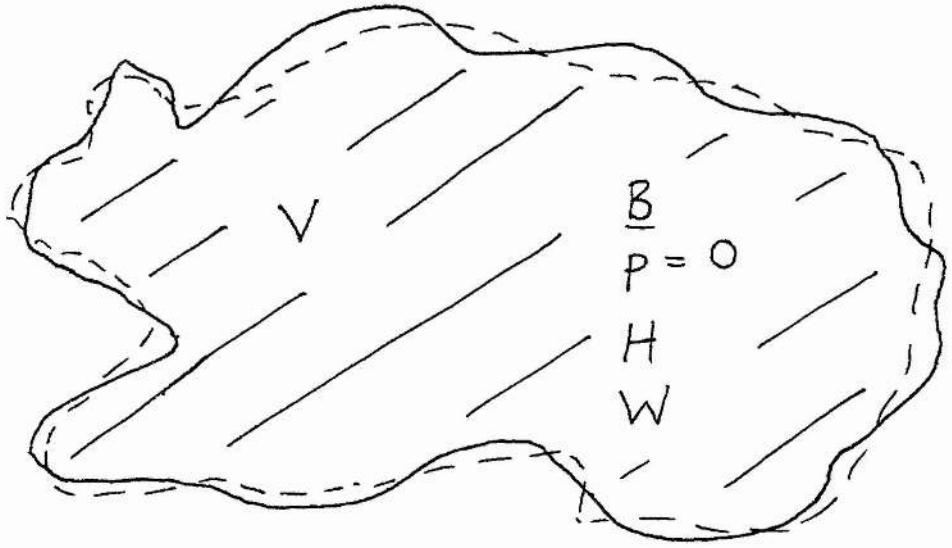

VOLUME OF PLASMA

BOUNDED BY A VARIABLE

MAGNETIC SURFACE,

WITH PHYSICAL VARIABLES SHOWN.

V'

$\underline{B} = \underline{0}$

$p = p(r)$

Figure 7.1

Then the magnetic energy of the field within V is

$$W = \frac{1}{2\mu_0} \int_V (\nabla \times \underline{A})^2 dV \tag{7.2}$$

and the magnetic helicity associated with it is

$$H = \int_V \underline{A} \cdot (\nabla \times \underline{A}) dV . \tag{7.3}$$

Notice that, since the bounding surface S is a flux surface, the expression (7.3) is gauge invariant and so is automatically the relative helicity.

In the exterior region V' we recall that there is a gas pressure $p(\underline{r})$ and zero field, whereas in the internal region V we have zero gas pressure but a magnetic field pressure $B^2/2\mu_0$. Hence the appropriate pressure balance on S may be written

$$[(\nabla \times \underline{A})^2]_S = 2\mu_0 [p]_S . \tag{7.4}$$

Let us denote by ξ a small displacement from some (assumed) equilibrium state of the system. In particular, we are interested in the displacement field on the boundary S. Given such a displacement, the energy of the system may involve changes in three ways, as follows. First, the vector potential $\underline{A}$ may change. Second, the boundary S may be displaced from its original position, which changes the limits in the integral (7.2). Third, if S does move, it must do mechanical work against the external gas pressure $[p]_S$, which changes the energy content of V' by an amount

$$\delta U = \int_S p (\underline{\xi} \cdot d\underline{S}) \tag{7.5}$$

where $d\underline{S}$ points out of V. We assume that there is no heat flow across the boundary.

All three of the above effects must be taken into account when considering the minimization of the energy of the whole system.

7.3 Solution of the Problem

7.3.1 Minimization Process

Since we are to extremize the total energy of the system subject to the constraint that the relative helicity H associated with the plasma in V remain fixed, we define the quantity

$$F = (W+U) - \frac{\lambda}{2\mu_0} H \tag{7.6}$$

where $\lambda/2\mu_0$ is a Lagrange multiplier and U represents the internal energy of the system.

With the definitions (7.2), (7.3) and (7.5) we see that the first variation of (7.6) is

$$2\mu_0 \delta F = \int_V 2\,\underline{B}\cdot(\underline{\nabla}\times\delta\underline{A})\,dV + \int_S B^2(\underline{\xi}\cdot d\underline{S}) + \int_S 2\mu_0 p(\underline{\xi}\cdot d\underline{S}) - \lambda\left\{\int_V(\delta\underline{A}\cdot\underline{B} + \underline{A}\cdot(\underline{\nabla}\times\delta\underline{A}))dV + \int_S(\underline{A}\cdot\underline{B})(\underline{\xi}\cdot d\underline{S})\right. \tag{7.7}$$

We now use the vector identity

$$\underline{A}\cdot(\underline{\nabla}\times\delta\underline{A}) = \delta\underline{A}\cdot(\underline{\nabla}\times\underline{A}) + \underline{\nabla}\cdot(\delta\underline{A}\times\underline{A}) \tag{7.8}$$

on the terms in (7.7) involving $\nabla\times\delta\underline{A}$, and apply the divergence theorem. Setting δF to zero, we obtain the expression

$$2\int_V \delta\underline{A}\cdot(\underline{\nabla}\times\underline{B} - \lambda\underline{B})dV + \int_S \delta\underline{A}\times(2\underline{B}-\lambda\underline{A})\cdot d\underline{S} + \int_S (B^2 - \lambda\,\underline{A}\cdot\underline{B} + 2\mu_0 p)(\underline{\xi}\cdot d\underline{S}) = 0 . \tag{7.9}$$

From the induction equation (1.21), we have that, on the boundary surface S,

$$\delta \underline{A} = \underline{\xi} \times \underline{B} \quad . \tag{7.10}$$

(Note that, since δF is gauge-invariant, there is no loss of generality in employing this particular gauge.) Thus

$$\int_S \delta \underline{A} \times (2\underline{B} - \lambda \underline{A}) \cdot d\underline{S} = \int_S (2\underline{B} - \lambda \underline{A}) \cdot \underline{\xi} (\underline{B} \cdot d\underline{S}) - \int_S (2\underline{B} - \lambda \underline{A}) \cdot \underline{B} (\underline{\xi} \cdot d\underline{S}) \quad . \tag{7.11}$$

For the purposes of the present calculation $\underline{B} \cdot d\underline{S} = 0$, so that (7.9) transforms to

$$2 \int_V \delta \underline{A} \cdot (\nabla \times \underline{B} - \lambda \underline{B}) dV + \int_S (2\mu_0 p - B^2)(\underline{\xi} \cdot d\underline{S}) = 0 \quad . \tag{7.12}$$

The surface integral term in (7.12) expresses the force balance at the boundary. Thus if (7.4) is satisfied, we obtain

$$\int_V \{ \delta \underline{A} \cdot (\nabla \times \underline{B} - \lambda \underline{B}) \} dV = 0 \quad , \tag{7.13}$$

Finally, since $\delta \underline{A}$ is an arbitrary quantity at all points in V, the integrand in (7.13) must necessarily vanish identically, giving us the result

$$\nabla \times \underline{B} = \lambda \underline{B} \tag{7.14}$$

where λ, being a Lagrange multiplier, is a constant uniform throughout V.

7.3.2 Interpretation of the Result

Equation (7.14) indicates that, under the conditions we have specified, an extremum of the magnetic field energy is produced by a linear, force-free field, thus extending the

previously known result for fixed boundaries to the case of pressure-confined free surfaces bounding V.

Dixon, Berger, Browning and Priest (1988) show how the above result may be extended further to include the effect of line-tying of coronal fields to the photosphere, assuming the photosphere is rigid, that is, $\underline{\xi} = \underline{0}$ there. The corona is divided into a number of independent flux regions, some or all of which have flux tied to the surface of the sun. Each of the regions is confined by the magnetic pressure of surrounding regions. The analysis is essentially similar to that employed above.

We now discuss some applications of the above theory.

7.4 Axi-Symmetric Flux-Tube Model

7.4.1 Geometry

In this example we shall consider plasma confined by a uniform external gas pressure so that it assumes the shape of a straight cylindrical flux-tube of circular cross-section but with a radius R which is capable of variation (see Figure 7.2). We adopt cylindrical polar co-ordinates (r,ϕ,z) and assume, for simplicity, that all quantities depend only on the radial co-ordinate r, so that the cylinder is constrained to expand or contract in a purely axi-symmetric manner.

So, outside the cylinder we have a uniform gas pressure p_0, but no magnetic field; inside the tube we neglect the gas pressure ($\beta \ll 1$) but have a non-zero magnetic field

$$\underline{B} = B_0 \left(0, B_\phi(r), B_z(r)\right) . \qquad (7.15)$$

There are two conserved quantities in the cylinder, namely the magnetic helicity H and the magnetic flux ψ, and we invoke a pressure balance at the boundary of the cylinder.

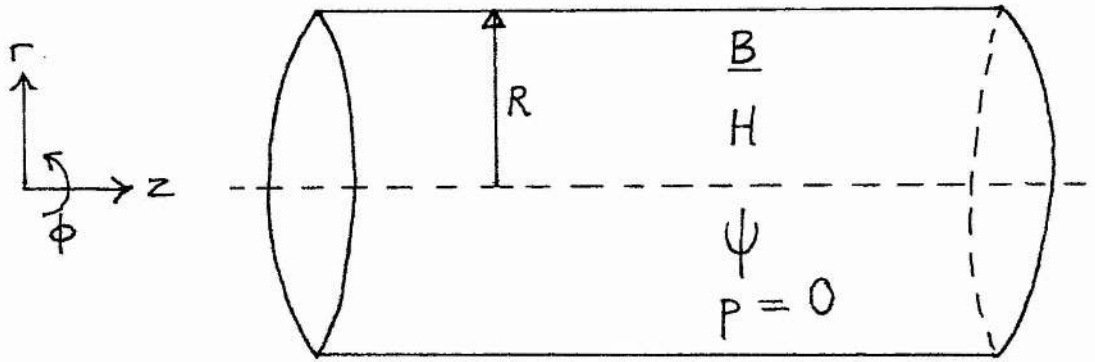

MODEL OF A STRAIGHT CYLINDRICAL FLUX TUBE OF VARIABLE RADIUS WITH RELEVANT PARAMETERS.

$$\underline{B} = \underline{0}$$

$$P = P_e$$

Figure 7-2

7.4.2 Minimum Energy State : Physical Quantities

Applying the result of the extended Woltjer principle as given in Section 7.3, the least-energy configuration of the magnetic field is a 'constant-α' state of the form

$$\underline{B} = B_0 \left(0, J_1(\alpha r), J_0(\alpha r)\right) \tag{7.16}$$

which, it can be verified, satisfies

$$\nabla \times \underline{B} = \alpha \underline{B} \tag{7.17}$$

and is divergence-free.

The 'toroidal' flux ψ is given by

$$\psi = 2\pi \int_0^R r B_z(r)\, dr \tag{7.18}$$

which using the field (7.16) we find to be

$$\psi = \frac{2\pi B_0 R^2 J_1(\alpha R)}{\alpha R} \,. \tag{7.19}$$

This quantity is conserved in our isolated tube.

Next, we wish to calculate the relative helicity (per unit length in the z-direction) of the field (7.16). To do this, we need two vector potentials : one corresponding to the field (7.16), and the other corresponding to the potential field with the same boundary conditions and flux. In general, the vector potential for (7.16) may be written

$$\underline{A} = B_0 \left(f(r), \frac{J_1(\alpha r)}{\alpha} + \frac{c_1}{r}, \frac{J_0(\alpha r)}{\alpha} + c_2 \right) \tag{7.20}$$

in which f is an arbitrary function and c_1, c_2 are constants. The required potential field is

$$\underline{B}_0 = \frac{2B_0 J_1(\alpha R)}{\alpha R} (0, 0, 1) \tag{7.21}$$

for which the simplest vector potential is

$$\underline{A}_0 = B_0 \frac{J_1(\alpha R)}{\alpha R} (0, r, 0) . \tag{7.22}$$

To construct the gauge-invariant relative helicity from (7.16), (7.20), (7.21) and (7.22), (see, for example, Finn and Antonsen, 1985) we equate the tangential components of (7.20) and (7.22) at the boundary $r = R$, noting that we may take $f(r) = 0$ and that $c_1 = 0$ in order that $\underline{A}$ remain finite on the axis. Hence we deduce that

$$\underline{A} = B_0 \left(0, \frac{J_1(\alpha r)}{\alpha}, \frac{J_0(\alpha r) - J_0(\alpha R)}{\alpha} \right) \tag{7.23}$$

and the relative helicity is then defined by

$$H = 2\pi \int_0^R r (\underline{A} \cdot \underline{B} - \underline{A}_0 \cdot \underline{B}_0) \, dr \tag{7.24}$$

where we note from (7.21) and (7.22) that

$$\underline{A}_0 \cdot \underline{B}_0 = 0 , \tag{7.25}$$

Therefore, substituting (7.16) and (7.23) into the integral expression (7.24) gives the result

$$H = \frac{2\pi R^3 B_0^2}{(\alpha R)^2} \{ \alpha R J_0^2(\alpha R) - 2 J_0(\alpha R) J_1(\alpha R) + \alpha R J_1^2(\alpha R) \} \tag{7.26}$$

per unit length in the z-direction.

To determine the external pressure p_e in terms of the magnitude of the magnetic field, we note that the pressure balance at $r = R$ requires that

$$p_e = \frac{|\underline{B}(R)|^2}{2\mu_0} . \tag{7.27}$$

Hence from the field (7.16) we deduce that the external pressure is

$$p_e = \frac{B_0^2 \{J_0^2(\alpha R) + J_1^2(\alpha R)\}}{2\mu_0} \tag{7.28}$$

expressed in terms of the tube radius R and the magnitude B_0 of the internal field.

Two further quantities of interest are the magnetic energy per unit length, which we calculate to be

$$W = \frac{\pi B_0^2 R^2}{\mu_0 (\alpha R)} \{\alpha R J_0^2(\alpha R) - J_0(\alpha R) J_1(\alpha R) + \alpha R J_1^2(\alpha R)\} \tag{7.29}$$

and the z-component of the field (7.16) on the boundary r = R , which we shall write as

$$B_z = B_0 J_0(\alpha R) . \tag{7.30}$$

7.4.3 Deductions : Dimensionless Quantities

We shall now investigate the results of the previous section graphically, first forming various dimensionless variables, as follows.

From (7.19), (7.26) and (7.28) we can form the dimensionless parameter

$$q_1(\alpha R) = \frac{\mu_0 p_e \psi^6}{H^4} \equiv \frac{p_e}{p_{e0}} \tag{7.31}$$

which we use as a measure of p_e when ψ and H are regarded as constant. Then, once p_e is chosen, αR is determined implicitly. We can also, in a similar fashion, define the dimensionless quantity

$$q_2(\alpha R) = \frac{R}{\psi^2} H \equiv \frac{R}{R_0} . \qquad (7.32)$$

Thus the variation of the equilibrium radius of the tube with external pressure may be determined in principle by eliminating αR between (7.31) and (7.32) in the case where ψ and H do not vary.

For the force-free parameter α we define

$$q_3(\alpha R) = \frac{\alpha R}{q_2(\alpha R)} \equiv \frac{\alpha}{\alpha_0} \qquad (7.33)$$

where ψ and H are constant. Continuing in this vein, by defining

$$q_4(\alpha R) = \frac{\mu_0 \psi^2}{H^2} W \equiv \frac{W}{W_0} \qquad (7.34)$$

and

$$q_5(\alpha R) = \frac{B_0 \psi^3}{H^2} J_0(\alpha R) \equiv \frac{B_z}{B_{z0}} \qquad (7.35)$$

we have dimensionless measures of the energy and boundary 'toroidal' field, again where ψ and H are fixed.

We next use the results (7.19), (7.26), (7.28), (7.29) and (7.30) to evaluate the q_n (n = 1,2,3,4,5) explicitly, and find that the results are

$$\frac{p_e}{p_0} = \frac{2\pi^2(\alpha R)^2 J_1^6(\alpha R)\{J_0^2(\alpha R) + J_1^2(\alpha R)\}}{\{\alpha R J_0^2(\alpha R) - 2 J_0(\alpha R) J_1(\alpha R) + \alpha R J_1^2(\alpha R)\}^4} \qquad (7.36)$$

$$\frac{R}{R_0} = \frac{\{\alpha R J_0^2(\alpha R) - 2 J_0(\alpha R) J_1(\alpha R) + \alpha R J_1^2(\alpha R)\}}{2\pi J_1^2(\alpha R)} \qquad (7.37)$$

$$\frac{\alpha}{\alpha_0} = \frac{2\pi(\alpha R)J_1^2(\alpha R)}{\{\alpha R J_0^2(\alpha R) - 2J_0(\alpha R)J_1(\alpha R) + \alpha R J_1^2(\alpha R)\}} \tag{7.38}$$

$$\frac{W}{W_0} = \frac{\pi(\alpha R)J_1^2(\alpha R)\{\alpha R J_0^2(\alpha R) - J_0(\alpha R)J_1(\alpha R) + \alpha R J_1^2(\alpha R)\}}{\{\alpha R J_0^2(\alpha R) - 2J_0(\alpha R)J_1(\alpha R) + \alpha R J_1^2(\alpha R)\}^2} \tag{7.39}$$

and

$$\frac{B_z}{B_{z0}} = \frac{2\pi(\alpha R)J_0(\alpha R)J_1^3(\alpha R)}{\{\alpha R J_0^2(\alpha R) - 2J_0(\alpha R)J_1(\alpha R) + \alpha R J_1^2(\alpha R)\}^2} \tag{7.40}$$

In all of the the above five expressions, the flux ψ and the helicity H are held constant.

We wish also to obtain variations of quantities with the relative helicity (per unit length) H , this time keeping the flux ψ and the external pressure p_e invariant. To do this, we must invent new dimensionless parameters. First, we define

$$q_6(\alpha R) = \frac{H}{(\mu_0 p_e \psi^6)^{1/4}} \equiv \frac{H}{H_0} \tag{7.41}$$

which is a measure of the helicity.

For the tube radius we have

$$q_7(\alpha R) = R\left(\frac{\mu_0 p_e}{\psi^2}\right)^{1/4} \equiv \frac{R}{R_1} \tag{7.42}$$

and for the force-free constant we define

$$q_8(\alpha R) = \alpha\left(\frac{\psi^2}{\mu_0 p_e}\right)^{1/4} \equiv \frac{\alpha}{\alpha_1} . \tag{7.43}$$

In much the same way, we have

$$q_9(\alpha R) = W\left(\frac{\mu_0}{p_e \psi^2}\right)^{1/2} \equiv \frac{W}{W_1} \tag{7.44}$$

for the magnetic energy, and finally

$$q_{10}(\alpha R) = \frac{B_0 J_0(\alpha R)}{(\mu_0 p_e)^{1/2}} \equiv \frac{B_z}{B_{z1}} \tag{7.45}$$

for the component of the boundary field in the z-direction.

Again using (7.19), (7.26), (7.28), (7.29) and (7.30), we evaluate the q_n (n = 6,7,8,9,10) explicitly, so that when ψ and p_e are fixed

$$\frac{H}{H_0} = \frac{2^{1/4}\{\alpha R J_0^2(\alpha R) - 2J_0(\alpha R)J_1(\alpha R) + \alpha R J_1^2(\alpha R)\}}{(2\pi\alpha R)^{1/2} J_1^{3/2}(\alpha R)\{J_0^2(\alpha R) + J_1^2(\alpha R)\}^{1/4}} \tag{7.46}$$

$$\frac{R}{R_1} = \left[\frac{(\alpha R)^2\{J_0^2(\alpha R) + J_1^2(\alpha R)\}}{8\pi^2 J_1^2(\alpha R)}\right]^{1/4} \tag{7.47}$$

$$\frac{\alpha}{\alpha_1} = \left[\frac{8\pi^2(\alpha R)^2 J_1^2(\alpha R)}{\{J_0^2(\alpha R) + J_1^2(\alpha R)\}}\right]^{1/4} \tag{7.48}$$

$$\frac{W}{W_1} = \frac{\{\alpha R J_0^2(\alpha R) - J_0(\alpha R)J_1(\alpha R) + \alpha R J_1^2(\alpha R)\}}{2^{1/2} J_1(\alpha R)\{J_0^2(\alpha R) + J_1^2(\alpha R)\}^{1/2}} \tag{7.49}$$

and

$$\frac{B_z}{B_{z1}} = \frac{2^{1/2} J_0(\alpha R)}{\{J_0^2(\alpha R) + J_1^2(\alpha R)\}^{1/2}} . \tag{7.50}$$

In Figures 7.3a to 7.3d inclusive we have plotted, using αR as the implicit parameter, the quantities (7.37), (7.38), (7.39) and (7.40) as functions of the pressure variable (7.36); whereas is in Figures 7.4a through 7.4d we show the variation of the parameters (7.47), (7.48), (7.49) and (7.50) with the helicity variable (7.46).

The arrows on the graphs indicate the directions of increase of the parametric

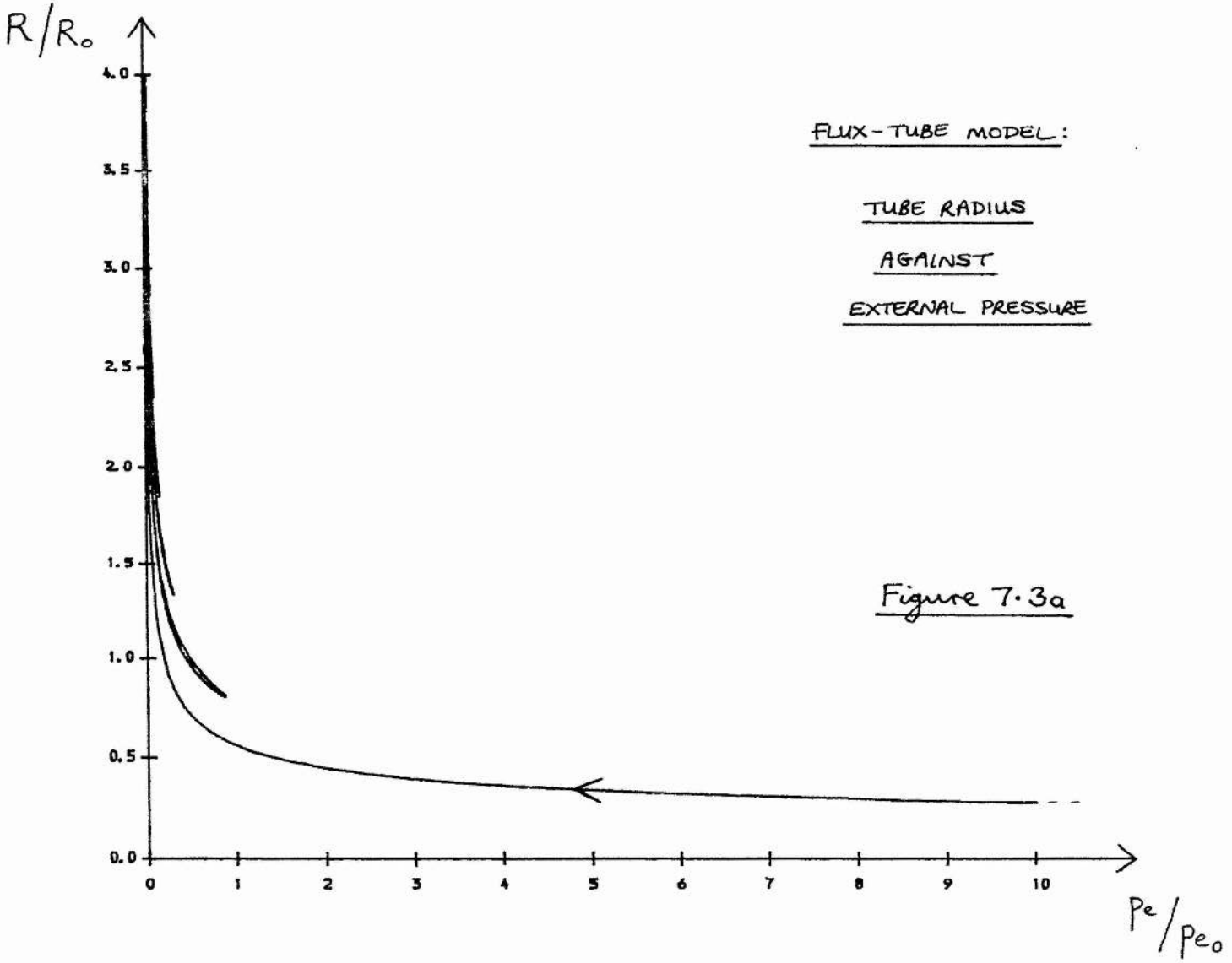

FLUX-TUBE MODEL:

TUBE RADIUS

AGAINST

EXTERNAL PRESSURE

Figure 7·3a

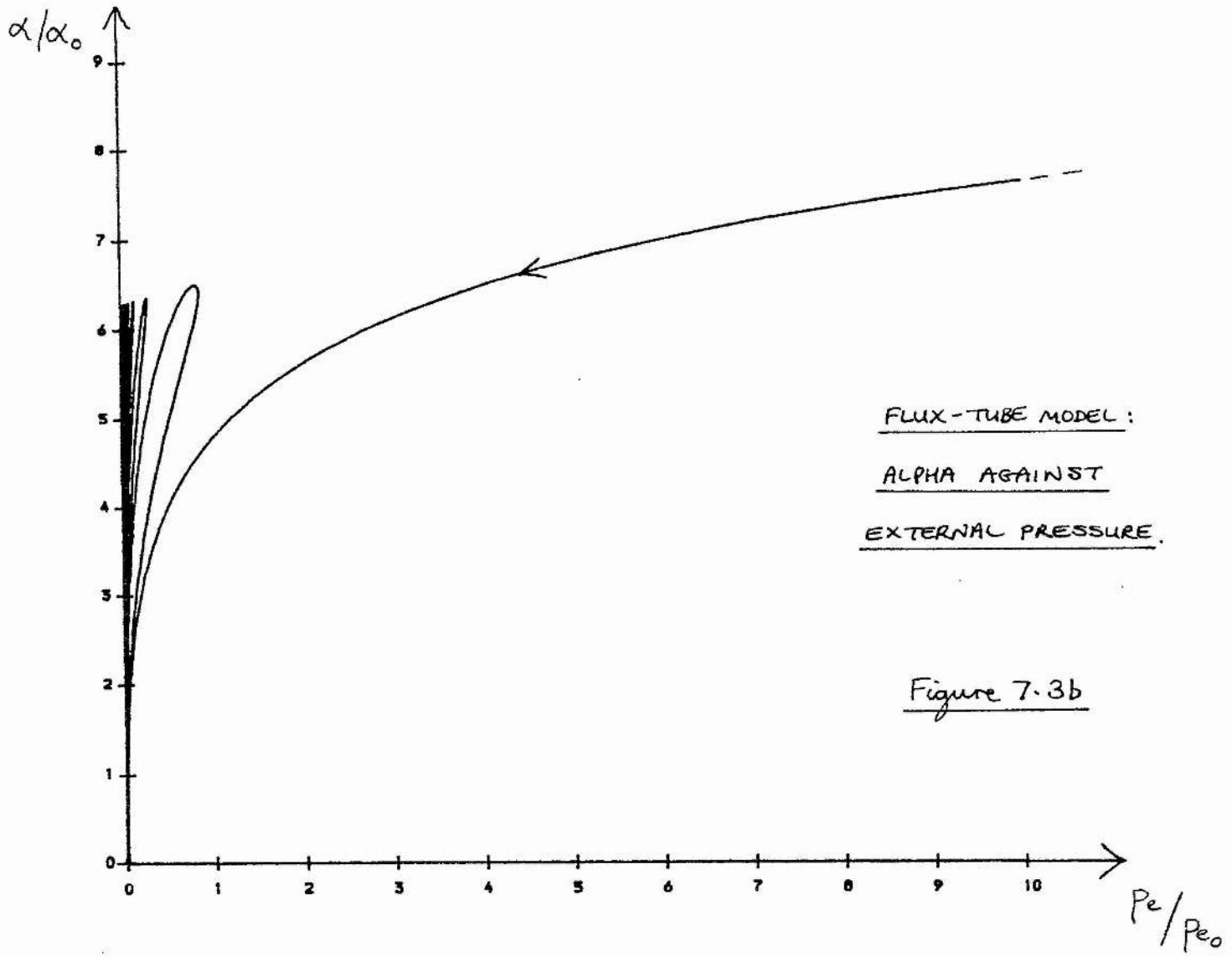

FLUX-TUBE MODEL:

ALPHA AGAINST

EXTERNAL PRESSURE.

Figure 7.3b

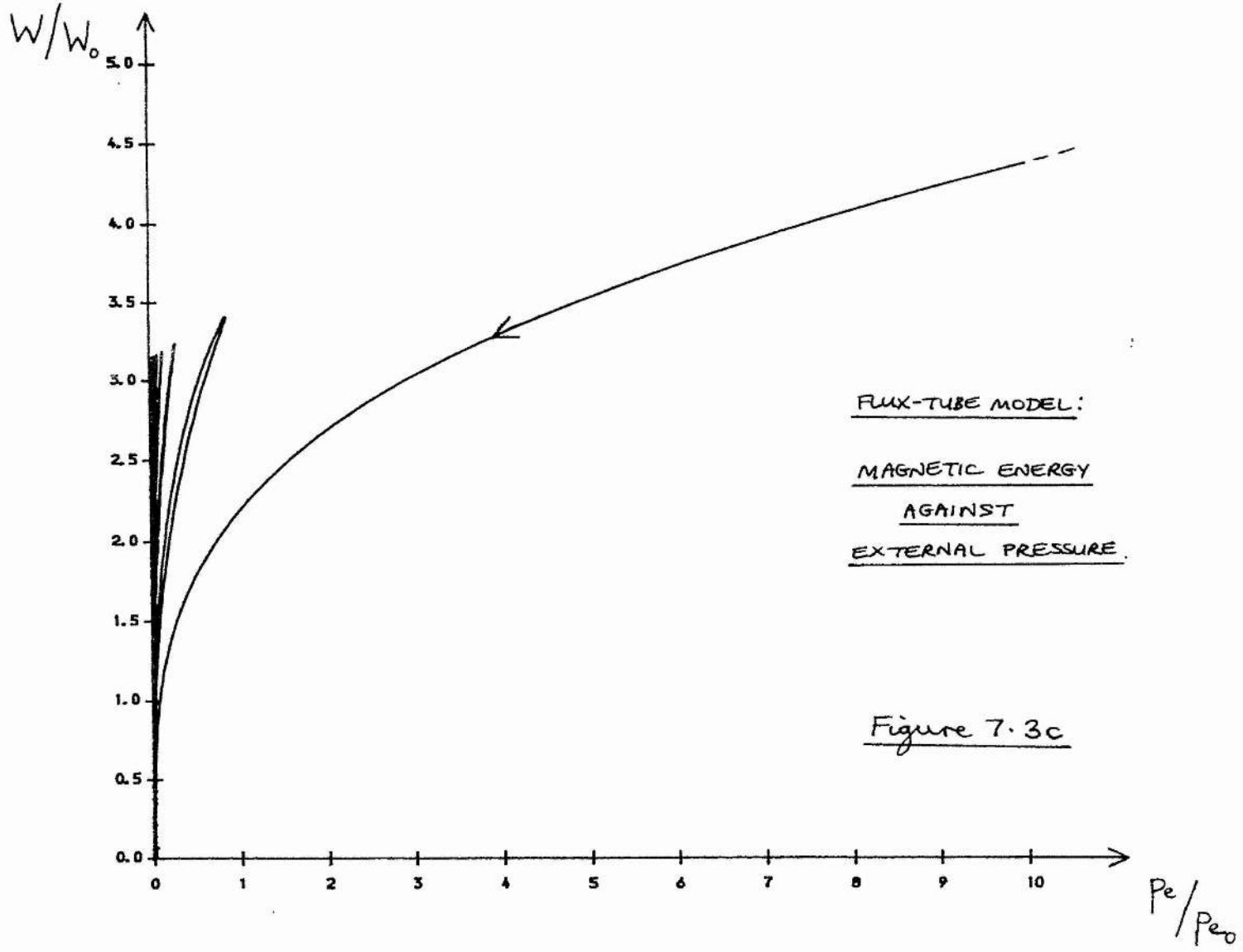
W/W₀
5.0
4.5
4.0
3.5
3.0
2.5
2.0
1.5
1.0
0.5
0.0
0
1
2
3
4
5
6
7
8
9
10
Pe/Pe₀
FLUX-TUBE MODEL:
MAGNETIC ENERGY
AGAINST
EXTERNAL PRESSURE.

Figure 7.3c

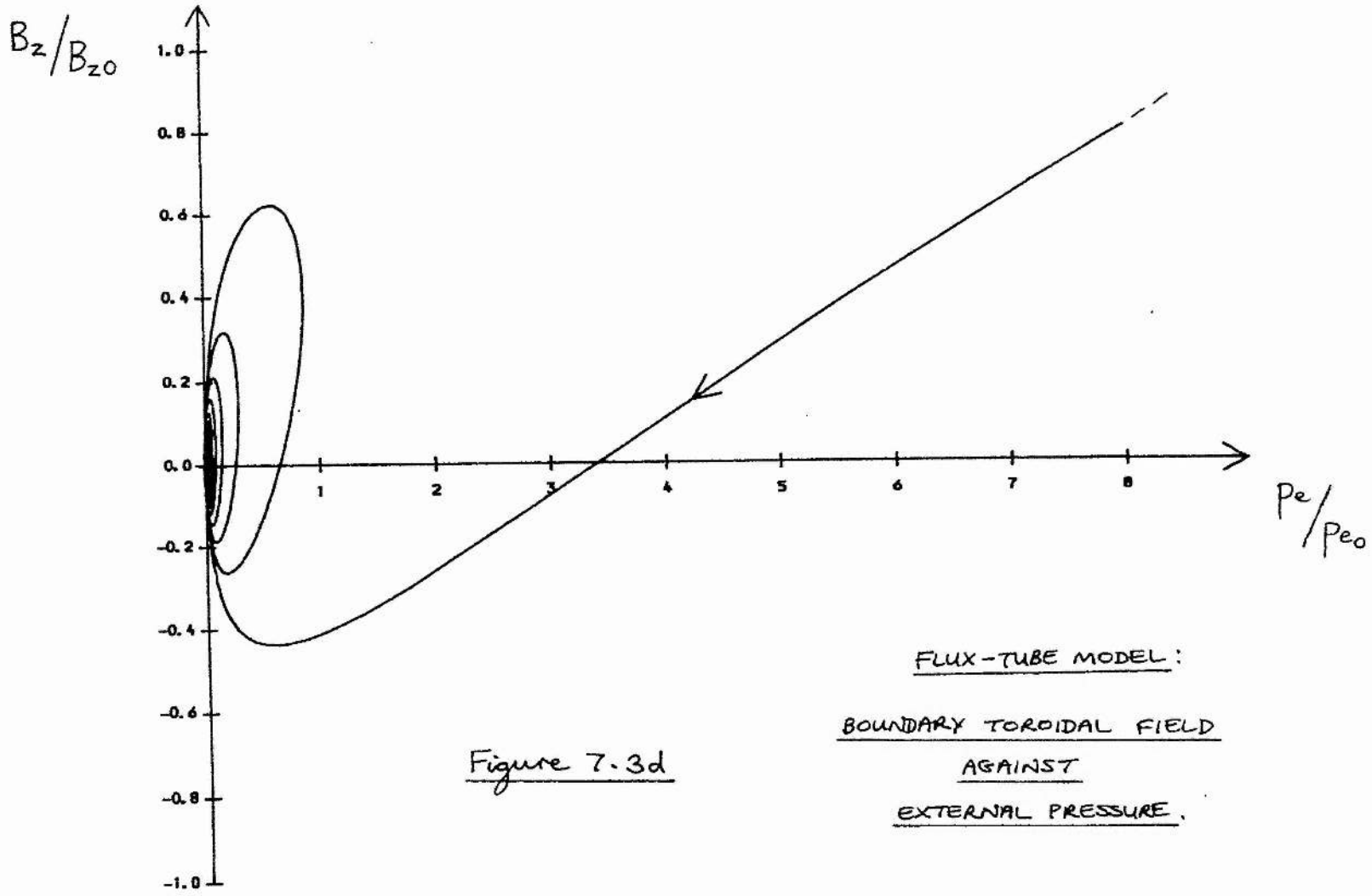

Figure 7.3d

FLUX-TUBE MODEL:

BOUNDARY TOROIDAL FIELD AGAINST EXTERNAL PRESSURE.

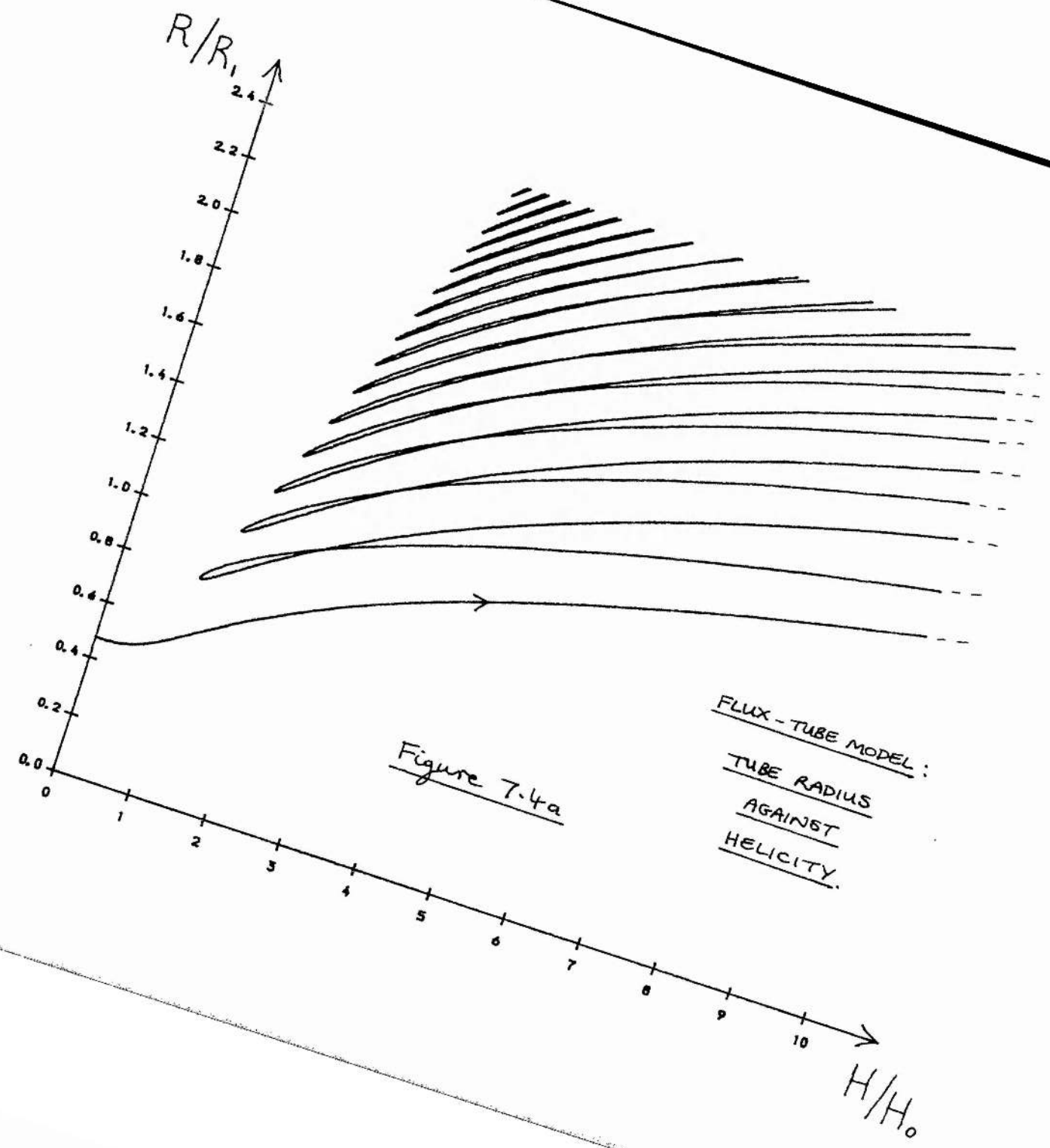

Figure 7.4a

FLUX-TUBE MODEL:
TUBE RADIUS
AGAINST
HELICITY.

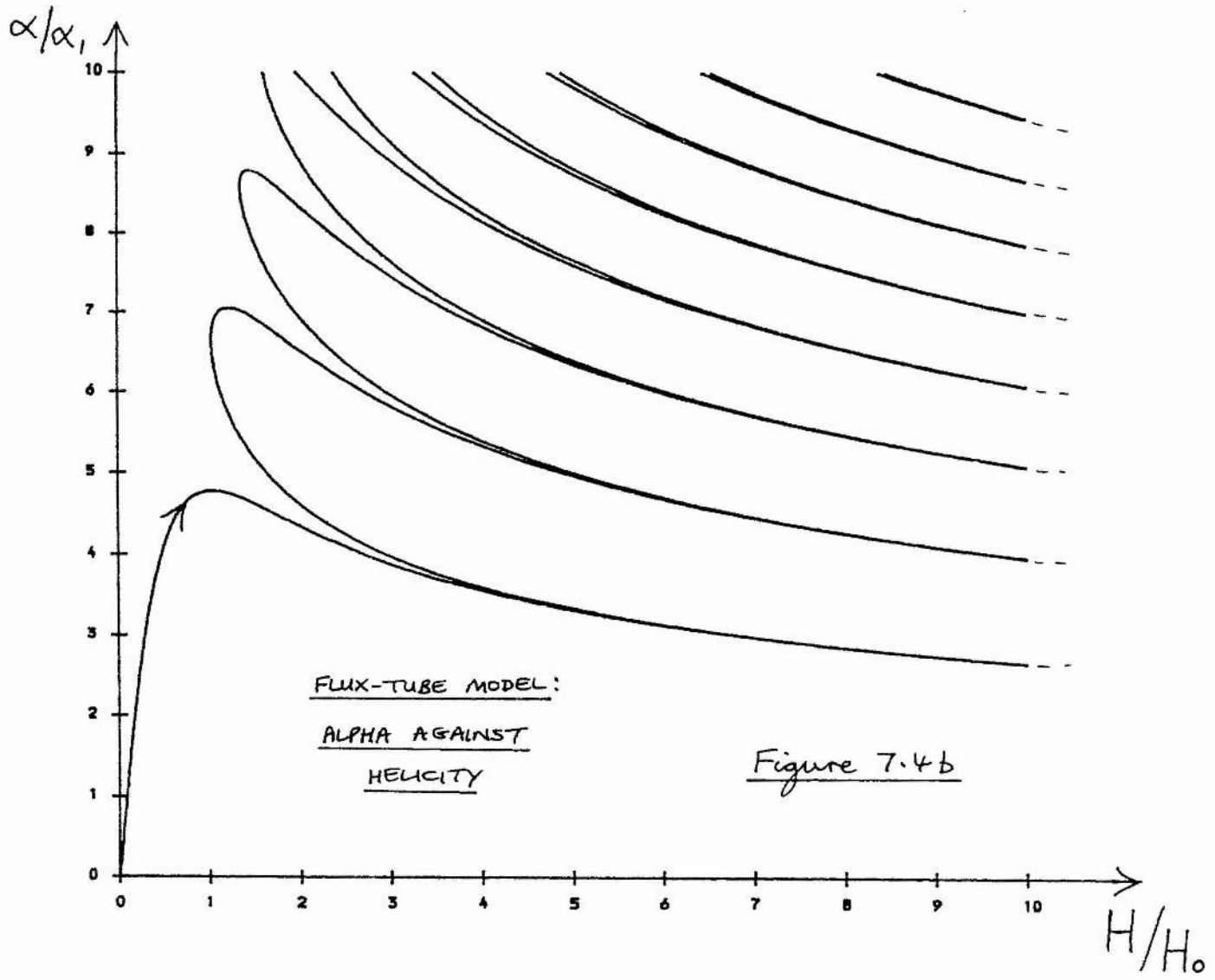
α/α₁
10
9
8
7
6
5
4
3
2
1
0
0
1
2
3
4
5
6
7
8
9
10
H/H₀
FLUX-TUBE MODEL:
ALPHA AGAINST
HELICITY

Figure 7.4b

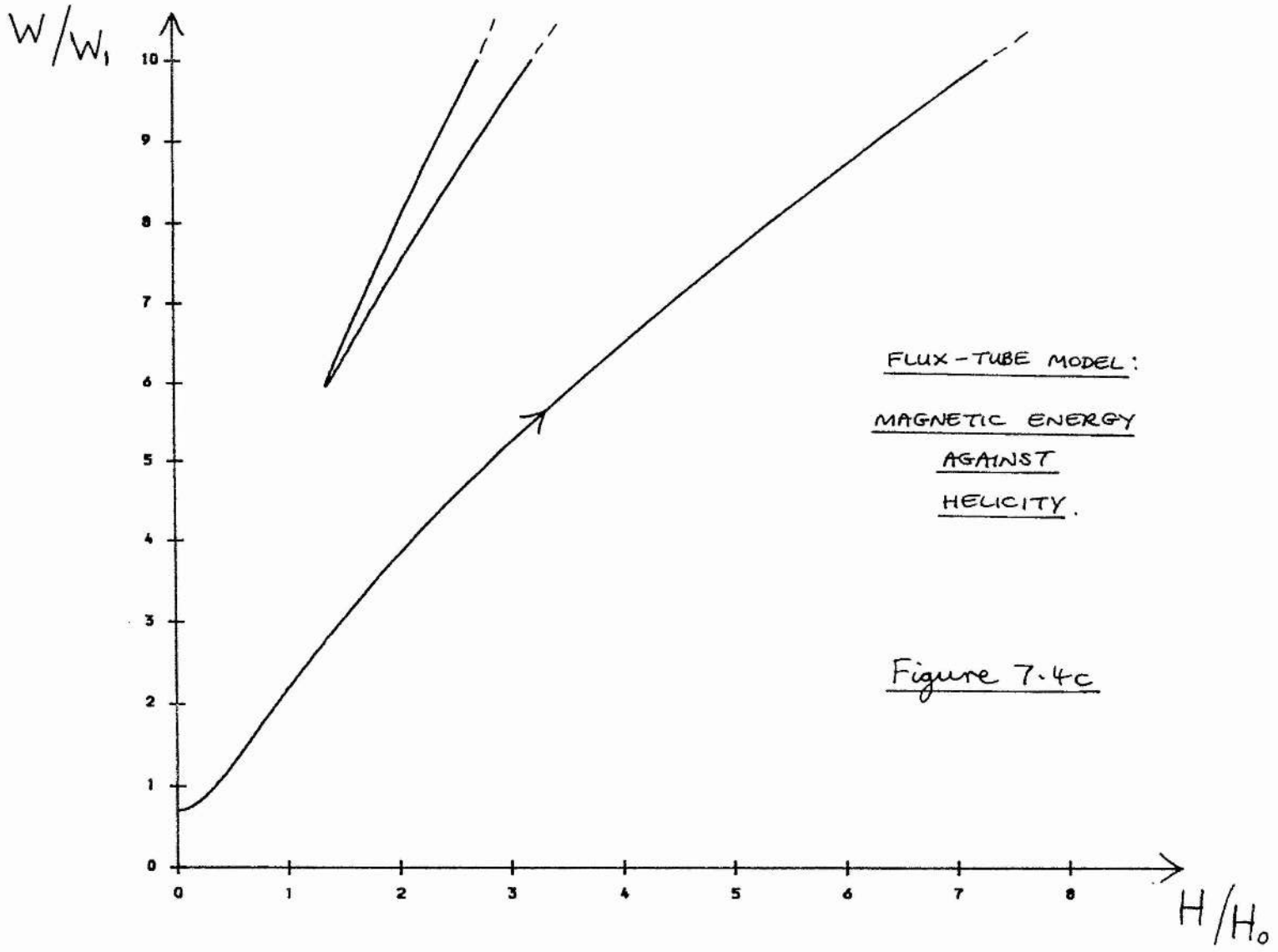

FLUX-TUBE MODEL:

MAGNETIC ENERGY

AGAINST

HELICITY.

Figure 7.4c

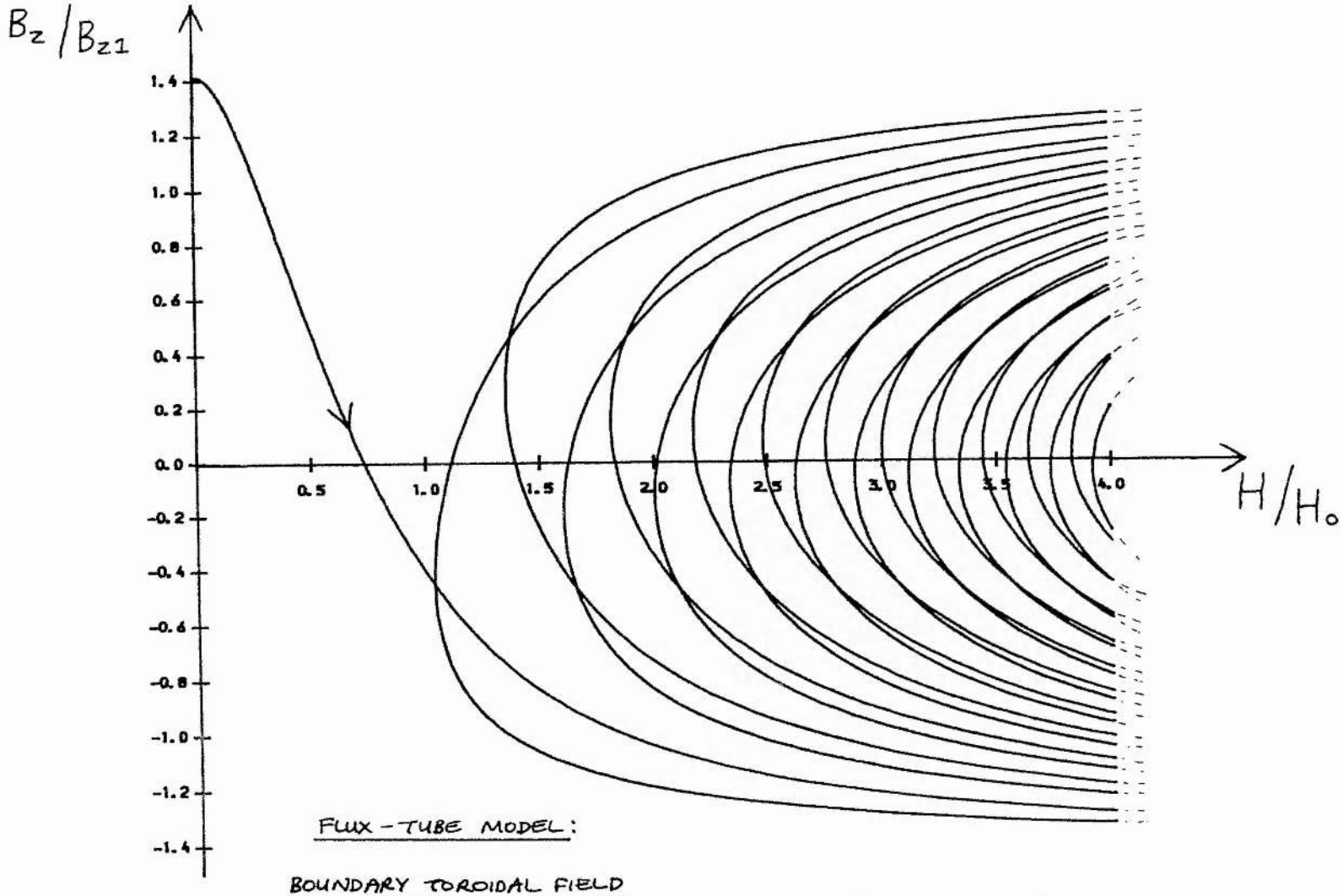

FLUX-TUBE MODEL:

BOUNDARY TOROIDAL FIELD

AGAINST HELICITY.

Figure 7.4d

variable αR. In addition, the arrow labels on each plot what may be termed the 'principal branch' of the graph, an important characteristic. In particular, inspection of Figures 7.3c and 7.4c shows that the principal branch represents the state of minimum energy of the magnetic field in each case, whether pressure or helicity is the independent variable. Further, by comparing Figure 7.3b with Figure 7.3c, or Figure 7.4b with Figure 7.4c, we deduce that the lowest value of the magnetic field energy corresponds to the lowest value of α for any particular value of the independent variable, and notably this occurs when W and α assume 'principal values'.

7.5 Two Spheromak Models

(a) Magnetically Isolated Spheromak

7.5.1 Spheromak Equilibrium

As a second example, consider the "m = 0, n = 1" solution of

$$\nabla \times \underline{B} = \alpha \underline{B} \tag{7.51}$$

in a sphere. This axi-symmetric solution has components in spherical polar co-ordinates (r,θ,ϕ) which may be written

$$B_r = 2B_0 \frac{1}{\alpha r} j_1(\alpha r) \cos\theta \tag{7.52}$$

$$B_\theta = -B_0 \frac{1}{\alpha r} \frac{d}{dr}\{r j_1(\alpha r)\} \sin\theta \tag{7.53}$$

and

$$B_\phi = B_0 j_1(\alpha r) \sin\theta \,. \tag{7.54}$$

Here B_0 represents the amplitude of the field, and $j_1(x)$ is a spherical Bessel function which in terms of the more familiar trigonometric functions is defined as

$$j_1(x) \equiv \frac{\sin x}{x^2} - \frac{\cos x}{x} \quad , \tag{7.55}$$

Now in general, on some spherical boundary r = a (say), the solution (7.52) - (7.54) above does not by itself satisfy the homogeneous boundary condition $B_r(a) = 0$, unless αa happens to be a zero of $j_1(x)$. The lowest such eigenvalue is

$$\alpha a = 4.49\ldots, \tag{7.56}$$

for which we have the lowest energy.

We shall proceed as follows. Consider a sphere of plasma of variable radius a, which is confined by suitable external pressure forces such that αa retains the value given by (7.56) at all times. Then we should expect the field inside the spherical volume to be the 'classical spheromak' which we have sketched in Figure 7.5. On the boundary, we note from (7.52), (7.54) and (7.56) that both B_r and B_ϕ vanish. Hence the magnetic pressure operating at the boundary is, from (7.53),

$$\left.\frac{B^2}{2\mu_0}\right|_{r=a} = \left.\frac{B_\theta^2}{2\mu_0}\right|_{r=a} = \frac{1}{2\mu_0}\frac{B_0^2}{(\alpha a)^2}\left[\left.\frac{d}{dr}\{r j_1(\alpha r)\}\right|_{r=a}\right]^2 \sin^2\theta \tag{7.57}$$

Clearly the pressure is not constant over the surface of the sphere, but varies in magnitude with the angle θ. Using the identity

$$\frac{d}{dx}\{j_1(x)\} = j_0(x) - \frac{2}{x} j_1(x) \quad , \tag{7.58}$$

(7.57) may be re-written in the form

$$p_e = \frac{B_0^2}{2\mu_0} j_0^2(\alpha a) \sin^2\theta \tag{7.59}$$

RADIUS a

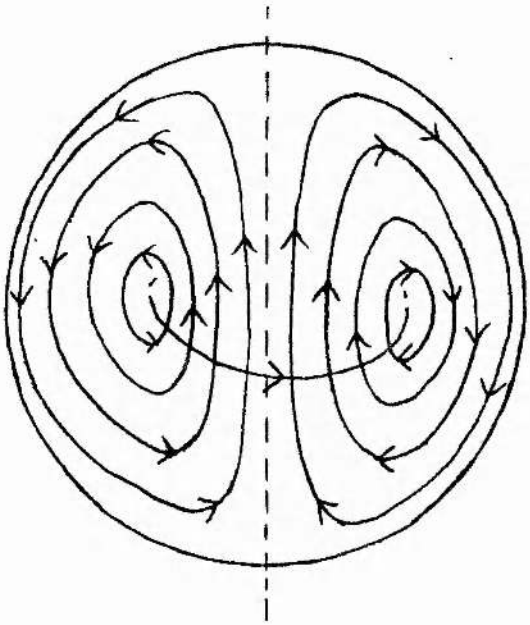

IDEALIZATION OF CLASSICAL SPHEROMAK CONFIGURATION.

Figure 7.5

where p_e denotes the confining pressure on the boundary and from now on αa is assumed to take the value αa as given by (7.56).

According to the theory of Sections 7.2 and 7.3, then, providing we can maintain the confining pressure (7.59), the linear force-free field, as given by (7.52) - (7.54), with parameter α, given by (7.56), is the predicted minimum-energy state for a spheromak of variable radius.

7.5.2 Physical Quantities

The parameters of our problem are the (relative) helicity H, the force-free constant α, the radius of the sphere a, the magnitude of the magnetic field B_0, the external pressure p_e and the field energy W.

For this problem one can show, since S here is a magnetic surface and both V and V' are simply-connected (see Section 4.14), that

$$H = \frac{1}{\alpha} \int_V \underline{B} \cdot \underline{B} \, dV . \tag{7.60}$$

So, upon substituting the components of $\underline{B}$ from (7.52), (7.53) and (7.54) into (7.60) and performing the integration using various identities, we find that

$$H = \frac{16\pi B_0^2 a^4}{3(\alpha a)^4} \int_0^{\alpha a} x^2 j_1^2(x) \, dx . \tag{7.61}$$

This integral can in turn be evaluated using (7.55) to convert the integrand to an expression involving trigonometric functions. The resulting definite integral may then be reconverted to spherical Bessel function form using the relations

$$\sin x \equiv x j_0(x) \tag{7.62}$$

and

$$\cos x \equiv j_0(x) - x j_1(x) . \tag{7.63}$$

We therefore find that

$$H = \frac{8\pi B_0^2 a^4}{3(\alpha a)^3} \{ 1 - j_0^2(\alpha a) \} \tag{7.64}$$

is the correct expression for the helicity of the configuration.

Next, consider the energy

$$W = \frac{1}{2\mu_0} \int_V \underline{B} \cdot \underline{B} \, dV \tag{7.65}$$

which by (7.60) may also be written in terms of the helicity as

$$W = \frac{1}{2\mu_0} \alpha H . \tag{7.66}$$

Hence by comparison with the result (7.64) we immediately deduce that

$$W = \frac{4\pi B_0^2 a^3}{3\mu_0 (\alpha a)^2} \{ 1 - j_0^2(\alpha a) \} \tag{7.67}$$

is the expression for the magnetic energy of the system.

We define the 'pressure amplitude' p_0 to be the maximum of the confining pressure p_e, as given by (7.59), so we write

$$p_e = p_0 \sin^2\theta \tag{7.68}$$

and hence from (7.59) we have

$$p_0 = \frac{B_0^2}{2\mu_0} j_0^2(\alpha a) . \tag{7.69}$$

For interest, we note that

$$j_0^2(\alpha a) = 4.472 \times 10^{-2} \tag{7.70}$$

and

$$1 - j_0^2(\alpha a) = 0.953 \,. \tag{7.71}$$

We are now able to make some deductions from the above.

7.5.3 Deductions

By eliminating B_0^2 between (7.64) and (7.69) we can form the constant

$$\frac{H}{p_0 a^4} = \frac{16\mu_0\pi\{1 - j_0^2(\alpha a)\}}{3(\alpha a)^3 j_0^2(\alpha a)} \,. \tag{7.72}$$

Thus, for p_0 fixed,

$$H \propto a^4 \,, \tag{7.73}$$

so that the radius of the sphere increases monotonically with the helicity present. Similarly, if helicity H is held constant,

$$p_0 \propto \frac{1}{a^4} \,, \tag{7.74}$$

so that increasing the external pressure has the effect of decreasing the radius, as we should expect intuitively.

From (7.66) we have

$$\frac{H}{aW} = \frac{2\mu_0}{(\alpha a)} = \text{CONSTANT}\ , \tag{7.75}$$

so that for constant helicity H the magnetic energy of the field is inversely proportional to the radius of the sphere. Using (7.72) we deduce also when H is fixed that the energy W is proportional to the fourth root of the pressure amplitude p_0. Hence, applying an increase in external pressure decreases the radius and increases the energy at a particular fixed value of the helicity.

We may replace the radius a in (7.72) and (7.75) above by

$$\alpha = \frac{4.49}{a} \tag{7.76}$$

from (7.56). Now α behaves as the reciprocal of a. Hence the counterpart of (7.75) is

$$\frac{\alpha H}{W} = \text{CONSTANT}\ , \tag{7.77}$$

so, for fixed H, the value of α increases in direct proportion to W, and so on.

Finally, (7.69) tells us that

$$\frac{p_0}{B_0^2} = \frac{\bar{j}_0^2(\alpha a)}{2\mu_0} = \text{CONSTANT}\ , \tag{7.78}$$

expressing the condition that increasing the size of the external pressure amplitude increases the strength of the confined field, independently of H, W or α explicitly.

(b) Spheromak in Ambient Magnetic Field

7.5.4 Description

Consider the following variation on the preceding spheromak example. Imagine

now a spheromak to be immersed in a stream of ambient flux which is in turn enclosed within a fixed cylindrical container of radius R_0. We assume the spheromak to remain always spherical, having at any time some radius $a < R_0$, to be determined. We have sketched the arrangement in Figure 7.6. [The configuration shown is intended to model the formation of as spheromak by injection of helicity into the supporting vessel in a laboratory experiment.]

In the central spheromak region we adopt the axi-symmetric, constant-α solution given by (7.52) - (7.54) in which αa assumes the eigenvalue (7.56). In the surrounding region, sufficiently far from the spheromak, we assume a uniform magnetic field of magnitude B_e. In addition, we make the assumption that the ambient field is uniform in the narrowest part, indicated in Figure 7.6 by the dotted lines PP'. The field strength in this region is denoted by B_{e0}.

7.5.5 Physical Quantities

The conservation of magnetic flux down the cylinder implies that

$$B_e R_0^2 = B_{e0} (R_0^2 - a^2) \tag{7.79}$$

and the balance of pressure at P implies, using (7.59), that

$$B_{e0}^2 = B_0^2 j_0^2 (\alpha a) . \tag{7.80}$$

Eliminating B_{e0} between (7.79) and (7.80), we obtain the relationship between the internal (spheromak) field and the external (ambient) field in the form

$$B_0^2 = \frac{B_e^2}{j_0^2(\alpha a)\left(1 - \frac{a^2}{R_0^2}\right)^2} , \tag{7.81}$$

Notice that (7.81) involves the ratio a/R_0.

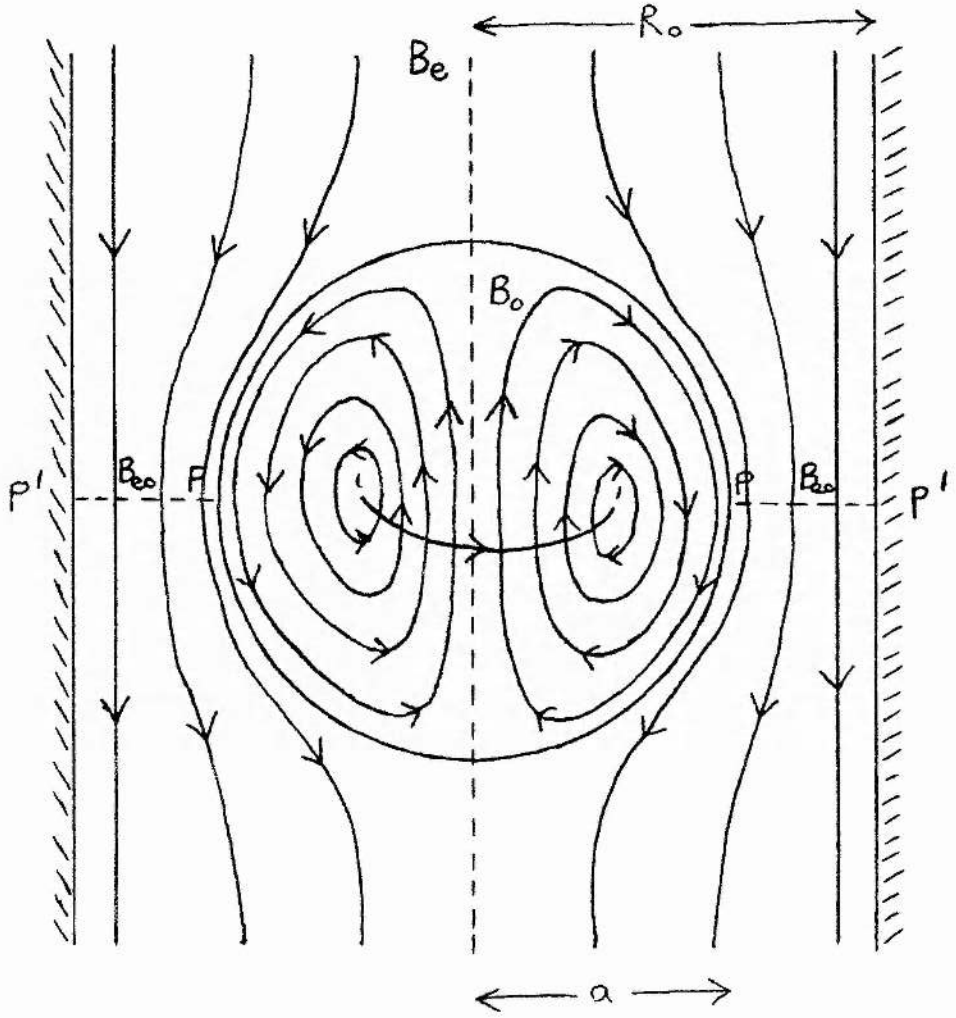

SPHEROMAK IN AMBIENT MAGNETIC FIELD.

Figure 7.6

Using (7.81), we eliminate the quantity B_0^2 from (7.64) and (7.67), giving

$$H = \frac{8\pi B_e^2 a^4 \{1 - j_0^2(\alpha a)\}}{3(\alpha a)^3 j_0^2(\alpha a)\left(1 - \frac{a^2}{R_0^2}\right)^2} \tag{7.82}$$

as the expression for the magnetic helicity, and

$$W = \frac{4\pi B_e^2 a^3 \{1 - j_0^2(\alpha a)\}}{3\mu_0 (\alpha a)^2 j_0^2(\alpha a)\left(1 - \frac{a^2}{R_0^2}\right)^2} \tag{7.83}$$

for the magnetic energy of the spheromak. In a similar way to the other spheromak example, we now make various deductions concerning the parameters of the system.

7.5.6 Deductions

First, note that (7.82) may with advantage be re-written in the form

$$H = H_0 \frac{(a^2/R_0^2)^2}{(1 - a^2/R_0^2)^2} \tag{7.84}$$

where

$$H_0 = \frac{8\pi B_e^2 R_0^4 \{1 - j_0^2(\alpha a)\}}{3(\alpha a)^3 j_0^2(\alpha a)}, \tag{7.85}$$

a constant, so that H is a function of the ratio a^2/R_0^2. The graph of (7.84) is sketched in Figure 7.7. Solving (7.84) for a^2/R_0^2, we have alternatively

$$\frac{a^2}{R_0^2} = \frac{1}{1 + (H/H_0)^{-1/2}} \tag{7.86}$$

from which we deduce that, as H increases without bound, the proportion of the container occupied by the spheromak increases with the limiting radius of the spheromak being the

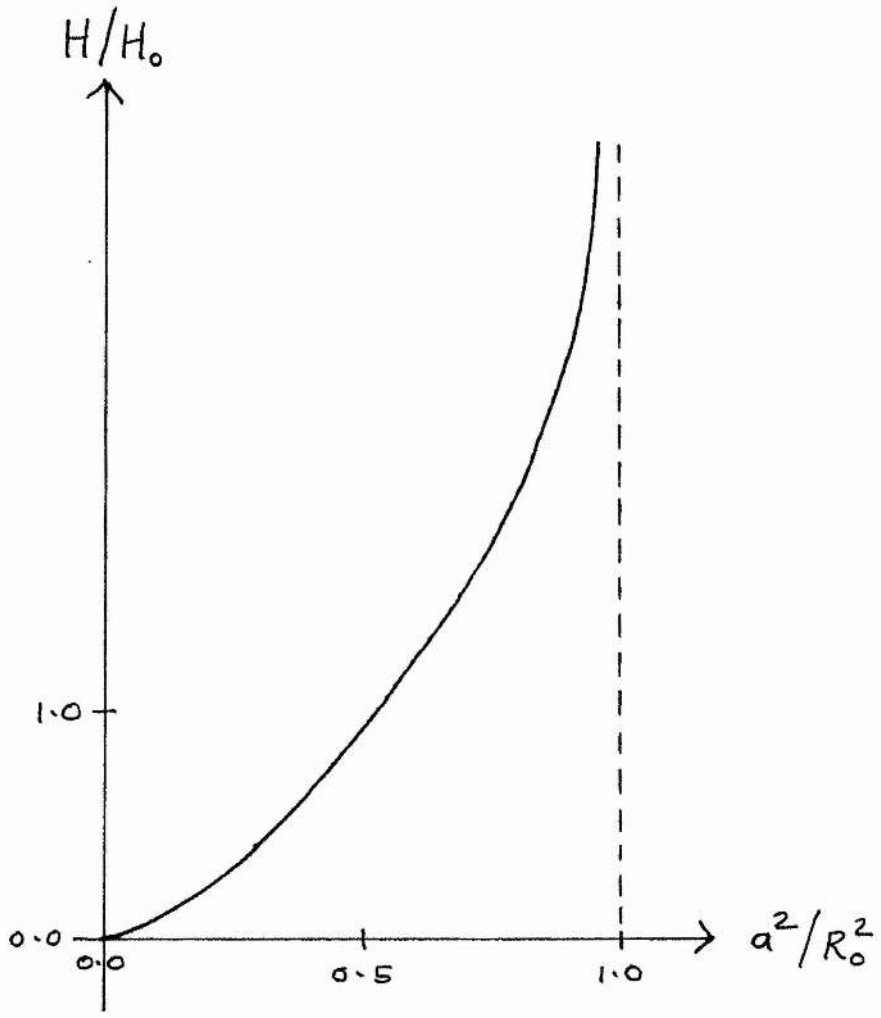

Figure 7.7

SPHEROMAK IN AMBIENT FIELD:

SKETCH OF HELICITY AGAINST

SQUARE OF SPHERDMAK RADIUS.

radius of the supporting vessel. We note also from (7.84) that $H = 0$ implies $a^2/R_0^2 = 0$, so that if there is no helicity then there is no spheromak.

Making the definition

$$\alpha_0 = \frac{4.49}{R_0} \tag{7.87}$$

we deduce using (7.56) that

$$\frac{a^2}{R_0^2} = \frac{\alpha_0^2}{\alpha^2} \, . \tag{7.88}$$

Thus, replacing the expression a^2/R_0^2 in (7.84) using (7.88), we find the helicity is

$$H = \frac{H_0}{\{(\alpha/\alpha_0)^2 - 1\}^2} \tag{7.89}$$

in terms of α . The graph of (7.89) is shown in Figure 7.8. If we solve (7.89) for $(\alpha/\alpha_0)^2$, we obtain

$$\left(\frac{\alpha}{\alpha_0}\right)^2 = 1 + \frac{1}{(H/H_0)^{1/2}} \tag{7.90}$$

which is the correct root, since

$$\alpha R_0 > \alpha a \, . \tag{7.91}$$

Thus we see that increasing the helicity decreases α/α_0 until it approaches a limiting value of 1 , corresponding to the limit $R_0 = a$ (see also Figure 7.7).

From (7.82) and (7.83) we note that

$$\frac{W}{H} = \frac{1}{2\mu_0 a} \, , \tag{7.92}$$

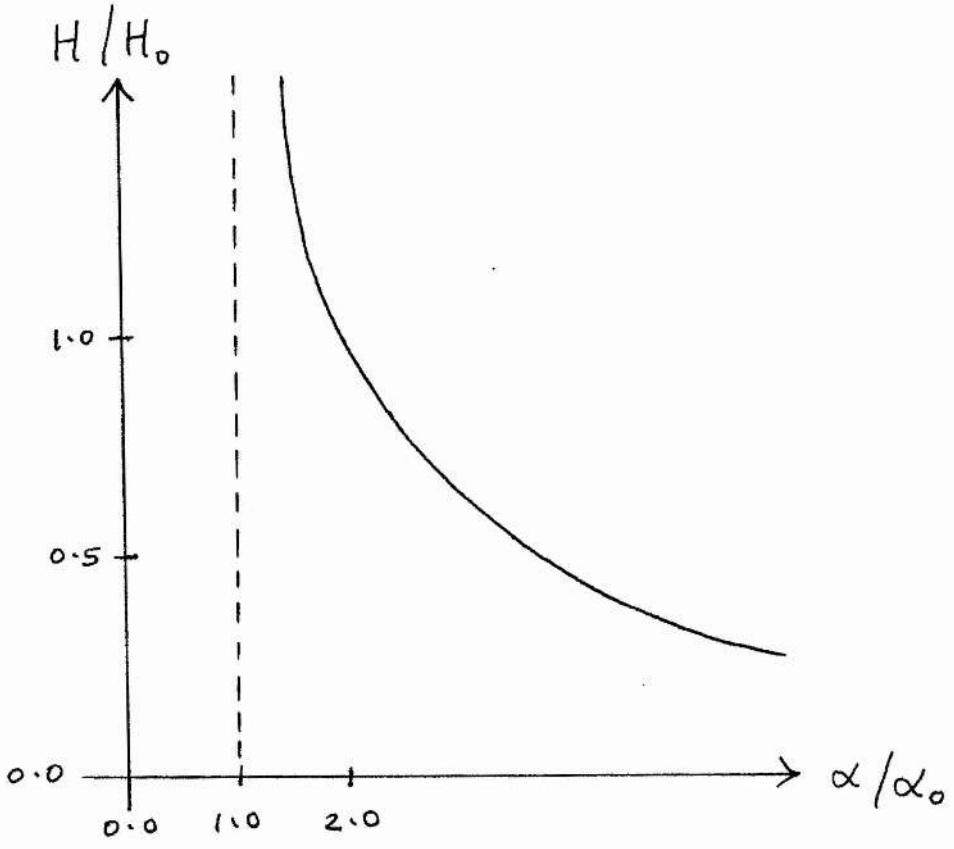

Figure 7.8

SPHEROMAK IN AMBIENT FIELD:

SKETCH OF HELICITY AGAINST

ALPHA OF SPHEROMAK FIELD.

or

$$\frac{W}{W_0} = \frac{R_0}{a}\,\frac{H}{H_0} \tag{7.93}$$

where

$$W_0 \equiv H_0 / 2\mu_0 R_0 \,. \tag{7.94}$$

Thus, substituting in (7.93) for a/R_0 from (7.84), the former becomes

$$\frac{W}{W_0} = \frac{H}{H_0}\left\{1 + \frac{1}{(H/H_0)^{1/2}}\right\}^{1/2}, \tag{7.95}$$

which relates the energy and helicity. From (7.95) we that the energy vanishes if the helicity vanishes, and $W/W_0 \to \infty$ as $H/H_0 \to \infty$. Also, at large values, the graph of energy against helicity differs little from a straight line, and near the origin

$$\frac{W}{W_0} \sim \left(\frac{H}{H_0}\right)^{3/4} . \tag{7.96}$$

The graph of (7.95) is shown in Figure 7.9, and from this we should expect quantities to vary with W in much the same way as they varied with H.

Eliminating H/H_0 between (7.84) and (7.93), we get

$$\frac{W}{W_0} = \frac{(a^2/R_0^2)^{3/2}}{(1 - a^2/R_0^2)^2} , \tag{7.97}$$

the graph of which is given in Figure 7.10. [Notice the resemblance between Figures 7.7 and 7.10.] Similarly, since from (7.76) and (7.87) we have

$$\frac{a}{R_0} = \frac{\alpha_0}{\alpha} . \tag{7.98}$$

This may be used with (7.89) and (7.93) to produce for the energy the alternative result

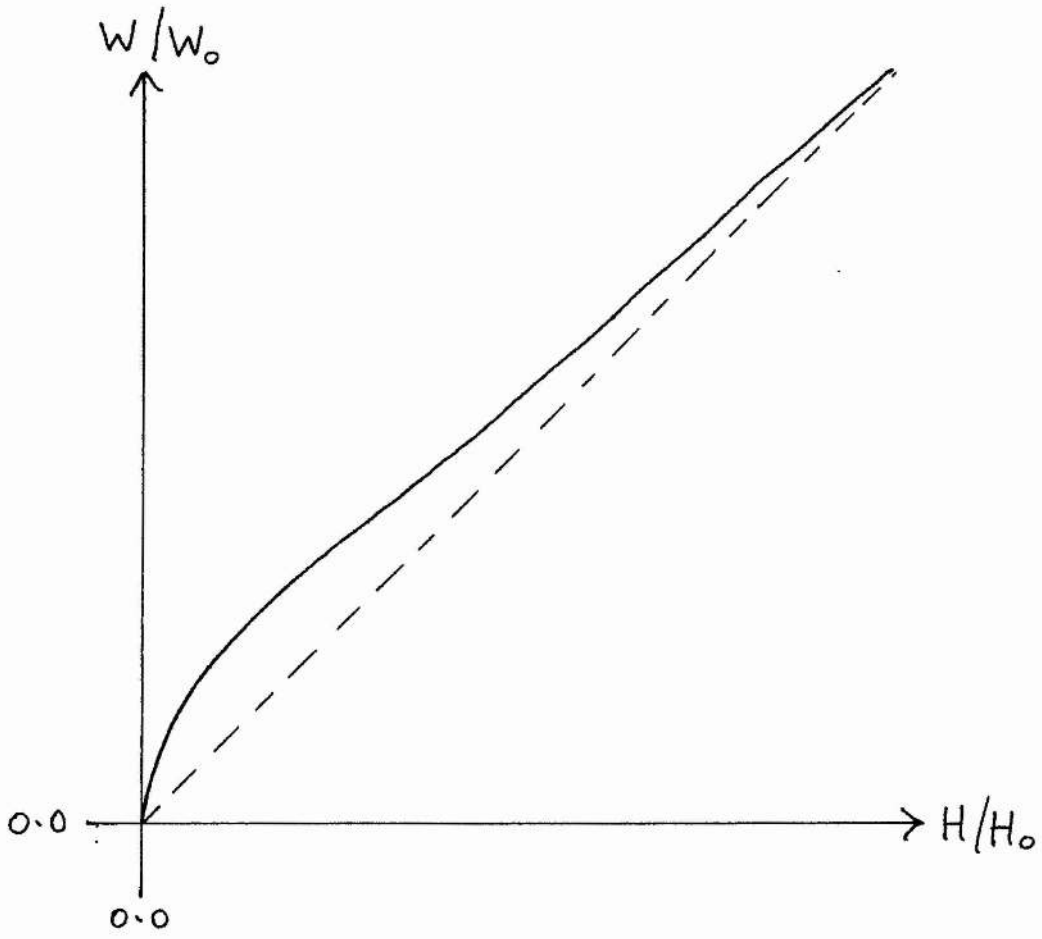

Figure 7.9

SPHEROMAK IN AMBIENT FIELD:

SKETCH OF MAGNETIC ENERGY

AGAINST SPHEROMAK HELICITY.

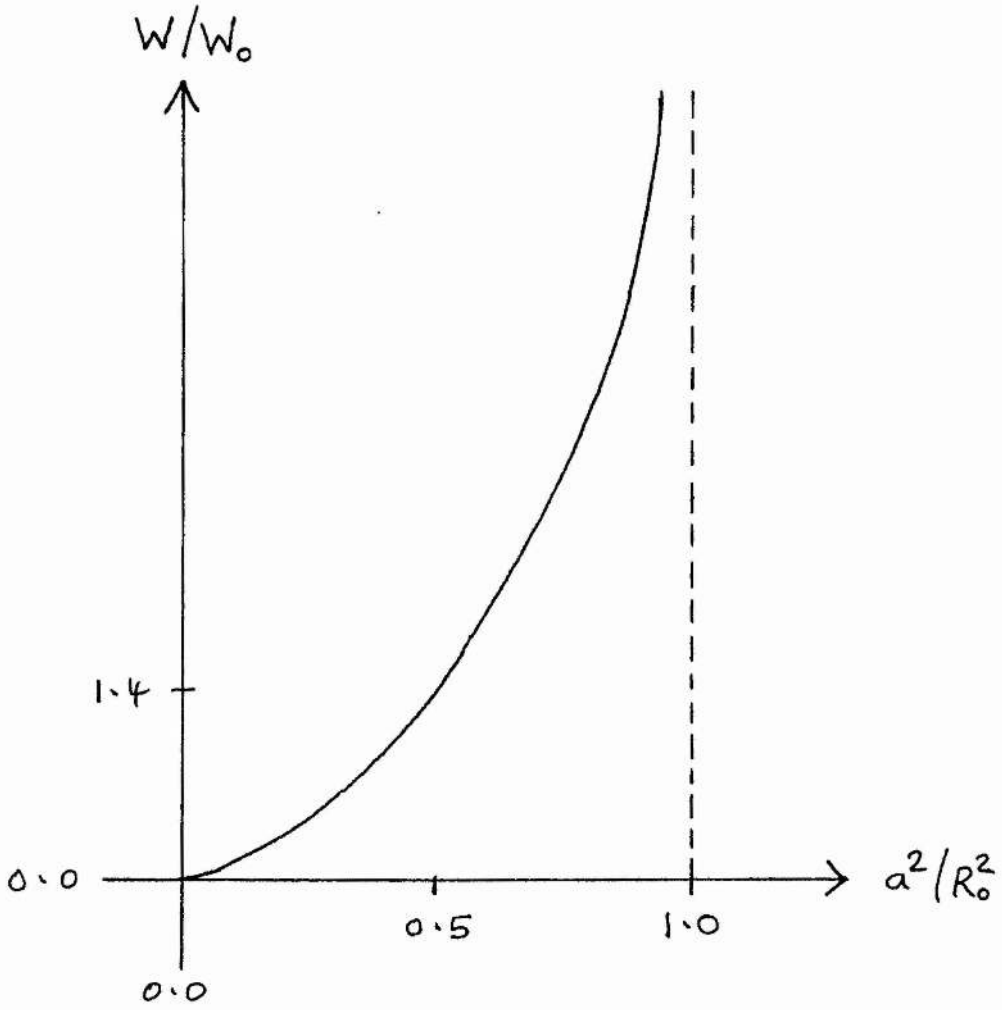

Figure 7.10

SPHEROMAK IN AMBIENT FIELD:

SKETCH OF MAGNETIC ENERGY AGAINST SQUARE OF RADIUS.

$$\frac{W}{W_0} = \frac{(\alpha^2/\alpha_0^2)^{1/2}}{(\alpha^2/\alpha_0^2 - 1)^2} \tag{7.99}$$

in terms of the α of the field. The graph of (7.99) is sketched in Figure 7.11 and is seen to be very similar in appearance to Figure 7.8. We notice that in Figures 7.7 and 7.10 the value of a^2/R_0^2 is limited above by unity, whereas in Figures 7.8 and 7.11 the value of α^2/α_0^2 is limited below by unity.

7.6 Conclusion to Chapter

We have shown in this chapter how to modify Woltjer's principle concerning the minimum-energy state of a plasma to include the case of free, homogeneous boundaries ($\underline{B}\cdot\underline{n} \equiv 0$), and have indicated how to accommodate fixed, inhomogeneous ($\underline{B}\cdot\underline{n} \not\equiv 0$) boundaries. These boundary conditions are of special importance in solar physics. The closed field solar corona may be regarded as being split up into distinct regions, each region bounded by a free, homogeneous boundary in the corona, together with a fixed, inhomogeneous boundary at the photosphere.

The theory may be of use not only in other astrophysical contexts (for example, in jets and accretion discs) but also in the laboratory regime (for example, spheromaks) where plasma confinement necessarily entails the formation of boundary confining surfaces which are not solid conducting walls.

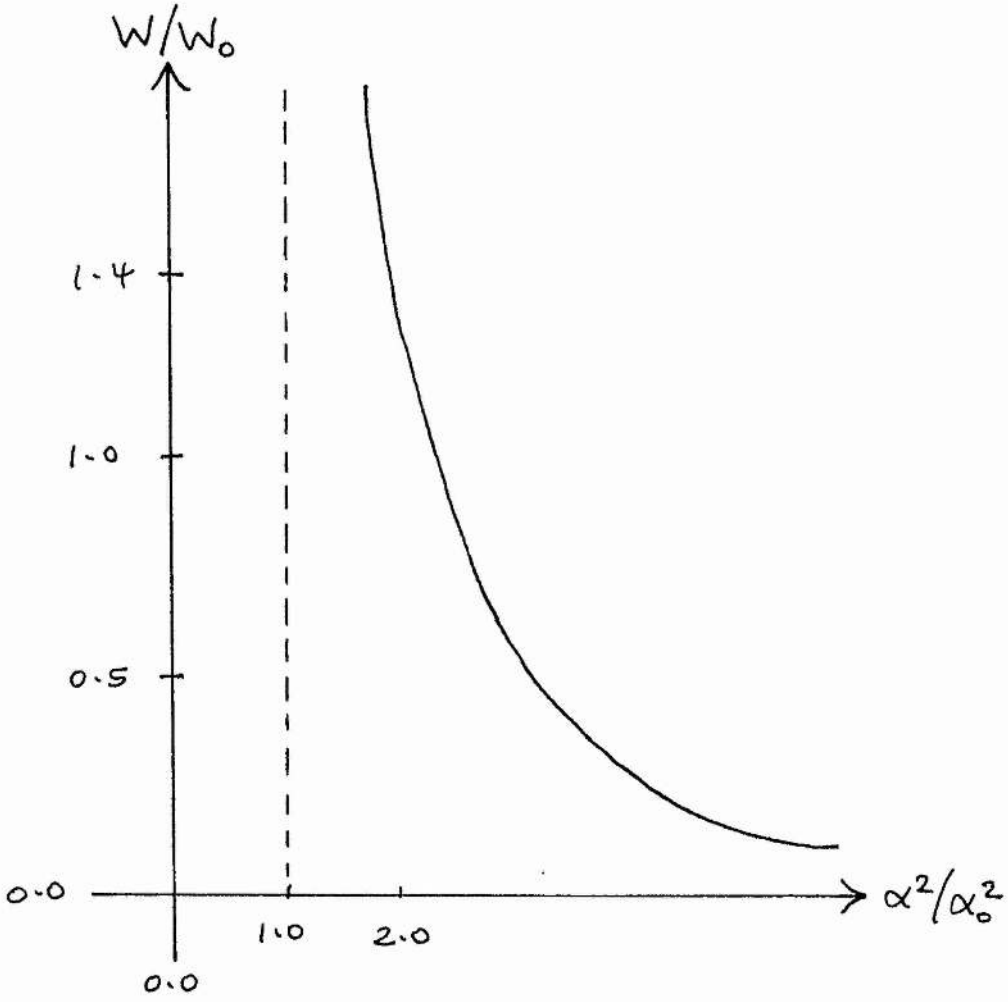

Figure 7.11

SPHEROMAK IN AMBIENT FIELD:

SKETCH OF MAGNETIC ENERGY

AGAINST SQUARE OF

SPHEROMAK ALPHA.

CHAPTER EIGHT : CONCLUSION TO THESIS

8.1 Summary

In the six chapters which form the main body of this thesis we have seen various aspects of the study of force-free equilibria and of the associated field of magnetic helicity, its conservation and evolution. In discussing these ideas, we have provided examples of applications in both solar coronal and laboratory regimes; in addition, we have extended existing theory to an astrophysical context.

The first problem addressed was that of the heating of the solar corona by means of the evolution of a magnetic configuration, chosen to model the field associated with a monopolar sunspot. In this model, the coronal field is twisted in response to the slow motions of the foot-points of an initially linear, force-free field anchored into the dense photosphere. The helicity of the field changes (ideally) according to an evolution equation developed by Heyvaerts and Priest (1984), and depends on the photospheric velocity field; it produces an intermediate non-linear, force-free field. This last field is then assumed to relax in the manner of Taylor (1974) to the linear, force-free field with the same helicity, releasing an amount of heat in the process, in order of magnitude sufficient to heat the corona to observed temperatures. The actual evolution of the coronal structure, frozen into the photosphere, is considered to be a concatenation of such elementary steps. The form of the heating-rate was found to be very similar to that of Heyvaerts and Priest (1984), and as such appears to differ only in terms of geometrical factors.

Taylor (1986) has provided an interesting analysis of equilbrium fields in plasmas confined in a cylindrical container, of basic applicability to the Reversed-Field Pinch (RFP) device in the laboratory. Using his own Hypothesis (Taylor, 1974) he was able to account

for certain features of actual experimental data, among these being the reversal of the toroidal field near the container wall and the onset of a helical distortion to the initial axi-symmetric state. The first of these is explained simply in terms of the equilibrium state being a linear, force-free field, whilst the second relies on the result that of two possible fields having the same helicity and boundary conditions, the one of lower energy is the one of lower alpha. Our aim was to search for similar behaviour in the solar coronal context. Thus, starting with the "sunspot equilibrium" of Chapter Two, we attempted to find a three-dimensional equilibrium which was a minimum-energy state, based on the field decaying to zero at a great height above the photosphere and the radial component being zero on some fixed cylinder. It was found that under these conditions a general non-axisymmetric equilibrium which isolates just two modes, one axi-symmetric and the other "helical", is not possible. Such a difference in behaviour between the solar and the laboratory problems is satisfactorily accounted for by the difference in the respective boundary conditions. It was, however, found possible to set up a theory of general, axi-symmetric fields in the solar corona such that if the form of the normal field at the photosphere is known, then the relaxed field in the entire region above the photosphere within some fixed cylinder may be calculated. Since such normal field components are measurable, it may actually be possible to construct models of the solar corona by this method, assuming the fields are linear and force-free.

In the next topic of discussion in this thesis, we turned to the laboratory environment, and in particular to models of spheromaks. Our attention was confined to cases in which magnetic flux crosses the boundary of the spherical volume, that is, to "inhomogeneous" boundary conditions, the relevance of this being that in actual laboratory experiments the boundary of the containing vessel is unlikely to be a magnetic surface. Superficially, a problem associated with this is the gauge-variance of magnetic helicity (except in the case of boundaries which are magnetic surfaces). However, the adoption of one of the gauge-invariant forms of helicity (for example, Berger and Field, 1984) deals with this particular difficulty. It was found that a general, axi-symmetric boundary condition for the radial field may be expressed as an infinite sum of Legendre polynomials in the argument $\cos\theta$, and we began by taking the first physically acceptable term in the

series, namely $B_r = P_1(\cos\theta)$, matching onto a straight field outside the sphere. The main objective was to investigate whether a three-dimensional equilibrium was possible for this boundary condition, but it was found that for all values of the relative helicity the minimum-energy state is axi-symmetric. With the next term of the series, namely $B_r = P_2(\cos\theta)$, corresponding to a hyperbolic potential field outside the sphere, the situation is apparently very different, with the result that for high enough values of the relative helicity a mixed (symmetric + asymmetric) state is indeed possible. Some examples of the general boundary condition were then considered in the form of point sources located on the boundary of the sphere (c.f. Turner, 1984). At this stage it became apparent that if only the tiniest amount of the "$P_1(\cos\theta)$" component is present on the boundary then the lowest-energy state is necessarily axi-symmetric. This is essentially because there is a singular value of alpha associated with this component which is smaller in magnitude than the eigenvalue associated with the lowest-energy mixed state, hence as one increases the value of the magnetic helicity the field "blows up" before the value of alpha required for the non-axi-symmetric state is reached. It is interesting to note how little the appearance of the graphs relating the three quantities magnetic helicity, magnetic energy and alpha change when the boundary conditions, or even the geometry, are changed. We remark that some of the point source solutions calculated may be of use in the description of "gun-injection" type spheromaks (Hammer, 1984).

The final problem considered in the present thesis is that of the extension of the theorem of Woltjer (1958) concerning the minimization of the magnetic energy of a structure to include the case where the boundary of the volume of plasma is not fixed but is free to move under the influence of external pressure forces of a plasma or magnetic origin. The constraints used are the invariance of the magnetic helicity and the balance of the pressure forces at the free boundary. It was found possible to incorporate an external pressure distribution which depends in an arbitrary way upon the three spatial co-ordinates, and the result for simply connected volumes was easily generalized to multiply connected ones. The shape of the free boundary can also be arbitrary, and "inhomogeneous" sections can be introduced into the boundary provided that they are fixed in space, with obvious identification with the photosphere of the sun. This extended theorem will be of use in

both an astrophysical setting, where most, if not all, boundaries are free, and in the laboratory, where plasmas are confined away from the solid walls of containing vessels. Three prototype applications of the use of the new form of the theorem are provided in the text.

8.2 Suggestions for Future Work

To conclude, we suggest some possible topics, prompted by the present work, for future investigation.

There exists the possibility using the Taylor-Heyvaerts method of Chapter Two of producing a theory which does not rely on unknown parameters (such as ε and γ) and which describes a truly continuous evolution rather than a series of discrete steps. It is not at once clear how to quantify the reconnection time in this model; it may well be easier to tackle the problem of the continuity of the reconnection and field evolution first. The method as it stands could be applied to a further range of equilibrium state configurations, perhaps to more "realistic" fields. However, since the expression for the heating-rate in transferring from one geometry to another remains essentially the same, this is probably of questionable value.

With regard to the development of models of spheromak devices (and other laboratory machines), a suggestion might be to develop the kind of solutions calculated in Chapters Four, Five and Six to more "realistic" shapes for the containing vessels. Perhaps one could try adopting an ellipsoidal co-ordinate system in order to investigate the effects of non-sphericity on the nature of relaxed states : indeed, various other stability aspects of spheromaks could be studied. Further calculations based on the results already obtained might include the determination of the proportion of the total volume of the vessel occupied by island regions; this information is of use to those in the fusion programme interested in the amount of confinement of plasma.

Finally, the extended theorem of Chapter Seven could be used to generalize the spheromak solutions of the three preceding chapters to cases where the boundaries are not defined by solid walls. Thus one could make an attempt to model the effects of the "space" between the central plasma region and the inner surface of the containing vessel, resulting in more accurate prediction of the magnitude of the magnetic field near the outer boundaries of certain laboratory configurations, particularly if the finite electrical conductivity of these regions is also taken into account.

REFERENCES

Abramowitz, M. and Stegun, I. A., *Handbook of Mathematical Functions,* Dover Publications, Inc., New York (1972)

Berger, M. A., *Geophys. Astrophys. Fluid Dyn.* **30**, 79 (1984)

Berger, M. A. and Field, G. B., *J. Fluid Mech.* **147**, 133 (1984)

Bodin, H. A. B. and Newton, A. A., *Nucl. Fusion* **20**, 1225 (1980)

Browning, P. K. and Priest, E.R., *Astron. Astrophys.* **159**, 129 (1986)

Browning, P. K., Sakurai, T. and Priest, E. R., *Astron. Astrophys.* **158**, 217 (1986)

Chandrasekhar, S. and Kendall, P. C., *Astrophys. J.* **126**, 457 (1957)

Chiuderi, C., in "Solar and stellar magnetic fields : origins and coronal effects" , *I.A.U. Symp.* (ed. J. O. Stenflo) **102**, 375 (1983)

Dixon, A. M., Berger, M. A., Browning, P. K. and Priest, E. R., to appear in *Astron. Astrophys.* (1988)

Dixon, A. M., Browning, P. K. and Priest, E. R., *Geophys. Astrophys. Fluid Dyn.* **40**, 293 (1988)

Dixon, A. M., Browning, P. K., Bevir, M. K., Gimblett, C. G. and Priest, E. R., preprint, to be submitted to *J. Plasma Phys.* (1988)

Finn, J. H. and Antonsen, T. M., *Comments Phys. Contr. Fusion* **9**, 111 (1985)

Hammer, J. H., p. 319 in *Magnetic Reconnection in Space and Laboratory Plasmas* (ed. E. W. Hones, Jr.), American Geophysical Union, Washington, D. C. (1984)

Heyvaerts, J., in *The Hydromagnetics of the Sun* , ESA SP-220, 123 (1984)

Heyvaerts, J. and Priest, E. R., *Astron. Astrophys.* **137**, 63 (1984)

Hollweg, J. V., in *Solar Wind Five* (ed. M. Neugebauer), NASA 5 (1983)

Hugill, J., in *Plasma Physics and Nuclear Fusion Research* (ed. R. D. Gill), Academic Press Inc. (London) Ltd. (1981)

Jarboe, T. R., Henins, I., Sherwood, A. R., Barnes, C. W. and Hoida, H. W., *Phys. Rev. Lett.* **51**, 39 (1983)

Jarboe, T. R., Barnes, C. W., Henins, I., Hoida, H. W., Knox, S. O., Linford, R. K. and Sherwood, A. R., *Phys. Fluids* **27**, 13 (1984)

Jensen, T. H. and Chu, M. S., *Phys. Fluids* **27**, 281 (1984)

Kippenhahn, R. and Schluter, A., *Zs. Ap.* **43**, 36 (1957)

Kuperus, M. and Raadu, M. A., *Astron. Astrophys.* **31**, 189 (1974)

Kuperus, M. and Heyvaerts, J., *Ann. Phys.* (France) **5**, 483 (1980)

Lawson, J. D., *Proc. Phys. Soc. B* **70**, 6 (1957)

Mangulis, V., *Handbook of Series for Scientists and Engineers* , Academic Press (1965)

Moffatt, H. K. *J. Fluid Mech.* **35**, 117 (1969)

Parker, E. N., *Astrophys. J.* **174**, 499 (1972)

Parker, E. N., *Astrophys. J.* **244**, 631 (1981)

Parker, E. N., *Astrophys. J.* **264**, 635 (1983a)

Parker, E. N., *Astrophys. J.* **264**, 642 (1983b)

Priest, E. R., *Solar Magnetohydrodynamics* , D. Reidel Publishing Company, Dordrecht, Holland, (1982)

Reiman, A., *Phys. Fluids* **24**, 596 (1981)

Rosenbluth, M. N. and Bussac, M. N., *Nucl. Fusion* **19**, 489 (1979)

Schatzman, E., *I.A.U. Symp.* **22**, 337 (1965)

Taylor, J. B., *Phys. Rev. Lett.* **33**, 1139 (1974)

Taylor, J. B., *Rev. Modern Phys.* **58**, 741 (1986)

Turner, W. C., Goldenbaum, G. C., Granneman, E. H. A., Hammer, J. H., Hartman, C. W., Prono, D. S. and Taska, J., *Phys. Fluids* **26**, 1965 (1983)

Turner, L., *Phys. Fluids* **27**, 1677 (1984)

Van Ballegooijen, A. A., *Astrophys. J.* **298**, 421 (Paper I) (1985)

Woltjer, L., *Proc. Nat. Acad. Sci. USA* **44**, 489 (1958)